

**CYTOTOXIC ACTIVITIES, APOPTOTIC INDUCTION
AND MITOCHONDRIAL STUDIES OF SELECTED
CATIONIC SCHIFF BASES FROM THE
THIOSEMICARBAZONE FAMILY**

SARAVANA KUMAR SINNI AH

**FACULTY OF SCIENCE
UNIVERSITY OF MALAYA
KUALA LUMPUR**

2016

CYTOTOXIC ACTIVITIES, APOPTOTIC INDUCTION AND
MITOCHONDRIAL STUDIES OF SELECTED CATIONIC SCHIFF
BASES FROM THE THIOSEMICARBAZONE FAMILY

SARAVANA KUMAR SINNIAH

THESIS SUBMITTED IN FULFILMENT OF THE REQUIREMENTS
FOR THE DEGREE OF DOCTOR OF PHILOSOPHY

FACULTY OF SCIENCE
UNIVERSITY OF MALAYA
KUALA LUMPUR

2016

UNIVERSITY OF MALAYA
ORIGINAL LITERARY WORK DECLARATION

Name of Candidate: Saravana Kumar Sinniah

Registration/Matric No: SHC110040

Name of Degree: DOCTOR OF PHILOSOPHY

Title of Project Paper/Research Report/Dissertation/Thesis ("this Work"):

CYTOTOXIC ACTIVITIES, APOPTOTIC INDUCTION AND
MITOCHONDRIAL STUDIES OF SELECTED CATIONIC SCHIFF BASES
FROM THE THIOSEMICARBAZONE FAMILY

Field of Study: Biochemistry

I do solemnly and sincerely declare that:

- (1) I am the sole author/writer of this Work;
- (2) This Work is original;
- (3) Any use of any work in which copyright exists was done by way of fair dealing and for permitted purposes and any excerpt or extract from, or reference to or reproduction of any copyright work has been disclosed expressly and sufficiently and the title of the Work and its authorship have been acknowledged in this Work;
- (4) I do not have any actual knowledge nor do I ought reasonably to know that the making of this work constitutes an infringement of any copyright work;
- (5) I hereby assign all and every rights in the copyright to this Work to the University of Malaya ("UM"), who henceforth shall be owner of the copyright in this Work and that any reproduction or use in any form or by any means whatsoever is prohibited without the written consent of UM having been first had and obtained;
- (6) I am fully aware that if in the course of making this Work I have infringed any copyright whether intentionally or otherwise, I may be subject to legal action or any other action as may be determined by UM.

Candidate's Signature

Date:

Subscribed and solemnly declared before,

Witness's Signature

Date:

Name:

Designation:

ABSTRACT

Thiosemicarbazone (TSC) is a Schiff base that has been receiving considerable attention owing to its promising biological implication and remarkable pharmacological properties such as anti-tumor, anti-viral, anti-microbial and anti-parasitic. Currently, the most promising drug candidate of this class would be Triapine (3-aminopyridine-2-carboxaldehyde thiosemicarbazone) which has entered phase II clinical trials as a potent anti-cancer chemotherapeutic agent. In the present study, Schiff base ligands from (3-formyl-4-hydroxy-phenyl)methyl-triphenyl-phosphonium (**T**) and varied substituents at N4 atom namely thiosemicarbazide itself [**(tsc)T**], 4-phenylthiosemicarbazide [**P(tsc)T**], 4,4-fluorophenylthiosemicarbazide [**FP(tsc)T**], 4-ethylthiosemicarbazide [**E(tsc)T**], 4,4-ethylphenylthiosemicarbazide [**EP(tsc)T**], 4-methylthiosemicarbazide [**M(tsc)T**] and 4,4-dimethyl thiosemicarbazide [**DM(tsc)T**] were synthesized by condensation reactions. These compounds have been characterised by IR, NMR, HRMS and X-ray crystallography and were in confirmation with the proposed structures. Growth inhibitory effect of the compounds were performed against six human cell lines, namely PC-3 (prostate adenocarcinoma), A549 (non-small cell lung cancer), MCF7 (breast carcinoma), MDA-MB-231 (breast adenocarcinoma), HCT 116 (colorectal carcinoma) and RWPE-1 (prostate normal). MTT assay indicated that [**P(tsc)T**], [**FP(tsc)T**], [**EP(tsc)T**] and [**DM(tsc)T**] exhibit significant inhibitory effect on PC-3 cells with least damage to RWPE-1 cells. These four cytotoxic compounds induce prominent morphological changes such as rounding, shrinkage, membrane blebbing and the loss of cell to cell contacts compared to untreated cells which were affirmed by AO/EB assay. The untreated cells were stained uniformly green; meanwhile most of the cells treated with 50 μ M or higher concentration for 48 and 72 hours were stained bright orange to red, indicating late apoptosis and/or necrosis phase. These results were further

supported by Annexin V/PI assay which clearly indicated that the compounds induce apoptosis in PC-3 cells. The untreated cells showed approximately 90 % cell viability meanwhile cells treated with 100 μ M of the compounds for 72 hours showed approximately 50 % drop in cell viability, indicating that these compounds demonstrate cytotoxic properties in dose- and time-dependent manner. Furthermore, the cell cycle assay results showed that the cell cycle was arrested in G0/G1 phase when treated with the compounds for 72 hours. Mitochondrial membrane potential assay result also implied that the apoptosis could be due to mitochondria mediated pathway by showing a steady drop in polarized cells with increasing dose for treatment duration of 24 hours. In conclusion, the results obtained showed that the newly synthesized compounds induce significant cytotoxic properties by inhibiting highly metastasis prostate cancer cell line growth. Taken together, these data suggest that the newly synthesized TSC compounds warrant further systematic investigation as anti-cancer agent, and they can serve as building blocks for further modifications.

ABSTRAK

Tiosemikarbazon (TSC) adalah bes Schiff yang menerima tumpuan kerana implikasi biologi dan sifat-sifat farmakologi seperti anti-kanser, anti-virus, anti-mikrob dan anti-parasit. Kini, calon ubat yang paling berbakat dalam kelas ini ialah triapina (3-aminopiridina-2-karbsaldehid tiosemikarbazon) yang telah memasuki ujian klinikal fasa II sebagai ejen anti-kanser kemoterapi. Dalam kajian ini, ligan-ligan bes Schiff dari (3-formil-4-hidroksi-fenil)metil-trifenil-phosphonium (T) dan pelbagai kumpulan penukar-ganti pada atom N4, iaitu tiosemikarbazida [**tscT**], 4-feniltiosemikarbazida [**P(tsc)T**], 4,4-fluorofeniltiosemikarbazida [**FP(tsc)T**], 4-etiltiosemikarbazida [**E(tsc)T**], 4,4-etilfeniltiosemikarbazida [**EP(tsc)T**], 4-metiltiosemikarbazida [**M(tsc)T**] dan 4,4-dimetiltiosemikarbazida [**DM(tsc)T**] telah disintesis melalui reaksi-reaksi kondensasi. Struktur sebatian-sebatian ini telah dikesahkan dengan menggunakan IR, NMR, HRMS dan kristalografi sinar-X. Aktiviti perencatan pertumbuhan sebatian-sebatian ini telah dijalankan atas empat titisan sel manusia, iaitu PC-3 (adenokarsinoma prostat), A549 (kanser paru-paru), MCF-7 (karsinoma payudara) MDA-MB-231 (adenokarsinoma paru-paru), HCT116 (karsinoma kolon) dan RWPE-1 (prostat biasa). Eksperimen MTT menunjukkan bahawa [**P(tsc)T**], [**FP(tsc)T**], [**EP(tsc)T**] dan [**DM(tsc)T**] mempunyai kesan perencatan yang ketara pada sel PC-3 tetapi tidak menunjukkan perencatan pada pertumbuhan sel RWPE-1. Dalam esei AO/EB, keempat-empat sebatian sitotoksik ini menunjukkan perubahan morfologi yang ketara seperti pembulatan, pengecutan, “*membrane blebbing*” dan kehilangan hubungan sel ke sel berbanding dengan sel-sel tanpa rawatan. Sel-sel tanpa rawatan menunjukkan warna hijau secara seragam; manakala kebanyakan sel-sel yang dirawat dengan 50 µM sebatian dan ke atas menunjukkan warna jingga terang dan merah dalam tempoh rawatan 48 dan 72 jam. Ini menunjukkan fasa apoptosis lewat dan/atau nekrosis. Hasil kajian ini turut disokong

oleh esei Annexin V/PI yang menunjukkan dengan jelas sebatian-sebatian ini menyebabkan apoptosis dalam sel PC-3. Sel-sel tanpa rawatan menunjukkan kira-kira 90 % sel yang berdaya hidup sementara sel yang dirawat dengan 100 μ M sebatian dalam tempoh 72 jam menunjukkan kira-kira 50 % penurunan sel berdaya hidup. Ini menunjukkan bahawa sebatian-sebatian ini mempamerkan ciri-ciri sitotoksik bergantung kepada dos dan tempoh rawatan. Tambahan lagi, hasil kajian eksperimen kitar sel menunjukkan bahawa kitaran sel berhenti pada fasa G0/G1 apabila dirawat dengan sebatian untuk tempoh 72 jam. Esei keupayaan membran mitokondria juga menunjukkan bahawa apoptosis mungkin berlaku melalui laluan pengantara mitokondria dengan penurunan polarisasi sel yang stabil bersama peningkatan dos untuk tempoh rawatan 24 jam. Kesimpulannya, hasil kajian yang diperolehi menunjukkan bahawa sebatian-sebatian yang baru disintesis ini mempunyai kesan sitotoksik yang ketara dalam penghalangan pertumbuhan titisan sel kanser prostat yang sangat metastasis. Diambil bersama, data-data tersebut mencadangkan bahawa kajian anti-kanser yang lebih mendalam bagi sebatian-sebatian TSC yang baru disintesis ini perlu diteruskan, dan sebatian-sebatian ini boleh berfungsi sebagai blok binaan untuk pengubahsuaian selanjutnya.

ACKNOWLEDGEMENTS

I would like to express my heartfelt gratitude and appreciation to my supervisors, Dr Sim Kae Shin from Institute of Biological Sciences and Dr Tan Kong Wai from Department of Chemistry, Faculty of Science for their continuous supervision, advices, guidance and the precious time that they have devoted for this research. I would like to thank them for their patience and many hours of hardwork in discussing various approaches throughout my project.

I would also like to thank Prof Dr Ng Seik Weng from Department of Chemistry for his guidance and advice in solving the crystal structures. In addition, I am very grateful to my fellow labmates from Department of Chemistry, Mr Lee Sze Koon, Mr Heng Mok Piew and Miss Chew Shin Thung for their assistance in chemistry work and true friendships.

My sincere appreciation to all my fellow labmates from Institute of Postgraduate Studies laboratory, Mr Suerialoasan, Mr Faizan Naeem, Mr Eric Saw Wen Shang, Miss Faezah Mohamad, Miss Hazwani Mat Saad, Miss Chan Sweet Rie and Miss Amal Rhaffor for their help, moral support and friendship in providing a conducive working environment. Special thanks to Mr Teoh Wuen Yew for his continuous encouragement and working hand in hand since Bachelor of Science, which truly has inspired me to complete this study.

I would like to acknowledge the Ministry of Higher Education (MOHE) for MyBrain15 MyPhD scholarship that keep me financially sound throughout the study period. I would like to express my utmost appreciation to Toray Science Foundation for awarding me Science and Technology Research Grant (55-02-03-1060). This research project was also funded by University of Malaya (PPP PV015/2012A and UMRG-RG049/11BIO).

Last but not least, my deepest appreciation and love to my wife, Teh Pei Pei for her understanding and endless patience all these years. I am also very thankful to my loving parents Mr Sinniah and Madam Khoo Ee Lan, my sweet sisters Jeevasulochana and Sumathy, my caring brother Sasee Kumar, my supportive niece Rishaini and my dearest nephews Vinod, Divenesh and Suhinesh for their love, support, believed in me and made me believe in myself. I owe my achievement to them.

University of Malaya

TABLE OF CONTENTS

	Page
ABSTRACT	iii
ABSTRAK	v
ACKNOWLEDGEMENT	vii
TABLE OF CONTENTS	ix
LIST OF FIGURES	xvi
LIST OF TABLES	xix
LIST OF SYMBOLS AND ABBREVIATIONS	xx
LIST OF APPENDICES	xxiii
CHAPTER	
1 INTRODUCTION	1
2 LITERATURE REVIEW	8
2.1 Schiff bases	8
2.2 Thiosemicarbazones	9
2.2.1 Mono-thiosemicarbazones and bis-thiosemicarbazones	10
2.2.2 Antitumor activity of thiosemicarbazones	11
2.3 Triphenylphosphonium	13
2.4 Triapine	15
2.5 Cancer	17
2.5.1 Hallmark of cancer	18
2.5.1.1 Self-sufficiency in growth signals	18
2.5.1.2 Insensitivity to antigrowth signals	19
2.5.1.3 Evading apoptosis	19
2.5.1.4 Limitless replicative potential	20
2.5.1.5 Sustained angiogenesis	20
2.5.1.6 Tissue invasion and metastasis	21

2.5.2	Hallmark of cancer: The next generation	21
2.5.2.1	Enabling characteristic: Genome instability and mutation	22
2.5.2.2	Enabling characteristic: Tumor-promoting inflammation	22
2.5.2.3	Emerging hallmark: Reprogramming energy metabolism	23
2.5.2.4	Emerging hallmark: Evading immune destruction	23
2.6	Apoptosis	23
2.6.1	Intrinsic and extrinsic apoptotic pathways	24
2.7	Necrosis	26
2.7.1	Necroptosis or programmed necrosis	27
2.8	Cell Cycle	28
2.8.1	Cell cycle checkpoints	29
2.9	Human cell lines used	29
2.9.1	Prostate cancer	30
2.9.2	Markers for prostate cancer	31
2.10	Mitochondria	32
2.10.1	Mitochondria as the key regulator of apoptosis	33
2.10.2	Mitochondria and cancer	33
2.10.2.1	Mitochondria-targeted anticancer compounds	34
3	MATERIALS AND METHODS	36
3.1	Chemistry	36
3.1.1	Materials and solutions	36
3.1.2	Physical measurements	36
3.1.3	Syntheses	36

3.1.3.1	Synthesis of 5-(chloromethyl)-2-hydroxybenzaldehyde	36
3.1.3.2	Synthesis of (3-formyl-4-hydroxyphenyl)methyltriphenylphosphonium (T)	36
3.1.3.3	Synthesis of [3-[(E)-(carbamothioylhydrazono)methyl]-4-hydroxyphenyl] methyltriphenylphosphonium chloride (tsc)T	38
3.1.3.4	Synthesis of [4-hydroxy-3-[(E)-(phenylcarbamothioylhydrazono)methyl]phenyl] methyl-triphenyl-phosphonium chloride P(tsc)T	39
3.1.3.5	Synthesis of [3-[(E)-(4-fluorophenyl)carbamothioylhydrazono]methyl]-4-hydroxyphenyl]methyl-triphenyl-phosphonium chloride FP(tsc)T	40
3.1.3.6	Synthesis of [3-[(E)-(ethylcarbamothioylhydrazono)methyl]-4-hydroxyphenyl] methyltriphenylphosphonium chloride E(tsc)T	41
3.1.3.7	Synthesis of [3-[(E)-(4-ethylphenyl)carbamothioylhydrazono]methyl]-4-hydroxyphenyl]methyl-triphenyl-phosphonium chloride EP(tsc)T	42
3.1.3.8	Synthesis of [4-hydroxy-3-[(E)-(methylcarbamothioylhydrazono)methyl]phenyl] methyltriphenylphosphonium chloride M(tsc)T	43

3.1.3.9	Synthesis of [3-[(E)- (dimethylcarbamothioylhydrazono) methyl]- 4-hydroxyphenyl] methyltriphenylphosphonium chloride DM(tsc)T	44
3.2	Biological studies	45
3.2.1	Materials	45
3.2.2	<i>In vitro</i> cytotoxicity assay	45
3.2.2.1	Cell culture	45
3.2.2.2	MTT cytotoxicity assay	47
3.2.3	Morphological assessment of apoptotic cells by phase- contrast inverted microscope	48
3.2.4	Cell death observation by acridine orange and ethidium bromide (AO/EB) double staining	49
3.2.5	Cell death detection using Annexin V-FITC/PI double staining by flow cytometry	50
3.2.6	Cell cycle arrest analysis using flow cytometry	51
3.2.6.1	Cell sample preparation	51
3.2.6.2	Staining procedure	52
3.2.7	Mitochondrial transmembrane potential ($\Delta\Psi_m$) assessment assay using flow cytometry	52
3.2.7.1	Preparation of 1x solution buffer	54
3.2.7.2	Preparation of JC-1 stock solution (one vial)	54
3.2.7.3	Preparation of JC-1 working solution	54
3.2.7.4	Preparation and staining of cells with JC-1	55
3.2.8	Statistical analyses	56

4	RESULTS AND DISCUSSION	57
4.1	Synthesis and characterization	57
4.2	Infrared spectra	59
4.3	¹ H NMR and ¹³ C NMR	59
4.4	X-ray crystal structures	60
4.5	Growth inhibitory effect of thiosemicarbazone compounds on human cancer cells as determined by MTT assay	70
4.6	Modes of cell death of selected compounds	74
4.6.1	Modes of cell death with P(tsc)T	77
4.6.1.1	Morphological assessment of apoptotic cells by phase-contrast inverted microscope for [P(tsc)T]	77
4.6.1.2	Morphological observation of apoptosis cells by fluorescent microscope for [P(tsc)T]	80
4.6.1.3	Annexin V-FITC/PI double staining study using flow cytometry for [P(tsc)T]	83
4.6.1.4	Cell cycle analysis using flow cytometry for [P(tsc)T]	85
4.6.1.5	JC-1 Mitochondrial transmembrane potential ($\Delta\psi_m$) assay for [P(tsc)T]	87
4.6.2	Modes of cell death with FP(tsc)T	88
4.6.2.1	Morphological assessment of apoptotic cells by phase-contrast inverted microscope for [FP(tsc)T]	88
4.6.2.2	Morphological observation of apoptosis cells by fluorescent microscope for [FP(tsc)T]	91
4.6.2.3	Annexin V-FITC/PI double staining study using flow cytometry for [FP(tsc)T]	93

4.6.2.4	Cell Cycle analysis using flow cytometry for [FP(tsc)T]	95
4.6.2.5	JC-1 Mitochondrial transmembrane potential ($\Delta\psi_m$) assay for [FP(tsc)T]	97
4.6.3	Modes of cell death with EP(tsc)T	98
4.6.3.1	Morphological assessment of apoptotic cells by phase-contrast inverted microscope for [EP(tsc)T]	98
4.6.3.2	Morphological assessment of cells stained with acridine orange/ethidium bromide double staining using fluorescent microscope for [EP(tsc)T]	100
4.6.3.3	Annexin V-FITC/PI double staining study using flow cytometry for [EP(tsc)T]	102
4.6.3.4	Cell cycle analysis using flow cytometry for [EP(tsc)T]	104
4.6.3.5	JC-1 Mitochondrial transmembrane potential ($\Delta\psi_m$) assay for [EP(tsc)T]	106
4.6.4	Modes of cell death with DM(tsc)T	107
4.6.4.1	Morphological assessment of apoptotic cells by phase-contrast inverted microscope for [DM(tsc)T]	108
4.6.4.2	Morphological assessment of cells stained with acridine orange/ethidium bromide double staining using fluorescent microscope for [DM(tsc)T]	110
4.6.4.3	Annexin V-FITC/PI double staining study using flow cytometry for [DM(tsc)T]	112

4.6.4.4	Cell cycle analysis using flow cytometry for [DM(tsc)T]	114
4.6.4.5	JC-1 Mitochondrial transmembrane potential ($\Delta\psi_m$) assay for [DM(tsc)T]	116
4.7	General discussion	117
5	CONCLUSIONS AND RECOMMENDATION	120
	REFERENCES	122
	LIST OF PUBLICATIONS	136
	PAPERS PRESENTED IN CONFERENCE	136
	APPENDICES	137

University of Malaya

LIST OF FIGURES

Figure		Page
1.1	Proposed structure for all the compounds	6
1.2	General flow chart of research activities	7
2.1	Cationic Schiff bases reaction pathway	8
2.2	Structure of Mono-thiosemicarbazone	10
2.3	Structure of Bis-thiosemicarbazone	11
2.4	Structure of triphenylphosphane	14
2.5	Structure of MitoQ	15
2.6	3-aminopyridine-2-carboxaldehyde thiosemicarbazone (Triapine)	17
3.1	Flow chart of JC-1 assay	53
4.1	Reaction scheme and structures of synthesized compounds	58
4.2	ORTEP diagram of C ₂₇ H ₂₅ N ₃ OPS.Cl [(tsc)T]	68
4.3	ORTEP diagram of C ₃₃ H ₂₉ N ₃ OPS.Cl [P(tsc)T]	68
4.4	ORTEP diagram of C ₂₉ H ₂₉ N ₃ OPS.Cl [E(tsc)T]	69
4.5	ORTEP diagram of C ₃₃ H ₂₈ FN ₃ OPS.Cl [FP(tsc)T]	69
4.6	ORTEP diagram of C ₂₉ H ₂₉ N ₃ OPS.Cl.3H ₂ O [DM(tsc)T]	70
4.7	Morphological observation of PC-3 cells treated with the [P(tsc)T] at concentration of 10, 30, 50 and 100 μ M under phase-contrast inverted microscope (magnification 50x) for 24, 48 and 72 hours	79
4.8	Cell death morphological changes in PC-3 cells treated with [P(tsc)T] compound for 24, 48 and 72 hours detected by acridine orange and ethidium bromide (AO/EB) double staining	82
4.9	Annexin V/PI assay against PC-3 cell lines treated with [P(tsc)T] at concentrations of 10, 30 and 50 μ M for 24, 48 and 72 hours	84
4.10	Results for cell cycle analysis against PC-3 cells treated with [P(tsc)T] at concentration of 10, 30 and 50 μ M for 24, 48 and 72 hours	86

4.11	Mitochondrial membrane potential analysis against PC-3 cells treated with [P(tsc)T] at concentration of 10, 30 and 50 μ M for 24 hours	87
4.12	Morphological observation of PC-3 cells treated with the [FP(tsc)T] at concentration of 10, 30, 50 and 100 μ M under phase-contrast inverted microscope (magnification 50x) for 24, 48 and 72 hours	90
4.13	Cell death morphological changes in PC-3 cells treated with [FP(tsc)T] compound for 24, 48 and 72 hours detected by acridine orange and ethidium bromide (AO/EB) double staining	92
4.14	Annexin V/PI assay against PC-3 cell lines treated with [FP(tsc)T] compound at concentration of 30, 50 and 100 μ M for 24, 48 and 72 hours	94
4.15	Results for cell cycle analysis against PC-3 cells treated with [FP(tsc)T] at concentration of 10, 30 and 50 μ M for 24, 48 and 72 hours	96
4.16	Mitochondrial membrane potential analysis against PC-3 cells treated with [FP(tsc)T] at concentration of 10, 30 and 50 μ M for 24 hours	97
4.17	Morphological observation of PC-3 cells treated with the [EP(tsc)T] at concentration of 10, 30, 50 and 100 μ M under phase-contrast inverted microscope (magnification 50x) for 24, 48 and 72 hours	99
4.18	Cell death morphological changes in PC-3 cells treated with [EP(tsc)T] compound for 24, 48 and 72 hours detected by acridine orange and ethidium bromide (AO/EB) double staining	101
4.19	Annexin V/PI assay against PC-3 cell lines treated with [EP(tsc)T] at concentrations of 10, 30 and 50 μ M for 24, 48 and 72 hours	103
4.20	Cell cycle analysis by flow cytometry in PC-3 cells treated with [EP(tsc)T] at concentration of 10, 30 and 50 μ M for 24, 48 and 72 hours	105

4.21	Mitochondrial membrane potential analysis against PC-3 cells treated with [EP(tsc)T] at concentration of 10, 30 and 50 μ M for 24 hours	106
4.22	Morphological observation of PC-3 cells treated with the [DM(tsc)T] at concentration of 30, 50 and 100 μ M under phase-contrast inverted microscope (magnification 50x) for 24, 48 and 72 hours	109
4.23	Cell death morphological changes in PC-3 cells treated with [DM(tsc)T] compound for 24, 48 and 72 hours detected by acridine orange and ethidium bromide (AO/EB) double staining	111
4.24	Annexin V/PI assay against PC-3 cell lines treated with [DM(tsc)T] at concentrations of 30, 50 and 100 μ M for 24, 48 and 72 hours	113
4.25	Cell cycle analysis by flow cytometry in PC-3 cells treated with [DM(tsc)T] at concentration of 10, 30 and 50 μ M for 24, 48 and 72 hours	115
4.26	Mitochondrial membrane potential analysis against PC-3 cells treated with [DM(tsc)T] at concentration of 10, 30 and 50 μ M for 24 hours	116

LIST OF TABLES

Table		Page
4.1	Crystallographic data for (tsc)T and P(tsc)T	62
4.2	Crystallographic data for FP(tsc)T and E(tsc)T	63
4.3	Crystallographic data for DM(tsc)T	64
4.4	Selected bond lengths and angles for (tsc)T and P(tsc)T	65
4.5	Selected bond lengths and angles for FP(tsc)T and E(tsc)T	66
4.6	Selected bond lengths and angles for DM(tsc)T	67
4.7	Growth inhibitory effect (IC_{50} μ M) of tested compounds	73

University of Malaya

LIST OF SYMBOLS AND ABBREVIATIONS

AO/EB	: Acridine orange/ethidium bromide
ATCC	: American Type Culture Collection
AV/PI	: Annexin V-FITC/ Propidium Iodide
A549	: Human non-small cell lung cancer cell line
C	: Carbon
CCDC	: Cambridge crystallographic data centre
CDCl ₃	: Deuterated chloroform
CHN	: Carbon Hydrogen Nitrogen elemental analysis
Cisplatin	: Cis-diamminedichloroplatinum(II)
°C	: Degree Celcius
DNA	: Deoxyribonucleic acid
DMF	: Dimethylformamide
DMSO	: Dimethylsulfoxide
DM(tsc)T	: [3-[(Z)-(dimethylcarbamothioylhydrazono)methyl]-4-hydroxyphenyl] methyltriphenylphosphonium chloride
EMEM	: Eagle's Minimal Essential Medium
E(tsc)T	: [3-[(Z)-(ethylcarbamothioylhydrazono)methyl]-4-hydroxyphenyl] methyltriphenylphosphonium chloride
EP(tsc)T	: [3-[(E)-[(4-ethylphenyl)carbamothioylhydrazono]methyl]-4-hydroxy-phenyl]methyl-triphenyl-phosphonium chloride
FBS	: Fetal bovine serum
FP(tsc)T	: [3-[(Z)-[(4-fluorophenyl)carbamothioylhydrazono]methyl]-4-hydroxy-phenyl]methyl-triphenyl-phosphonium chloride
g	: Gram

HCT116	:	Human colon colorectal carcinoma cell line
h	:	Hour
^1H	:	Proton
HRMS	:	High Resolution Mass Spectrometry
H_2O	:	Water
IR	:	Infrared
IC_{50}	:	Inhibition concentration at 50%
JC-1	:	5',6,6'-tetrachloro-1,1',3,3'-tetraethylbenzimidazolylcarbocyanine-iodide
KBr	:	Potassium bromide
L	:	Litre
μg	:	Microgram
mg	:	Milligram
μl	:	Microliter
mL	:	Milliliter
MCF7	:	Hormone dependent breast adenocarcinoma cell line
MDA-MB-231	:	Non hormone dependent breast adenocarcinoma cell line
MeOH	:	Methanol
MS	:	Mass Spectrometry
MTT	:	(3-(4,5-Dimethylthiazol-2-yl)-2,5-Diphenyltetrazolium Bromide)
M(tsc)T	:	[4-hydroxy-3-[(Z)-(methylcarbamothioylhydrazono)methyl]phenyl]methyltriphenylphosphonium chloride
NaCl	:	Sodium chloride
Na_2CO_3	:	Sodium carbonate
NaHCO_3	:	Sodium bicarbonate
NMR	:	Nuclear magnetic resonance

Nm	:	Nanometer
OD	:	Optical density
PBS	:	Phosphate buffered saline
PC-3	:	Prostate adenocarcinoma
PI	:	Propidium iodide
P(tsc)T	:	[4-hydroxy-3-[(Z)-(phenylcarbamothioylhydrazono)methyl]phenyl]methyl-triphenyl-phosphonium chloride
RPM	:	Rotation per minute
RPMI	:	Roswell Park Memorial Institute medium
RWPE-1	:	Human prostate normal cell line
SI	:	Selectivity index
T	:	(3-formyl-4-hydroxyphenyl)methyltriphenylphosphonium
(tsc)T	:	[3-[(Z)-(carbamothioylhydrazono)methyl]-4-hydroxyphenyl]methyltriphenylphosphonium chloride
UV	:	Ultraviolet
vs	:	Versus
%	:	Percentage
$\Delta\psi_m$:	Mitochondrial membrane potential

LIST OF APPENDICES

Appendix		Page
1	IR spectrum of T	137
2	IR spectrum of T(tsc)T	138
3	IR spectrum of P(tsc)T	139
4	IR spectrum of FP(tsc)T	140
5	IR spectrum of E(tsc)T	141
6	IR spectrum of EP(tsc)T	142
7	IR spectrum of M(tsc)T	143
8	IR spectrum of DM(tsc)T	144
9	¹ H NMR of T	145
10	¹ H NMR of T(tsc)T	146
11	¹ H NMR of P(tsc)T	147
12	¹ H NMR of FP(tsc)T	148
13	¹ H NMR of E(tsc)T	149
14	¹ H NMR of EP(tsc)T	150
15	¹ H NMR of M(tsc)T	151
16	¹ H NMR of DM(tsc)T	152
17	¹³ C NMR of T	153
18	¹³ C NMR of T(tsc)T	154
19	¹³ C NMR of P(tsc)T	155
20	¹³ C NMR of FP(tsc)T	156
21	¹³ C NMR of E(tsc)T	157
22	¹³ C NMR of EP(tsc)T	158
23	¹³ C NMR of M(tsc)T	159

24	^{13}C NMR of DM(tsc)T	160
25	HRMS of T	161
26	HRMS of T(tsc)T	162
27	HRMS of P(tsc)T	163
28	HRMS of FP(tsc)T	164
29	HRMS of E(tsc)T	165
30	HRMS of EP(tsc)T	166
31	HRMS of M(tsc)T	167
32	HRMS of DM(tsc)T	168

University of Malaya

CHAPTER 1

INTRODUCTION

Cancer is one of the most widespread and feared disease in the world today and it is the second leading cause of death after cardiovascular disease. Cancer is a disease characterized by uncontrolled cell growth whereby the cells divide continuously forming lumps and mass of abnormal cells consequently interfering or blocking organs' and/or tissues' normal function. A cancer is usually named after the part of the body where it first started to manifest and this is known as the primary site or the primary cancer. If the cancer cells spread from the primary cancer site to other body parts and/or organs, it is called secondary cancer or a metastasis. Metastasis is the major cause of cancer related mortality (Spano et al., 2012).

Cancer is the most notorious disease which caused the most devastating economic burden in the world. Researchers from Oxford University and King's College London found that the total economic cost of cancer across the 27 European united countries was EUR 126 billion in 2009 (Luengo-Fernandez et al., 2013). According to Global oncology trend report by Intercontinental Marketing Services (IMS) institute of healthcare information, global spending on cancer medications rose to USD 100 billion in 2014.

The current common approaches in treating cancer are radiation therapy, surgery and cytotoxic drugs. All of the mentioned approaches have some limitations whereby they are mainly used in the treatment of primary cancer except for cytotoxic drugs. Most of the cytotoxic drugs used for cancer treatment will interfere with normal DNA functions whereby keeping the cell from reproducing. These chemotherapeutic drugs are known as alkylating agents, which can lead to gastrointestinal side effects and acute

leukemia whereby the risk is higher with higher dose treatment. The platinum drugs such as cis-platin, carboplatin and oxaliplatin are grouped with alkylating agents as they kill in the similar ways (Scholar, 2007). Cytotoxic drugs can be very toxic to normal cells unless it is very specific in targeting only cancerous cells.

A major challenge in modern drug design technology is to come out with a drug that will be more selective towards cancerous cells and thus having lesser side effects on healthy cells. A better understanding behind the mechanism of the Warburg effect (enhanced glucose uptake, high rate of glycolysis and increased in lactic acid production as a byproduct of the glycolytic pathway) that has caught the attention of many scientist whereby people believes that Warburg effect may ultimately lead to a more effective treatment of cancer (Wu & Zhao, 2013). In the context of cancer therapy, the mitochondrion has been recognized as the primary location of several potential drug targets.

The mitochondrion is an important organelle that mediates numerous critical processes in eukaryotic cells. There are burgeoning data suggesting mitochondrion is the crucial regulators of the apoptotic intrinsic pathway as it plays a crucial role in the production of ATP and the metabolites necessary in the fulfillment of bioenergetic and the biosynthesis demand of the cell hence for the survival of eukaryotic cells (D'Souza et al., 2011; Fulda et al., 2010). Furthermore, mitochondrion plays a major role in non-apoptotic cell death and in necroptosis (regulated necrosis). Therefore, mitochondrial-targeted compounds would represent a promising approach to eradicate chemotherapy-refractory cancer cells.

One of the most effective ways in delivering the molecule of interest to mitochondria is by conjugating the bioactive molecules to lipophilic cations such as triphenylphosphonium (TPP). The hydrophobic surface and the large ionic radius

enable the TPP cation to move directly and rapidly through biological phospholipid bilayers without requiring any protein transporter (Ross et al., 2005). The accumulation of lipophilic cations inside the mitochondrial matrix is driven by the differences in electrochemical gradient that generates a negative charge in the matrix (Ono et al., 1994). Thus, in an attempt to deliver our compound of interest to the mitochondria, TPP was conjugated to the compound of interest in present study.

The anticancer drug, 3-aminopyridine-2-carboxaldehyde thiosemicarbazone, known commercially as Triapine, is a Schiff base that can be synthesized by reaction of an aromatic aldehyde and thiosemicarbazide has reached phase II clinical trials (Finch et al., 2000; Finch et al., 1999). Schiff base is an important class of organic compounds and literature on cationic Schiff bases, particularly in the context of their medicinal uses, is sparse, with references being limited to research carried out on their interactions with DNA and microorganisms. Interestingly, Schiff bases of the thiosemicarbazones family having a substituent at the N(4) atom are known to show enhanced cytotoxic properties (Pervez et al., 2011). The common structural features of these compounds are azomethine or imine group with the general formula of $RHC=N-R_1$. Azomethine groups are shown to be present in various natural, naturally derived and non-natural compounds. In addition, Azomethine group has been outlined as the key factor for their broad range of biological properties.

In view of these facts and as part of our extensive research to rapidly synthesize bioactive compounds, the present work was intended for the synthesis of thiosemicarbazones family having various substituents at the N(4) atom; bound to lipophilic cations such as triphenylphosphonium moiety. In this study, we proposed several Schiff bases from the thiosemicarbazides family to be used as the starting material. The proposed thiosemicarbazides are thiosemicarbazide **[(tsc)]** on its own, 4-

phenylthiosemicarbazide **[P(tsc)]**, 4-fluorophenylthiosemicarbazide **[FP(tsc)]**, 4-ethylthiosemicarbazide **[E(tsc)]**, 4-ethylphenylthiosemicarbazide **[EP(tsc)]**, 4-methylthiosemicarbazide **[M(tsc)]** and lastly 4,4-dimethyl thiosemicarbazide **[DM(tsc)]**.

The proposed structures of the starting material (3-formyl-4-hydroxyphenyl)methyltriphenylphosphonium (**T**) followed by all the seven compounds in order namely [3-[(Z)-(carbamothioylhydrazono)methyl]-4-hydroxyphenyl]methyltriphenylphosphonium chloride **[(tsc)T]**, [4-hydroxy-3-[(Z)-(phenylcarbamothioylhydrazono)methyl]phenyl]methyl-triphenyl-phosphonium chloride **[P(tsc)T]**, [3-[(Z)-[(4-fluorophenyl)carbamothioylhydrazono]methyl]-4-hydroxy-phenyl]methyl-triphenyl-phosphonium chloride **[FP(tsc)T]**, [3-[(Z)-(ethylcarbamothioylhydrazono)methyl]-4-hydroxyphenyl]methyltriphenylphosphonium chloride **[E(tsc)T]**, [3-[(E)-[(4-ethylphenyl)carbamothioylhydrazono]methyl]-4-hydroxy-phenyl]methyl-triphenyl-phosphonium chloride **[EP(tsc)T]**, [4-hydroxy-3-[(Z)-(methylcarbamothioylhydrazono)methyl]phenyl] methyltriphenylphosphonium chloride **[M(tsc)T]** and lastly [3-[(Z)-(dimethylcarbamothioylhydrazono)methyl]-4-hydroxyphenyl] methyltriphenylphosphonium chloride **[DM(tsc)T]** are illustrated in Figure 1.1.

The eight compounds were subjected to *in vitro* cytotoxicity test using 3-(4,5-dimethylthiazol-2-yl)-2,5-diphenyltetrazolium bromide (MTT) assay against six human cell lines, namely prostate adenocarcinoma (PC-3), non-small cell lung cancer (A549), hormone dependent breast adenocarcinoma (MCF7), hormone independent breast adenocarcinoma (MDA-MB-231), colon colorectal carcinoma (HCT 116) and normal prostate (RWPE-1). The cytotoxic compounds were then subjected to the next in depth

study on induction of cell death. In present study, induction of cell death was evaluated both quantitative and qualitative by morphological assessment, acridine orange and ethidium bromide double staining assay (AO/EB), Annexin V-FITC/PI double staining study (AV/PI), cell cycle analysis and lastly mitochondrial membrane potential investigation ($\Delta\Psi_m$). The outline of general procedures in present study is shown in Figure 1.2.

Objectives of study

The main objectives of the present study were as follows:

- i. To synthesize compounds with high lipophilicity and better cytoselectivity properties.
- ii. To determine structure activity relation (SAR) of the compounds.
- iii. To evaluate growth inhibitory properties of the compounds.
- iv. To investigate possible mechanisms of cell death elicited on selected thiosemicarbazone compounds.
- v. To understand the involvement of mitochondria mediated apoptosis by the selected compounds

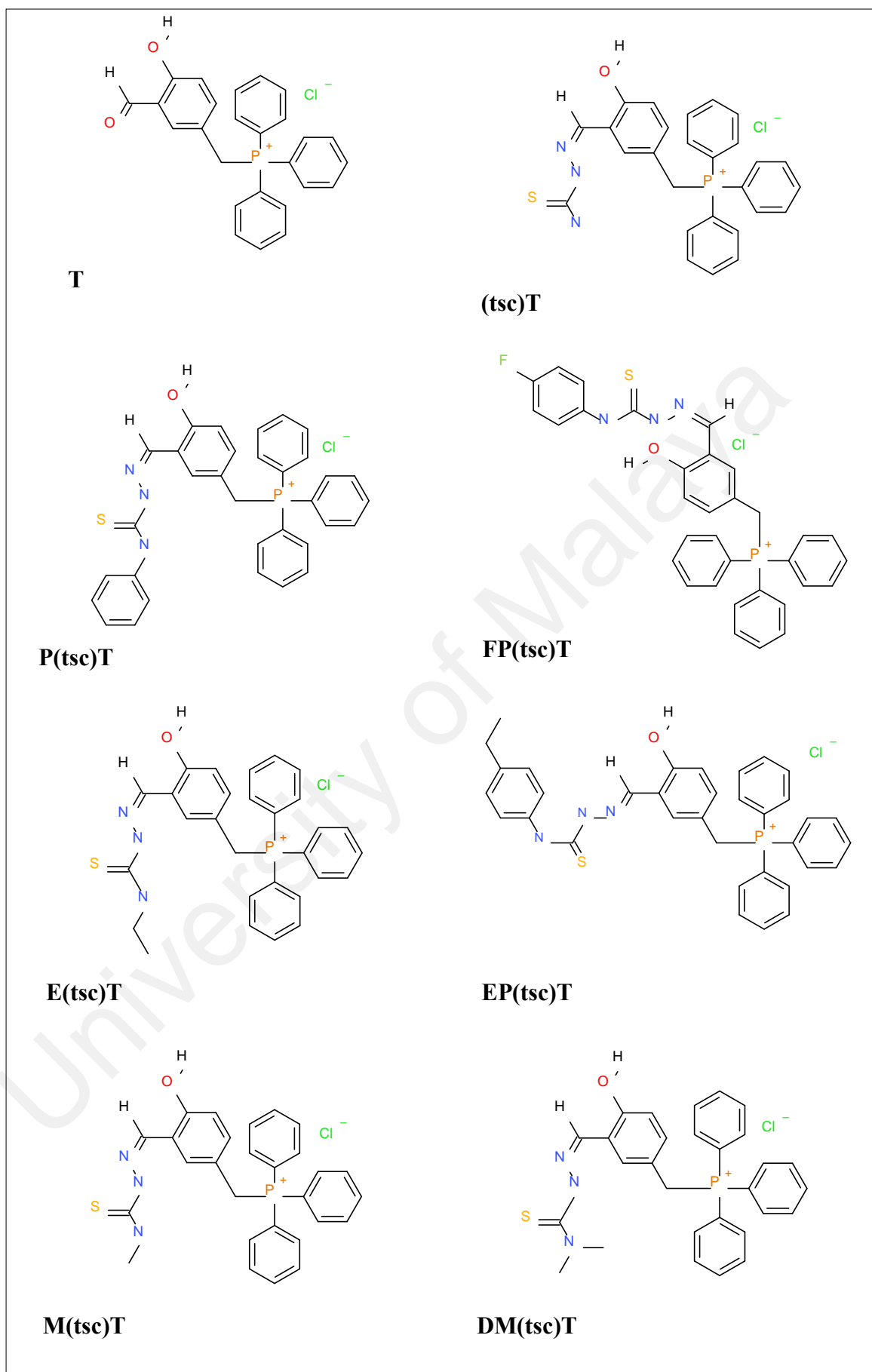


Figure 1.1: Proposed structure of compounds in the present study

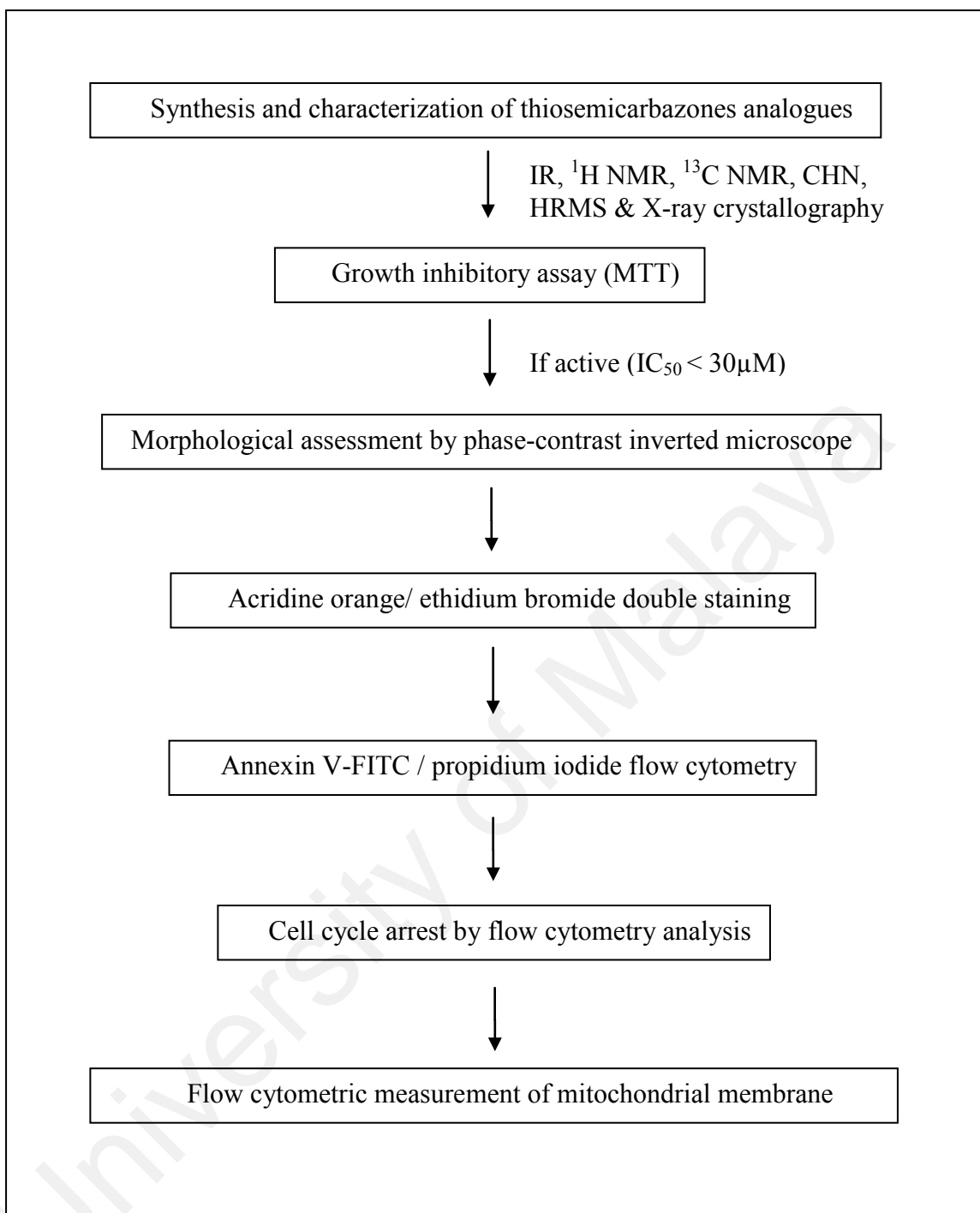


Figure 1.2: Outline of general procedures

CHAPTER 2

LITERATURE REVIEW

2.1 Schiff bases

Schiff bases were first reported by Hugo Schiff in 1864 (Schiff, 1864). This important class of organic compounds is formed by condensation of an aldehyde or ketone (carbonyl group) with primary amine as shown in Figure 2.1.

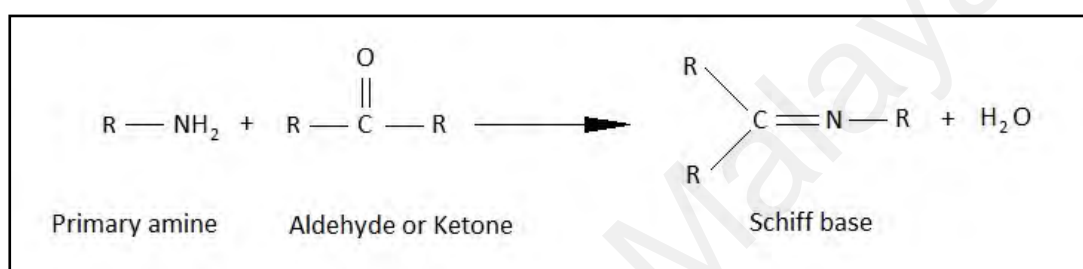


Figure 2.1: Schiff bases reaction pathway

Structurally, Schiff bases are also known as imine or azomethine in which the carbonyl group (C=O) is replaced by imine or azomethine through condensation. This formation generally takes place under acids or base catalysis or with heat. The reaction is driven to completion by separation of the product or by removal of water or both. Schiff bases can be hydrolyzed back to aldehydes or ketone and amines by aqueous acid or base. Their ability to form carbon-nitrogen bonds makes them an important intermediate in a number of enzymatic reactions involving interactions of an enzyme with an amino or a carbonyl group.

Aromatic aldehydes having an effective conjugation system form stable Schiff bases while aliphatic aldehydes are relatively unstable and are readily polymerize. Schiff base ligands with aldehyde are formed more readily than with ketone (carbonyl carbon). These groups are present in various natural and synthetic compounds whereby

have been shown to be critical for their biological activities. It has become an important class of compounds in medicinal and pharmaceutical field as well.

One particular set of Schiff bases that has been aggressively studied for the past decade is thiosemicarbazones which attract considerable pharmaceutical interest with its broad spectrum of chemotherapeutic (Beckford et al., 2011). Varied substituent possess a wide range of biological properties includes antitumor (Liu et al., 1992), antibacterial (Aljahdali & El-Sherif, 2013), antiviral (Castro et al., 2014) and antiparasitic (Adams et al., 2013) properties as well as other industrially important activities, including anticorrosion (Khamis et al., 2000) and antifouling (Tadros & El-Batouti, 2004) effects.

2.2 Thiosemicarbazones

Thiosemicarbazones ($R^1R^2C^2=N^3-N^2(H)-C^1(=S)N^1R^3R^4$) constitute an important class of N, S donor ligands, which was first reviewed by Akbar Ali and Livingstone in 1974 (Akbar Ali & Livingstone, 1974). Research on thiosemicarbazones started from early 20th century, but the first report on its medical applications began to appear in the fifties as a drug against tuberculosis (Shane et al., 1951) and leprosy (Ryrie, 1950).

In the sixties, antiviral properties of thiosemicarbazone were discovered and extensive investigation of this compound eventually led to the commercialization of methisazone, Marboran (Bauer & Apostolov, 1966). Methisazone or 1-methylisatin 3-thiosemicarbazone was shown to inhibit multiplication of vaccinia and smallpox viruses (Ferguson, 1964) in mice and also effective in the treatment of eczema vaccinatum (Turner et al., 1962) and vaccinia gangrenosa (Jaroszyńska-Weinberger, 1970).

Thiosemicarbazones of various aldehydes and ketones has been paid considerable attention among organic ligands due to various donor atoms present in them and their ability to change their denticity depending on the starting reagents and

reaction conditions. Structure activity relationship studies revealed that the presence of bulky group attached at terminal N(4) position significantly enhances the pharmacological activity of these compounds (Joseph et al., 2006). Antitumor activity of N(4)-phenyl thiosemicarbazones was shown to be higher compared with unsubstituted thiosemicarbazones (Hussein et al., 2015; Soares et al., 2012).

2.2.1 Mono-thiosemicarbazones and bis-thiosemicarbazones

Thiosemicarbazones can be broadly classified as mono-thiosemicarbazones and bis-thiosemicarbazones. Mono-thiosemicarbazones are the compounds whereby one group (C=O) from an aldehyde/ketone and one NH₂ group from thiosemicarbazide condense forming a (C=N) linkage by elimination of water molecule. Mono-thiosemicarbazone ligand has different substituents at R₁, R₂, R₃ and R₄ positions. Structure of mono-thiosemicarbazone is shown in Figure 2.2.

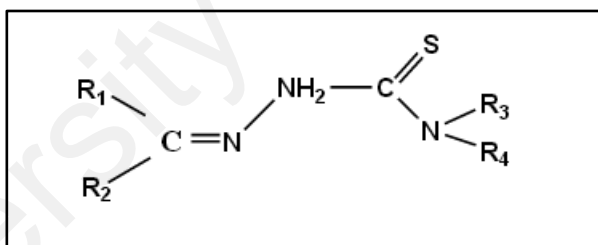


Figure 2.2: Structure of mono-thiosemicarbazone

Bis-thiosemicarbazone on the other hand are the compound whereby two groups (C=O) from an aldehyde/ketone and two NH₂ group from two thiosemicarbazides condense forming a (C=N) linkage by elimination of two water molecules. Bis-thiosemicarbazones constitutes of two arms connected by a ring or a C-C bond as shown in Figure 2.3.

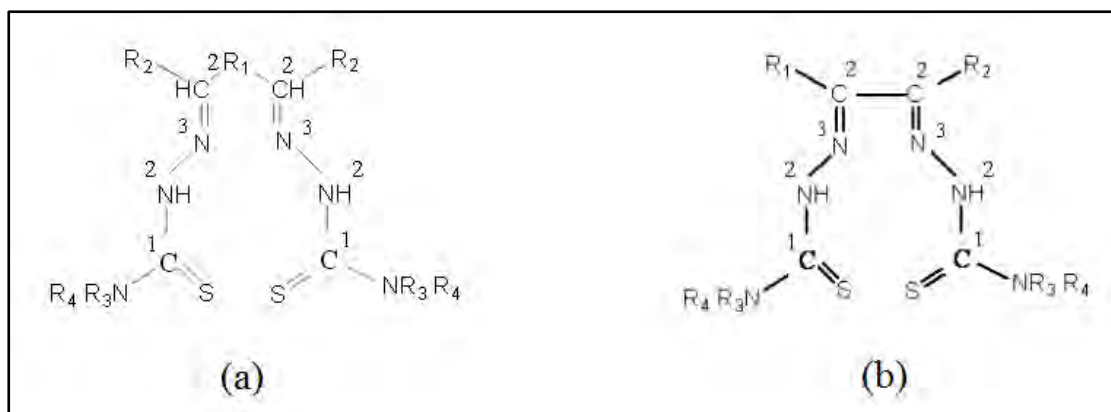


Figure 2.3: Structure of bis-thiosemicarbazone *via* (a) ring formation (b) C-C bond formation.

2.2.2 Antitumor activity of thiosemicarbazones

A lot of research has been aimed to the discovery of new drugs for cancer treatments. Thiosemicarbazones possess a vast range of pharmacological versatility and a number of its derivatives were synthesized and reported as potential antitumor. The antitumor activity of thiosemicarbazone has always been attributed to their ability to act as inhibitors of ribonucleotide reductase (RR), a key enzyme in the biosynthesis of DNA precursors (Finch et al., 2000).

Literatures on thiosemicarbazones with N(4) substitution showed that presence of bulky group at N(4) positions of the thiosemicarbazone moiety enhances its biological activity (Akgemci et al., 2015). In one of the structure and activity study showed that 2-hydroxy-5-methoxyacetophenone thiosemicarbazone with the presence of the ethyl group at N(4) position decreased the potential antiproliferative effect of the compound meanwhile phenyl group at N(4) position enhances the antiproliferative potential of the compound (Akgemci et al., 2015). Similarly in another study whereby four new thiosemicarbazone was synthesized and the results showed that substitution of phenolic groups at terminal thioamide nitrogen enhances the biological significance of

thiosemicarbazone (Hussein et al., 2015). A study on isatin- β -thiosemicarbazones showed that variable chelators scaffold express variable toxicity. Analysis on structure and activity relationships showed that NNS and NNN donor chelators showed enhances cytotoxicity in comparison with ONS derivatives (Pape et al., 2016).

In the recent report, 3,5-diacetyl-1,2,4-triazol mono(4-phenylthiosemicarbazone) ligand and its palladium (II) and platinum (II) complexes were synthesized. This compounds were tested against three cell lines namely breast cancer, epithelial ovarian cancer and resistant epithelial ovarian cancer. The results showed that the free ligand presents the best antiproliferative profile in comparison with the complexes. This report indicates that incorporation of palladium or platinum in to the ligand gives unfavorable effect on cytotoxicity. DNA binding studies address that direct interaction with DNA is part of the mechanism of action of this compound (Matesanz et al., 2016).

A series of 5,6-disubstituted pyridine-2,3-dione-3-thiosemicarbazone derivatives were synthesized. Antiproliferative assay indicates that most of the compounds synthesized exhibited antiproliferative activity against breast cancer, colon cancer and hepatocellular cancer cell line. The structure activity relationship indicated that benzylation of the thiosemicarbazones reduced the biological activity meanwhile substitution with methyl, chloro, fluoro or bromo enhances the compounds with most favorable antiproliferative activity (Xie et al., 2014).

A number of iron chelators have demonstrated anticancer activity *in vitro* and *in vivo*, including clinical trials. Rapidly dividing cells requires higher amount of iron compared to normal cells and this creates a therapeutic avenue for selective inhibition of cancer cell growth (Mrkvičková et al., 2007). Thiosemicarbazone iron chelators have demonstrated great promise as anticancer agents. The 2-benzoylpyridine thiosemicarbazone chelators have demonstrated potent antiproliferative effects against

neuroepithelioma cells. Structure activity analysis revealed that mono-or di-methoxy substitution at the phenyl ring reduces its antiproliferative activity meanwhile methoxy group substitution at the phenyl ring enhances the iron chelation efficacy (Lukmantara et al., 2013). Similarly quinoline-based thiosemicarbazone analogs have been shown to possess greater anticancer activity than the gold-standard iron chelator desferrioxamine. These analogs were tested against cancer and non neoplastic cells including human SK-N-MC neuroepithelioma, colon cancer cell lines and normal human dermal fibroblast (Serda et al., 2012).

2.3 Triphenylphosphonium

Phosphonium salts have huge potential with the application in chemistry, biology and pharmacology. This phosphonium salt has been used in obtaining [^{18}F] probes for myocardial perfusion imaging using PET/CT, delivering radiometal chelates to tumor cells and used as a transporter for various therapeutic agents (H. Yuan et al., 2013). There is vast literatures showing that lipophilic triphenylphosphonium cation, has been conjugated to an antioxidant moiety; to give a new compound called MitoQ. This compound has been widely used to prevent mitochondrial oxidative damage which leads to a range of degenerative diseases (Kelso et al., 2001; Murphy & Smith, 2007). Triphenylphosphine is widely used in the synthesis of organic and organometallic compounds and it exists as relatively air stable, colorless crystals at room temperature. This compound is soluble in non-polar organic solvents such as benzene and diethyl ether.

Triphenylphosphine can be easily prepared in laboratory by reacting phosphorus trichloride with phenylmagnesium bromide or phenyllithium. This salt can be reacted with alcohols, alkyl halides and carboxylic acids giving rise to a range of chemical

compounds with wide applicability. Another well-known reaction is Wittig reaction whereby an aldehyde or ketone reacts with triphenyl phosphonium ylide to give an alkene and triphenylphosphine oxide. In biological research, the lipophilic and cationic properties of tetraphenylphosphonium makes it a good candidate in demonstrating the existence of electrochemical potential across the mitochondrial membrane (Millard et al., 2010).

The hydrophobic surface and large ionic radius enable triphenylphosphonium cation to move directly and rapidly through the mitochondrial phospholipid bilayer without the help of any protein transporter. Some phosphonium salts have been reported to show antiproliferative activity in some cancer cell lines (Abu-Gosh et al., 2009; Finichiu et al., 2013; Ross et al., 2005). Copper complexes with phosphonium containing hydrazone ligand for instance have shown to exhibit cytotoxicity activity against PC-3 cells as reported by Chew *et al.* (2014). Another multifunctional phosphonium–lanthanide compounds which possess paramagnetism, luminescence, and tumor mitochondrial targeting properties showed to exhibit selective tumor targeting properties towards breast cancer cells (M. Li et al., 2012). The chemical structure of triphenylphosphane is illustrated in Figure 2.4 and Mito Q is illustrated in Figure 2.5.

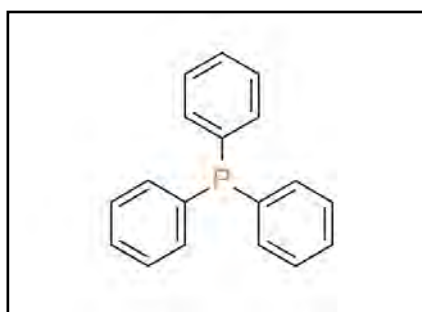


Figure 2.4: Structure of triphenylphosphane

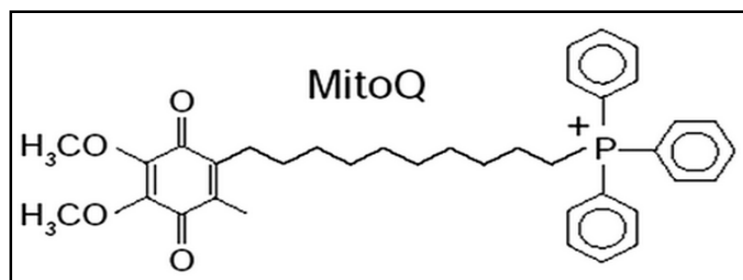


Figure 2.5: Structure of MitoQ (Mitchell et al., 2011)

2.4 Triapine

A good example of thiosemicarbazone would be the anticancer drug 3-aminopyridine-2-carboxaldehyde thiosemicarbazone (3-AP, Triapine®, Vion Pharmaceuticals Inc, New Haven, CT) which has been developed and reached phase II clinical trial (Finch et al., 2000; Finch et al., 1999). The chemical structure of Triapine is illustrated in Figure 2.5. Triapine is a potent small molecule inhibitor of ribonucleotide reductase (RR), which is an important enzyme in the synthesis of deoxynucleotides. RR catalyzes the reduction of ribonucleotides to deoxyribonucleotides which provides a fundamental platform for DNA replication, repair of damage DNA and cellular growth. It is proven that there is a strong correlation between the activity of the enzyme and intracellular pools of deoxyribonucleotides.

RR is composed of two homodimeric subunits, which are two identical R1 subunits and two identical R2 subunits. R1, the larger subunit contains the binding sites for the ribonucleotide substrates as well as for allosteric effectors. The R2 subunit contains a tyrosyl free radical which requires an iron center necessary for the reduction reaction whereby both iron and tyrosyl radical are essential for the catalytic activity (Finch et al., 2000). The R2 subunit is inhibited by hydroxyurea (HU) and Triapine.

HU is the first agent used to target RR by inactivating the non-heme iron in R2 subunit. However, HU has limited effectiveness as an anticancer agent due to its

relatively low affinity for RR and short half-life in human (Wadler et al., 2004). In addition, HU showed severe hematological and gastrointestinal side effects which hinder its further clinical development (Murren et al., 2003).

Clinical research studies of HU suggest development of more potent RR inhibitors would be a great contribution in cancer chemotherapy regimens. RR is a well-established target for cancer chemotherapy because tumor cells have faster proliferation which equals to higher expression of RR in it. This leads to the discovery of Triapine as the potent inhibitor of the R2 subunit which is 100-1000 folds more effective in comparison with HU. Furthermore, Triapine inhibits some of the tumor cell lines that are previously resistant to HU. Acting very similar to HU, Triapine quenches tyrosyl free radical in R2 subunit of the enzyme and act as an iron chelator. Triapine is most likely reported to inhibit the cell cycle at the S phase as RR is expressed principally in this phase (Karp et al., 2008; Shao et al., 2006; Trondl et al., 2014; Wadler et al., 2004).

Unfortunately, Triapine showed adverse side effects at the same time. In patients with metastatic renal cell carcinoma, Triapine showed grade 3 or 4 side effects such as acute reaction of hypoxia, hypotension and methemoglobinemia (Knox et al., 2007). One of the common side effects observed in patients treated with iron chelators is reversible myelo-suppression. Myelo-suppression can lead to serious conditions like anemia, severe bleeding, granulocytopenia/agranulocytosis and life threatening infections due to the lack of circulating neutrophils (Galanello, 2007).

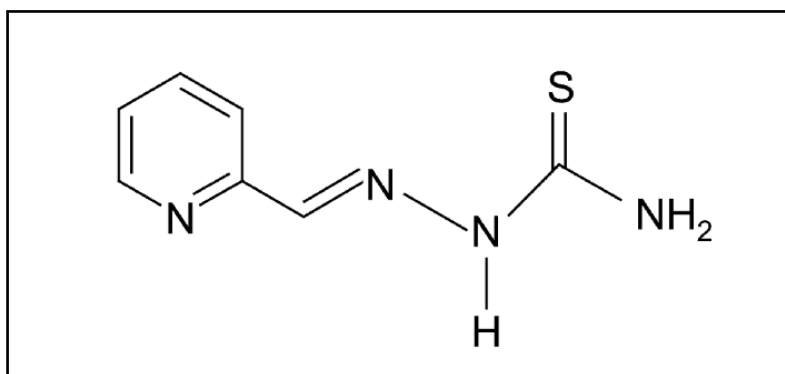


Figure 2.6: Structure of 3-aminopyridine-2-caboxaldehyde thiosemicarbazone (Triapine) (Finch et al., 1999)

2.5 Cancer

Cardiovascular is the leading cause of death in developed and developing countries and it is closely followed by cancer as the second leading cause of death. The treatment for cancer still remains an important and challenging entity. Cancer is a disease of the cells (from the Latin word meaning “small room”), which is the basic structural, functional and biological unit of all known living organisms. The human body is composed of trillions of cells to provide structure for the body, absorb nutrients and convert them into energy to carry out daily routines. The number of cells in a multicellular organism is tightly regulated, not by just controlling the rate of cell division, but also controlling the rate of cell death. If the cells are no longer needed, they will undergo programmed cell death or commonly known as apoptosis (from a Greek word meaning “falling off”) (Hengartner, 2000; Meier et al., 2000). A cell is replicated by genes and whenever these genes grow or multiply abnormally into a lump (tumor), it becomes cancer.

Tumor cells can be classified into two categories which are benign and malignant cells. Benign tumors are non-cancerous growth in the body, whereby most often they can be removed and they do not spread to other parts of the body. Malignant tumors, on the other hand, are made up of cells that grow out of control. These cells can

invade into nearby tissues and spread to other parts of the body. This process is known as metastasis and metastases keep the name of the original cancer location.

2.5.1 Hallmark of cancer

The hallmarks of cancer were extensively discussed in a review by Douglas Hanahan and Robert Weinberg published in the Cell journal, year 2000. The complexity of cancer can be narrowed down to the common traits that a normal cell acquires in order to transform into cancer. These are the characteristics that distinguish between normal and cancerous cells (Douglas Hanahan & Weinberg, 2000).

2.5.1.1 Self-sufficiency in growth signals

The first hallmark of cancer is defined as self-sufficiency in growth signals. The cells are the basic unit of structure in all organisms and also the basic unit of reproduction. Similar cells from the same origin ensembles to form a tissue and multiple tissues group together to form organs. All the cells of an organ must work and communicate as a complete system in order to function properly. Cancerous cell on the other hand do not work as a system whereby they do not require any hormones and/or signals for them to grow or divide. Cancer cells have the ability to produce their own signals which is known as autocrine signaling; by continuously activating the signaling pathway and destroying the cell growth regulator proteins. These transformed cells lead to an increased cell growth and cell division within the tumor.

2.5.1.2 Insensitivity to antigrowth signals

The second hallmark of cancer defined as insensitivity to antigrowth signals. Within a normal tissue, there are numerous antigrowth signals which can block cell proliferation to maintain tissue homeostasis. These processes are carefully maintained in order by proteins known as tumor suppressor genes. In cancer cells, unfortunately these genes are mutated and/or altered, which drives the cancer cells to grow and divide continuously even when the cell has severe abnormalities. In addition cancer cells do not have contact inhibition like the normal cells whereby the cells stop dividing once the space is filled up or the cell touches another cell. Cancer cells will continue to grow and divide regardless of their surroundings.

2.5.1.3 Evading apoptosis

The third hallmark of is defined as evading apoptosis whereby the normal cells have the capability to initiate cell suicide; a process known as apoptosis. This step is required for organisms to grow and develop while maintaining the homeostasis of the tissue in the body. This is the body system methods of limiting growth and discarding the cells with damaged DNA to prevent further damage. Cancer cells however have lost this ability and apoptosis is not activated under any conditions. In addition, report shows that cancer cells become resistant to apoptosis through mutation at *p53* tumor suppressor gene (Harris, 1996).

2.5.1.4 Limitless replicative potential

The fourth hallmark of cancer is defined as limitless replicative potential. Normal cells do not have the ability to divide indefinitely therefore the cells die after a certain number of divisions. This is caused by a small region at the end of the chromosomes known as telomeres. Telomeric DNA shortens every time the DNA is copied and eventually the DNA reaches a critical point whereby it activates senescence, so the cell stops dividing. Cancer cells have the ability to bypass this barrier, whereby they are able to manipulate the enzymes in order to increase the length of telomeres on every replication. Early work by Hayflick showed that cells can continue replicating by disabling their pRb and p53 tumor suppressor proteins, allowing these cells to continue multiplying until they reach a stage called crisis (Hayflick, 1997). Most tumor cells are immortalized.

2.5.1.5 Sustained angiogenesis

The fifth hallmark of cancer is defined as sustained angiogenesis. Angiogenesis is a normal and essential process in the formation and development of the embryonic tissues, where else in adult angiogenesis is only switched on during the physiological process such as wound healing or during the female reproductive cycle. The oxygen and nutrients supplied by the vasculature are crucial for cell function and survival and the cells must be close to the blood vessels to get enough oxygen for them to survive. During angiogenesis this closeness is maintained by coordination of growth of vessels and parenchyma. Once a tissue is formed the angiogenesis process occurs in a transitory and carefully regulated manner. In normal cells, the angiogenesis will be switched off, where else the cancer cells acquires the ability to exploit these normal physiological processes by activating the angiogenic switch for production of new vasculature. This

capability ensures that cancer cells are able to receive a continual supply of oxygen and other nutrients for its expanding tumor (D. Hanahan & Folkman, 1996).

2.5.1.6 Tissue invasion and metastasis

The sixth hallmark of cancer is defined as tissue invasion and metastasis. During the development of most types of human cancer, the primary tumor masses will have the ability to invade neighboring tissues and some will travel to distant sites where they may succeed in founding new colonies. These distant and new settlements of tumor cells (metastases) are the cause of 90% of human cancer death (Sporn, 1996). It is a complex multisteps process that starts with local invasion of the surrounding tissues followed by invading the circulatory system and exiting this system to colonize new tissues.

2.5.2 Hallmark of cancer: The next generation

In the year 2011, cancer researcher Douglas Hanahan and Robert Weinberg have published another review article titled Hallmark of cancer: The next generation; as an update to the previous article. Extensive research in this field suggests that two additional hallmark of cancer are involved in the pathogenesis of some or perhaps all cancers and labeled as emerging hallmarks. Hallmark of cancer is defined as acquired functional capabilities that allow cancer cells to survive proliferate and disseminate. Their acquisition is made possible by two enabling characteristics which are described in this new article (Douglas Hanahan & Weinberg, 2011).

2.5.2.1 Enabling characteristic: Genome instability and mutation

The seventh hallmark of cancer which is an enabling characteristic defined as genome instability and mutation. The normal cells have extraordinary ability of genome maintenance systems which are able to detect and rectify defects in the DNA to ensure that spontaneous mutations in the cells are very low during each cell generation. Cancer cells often increase the rate of mutation through breakdown of the genomic maintenance machinery and/or increased sensitivity to mutagenic agents. This genomic maintenance machinery often referred as the caretakers of the genome and their functions can be lost during the course of tumor progression (Negrini et al., 2010). This finding concludes that defects in the genome maintenance and genome instability are clearly an enabling characteristic associated with the acquisition of hallmark capabilities.

2.5.2.2 Enabling characteristic: Tumor-promoting inflammation

The eighth hallmark of cancer, also an enabling characteristic, is defined as tumor-promoting inflammation. In normal cells, the body's immune system recognizes and destroys any foreign materials and abnormal cells instantly. Research on the association between inflammation and cancer pathogenesis has been exploited comprehensively, and it demonstrated unanticipated, paradoxical effect whereby inflammation enhances tumorigenesis and progression. Inflammation can contribute to multiple hallmark capabilities, and is being evident in some cases; it is able to foster the development of incipient neoplasia into full-blown cancers (DeNardo et al., 2010). Therefore, inflammation can be considered an enabling characteristic as it contributes to the acquisition of core hallmark capabilities.

2.5.2.3 Emerging hallmark: Reprogramming energy metabolism

The ninth hallmark of cancer which is an emerging hallmark is defined as reprogramming energy metabolism. Otto Warburg in 1924, first observed this aberrant characteristic of cancer cell energy metabolism whereby cancer cells can reprogram their energy metabolism from aerobic to anaerobic glycolysis to allow oxygen deprived cells to continue generating ATP that are required for active cell proliferation.

2.5.2.4 Emerging hallmark: Evading immune destruction

The tenth and last hallmark of cancer; which is an emerging hallmark, is defined as evading immune destruction. When the human body's immune system is functioning properly, the body is able to detect and destroy foreign cells immediately. Cancer cells however have the ability to evade immune destruction by disabling components such as infiltrating CTLs and NK cells of the immune system that have been dispatched to eliminate them (Shields et al., 2010).

2.6 Apoptosis

Apoptosis, also known as programmed cell death, has now established its importance in many biological processes. It is used by multicellular organisms to execute any unwanted cells in a cascade of molecular events reflecting the presence of distinct well preserved molecular pathways. Programmed cell death establishes a homeostatic function, whereby it creates equilibrium of continuously renewing tissues, achieved by a steady state balance between cell replication and cell death (Galluzzi et al., 2009; Taylor et al., 2008).

Apoptosis is critical for numerous physiological processes such as embryogenesis, post-embryonic development, tissue homeostasis in continuously

renewing tissues, selective immune cell deletion and many other physiological processes. Therefore, it is not surprising deregulated apoptosis could lead to a wide array of diseases. Some of the acute and chronic pathologies such as Alzheimers, autoimmune disease, ischemic, infectious syndrome, toxic, AIDS and cancer are caused by apoptosis deregulation (Allen et al., 1997; Sheridan & Martin, 2010).

Apoptosis is initiated by pro-apoptotic stimuli which begin with rounding of cells and detachments from the surface and neighboring cells. It is followed with blebbing of the plasma membrane whereby the cells pinch into smaller membrane enclosed particles named apoptotic bodies. These apoptotic bodies are packed with cellular organelles and fragments of the nucleus. The cells that are undergoing apoptosis are readily differentiated from other cells, ingested and eaten by professional phagocytes or neighboring cells. Apoptotic bodies is surrounded by intact membranes which do not release their cellular constituents into the surrounding tissues during phagocytosis, thus preventing any inflammatory reaction associated with the apoptosis process nor removal of apoptotic cell (Elmore, 2007; Taylor et al., 2008).

2.6.1 Intrinsic and extrinsic apoptotic pathways

Both the intrinsic and extrinsic apoptotic pathway that involve cell membrane receptor- mediated interactions, play significant roles in normal development, tissue remodeling, aging, wound healing, immune response and maintaining homeostasis in the adult human body. The intrinsic pathway, also known as mitochondrial mediated pathway, is activated by vast array of stimulus, including radiation, cytotoxic drugs, cellular stress, cytoskeletal disruption, DNA damage, hypoxia and growth factor withdrawal (Green & Reed, 1998).

In this pathway, mitochondrial plays a crucial role by releasing cytochrome C which is an essential element to act as a critical inducer of programmed cell death. In the cytosol, cytochrome C binds and activates apoptotic activator 1 (Apaf-1) and procaspase 9 in the presence of ATP, forming “apoptosome”. This will initiate activation of caspase-9, an initiator caspase that is responsible for the intrinsic apoptosis pathway. This caspase-9 will trigger a caspase cascade activation involving caspase-3, caspase-6 and caspase-9 resulting in morphological and biochemical changes associated with apoptosis.

Out of the 12 known human caspases, six caspases, namely caspase-3, -6, -7, -8, -9 and -10 are involved in apoptosis. This caspases can be divided into two classes which is effector caspases (caspases-3, -6 and -7) which are responsible for most of the cleavages that disassemble the cell and initiator caspases (caspases-8 and -9) which initiates the proteolytic cascade. Mitochondria-targeted compounds that caused outer membrane permeabilization and intrinsic apoptosis in cancer cells also induce anticancer properties.

This intrinsic apoptotic pathway is regulated by BCL-2 family proteins, which shares one or more of the BCL-2 homology domains (BH1-BH4). There is also an anti-apoptotic member (BCL-2, BCL-X_L, BCL-W and MCL-1) of the family who works against the apoptotic inducer in cancer cells. This anti-apoptotic functions by sequestering the pro-apoptotic executioners of the MOMP (BAX and BAK).

In contrast to the intrinsic pathway, the extrinsic cell death pathway can function independently of mitochondria and is activated by binding to cell surface death receptors. This pathway is initiated by the binding of cytokines like TNF- α , TRAIL or FasL to the death receptors on the target cell surface. These death receptors on the cell surface are members of the tumor necrosis factor superfamily, which includes TNF

receptor-1, CD95, death receptor-3, TNF-related apoptosis inducing ligand receptor-1 and TRAIL-R2. Once bound, the receptor will be activated and the activated receptor will bind to a series of adaptor proteins which lead to the activation of procaspase-8. Once caspase-8 is activated, the execution phase of apoptosis is triggered (Elmore, 2007; McIlwain et al., 2013; Soengas & Lowe, 2003).

2.7 Necrosis

Necrosis is often defined as an accidental cell death, while apoptosis is frequently referred to “programmed cell death”. It has been widely accepted that apoptosis and necrosis are two distinct, mutually exclusive, modes of cell death. Necrosis generally represents a cell’s response to gross injury and can be induced by an overdose of cytotoxic agents. A classic example of necrotic cell death would be ischemia in which restriction of blood supply to tissues causes drastic depletion of oxygen, glucose and other nutrient factors, thus evoking massive necrotic death of endothelial cells and non-proliferating cells of surrounding tissues.

Among the agents that are capable of inducing necrotic cell death are various viruses, bacteria and protozoa. This necrosis can be activated by bacterial toxins, components of immune defense and peritoneal macrophages (Proskuryakov et al., 2003). Necrosis is identified morphologically by an increase in cell volume or better known as oncosis, swelling of organelles, plasma membrane rupture and subsequently release of intracellular contents and pro-inflammatory molecules causing induction of inflammation around the dying cell.

2.7.1 Necroptosis or programmed necrosis

Necrosis is often viewed as an accidental and unregulated cellular event; however, there is accumulating evidence showing that necrosis might not be accidental after all. With the discovery of signaling components for necrosis such as receptor interacting protein (RIP) kinases, poly (ADP-ribose) polymerase-1 (PARP-1), NADPH oxidases and calpains, this concept has recently been gaining ground (Ouyang et al., 2012). This regulated mechanism of passive cell death is termed as necroptosis or programmed necrosis.

Research findings showed that the same stimulants that could activate apoptosis such as TNF α , FasL and Trail ligands could also induce necroptosis activation as well (Kroemer et al., 2009). The final stage of necrotic destruction would be activation of proteases and in some cases this destruction is executed by caspases. Most of the time, inhibition of caspases will trigger necrosis cell death initiation. Apoptosis plays a major role in physiological cell death; however, under pathological conditions, necrosis is very common. Research also showed that necroptosis may act as a second line of defense against viral infections as viruses are able to inhibit apoptosis (Han et al., 2011; Kung et al., 2011). Therefore necroptosis is an important cellular death mechanism used in numerous human pathologies.

2.8 Cell Cycle

The cellular life cycle also known as cell cycle is a series of many processes that take place in a cell for a successful self-replication leading to its division and duplication (S phase) to produce two daughter cells (M phase). A cell cycle biologist focuses on the system which regulates the timing and frequency of DNA duplication and cell division. The cell cycle can be clearly divided into four different phases, namely mitosis (M), gap 1 (G1), DNA synthesis (S), gap 2 (G2) and resting phase (G0).

M phase, a phase where the cell divides into two new cells, occurs in four stages (prophase, metaphase, anaphase and telophase). This process will last between one to three hours. G1 phase is the time where the cell prepares to undergo cell division whereby it performs all the normal functions but starts to get bigger. In this phase, the cell begins to make protein in preparation to divide. The time for this phase can last from about eight hours to months. S phase is the time where the cell copies its DNA to make two sets of chromosomes. This phase would last between six to eight hours. G2 phase is the time for second growth phase where the cell makes more protein in preparation for cell division and this phase lasts about two to five hours. Lastly G0 phase is the resting phase or also known as a quiescent or dormant phase. At this stage the cell performs all its normal functions, but is not prepared to divide. Once the particular cell receives the signal to divide, it will move into G1 phase of the cell cycle.

2.8.1 Cell cycle checkpoints

Checkpoints are the regulators at which the progression of a cell to the next stage in the cycle can be halted under unfavorable condition. In the cell cycle there are three major checkpoints, namely G1, G2 and M (Sherr, 1996). A cell can only pass through these checkpoints in the presence of the necessary stimulatory signals and free from any DNA damage. If any of the conditions are not met and/or the damage cannot be rectified, the cell will be labeled for apoptosis. Defect in these checkpoints can lead to catastrophic consequences including cell death or uncontrolled growth of the cell (cancer). Each checkpoint consists of unique regulators, for example, at G1 checkpoints, damage to DNA and other external factors are evaluated. The G2 checkpoint ensures all of the chromosomes have been replicated and the DNA is in an optimum condition before entering mitosis. Lastly M checkpoint occurs at the end of the metaphase stage of mitosis. This checkpoint is also known as the spindle checkpoint as it determines whether the entire sister chromatids are correctly attached to the spindle microtubules (Elledge, 1996; Funk, 2001).

2.9 Human cell lines used

Cell lines are primary cultures that are transferred into the next culture vessel. PC-3 prostate cancer cell line was initiated from a bone metastasis of a grade IV prostatic adenocarcinoma of a 62 years old white man. This cell line does not express androgen receptors and prostate specific antigen, and are androgen independent. The PC-3 prostate cancer cells are also known to have high metastatic potential compared to other commonly used prostate cancer cell lines (Sobel & Sadar, 2005; Tai et al., 2011).

The MCF7 breast cancer cell line was derived from pleural effusion taken from a postmenopausal woman patient with metastatic breast cancer. This cell line has the

ability to process estrogen *via* estrogen receptors in cell cytoplasm which makes this cell line an estrogen positive control cell line. Thus, it is an ideal model to study hormone response in cancer studies (Levenson & Jordan, 1997). The MDA-MB-231 is also a cell line from breast cancer origin that is regarded as invasive *in vitro* and is used to identify genes and pathways that regulate metastasis to different sites. Most importantly, this cell line is generally known as triple-negative breast cancers which lacks expression of oestrogen, progesterone and ERBB2 receptors (Chavez et al., 2010).

The A549 cell line was first developed through removal and culturing of cancerous lung tissue. The A549 cells are human alveolar basal epithelial cells which are squamous in nature and responsible for the diffusion of substances such as water and electrolytes across the alveoli of lungs (Foster et al., 1998). The HCT 116 is a human colon cancer cell line that is commonly used to study cancer biology and often used as orthotopic model for colon cancer. This is a growth factor independent cell line and has been shown to be invasive and highly motile in *in vitro* studies (Rajput et al., 2008).

In this study, a normal human prostate cell line (RWPE-1) was used to determine the specificity for cancerous cells. RWPE-1 is an epithelial cell line derived from the normal adult human prostate and were transfected with a single copy of the human papilloma virus 18 to establish this cell line (Bello et al., 1997).

2.9.1 Prostate Cancer

Prostate cancer is the most common malignant tumor in men, and the second leading cause of mortality after skin cancer. The American Cancer Society's reported that in 2016, an estimated 180,890 men in the United States will be diagnosed with prostate cancer and out of this, it is estimated that about 26,120 deaths from prostate

cancer would occur (R. L. Siegel et al., 2016). Incidence of prostate cancer is increasing steadily in almost all countries, yet little is known about this disease (Grönberg, 2003; Xu et al., 2013). The first line treatment for prostate cancer is usually partial prosectomy or radiation to remove or destroy the cancerous cells (Gil-Araujo et al., 2013). In normal prostate tissues, the signaling pathways are regulated by androgen and it maintains a homeostatic state between growth and apoptosis of the glandular cells. However, in the abnormal tissues, the balance is disrupted and the continuous expression of androgen causes glandular cell growth and pathological changes.

The main androgens which stimulate prostate cancer cells growth are testosterone and dihydrotestosterone originates from the testicles. Therefore, androgen ablation therapy on the majority of patients showed positive results against androgen dependent cancer. However, this cancer eventually becomes androgen independent that continues to grow and metastasize. Androgen ablation therapy does not work on metastatic prostate cancer as the cells do not depend on hormones for growth anymore (Feldman & Feldman, 2001; Kaini & Hu, 2012; Suzuki et al., 2014; Taplin et al., 1995).

2.9.2 Markers for prostate cancer

The development and progression of prostate cancer is yet to be fully understood, but some of the markers that might be responsible for it have been identified. One of the possible markers could be mitogen-activated protein kinases (MAPK) family. Interleukin-8 (IL-8), also known as CXCL8, is a pro-inflammatory CXC chemokine. Expression of this IL-8 is primarily regulated by activator protein and /or nuclear factor κ B mediated transcriptional activity. The biological activity of IL-8 is mediated through binding of two cell-surface G protein-coupled receptors which is termed CXCR1 and CXCR2. This IL-8 signaling has been shown to induce activation of

AKT and also increase its expression in androgen independent prostate cancer cell lines. Increased AKT expression and activity are commonly detected in multiple forms of cancer (Waugh & Wilson, 2008).

Another marker, $IKK\alpha$, has been responsible for the augmented binding of CBP protein to NF- κ B than to p53. This event causes enhanced expression of NF- κ B target genes ultimately promoting cell proliferation. Apart from this, there has also been an association between $IKK\alpha$ and metastasis. High level of phosphorylated $IKK\alpha$ has been linked to progression of prostate carcinomas (Oeckinghaus et al., 2011).

2.10 Mitochondria

The mitochondrion is a cell's powerhouse, powering various functions of the cell and the organism as a whole. Its main function is to metabolize or break down carbohydrates and fatty acids in order to generate energy. Eukaryotic cells will use the energy in the form of ATP (adenosine triphosphate). These organelles have their own genome and are surrounded by two membranes (inner and outer membrane) with a small intermembrane space in between. The outer membrane encloses the entire content of the organelle, while the inner membrane folds inwards to form cristae and encloses the matrix. The surface of the inner mitochondrial membrane varies considerably between cell types or within a cell depending on its role which correlates with the rate of metabolic activity of the cell. Another function of the mitochondria is to synthesize protein for its own replication.

This organelle could work independently and execute its own transcription of DNA to RNA and translation of RNA to amino acid without depending on the cells. In recent years, researches were done to synthesize small molecules/nanocarriers for mitochondrial targeting and it is said that mitochondrial dysfunction is responsible for a

wide variety of human disorders such as neurodegenerative, neuromuscular diseases, diabetes, obesity and cancer.

2.10.1 Mitochondria as the key regulator of apoptosis

It is proven that mitochondria happen to be the key regulator of apoptosis by inducing a regulated energy dependent cell death pathway. This intrinsic apoptosis can be induced by a wide array of physiological or pathological cell stressors, such as toxins, viral infections, hypoxia, hyperthermia, free radicals and DNA damage. Intrinsic apoptosis involve mitochondrial outer membrane permeabilization (MOMP), a notable step whereby the cell is marked for ultimate destruction. This step is closely followed by release of cytochrome C and other apoptogenic proteins from the mitochondrial inter-membrane space into the cytosol. These proteins will activate a caspase cascade pathway which leads to proteolytic cleavage of intracellular proteins, DNA degradation, formation of apoptotic bodies and other apoptotic hallmark characteristics (D'Souza et al., 2011).

2.10.2 Mitochondria and cancer

Otto Warburg is the first person to discover the high rates of aerobic glycolysis observed in variety of tumor cell lines and this discovery prompted many scientists to study the underlying basis for the discrepancy in respiratory capacity, also known as “Warburg effect” (enhanced glucose uptake, high rate of glycolysis and increased in lactic acid production as a byproduct of the glycolytic pathway) (Warburg et al., 1927).

Research interest in the area of mitochondria has led to the discovery of several significant differences in the structure and function of this organelle between normal and cancerous cells. This includes differences in the size, number and shape of the

organelle, the rate of protein synthesis and organelle turnover and the polypeptide and lipid profiles of the inner mitochondrial membrane. In addition, it is found that mitochondrial membrane potential is notably higher in cancerous cell compared to normal epithelial cells (Modica-Napolitano & Weissig, 2015).

Alteration of mitochondrial genome sequence has been associated with a wide array of cancers. One of the common mutation in the mitochondrial genome is somatic mutation which have been observed in a wide array of cancer, including ovarian, uterine, liver, lung, colon, gastric, brain, bladder, prostate, breast, melanoma and leukemia (Modica-Napolitano & Singh, 2002). Scientists have been exploiting the differences in structural and functional characteristics that exist between the mitochondria of the normal cells and cancer cells which might serve as a target for selective killing of the cancer cells (Vyas et al., 2016).

Scientists have come out with a new term called “mitocan” (mitochondria and cancer) which is used to classify mitochondria targeting anticancer agents. A number of compounds which have shown efficacy in selective killing are delocalized lipophilic cations. These compounds have high lipophilicity and positive charge which forces them to selectively accumulate in the mitochondria of carcinoma cells, which is known to have higher negative membrane potential in comparison with normal cells. (160 mV in cancer cells vs 100 mV in control cells).

2.10.2.1 Mitochondria-targeted anticancer compound

Some of the compounds in this class are Rhodamine 123, dequalinium chloride and thiopyrylium AA-1. Research has shown that common anti-diabetic biguanide derivative, metformin, which is used in type 2 diabetes, may also be effective in the prevention and treatment of human cancer *via* inhibition of mitochondrial respiratory

function. This drug has effectively shown to reduce cancer incidence and cancer related mortality (Dowling et al., 2012). The fact that some of the mitochondria-targeted compounds have shown potent anticancer properties in preclinical and early clinical studies is very promising and these results warrant for further research and testing of these compounds as viable, single modality treatment options for human cancers.

University of Malaya

CHAPTER 3

MATERIALS AND METHODS

3.1 Chemistry

3.1.1 Materials and solutions

All reagents and solvents used for chemical synthesis were purchased from Merck unless stated otherwise.

3.1.2 Physical measurements

Infrared spectra were recorded from KBr discs on Perkin-Elmer Spectrum RX-1 spectrophotometer. ^1H NMR and ^{13}C NMR spectra were recorded in deuterated DMSO- d_6 on a JEOL JNM-LA400 or ECA 400 MHz instrument. Chemical shifts (δ) are given in ppm (parts per million). Elemental analyses were carried out on a Thermo Finnigan Eager 300 - CHNS elemental analyzer. HRMS were obtained on a JEOL AccuTOF mass spectrometer.

3.1.3 Syntheses

3.1.3.1 Synthesis of 5-(chloromethyl)-2-hydroxybenzaldehyde

All the reagents and solvents were obtained from commercial sources and used as supplied. Firstly, 2-hydroxybenzaldehyde (10.64 ml, 0.076 mol) was stirred with paraformaldehyde (5.05 g, 0.168 mol) and 50 ml of hydrochloric acid (fuming 37 %). The reaction mixture was then stirred at room temperature for 20 hours. After 20 hours, clumps of pinkish solid formed were filtered off. The solid was washed with 0.5 % sodium hydrogen carbonate (NaHCO_3) (R&M chemicals, U.K) solution and then with distilled water until the pH was closed to seven. It was crystallized using petroleum

ether to give white needle crystals. The crystals were dried under vacuum and kept for further synthesis. Similar studies had been carried out by (El-Sonbati et al., 2002; C. Huang et al., 2007).

3.1.3.2 Synthesis of (3-formyl-4-hydroxyphenyl) methyltriphenylphosphonium (T)

Briefly, 5-chloromethylsalicylaldehyde (0.170 g, 1 mmol) and triphenylphosphine (0.262 g, 1 mmol) were dissolved in 50 ml of toluene separately. Both solutions were mixed together and refluxed for three hours and cooled. The cooled whitish-yellow precipitated phosphonium salt was then filtered off and washed with diethyl ether. Slow evaporation of the compound in ethanol yielded white crystals. The crystals were filtered, washed with water, dried in the air and kept in desiccator over silica gel.

(Yield: 0.18 g, 41 %). Anal. Calc. for $C_{26}H_{22}O_2P.Cl$: (432.88): C, 72.22 %; H, 5.09 %. Found: C, 71.79 %; H, 5.21 %. FT-IR: (KBr, cm^{-1}): $\nu_{(O-H)}$: 3422 (w), $\nu_{(C-H)}$: 3021 (m), $\nu_{(C=O)}$: 1676 (s), $\nu_{(C-H)}$: 1438 (s), $\nu_{(C-O)}$: 1112 (s), $\nu_{(C-H)}$: 687 (s). s = strong, m = medium and w = weak

Characteristics 1H NMR (400MHz, DMSO- d_6 , TMS, s=singlet; d=duplet; m=multiplet) δ (ppm): 5.07-5.11 (2H, d, CH_2); 6.90 (1H, s, aromatic CH); 7.03-7.07 (1H, s, aromatic CH); 7.19-7.20 (1H, s, aromatic CH); 7.62-7.90 (15H, m, aromatic CH); 10.13 (1H, s, CHO); 11.03 (1H, s, OH). ^{13}C NMR (DMSO- d_6 , TMS, ppm 100MHz): 190.13 (C=O); 161.21 (C-OH); 117.67-138.62 (Ar); 27.92, 27.46 (CH_2). HRESIMS m/z 397.1356 (calculated for $C_{26}H_{22}O_2P$, 397.1352).

3.1.3.3 Synthesis of [3-[(E)-(carbamothioylhydrazono)methyl]-4-hydroxyphenyl] methyltriphenylphosphonium chloride (tsc)T

The (3-formyl-4-hydroxyphenyl) methyltriphenylphosphonium chloride (0.432 g, 1 mmol) and 3-thiosemicarbazide (0.091 g, 1 mmol) (Alfa Aesar) were dissolved in 30 ml and 20 ml of ethanol, respectively. Both solutions were mixed together and refluxed for four hours and cooled. The yellowish precipitate formed was filtered off using filter paper and washed again with ethanol to give pure Schiff base. The product was air dried at room temperature. Slow evaporation of the compound in ethanol yielded yellow crystals.

(Yield: 0.21 g, 42 %). Anal. Calc. for $C_{27}H_{25}N_3OPS.Cl$: (506.00): C, 64.16 %; H, 4.95 %; N, 8.32 %. Found: C, 63.95 %; H, 5.01 %; N, 8.22 %. FT-IR: (KBr, cm^{-1}): $\nu_{(O-H)}$: 3385 (w), $\nu_{(C=N)}$: 1598 (s), $\nu_{(C-H)}$: 1437 (s), $\nu_{(C-S)}$: 1108 (s), $\nu_{(C-S)}$: 838 (m), $\nu_{(C-H)}$: 686.52 (s). s = strong, m = medium and w = weak.

Characteristic 1H NMR (400MHz, DMSO- d_6 , TMS, s=singlet; d= duplet and m=multiplet) δ (ppm): 4.99-4.96 (2H, d, CH_2); 6.85-6.82 (1H, s, aromatic CH); 6.75-6.73 (1H, s, aromatic CH); 6.99 (1H, s, aromatic CH); 7.35 (1H, s, aromatic CH); 7.89-7.62 (15H, m, aromatic CH); 8.17 (1H, s, NH); 8.35 (1H, s, $CH=N$); 10.35 (1H, s, OH); 11.47 (1H, s, NH). ^{13}C NMR (DMSO- d_6 , TMS, ppm 100MHz): 179.06 (C=S); 156.85 (C-OH); 144.80 (C=N); 117.06-135.09 (Ar); 27.60, 27.13 (CH_2). HRESIMS m/z 470.1451 (calculated for $C_{27}H_{25}N_3OPS$, 470.1456).

3.1.3.4 Synthesis of [4-hydroxy-3-[(E)-(phenylcarbamothioylhydrazono)methyl]phenyl]methyl-triphenyl-phosphonium chloride P(tsc)T

The (3-formyl-4-hydroxy-phenyl) methyl-triphenyl-phosphonium chloride (0.382g, 1mmol) and 4-phenyl-3-thiosemicarbazide (0.168g, 1mmol) (Alfa Aesar) were dissolved in 30 ml and 20 ml of ethanol, respectively. Both solutions were then mixed together and refluxed for four hours and cooled. The yellowish precipitate formed was filtered off using filter paper and washed again with ethanol to give pure Schiff base. The product was air dried at room temperature.

(Yield: 0.32 g, 59 %). Anal. Calc. for $C_{33}H_{29}N_3OPS.Cl.CH_4O$: (614.14): C, 66.56 %; H, 5.38 %; N, 6.85 %. Found: C, 66.51 %; H, 5.15 %; N, 6.88 %. FT-IR: (KBr, cm^{-1}): $\nu_{(O-H)}$: 3303 (s), $\nu_{(C=N)}$: 1594 (m), $\nu_{(C-H)}$: 1438 (s), $\nu_{(C=S)}$: 1111 (s), $\nu_{(C-S)}$: 830 (m), $\nu_{(C-H)}$: 691 (s). s = strong, m = medium and w = weak.

Characteristic 1H NMR (400MHz, DMSO- d_6 , TMS, s=singlet; d= duplet and m=multiplet) δ (ppm): 5.00-4.97 (2H, d, CH_2); 6.83-6.75 (1H, s, aromatic CH); 7.41-7.39 (2H, s, aromatic CH_2); 7.52-7.44 (2H, m, CH_2); 7.70-7.59 (15H, m, aromatic CH); 7.81-7.77 (3H, m, CH_3); 8.30 (1H, s, aromatic CH); 9.45 (1H, s, $CH=N$); 10.41 (1H, s, OH); 11.87 (1H, s, NH). ^{13}C NMR (DMSO- d_6 , TMS, ppm 100MHz): 176.06 (C=S); 157.10 (C-OH); 139.21 (C=N); 117.12-135.49 (Ar); 31.23 (CH_2). HRESIMS m/z 546.1747 (calculated for $C_{33}H_{29}N_3OPS$, 546.1769).

3.1.3.5 Synthesis of [3-[(E)-[(4-fluorophenyl)carbamothioylhydrazono]methyl]-4-hydroxy-phenyl]methyl-triphenyl-phosphonium chloride FP(tsc)T

The (3-formyl-4-hydroxyphenyl) methyltriphenylphosphonium chloride (0.432 g, 1 mmol) and 4-(4-fluorophenyl)-3-thiosemicarbazide (0.186 g, 1 mmol) (Alfa Aesar) were dissolved in 30 ml and 20 ml of ethanol, respectively. Both solutions were mixed together and refluxed for four hours and cooled. The yellowish precipitate formed was filtered off using filter paper and washed again with ethanol to give pure Schiff base. The product was air dried at room temperature. Slow evaporation of the compound in methanol yielded yellow crystals. The crystals were kept in a desiccator over silica gel.

(Yield: 0.34 g, 55 %). Anal. Calc. for $C_{33}H_{28}FN_3OPS.Cl.CH_4O$: (632.13): C, 64.66 %; H, 5.07 %; N, 6.66 %. Found: C, 64.83 %; H, 4.71 %; N, 6.86 %. FT-IR: (KBr, cm^{-1}): $\nu_{(O-H)}$: 3328 (s), $\nu_{(C=N)}$: 1560 (m), $\nu_{(C-H)}$: 1438 (s), $\nu_{(C-S)}$: 1112 (s), $\nu_{(C-S)}$: 839 (s), $\nu_{(C-H)}$: 691 (s). s = strong, m = medium and w = weak.

Characteristic 1H NMR (400MHz, DMSO- d_6 , TMS, s=singlet; d= duplet and m=multiplet) δ (ppm): 5.05-5.01 (2H, d, CH_2); 6.82-6.80 (1H, s, aromatic CH); 7.27-7.24 (1H, s, aromatic CH); 7.28-7.27 (2H, m, CH_2); 7.80-7.60 (15H, m, aromatic CH); 7.85-7.80 (3H, m, CH_3); 8.32 (1H, s, aromatic CH); 9.51 (1H, s, $CH=N$); 10.50 (1H, s, OH); 11.91 (1H, s, NH). ^{13}C NMR (DMSO- d_6 , TMS, ppm 100MHz): 175.97 (C=S); 156.59 (C-OH); 135.05 (C=N); 114.85-134.92 (Ar); 27.80 (CH_2). HRESIMS m/z 564.1677 (calculated for $C_{33}H_{28}N_3OFPS$, 564.1675).

3.1.3.6 Synthesis of [3-[(E)-(ethylcarbamoithiylhydrazono)methyl]-4-hydroxyphenyl] methyltriphenylphosphonium chloride E(tsc)T

The (3-formyl-4-hydroxyphenyl) methyltriphenylphosphonium chloride (0.432 g, 1 mmol) and 4-ethyl-3-thiosemicarbazide (0.119 g, 1 mmol) (Alfa Aesar) were dissolved in 30 ml and 20 ml of ethanol, respectively. Both solutions were mixed together and refluxed for four hours and cooled. The yellowish precipitate formed was filtered off using filter paper. The precipitate was washed again with ethanol to give pure Schiff base. The product was air dried at room temperature.

(Yield: 0.28 g, 50 %). Anal. Calc. for $C_{29}H_{29}N_3OPS.Cl.C_2H_6O$: (580.12): C, 64.25 %; H, 6.04 %; N, 7.25 %. Found: C, 64.04 %; H, 5.60 %; N, 7.35 %. FT-IR: (KBr, cm^{-1}): $\nu_{(O-H)}$: 3290 (w), $\nu_{(C=N)}$: 1560 (m), $\nu_{(C-H)}$: 1439 (s), $\nu_{(C=S)}$: 1109 (s), $\nu_{(C=S)}$: 822 (w), $\nu_{(C-H)}$: 687 (m). s = strong, m = medium and w = weak.

Characteristic 1H NMR (400MHz, DMSO- d_6 , TMS, s=singlet; d= duplet and m=multiplet) δ (ppm): 5.02-4.99 (2H, d, CH_2); 6.80-6.77 (1H, s, aromatic CH); 6.86-6.83 (1H, s, aromatic CH); 7.27-7.22 (1H, s, aromatic CH); 7.45-7.40 (2H, d, CH_2); 7.69-7.54 (15H, m, aromatic CH); 7.83-7.78 (3H, m, CH_3); 8.32 (1H, s, NH); 9.48 (1H, s, $CH=N$); 10.50 (1H, s, OH); 11.87 (1H, s, NH). ^{13}C NMR (DMSO- d_6 , TMS, ppm 100MHz): 175.57 (C=S); 156.57 (C-OH); 138.63 (C=N); 116.57-134.96 (Ar); 27.79 (CH_2). HRESIMS m/z 498.1781 (calculated for $C_{29}H_{29}N_3OPS$, 498.1769).

3.1.3.7 Synthesis of [3-[(E)-[(4-ethylphenyl)carbamothioylhydrazono]methyl]-4-hydroxy-phenyl]methyl-triphenyl-phosphonium chloride EP(tsc)T

The (3-formyl-4-hydroxyphenyl) methyltriphenylphosphonium chloride (0.432 g, 1 mmol) and 4-ethylphenyl-3-thiosemicarbazide (0.195 g, 1 mmol) (Alfa Aesar) were dissolved in 30 ml and 20 ml of ethanol, respectively. Both solutions were mixed together and refluxed for four hours and cooled. The yellowish precipitate formed was filtered off using filter paper and washed again with ethanol to give pure Schiff base. The product was air dried at room temperature.

(Yield: 0.36 g, 57 %). Anal. Calc. for $C_{35}H_{33}N_3OPS.Cl$: (610.15): C, 68.97 %; H, 5.42 %; N, 6.90 %. Found: C, 68.45 %; H, 5.43 %; N, 6.83 %. FT-IR: (KBr, cm^{-1}): $\nu_{(O-H)}$: 3330 (s), $\nu_{(C=N)}$: 1600 (m), $\nu_{(C-H)}$: 1438 (s), $\nu_{(C=S)}$: 1108 (s), $\nu_{(C=S)}$: 845 (m), $\nu_{(C-H)}$: 687 (s). s = strong, m = medium and w = weak.

Characteristic 1H NMR (400MHz, $DMSO-d_6$, TMS, s=singlet; d= duplet and m=multiplet) δ (ppm): 2.49 (3H, m, CH_3); 4.98-4.94 (2H, d, CH_2); 6.75-6.73 (1H, s, aromatic CH); 6.82-6.80 (1H, s, aromatic CH); 7.25-7.24 (2H, s, aromatic CH_2); 7.46 (2H, m, CH_2); 7.67-7.48 (15H, m, aromatic CH); 7.81-7.77 (3H, m, CH_3); 8.28 (1H, s, aromatic CH); 9.37 (1H, s, $CH=N$); 10.41 (1H, s, OH); 11.80 (1H, s, NH). ^{13}C NMR ($DMSO-d_6$, TMS, ppm 100MHz): 176.11 (C=S); 157.05 (C-OH); 138.82 (C=N); 117.12-135.52 (Ar); 31.23 (CH_2). HRESIMS m/z 574.2105 (calculated for $C_{35}H_{33}N_3OPS$, 574.2082).

3.1.3.8 Synthesis of [4-hydroxy-3-[(E)-(methylcarbamothioylhydrazono) methyl] phenyl] methyltriphenylphosphonium chloride M(tsc)T

The (3-formyl-4-hydroxyphenyl) methyltriphenylphosphonium chloride (0.432 g, 1 mmol) and 4-methyl-3-thiosemicarbazide (0.105 g, 1 mmol) (Alfa Aesar) were dissolved in 30 ml and 20 ml of ethanol, separately. Both solutions were mixed together and refluxed for four hours and cooled. The yellowish precipitate formed was filtered off using filter paper and washed again with ethanol to give pure Schiff base. The product was air dried at room temperature.

(Yield: 0.22 g, 40 %). Anal. Calc. for $C_{28}H_{27}N_3OPS.Cl.H_2O$: (538.04): C, 62.57 %; H, 5.40 %; N, 7.82 %. Found: C, 62.90 %; H, 5.19 %; N, 7.74 %. FT-IR: (KBr, cm^{-1}): $\nu_{(O-H)}$: 3403 (w), $\nu_{(C=N)}$: 1560 (m), $\nu_{(C-H)}$: 1439 (s), $\nu_{(C=S)}$: 1110 (s), $\nu_{(C=S)}$: 824 (w), $\nu_{(C-H)}$: 687 (m). s = strong, m = medium and w = weak.

Characteristic 1H NMR (400MHz, DMSO- d_6 , TMS, s=singlet; d= duplet and m=multiplet) δ (ppm): 4.93-4.90 (2H, d, CH_2); 6.68 (1H, s, aromatic CH); 7.35 (1H, s, aromatic CH); 7.59 (1H, s, aromatic CH); 7.60 (1H, s, NH); 7.69-7.61 (15H, m, aromatic CH); 7.85-7.81 (3H, m, CH_3); 8.11 (1H, s, $CH=N$); 10.32 (1H, s, OH); 11.42 (1H, s, NH). ^{13}C NMR (DMSO- d_6 , TMS, ppm 100MHz): 177.99 (C=S); 156.73 (C-OH); 138.66 (C=N); 116.95-135.59 (Ar); 31.23 (CH_2). HRESIMS m/z 484.1607 (calculated for $C_{33}H_{29}N_3OPS$, 484.1612).

3.1.3.9 Synthesis of [3-[(E)-(dimethylcarbamothioylhydrazono)methyl]-4-hydroxyphenyl] methyltriphenylphosphonium chloride DM(tsc)T

The (3-formyl-4-hydroxyphenyl) methyltriphenylphosphonium chloride (0.432 g, 1 mmol) and 4-(4-Dimethyl)-3-thiosemicarbazide (0.119 g, 1 mmol) (Alfa Aesar) were dissolved in 30 ml and 20 ml of ethanol, respectively. Both solutions were mixed together and refluxed for four hours and cooled. The yellowish precipitate formed was filtered off using filter paper and washed again with ethanol to give pure Schiff base. The product was air dried at room temperature. Slow evaporation of the compound in ethanol yielded yellow crystals. The crystals were filtered, washed with water, dried in the air and kept in a desiccator over silica gel.

(Yield: 0.32 g, 55 %). Anal. Calc. for $C_{29}H_{29}N_3OPS.Cl.3H_2O$: (588.10): C, 59.28 %; H, 5.96 %; N, 7.16 %. Found: C, 59.43 %; H, 5.73 %; N, 7.62 %. FT-IR: (KBr, cm^{-1}): $\nu_{(O-H)}$: 3406 (s), $\nu_{(C=N)}$: 1560 (m), $\nu_{(C-H)}$: 1438 (s), $\nu_{(C=S)}$: 1111 (s), $\nu_{(C-S)}$: 832 (w), $\nu_{(C-H)}$: 691 (s). s = strong, m = medium and w = weak.

Characteristic 1H NMR (400MHz, DMSO- d_6 , TMS, s=singlet; d= duplet and m=multiplet) δ (ppm): 5.05-5.01 (2H, d, CH_2); 6.83-6.80 (1H, s, aromatic CH); 6.85 (1H, s, aromatic CH); 7.56-7.50 (3H, m, CH_3); 7.27-7.25 (2H, d, aromatic CH); 7.72-7.66 (13H, m, aromatic CH); 7.84-7.77 (3H, m, CH_3); 8.31 (1H, s, aromatic CH); 9.40 (1H, s, $CH=N$); 10.52 (1H, s, OH); 11.85 (1H, s, NH). ^{13}C NMR (DMSO- d_6 , TMS, ppm 100MHz): 175.61 (C=S); 156.61 (C-OH); 140.98 (C=N); 116.60-139.06 (Ar); 27.34-27.80 (CH_2). HRESIMS m/z 498.1761 (calculated for $C_{29}H_{29}N_3OPS$, 498.1769).

3.2 Biological studies

3.2.1 Materials

Anticancer agent cis-platin was purchased from Merck (Darmstadt, Germany), MTT (3-(4,5-Dimethylthiazol-2-yl)-2,5-diphenyltetrazolium bromide) was purchased from Sigma-Aldrich (Missouri, USA). Penicillin-Streptomycin as an antibacterial and amphotericin B solution as an antifungal were purchased from Sigma-Aldrich (St. Louis, MO, USA). Accutase solution as cell detacher and fetal bovine serum (FBS) used as an undefined supplement in cell culture, were purchased from Sigma-Aldrich (Missouri, USA). Phosphate-buffered saline (PBS) from Sigma-Aldrich (St. Louis, MO, USA) was purchased in tablet form, and each tablet was dissolved in 200 ml of distilled water. Dimethyl sulfoxide (DMSO) and Trypan blue were purchased from Sigma-Aldrich (St. Louis, MO, USA) as well. The mediums used for cell culture are RPMI 1640, DMEM and McCoy medium purchased from Sigma-Aldrich (St. Louis, MO, USA) and Keratinocyte Serum free medium purchased from Invitrogen (Carlsbad, CA, USA). (AO/EB) were purchased from Sigma-Aldrich (Missouri, USA).

3.2.2 *In vitro* cytotoxicity assay

3.2.2.1 Cell culture

The human cell lines used in this study were PC-3 (prostate adenocarcinoma), A549 (non-small cell lung cancer), MCF7 (breast adenocarcinoma), MDA-MB-231 (breast adenocarcinoma), HCT 116 (colon colorectal carcinoma) and RWPE-1 (prostate normal). The cell lines were purchased from American Type Culture Collection (Chicago, IL, USA). The PC-3, A549 and MCF7 cells were cultured in RPMI 1640 medium while MDA-MB-231 cells were cultured in DMEM medium and HCT 116 cells in McCoy medium. The RWPE-1 cells were maintained in keratinocyte serum

free medium supplemented with bovine pituitary extract (BPE) and human recombinant epidermal growth factor (EGF). The cells were cultured as monolayers in filtered 25 cm² culture flasks and maintained in exponential growth at 37 °C in a humidified atmosphere containing 5 % CO₂. When the cells reached 70 % confluence, they were harvested by incubating with Accutase at 37 °C for 10 minutes to obtain complete cell detachment. The cells were counted by standard laboratory methods using a hemocytometer method with an optimum cell number for 72 hours in 100 µl media per well. Cells were seeded in triplicate in 96-well tissue culture plates and incubated in CO₂ for 18 hours. After 18 hours, the medium was removed gently without causing cell detachment. The anticancer drugs ranging from 0.1 to 30 µM concentration dissolved in fresh medium were then added into designated wells, with the final volume of 200 µl. The plates were further incubated for 72 hours and wells with 0.5% DMSO omitting the anticancer drugs were used as negative control and empty wells were used as the blank.

Cryopreservation of cells

The cells were cultured as monolayers in filtered 25 cm² culture flasks and maintained in exponential growth at 37 °C in a humidified atmosphere containing 5 % CO₂. The cells to be cryopreserved were made free of infections from microorganisms (bacteria, yeast and mold). In addition, the cells were made to be viable and in exponential growth phase. When the cell growth reached 70 % confluence, they were harvested by incubating with Accutase at 37 °C for 10 minutes to obtain complete cell detachment. The cells were counted by standard laboratory methods using a hemocytometer method with 5 x 10⁵ cells per ml to be transferred into each cryovials. The cells were resuspended in complete growth medium supplemented with cryoprotective agents such as DMSO. Cryoprotective agents reduce the freezing point

of the medium and allow for a slower cooling rate, that greatly reduces the risk of ice crystal formation. These ice crystals can damage the cells and cause cell death. A volume of 1 ml resuspended cells with growth medium was transferred into each cryovials labeled with cell name, user name, date and medium used. The cryovials were stored in Mr Frosty from Nalgene (Penfield, NY, USA), overnight at -80 °C freezer. Mr Frosty is used to ensure a satisfactory and reproducible cooling rate when placed overnight. The following day, the frozen vials were transferred into a liquid nitrogen tank and stored in the gas phase above the liquid.

Revival of cells

The cryopreservation vials were thawed by gently agitating the vials in a water bath at 37 °C. To reduce the chances of contamination, the O-ring and cap were made sure to be kept above the water level. Thawing process was rapid, and once it was thawed, the vials were decontaminated by spraying with 70 % ethanol. The vial content was then transferred into 15 ml falcon tube and centrifuged at 1000 rpm for five minutes. The supernatant was discarded and the pellet was resuspended into 1 ml of fresh medium and transferred into 25 cm² tissue culture flask with complete culture medium. The flask was stored at 37 °C in a humidified atmosphere containing 5 % CO₂ and growth was observed under microscope on a daily basis.

3.2.2.2 MTT cytotoxicity assay

Firstly, MTT solution was prepared by weighing out 100 mg of MTT powder in 20 ml of PBS. The MTT solution was then filtered and stored at -20 °C in amber bottles before adding into each well (20 µl) and further incubated for three hours. Next, the medium was completely removed without disturbing the bottom and replaced with 200 µl of DMSO into each well. The plate was agitated for 15 minutes to completely dissolve the precipitants (Mosmann, 1983). The absorbance was detected at 570 nm with a reference wavelength at 690 nm on a Multiskan GO UV/Vis microplate spectrophotometer from Thermo Scientific (Waltham, MA, USA).

3.2.3 Morphological assessment of apoptotic cells by phase-contrast inverted microscope

Briefly, PC-3 cells were seeded in 35 mm culture dish (3×10^5 cells) and incubated in a CO₂ incubator for 18 hours. After incubation, the media were gently removed and 3 ml of fresh medium with selected compounds at concentration of 10, 30, 50 and 100 µM were added and further incubated for 24, 48 and 72 hours at 37 °C. The cells morphology were observed under Leica DMI 300B phase-contrast inverted microscope (Leica Microsystems, Germany) at 50x magnification and photographed (Reddy et al., 2013). The PC-3 cells plated with 0.5 % DMSO was used as negative control.

3.2.4 Cell death observation by acridine orange and ethidium bromide (AO/EB) double staining

Morphological changes of PC-3 cells were studied using AO/EB staining and observed under fluorescent microscopy. Briefly, PC-3 cells were seeded in 35 mm culture dish (3×10^5 cells) and incubated in a CO₂ incubator for 18 hours. PC-3 cells plated with 0.5 % DMSO was used as negative control. The cells were treated with selected compounds at concentrations of 30, 50 and 100 μ M with incubation period of 24, 48 and 72 hours at 37 °C. After incubation, the supernatant was collected and the adherent cells were detached with Accutase from each dish. Both floating and detached cells were pooled into 15 ml tube and centrifuged at 1000 g for five minutes at room temperature. The cells were washed with PBS and centrifuged again at 1000 g for five minutes at room temperature. The supernatant was carefully discarded and the pellet was resuspended in 25 μ l of PBS and 5 μ l of fluorochrome mixture (100 μ g/ml acridine orange and 100 μ g/ml EB in PBS). A volume of 10 μ l cell suspension was transferred to a glass slide and covered with cover slip. The samples were examined under an Olympus fluorescent inverted microscope (BX51-32F02) immediately with blue excitation mirror and image was captured using an Olympus camera (DP72) at 400x magnification (Rahmani-Nezhad et al., 2014).

3.2.5 Cell death detection using Annexin V-FITC/PI double staining by flow cytometry

The selected compounds were evaluated for their ability to induce cell death on PC-3 cells by annexin V-FITC fluorescein isothiocyanate apoptosis detection kit (BD Biosciences, Pharmingen San Diego, CA, USA). Firstly, PC-3 cells were seeded in 35 mm culture dish (3×10^5 cells) for sample treatment and additional three 35 mm culture dishes were prepared for controls (unstained, annexin dye only and propidium iodide dye only) which were used to set up compensation and quadrants. The cells were treated with concentrations of 30, 50 and 100 μM of selected compounds with incubation durations of 24, 48, and 72 hours at 37 °C. After incubation, the supernatant was collected and the adherent cells were detached with Accutase from each dish. Both floating cells and detached cells were pooled into 15 ml tube and centrifuged at 1000 g for five minutes at room temperature. The supernatant was discarded and the cell pellets were counted by standard laboratory methods using a hemocytometer to make sure the density does not exceed 1×10^6 cells per ml. Flow cytometric analysis was carried out according to the instruction manual in annexin V-FITC Apoptosis Detection Kit. The cells were washed twice in PBS and resuspended in 1 x binding buffer at a concentration of 1×10^6 cells per ml. A volume of 100 μl sample (1×10^5 cells) were transferred to 5 ml culture tube, followed by staining with 5 μl of annexin V-FITC and 5 μl of propidium iodide. The tubes were gently tapped and incubated for 15 minutes at room temperature in dark. Then, 1 x binding buffer (400 μl) was added to each tube and quantified by flow cytometry within an hour on a BD FACSCanto II system (Becton Dickinson, Mountain View, CA). At least 10,000 cells were counted in each sample.

3.2.6 Cell cycle arrest analysis using flow cytometry

The ability of selected compounds to arrest the cell cycle of PC-3 cell line was studied using CycleTEST PLUS DNA Reagent kit (BD Biosciences, Pharmingen San Diego, CA, USA) in this study. Briefly, PC-3 cells were seeded in 35 mm culture dish (3×10^5 cells) and treated with concentrations of 30 and 50 μM of selected compound for 24, 48 and 72 hours. After incubation, the supernatant was collected and adherent cells were detached with Accutase from each dish. Both floating cells and detached cells were pooled into 15 ml tube and centrifuged at 1000 g for five minutes at room temperature. The supernatant was discarded and cell pellets were resuspended in PBS. Flow cytometric analysis was carried out according to the instruction in CycleTEST PLUS DNA Reagent kit. The cell cycle procedures were divided into two steps which began with cell sample preparation from tissue culture, closely followed by staining procedure.

3.2.6.1 Cell sample preparation

Firstly, the cell suspension was centrifuged at 300 g for five minutes at room temperature. The supernatant was aspirated leaving approximately 50 μl to avoid unsettling the pellet. The pellet was resuspended in 1 ml of buffer solution by gently vortexing and centrifuge again for five minutes at 300 g at room temperature. The supernatant was similarly aspirated leaving approximately 50 μl to avoid disturbing the pellet. The pellet was resuspended in 1 ml of buffer solution by gently vortexing and counted by standard laboratory methods using a hemocytometer to adjust the cell density to 1×10^6 cells per ml with buffer solution. The cells were stained immediately or frozen for later testing.

3.2.6.2 Staining procedure

The cell suspensions were centrifuged at 400 g for five minutes at room temperature and the supernatant were emptied and dried onto a tissue. A volume of 250 μ l solution A (trypsin buffer) was added to each tube and gently mixed by tapping the tube by hand. The solution was allowed to react for ten minutes at room temperature. A volume of 200 μ l solution B (trypsin inhibitor and RNase buffer) was then added to each tube without removing solution A and gently mixed by tapping the tube again by hand. The solution A and B were further incubated for ten minutes at room temperature. Then, 200 μ l of solution C (propidium iodide stained solution) was added to each tube again without removing any solution and gently tapped prior further incubation for ten minutes in the dark on the ice. The sample was filtered using a culture tube with 35 μ M cell strainer cap and analyzed on flow cytometry BD FACSCanto II system (Becton Dickinson, Mountain View, CA) within three hours after addition of solution C. A total volume of 30,000 cells was counted in each sample. ModFit LT from Becton Dickinson was used to analyze the population in each cell cycle phase.

3.2.7 Mitochondrial transmembrane potential ($\Delta\Psi_m$) assessment assay using flow cytometry

In the present study, JC-1 (5,5',6,6'-tetrachloro-1,1',3,3'-tetraethylbenzimidazolcarbocyanine iodide) probe was utilized to measure mitochondrial depolarization in PC-3 cells using BDTM MitoScreen (BD Biosciences, Pharmingen San Diego, CA, USA). The mitochondrial transmembrane potential analysis was carried out according to instructions in manufacture protocol. The complete flow chart of this assay is illustrated in Figure 3.1. The assay was separated

into several steps prior to staining the cells with the dye which include preparation of 1x solution buffer, preparation of JC-1 stock solution and JC-1 working solution.

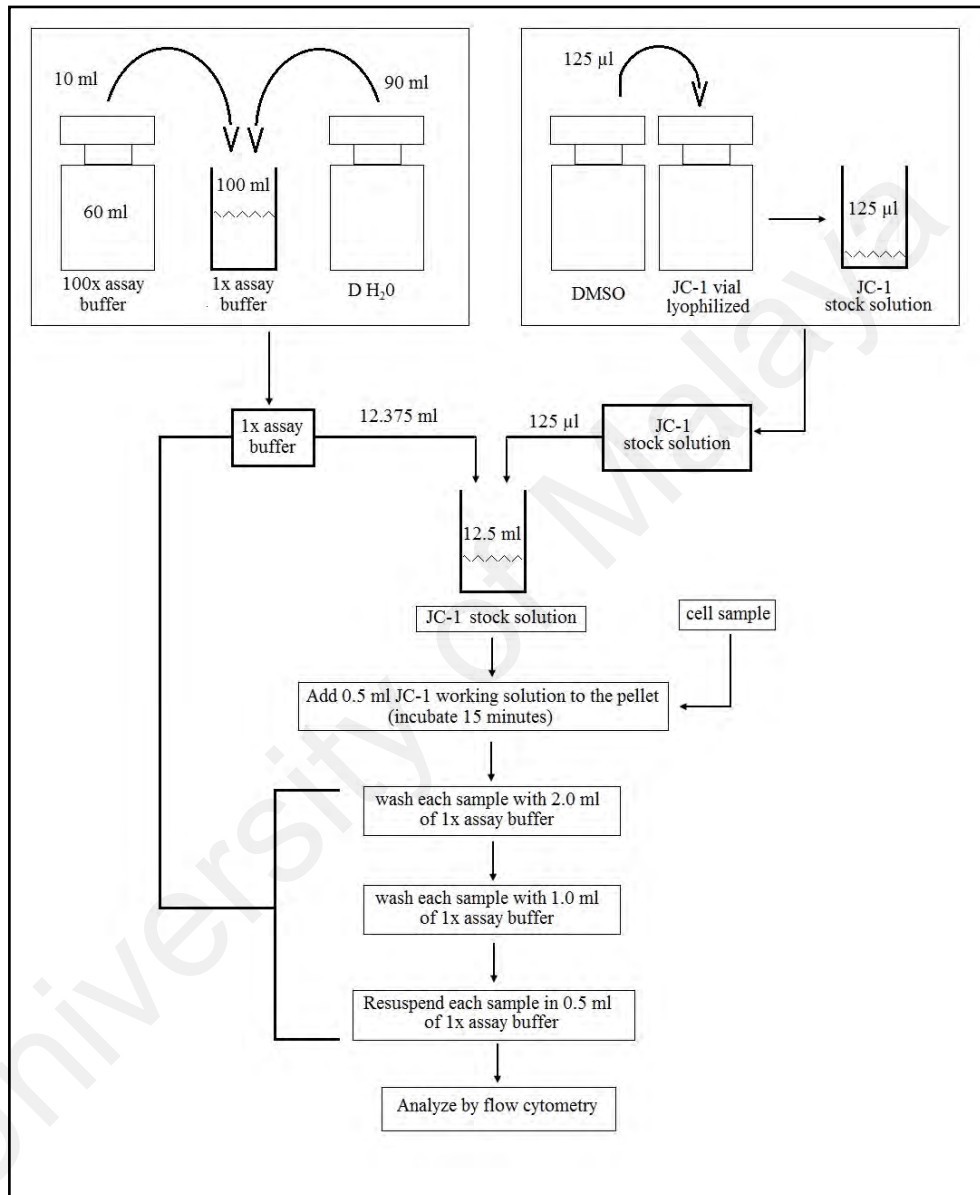


Figure 3.1: Flow chart of JC-1 assay

3.2.7.1 Preparation of 1x solution buffer

The buffer was formulated as reaction buffer and cell wash. The stock solution which was supplied as 10x concentrated, was then diluted to 1x. The 10x buffer was gently warmed in 37 °C water bath for 15 minutes to completely dissolve any salt crystals. The buffer was diluted in the ratio of 1:10 in distilled water by adding 90 ml of distilled water to 10 ml 10x assay buffer in 100 ml tube. The solution was stirred for five minutes and warm in 37 °C water bath prior using. Any unused diluted buffer (1x) was kept up to seven days at 2-8 °C.

3.2.7.2 Preparation of JC-1 stock solution (one vial)

The lyophilized JC-1 reagent was reconstituted with 125 µl of DMSO for every vial to give the stock solution. The vial was capped and inverted several times to fully dissolve the reagent. This stock solution was used immediately by diluting into working solution and the balance were aliquoted into several 1.5 ml microcentrifuge tubes wrapped with aluminium foils and stored at -20 °C freezer (used within six months). Repeated freeze and thaw was avoided to prevent disintegration of JC-1 stock solution.

3.2.7.3 Preparation of JC-1 working solution

The 1x assay buffer was warmed to 37 °C in water bath. The JC-1 working solution was prepared by diluting the JC-1 stock solution in ratio of 1:100 with pre-warmed 1x assay buffer. A volume of 125 µl JC-1 stock solution was added to 12.375 ml of pre-warmed assay buffer and each sample was added to 0.5 ml of JC-1 working solution. Therefore, 12.5 ml of working solution was sufficient to run 25 samples. The JC-1 working solution was vortexed thoroughly but there was some particulate matter consisting of JC-1 aggregates present. These aggregates were removed by centrifuging

at 1000 x g for 15 minutes and the clarified supernatant was transferred into another tube. All JC-1 solutions were used immediately and any leftover was discarded.

3.2.7.4 Preparation and staining of cells with JC-1

Briefly, PC-3 cells were seeded in 35 mm culture dish (3×10^5 cells) and incubated in a CO₂ incubator for 18 hours. PC-3 cells plated with 0.5 % DMSO was used as negative control. The media were gently removed and fresh medium with selected compound at concentrations of 10, 30 and 50 μ M were added and further incubated for 24 hours. After incubation, the supernatant was collected and the adherent cells were detached with Accutase from each dish. Both floating cells and detached cells were pooled into 15 ml tube and centrifuged at 1000 g for five minutes at room temperature. The supernatant was discarded and cell pellets were counted to make sure the density does not exceed 1×10^6 cells per ml. The cells were centrifuged again at 400g for five minutes at room temperature and the supernatant was gently removed. The freshly prepared JC-1 working solution (0.5 ml) was added to each pellet and vortexed to disrupt any cell to cell clumping. The cells were further incubated for 15 minutes at 37 °C in CO₂ incubator. After incubation, the cells were washed using 2 ml of 1x assay buffer to each tube and vortexed to prevent cell to cell clumping. This step was followed by centrifugation at 400 x g for five minutes and the supernatant was removed and discarded. The pellets were washed for the second time with 1 ml of assay buffer and all the steps were followed as previous. After second wash, the pellets were resuspended in 0.5 ml of 1x assay buffer and vortexed. A total volume of 50,000 cells were counted in each sample. Lastly, the samples were analyzed by flow cytometry BD FACSCanto II system (Becton Dickinson, Mountain View, CA).

3.2.8 Statistical analyses

The IC₅₀ values for cytotoxic activity were obtained from nonlinear regression using GraphPad Prism statistical software. Data were shown as mean ± standard deviation.

University of Malaya

CHAPTER 4

RESULTS AND DISCUSSION

4.1 Synthesis and characterization

The thiosemicarbazones were prepared by condensation reaction of (**T**) with thiosemicarbazide and its N-(4)-substituted derivatives in accordance to the reaction scheme shown in Figure 4.1. Compound **1** (3-formyl-4-hydroxyphenyl)methyltriphenylphosphonium (**T**) is white in color and compound **2-8**, in order namely thiosemicarbazide [**(tsc)**], 4-phenylthiosemicarbazide [**P(tsc)**], 4-fluorophenylthiosemicarbazide [**FP(tsc)**], 4-ethylthiosemicarbazide [**E(tsc)**], 4-ethylphenylthiosemicarbazide [**EP(tsc)**], 4-methylthiosemicarbazide [**M(tsc)**] and lastly 4,4-dimethyl thiosemicarbazide [**DM(tsc)**] are yellow in color. All compounds are non-hygroscopic, stable both in solid and solution phases; and highly soluble in methanol (MeOH), dimethyl sulfoxide (DMSO) and dimethylformamide (DMF). The compounds were characterized by infrared spectra (IR), Carbon Hydrogen Nitrogen elemental analysis (CHN), high resolution mass spectrometry (HRMS) proton nuclear magnetic resonance (^1H NMR) and carbon nuclear magnetic resonance (^{13}C NMR) which were in conformity with the structure of targeted compounds.

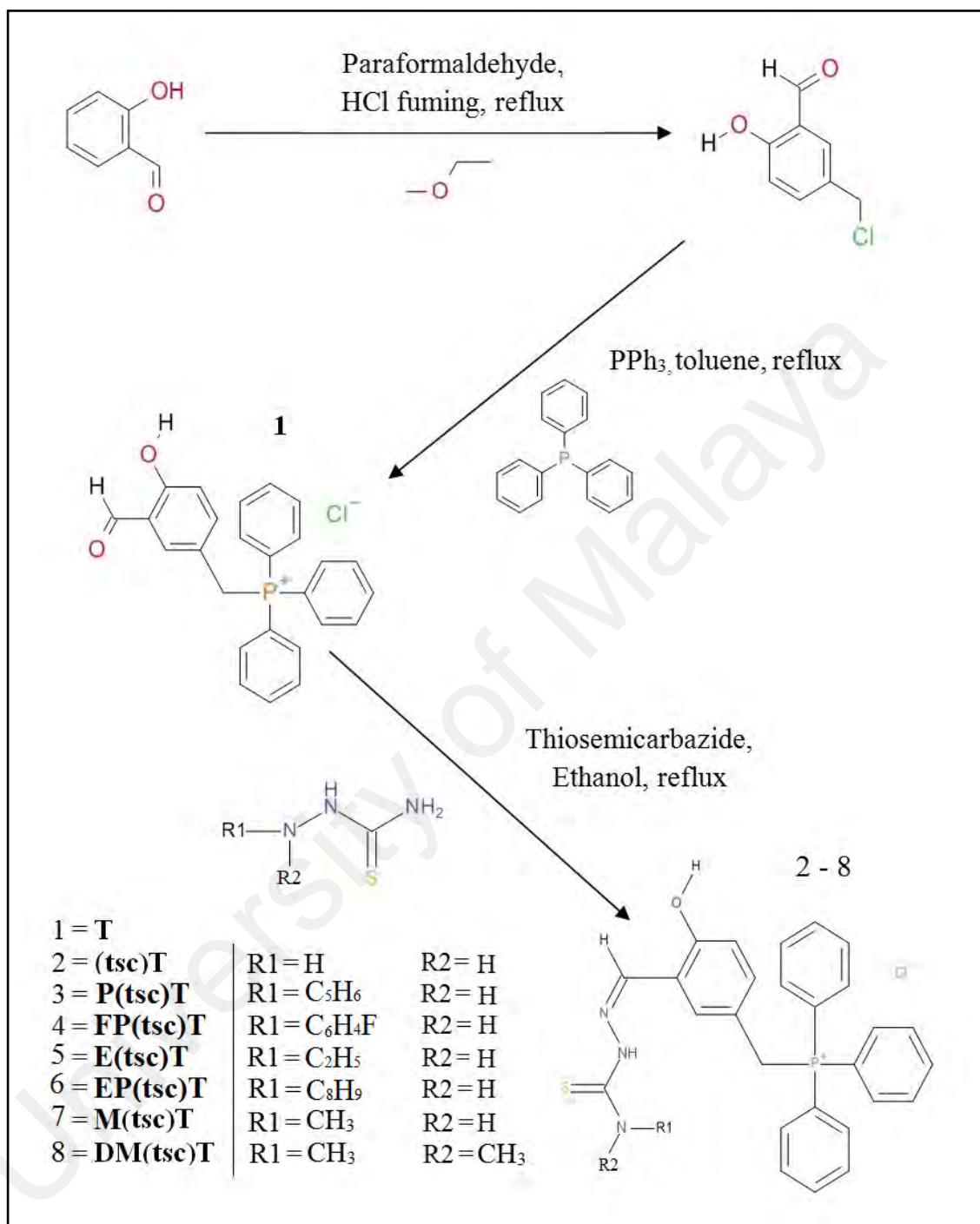


Figure 4.1: Reaction scheme and structures of synthesized compounds

4.2 Infrared spectra

The infrared spectra of ligands were analyzed in region of 4000 – 400 cm^{-1} . The IR spectrum of **T** showed the presence of band at 3021 cm^{-1} which is ascribed to aromatic $\nu(\text{C-H})$ stretch. The bands from 3290 to 3422 cm^{-1} are assigned to $\nu(\text{O-H})$ for all the compounds (Tan et al., 2012). Meanwhile, the bands from 3124 to 3176 are assigned to N-H stretching frequency (Alomar et al., 2013; Jagadeesh et al., 2015; Yildirim et al., 2014). In the IR spectrum of **T**, a strong band at 1676 cm^{-1} appeared but disappeared in all thiosemicarbazones is assigned to the stretching vibration of carbonyl $\nu(\text{C=O})$ (Anitha et al., 2013; Chew et al., 2014; Ebrahimi et al., 2015; Stringer et al., 2011). The IR spectra of **(tsc)T** showed IR absorption of 1598, meanwhile the rest of the compound showed IR absorption of 1560 cm^{-1} which are ascribed to the $\nu(\text{C=N})$ azomethine stretching frequencies (Anbazhagan & Sankaran, 2015; Gurumoorthy et al., 2015; Kiriy et al., 2004). Appearance of strong band in thiosemicarbazones for the region of 1108 to 1112 cm^{-1} and 822 to 839 cm^{-1} are ascribed to $\nu(\text{C-S})$ stretching vibration (Wiles et al., 1967). The above assignments are in good agreement with the literature values.

4.3 ^1H NMR and ^{13}C NMR

The ^1H -NMR spectra of the compounds are recorded in $\text{DMSO-}d_6$. In the ^1H -NMR spectrum of **T**, a complex multiplet that appeared in the region of 7.91 to 7.62 ppm is assigned to aromatic protons of triphenylphosphine (Chew et al., 2014; Kalaivani et al., 2014; Prabhakaran et al., 2006). Upon formation of Schiff base, the multiplet shifted upfield as presented in the experimental section. The aldehydic proton ($-\text{CHO}$) of **T** appeared in the spectrum at 10.13 ppm, but upon Schiff base formation there was no resonance attributable to ($-\text{CHO}$). Singlet observed at 8.11 to 9.48 ppm is

ascribed to the imine proton(-CH=N) (Eissa, 2013). The prominent doublet signal that appears in all compounds in the range of 5.00 ppm is assigned to the methylene CH₂ proton, whereas the multiplets that appear at the region of 7.60 to 7.89 ppm are ascribed to the aromatic proton of triphenylphosphine.

The ¹³C NMR spectra of the compounds are recorded in DMSO-*d*₆. The ¹³C NMR spectrum of compound **T**, showed chemical shift at 190.12 ppm and 161.21 ppm which is assigned to C=O and C-OH respectively. Upon the formation of Schiff base ligand, the chemical shift of (C=O) for compound **T** is replaced by azomethine carbon (C=N) for all thiosemicarbazone which appeared in the region of 135.05 to 144.80 ppm. The doublet that falls around 27.00 ppm is assigned to the methylene carbon for all compounds. Additionally the signal at 175.61 to 179.06 ppm is ascribed to (C=S) bond of thiosemicarbazones. The ¹H-NMR and ¹³C NMR spectral data are in good agreement with the literatures of the similar compounds therefore the results strongly affirm that the proposed compounds have been formed.

4.4 X-ray crystal structures

Single-crystal X-ray analysis reveals that all compounds crystallized in the monoclinic system except for **P(tsc)T** in the triclinic form. **(tsc)T**, **FP(tsc)T** and **DM(tsc)T** are having space group of P2₁/*c* whereas **P(tsc)T** having space group of P-1 and **E(tsc)T** having a space group of P2₁/*n*. Selected crystallographic data are given in Table 4.1, 4.2 and 4.3. Selected bond lengths and angles are given in Table 4.4, 4.5 and 4.6. Figure 4.2, 4.3, 4.4, 4.5 and 4.6 shows ORTEP plots of **(tsc)T**, **P(tsc)T**, **FP(tsc)T**, **E(tsc)T** and **DM(tsc)T** respectively. All the crystallized compound **(tsc)T**, **P(tsc)T**, **FP(tsc)T**, **E(tsc)T** and **DM(tsc)T** adopt an *E* configuration about the C=N bond with bond distances of 1.287(3), 1.285(2), 1.284(3), 1.281(4) and 1.282(3) Å respectively.

Presence of C=S bond is detected in **(tsc)T**, **P(tsc)T**, **FP(tsc)T**, **E(tsc)T** and **DM(tsc)T** with bond length of 1.688(2), 1.6813(16), 1.692(2), 1.675(3) and 1.693(3) Å respectively. The O-H and N-H hydrogen atoms are syn for **(tsc)T**, **P(tsc)T**, **FP(tsc)T** and **E(tsc)T** while it is anti in **DM(tsc)T** allowing for the formation of an intramolecular O--H...N hydrogen bond which stabilizes the molecule (Lobana & Castineiras, 2002; Velders et al., 2001). With respect to the central hydroxybenzene ring in the cation, the phosphonium-P atom lies to the ring with a torsion angle of 121.2° *via* P₁-C₉-C₇-C₈ for **(tsc)T**, whereas **P(tsc)T**, **FP(tsc)T**, **E(tsc)T** and **DM(tsc)T** showed torsion angle of 75.11°, 75.2°, 115.4° and 118.8° respectively *via* P₁-C₁₉-C₂₀-C₂₅. The hydrazone residue *via* N₃-C₂-C₃-C₈ for **(tsc)T** lies in a position of almost planar with torsion angle of -6.9°. **DM(tsc)T** and **E(tsc)T**, also showed planar torsion angle of -0.3° and 0.4 ° *via* N₁-C₂₆-C₂₄-C₂₃ and N₁-C₂₇-C₂₆-C₂₅ respectively for similar positions. **P(tsc)T** and **FP(tsc)T** have a torsion angle of 15.7 ° and 13.1 ° respectively *via* N₁-C₂₆-C₂₄-C₂₅ for similar positions.

Table 4.1: Crystallographic data for (tsc)T and P(tsc)T

	(tsc)T	P(tsc)T
Empirical Formula	C ₂₇ H ₂₅ N ₃ OPS.Cl	C ₃₃ H ₂₉ N ₃ OPS.Cl.CH ₄ O
Formula Weight	506.00	614.14
Crystal system	Monoclinic, P2 ₁ /c	Triclinic, P-1
<i>a</i> (Å)	9.6434 (6)	8.7119 (4)
<i>b</i> (Å)	10.3758 (8)	11.3037 (5)
<i>c</i> (Å)	25.2554 (15)	16.2991 (7)
α (°)	90	102.0448
β (°)	98.866	99.8760
γ (°)	90	99.6329
<i>V</i> (Å ³)	2496.8 (3)	1511.72 (12)
<i>Z</i>	4	2
<i>F</i> (000)	1056	634
<i>D_x</i> (Mg m ⁻³)	1.346	1.329
μ (mm ⁻¹)	0.33	0.28
<i>T</i> (K)	100(2)	293(2)
Crystal size (mm)	0.25 x 0.20 x 0.15	0.50 x 0.40 x 0.30
Crystal color, habit	Yellow, Block	Yellow, Block
Observed data [<i>I</i> > 2σ(<i>I</i>)]	4304	6096
R _{int}	0.067	0.025
θ_{\max} (°)	27.6	27.5
θ_{\min} (°)	2.9	1.9
<i>h</i>	-12→12	-11→11
<i>k</i>	-13→13	-14→14
<i>l</i>	-32→32	-21→21
<i>R</i> [<i>F</i> ² > 2σ(<i>F</i> ²)]	0.047	0.037
<i>wR</i> (<i>F</i> ²)	0.129	0.103
<i>S</i>	1.06	1.05
$\Delta\rho_{\max}$ (e Å ⁻³)	0.57	0.53
$\Delta\rho_{\min}$ (e Å ⁻³)	-0.42	0.58
CCDC no	1024893	1443549

Table 4.2: Crystallographic data for FP(tsc)T and E(tsc)T

	FP(tsc)T	E(tsc)T
Empirical Formula	C ₃₃ H ₂₈ FN ₃ OPS.Cl.CH ₄ O	C ₂₉ H ₂₉ N ₃ OPS.ClC ₂ H ₅ OH
Formula Weight	632.13	580.12
Crystal system	Monoclinic, P2 ₁ /c	Monoclinic, P2 ₁ /n
<i>a</i> (Å)	17.5495 (6)	9.9634 (5)
<i>b</i> (Å)	9.4617 (3)	17.6847 (10)
<i>c</i> (Å)	19.0569 (6)	16.0134 (7)
α (°)	90	90
β (°)	107.298 (4)	107.899
γ (°)	90	90
<i>V</i> (Å ³)	3021.24 (17)	2685.0 (2)
<i>Z</i>	4	4
<i>F</i> (000)	1248	1120
<i>D_x</i> (Mg m ⁻³)	1.319	1.321
μ (mm ⁻¹)	0.29	0.31
<i>T</i> (K)	100(2)	100(2)
Crystal size (mm)	0.30 x 0.25 x 0.20	0.15 x 0.10 x 0.05
Crystal color, habit	Yellow, Block	Yellow, Block
Observed data [<i>I</i> > 2 σ (<i>I</i>)]	4584	4655
R _{int}	0.041	0.040
θ_{\max} (°)	27.5	27.6
θ_{\min} (°)	2.4	2.4
<i>h</i>	17→22	-12→12
<i>k</i>	12→9	-14→23
<i>l</i>	24→16	-20→15
<i>R</i> [<i>F</i> ² > 2 σ (<i>F</i> ²)]	0.057	0.050
<i>wR</i> (<i>F</i> ²)	0.159	0.124
<i>S</i>	1.04	1.02
$\Delta\rho_{\max}$ (e Å ⁻³)	0.67	0.66
$\Delta\rho_{\min}$ (e Å ⁻³)	-0.39	0.66
CCDC no	1045490	1024896

Table 4.3: Crystallographic data for DM(tsc)T

DM(tsc)T	
Empirical Formula	C ₂₉ H ₂₉ N ₃ OPS.Cl.3H ₂ O
Formula Weight	588.10
Crystal system	Monoclinic, P2 ₁ /c
<i>a</i> (Å)	12.0678 (4)
<i>b</i> (Å)	15.8483 (4)
<i>c</i> (Å)	29.9653 (9)
α (°)	90
β (°)	90.444 (3)
γ (°)	90
<i>V</i> (Å ³)	5730.8 (3)
<i>Z</i>	8
<i>F</i> (000)	2400
<i>D_x</i> (Mg m ⁻³)	1.321
μ (mm ⁻¹)	0.30
<i>T</i> (K)	100(2)
Crystal size (mm)	0.40 x 0.30 x 0.20
Crystal colour, habit	Yellow, Block
Observed data [<i>I</i> > 2 σ (<i>I</i>)]	8976
<i>R</i> _{int}	0.044
θ_{\max} (°)	27.6
θ_{\min} (°)	2.2
<i>h</i>	15→15
<i>k</i>	20→20
<i>l</i>	38→27
<i>R</i> [<i>F</i> ² > 2 σ (<i>F</i> ²)]	0.057
<i>wR</i> (<i>F</i> ²)	0.143
<i>S</i>	1.02
$\Delta\rho_{\max}$ (e Å ⁻³)	0.60
$\Delta\rho_{\min}$ (e Å ⁻³)	-0.51
CCDC no	1024897

Table 4.4: Selected bond lengths and angles for (tsc)T and P(tsc)T

Atoms (Å, °)			
(tsc)T		P(tsc)T	
S1-C1	1.688 (2)	S1-C27	1.6813 (16)
P1-C10	1.794 (2)	P1-C7	1.7907 (16)
P1-C16	1.796 (2)	P1-C1	1.7925 (16)
P1-C22	1.797 (2)	P1-C13	1.7938 (16)
P1-C9	1.811 (2)	P1-C19	1.8068 (15)
O1-C4	1.364 (3)	O1-C23	1.3532 (18)
N1-C1	1.321 (3)	N1-C26	1.285 (2)
N2-C1	1.362 (3)	N1-N2	1.3780 (18)
N2-N3	1.378 (3)	N2-C27	1.357 (2)
N3-C2	1.287 (3)	N3-C27	1.343 (2)
C10-P1-C16	110.42 (11)	N3-C28	1.417 (2)
C10-P1-C22	110.05 (10)	C7-P1-C1	109.47 (7)
C16-P1-C22	108.31 (11)	C1-P1-C13	112.09 (7)
C10-P1-C9	111.97 (11)	C26-N1-N2	114.49 (13)
C16-P1-C9	108.06 (10)	C27-N2-N1	120.71 (13)
C22-P1-C9	107.92 (11)	N3-C27-N2	114.11 (14)
C1-N2-N3	117.87 (19)	N3-C27-S1	128.04 (12)
C2-N3-N2	117.3 (2)	N2-C27-S1	117.84 (12)
N1-C1-N2	117.8 (2)	O2-C34-C35	112.2 (5)
N1-C1-S1	122.40 (17)	C18-C13-P1	121.99 (12)
N2-C1-S1	119.82 (18)	C14-C13-P1	118.01 (12)
N3-C2-C3	118.3 (2)	P1-C1-C2-C3	-174.54 (13)
C1-N2-N3-C2	172.0 (2)	P1-C1-C6-C5	175.50 (12)
N3-N2-C1-N1	-0.4 (3)	C26-N1-N2-C27	-170.01 (14)
N3-N2-C1-S1	179.32 (16)	C1-P1-C19-C20	171.83 (11)
N2-N3-C2-C3	177.64 (19)	N2-N1-C26-C24	-177.63 (13)
		N1-N2-C27-N3	-0.6 (2)
		N1-N2-C27-S1	178.17 (11)

Table 4.5: Selected bond lengths and angles for FP(tsc)T and E(tsc)T

Atoms (\AA , $^\circ$)			
FP(tsc)T		E(tsc)T	
S1-C27	1.675 (3)	S1-C28	1.692 (2)
F1-C31	1.369(4)	P1-C7	1.791 (2)
O1-C23	1.356 (3)	P1-C13	1.792 (2)
N1-C26	1.281 (4)	P1-C19	1.800 (2)
N1-N2	1.379 (3)	P1-C1	1.804 (2)
N2-C27	1.352 (4)	O1-C23	1.356 (3)
N3-C27	1.349 (4)	N1-C27	1.284 (3)
C1-P1-C7	107.60 (14)	N1-N2	1.369 (2)
C1-P1-C13	112.86 (14)	N2-C28	1.358 (3)
C1-P1-C19	108.12 (14)	N3-C28	1.320 (3)
C23-O1-H1	111 (3)	C7-P1-C13	108.89 (11)
C26-N1-N2	115.8 (2)	C7-P1-C19	108.98 (11)
C27-N2-N1	119.5 (2)	C7-P1-C1	108.14 (10)
N1-N2-H2	122 (3)	C13-P1-C1	111.70 (11)
C27-N3-C28	127.2 (3)	C19-P1-C1	110.19 (11)
C27-N3-H3	116 (2)	C23-O1-H1	112 (2)
C28-N3-H3	116 (2)	C27-N1-N2	116.86 (19)
O1-C23-C22	122.6 (3)	C28-N2-N1	118.28 (19)
O1-C23-C24	117.8 (3)	N1-N2-H2	119.6 (17)
N1-C26-C24	120.7 (3)	C6-C1-P1	121.38 (19)
C29-C28-N3	119.1 (3)	C2-C1-P1	118.41 (18)
C33-C28-N3	120.7 (3)	N3-C28-S1	124.52 (17)
N3-C27-N2	113.9 (3)	N2-C28-S1	118.29 (17)
N3-C27-S1	125.8 (2)	C7-P1-C1-C6	90.1 (2)
N2-C27-S1	120.3 (2)	C27-N1-N2-C28	-176.6 (2)
C30-C31-F1	118.7 (3)	N2-N1-C27-C26	-179.7 (2)
F1-C31-C32	117.6 (3)	C29-N3-C28-S1	2.4 (4)
N1-N2-C27-N3	3.8 (4)	N1-N2-C28-N3	-4.9 (3)
N1-N2-C27-S1	-175.5 (2)	N1-N2-C28-S1	174.90 (18)
C26-N1-N2-C27	-172.7 (3)		

Table 4.6: Selected bond lengths and angles for DM(tsc)T

Atoms (Å, °)	
DM(tsc)T	
S1-C27	1.693 (3)
P1-C1	1.794 (3)
P1-C7	1.794 (3)
P1-C13	1.799 (3)
O1-C23	1.357 (3)
N1-C26	1.282 (3)
N1-N2	1.376 (3)
N2-C27	1.366 (3)
N3-C27	1.346 (3)
N3-C28	1.454 (4)
N3-C29	1.467 (4)
C1-P1-C7	110.38 (14)
C1-P1-C13	107.34 (13)
C7-P1-C13	108.71 (13)
C1-P1-C19	110.39 (13)
C7-P1-C19	111.46 (13)
C13-P1-C19	108.43 (13)
N3-C27-N2	115.5 (2)
N3-C27-S1	123.1 (2)
N2-C27-S1	121.4 (2)
C23-O1-H10	109 (2)
C26-N1-N2	119.3 (2)
C8-C7-P1	120.8 (2)
C26-N1-N2-C27	-179.6 (2)
C55-N4-N5-C56	174.1 (2)
N1-N2-C27-S1	3.7 (3)
N2-N1-C26-C24	-175.7 (2)
C28-N3-C27-S1	-173.7 (2)
N1-N2-C27-N3	-175.7 (2)

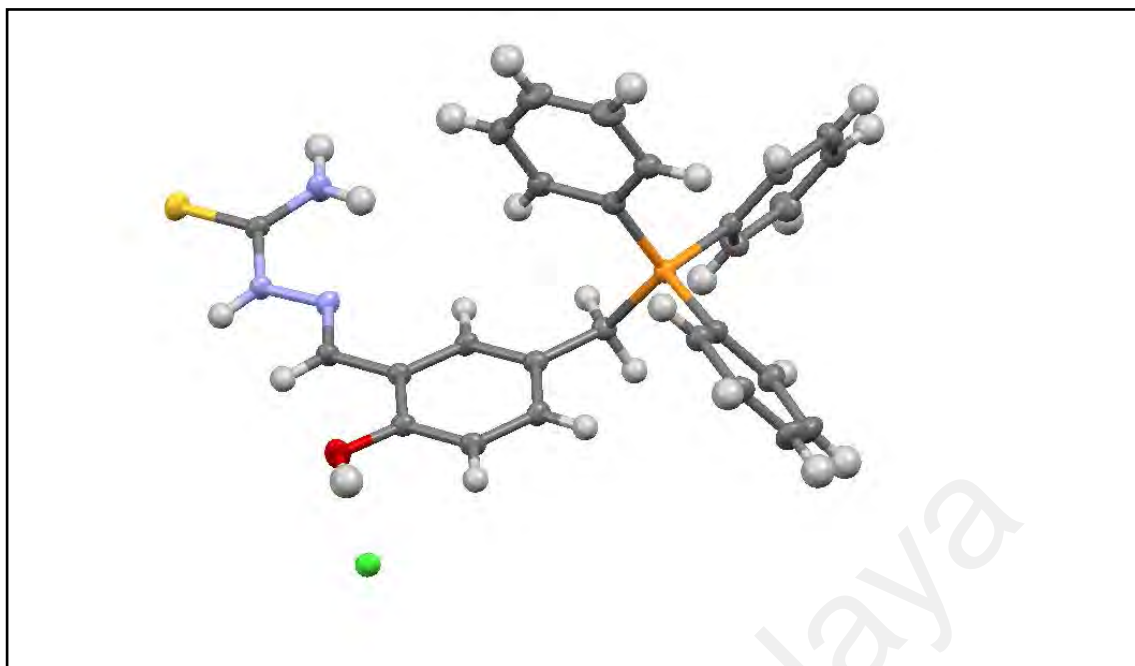


Figure 4.2: ORTEP diagram of $C_{27}H_{25}N_3OPS.Cl$ [(tsc)T]. Thermal ellipsoids are shown at 50 % probability.

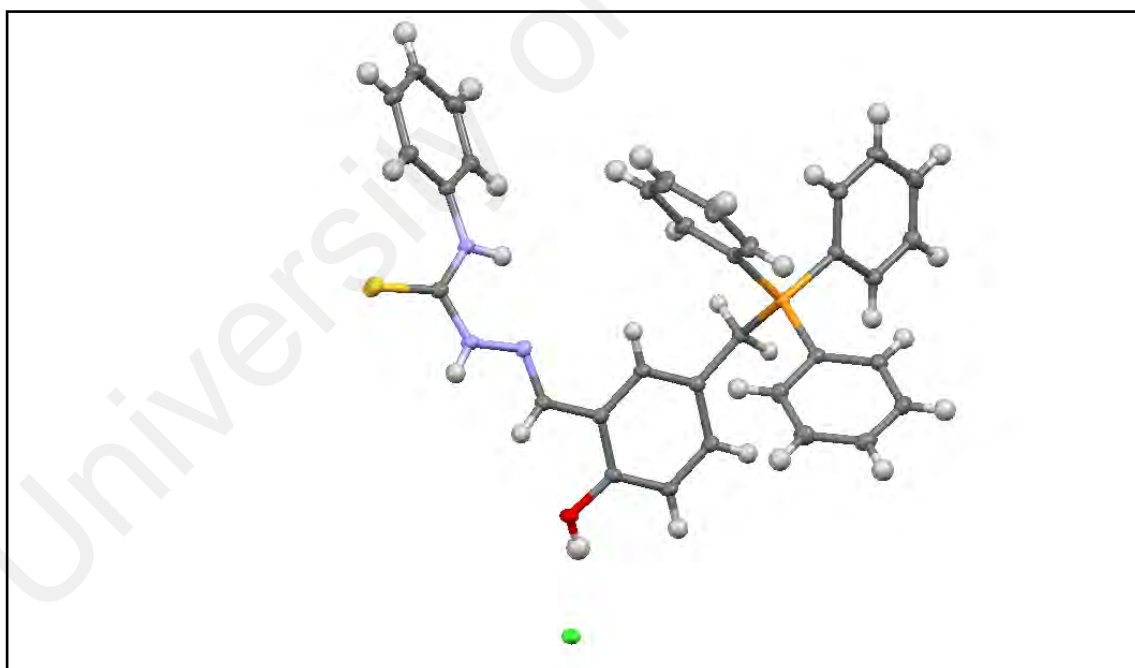


Figure 4.3: ORTEP diagram of $C_{33}H_{29}N_3OPS.Cl$ [P(tsc)T]. Thermal ellipsoids are shown at 50 % probability.

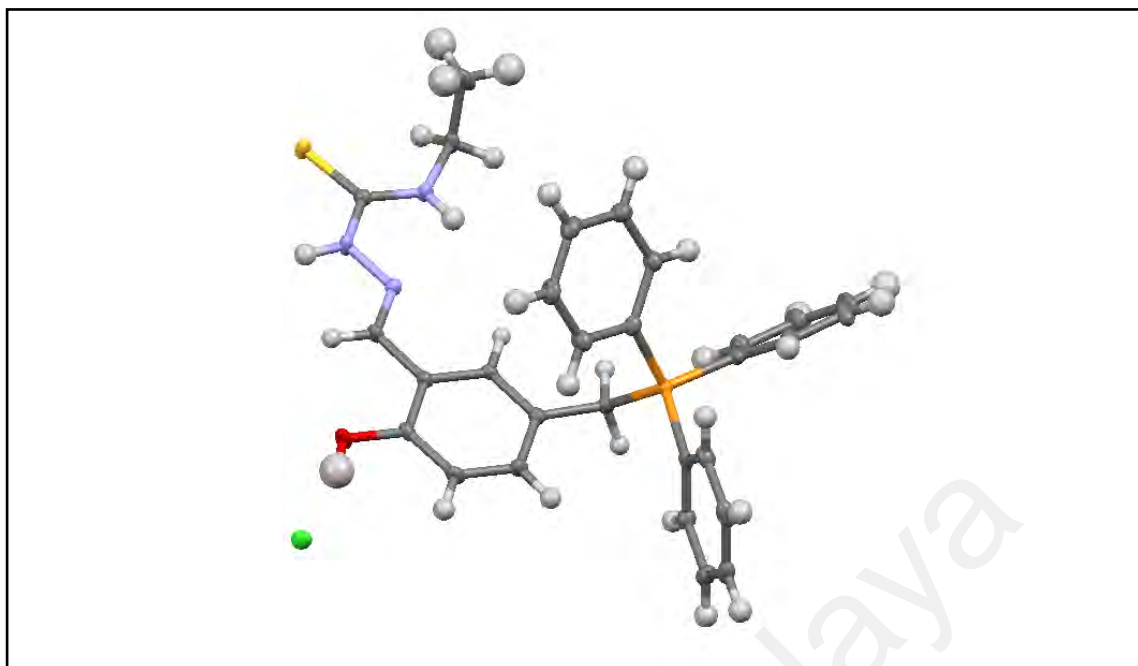


Figure 4.4: ORTEP diagram of C₂₉H₂₉N₃OPS.Cl [E(tsc)T]. Thermal ellipsoids are shown at 50 % probability.

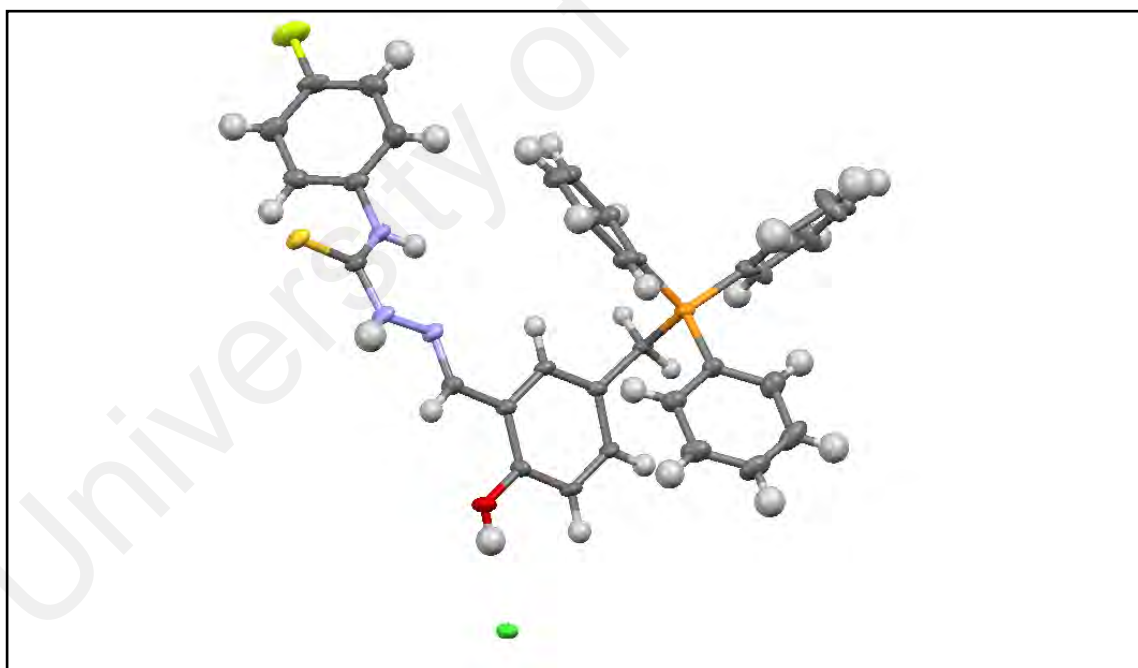


Figure 4.5: ORTEP diagram of C₃₃H₂₈FN₃OPS.Cl [FP(tsc)T]. Thermal ellipsoids are shown at 50 % probability.

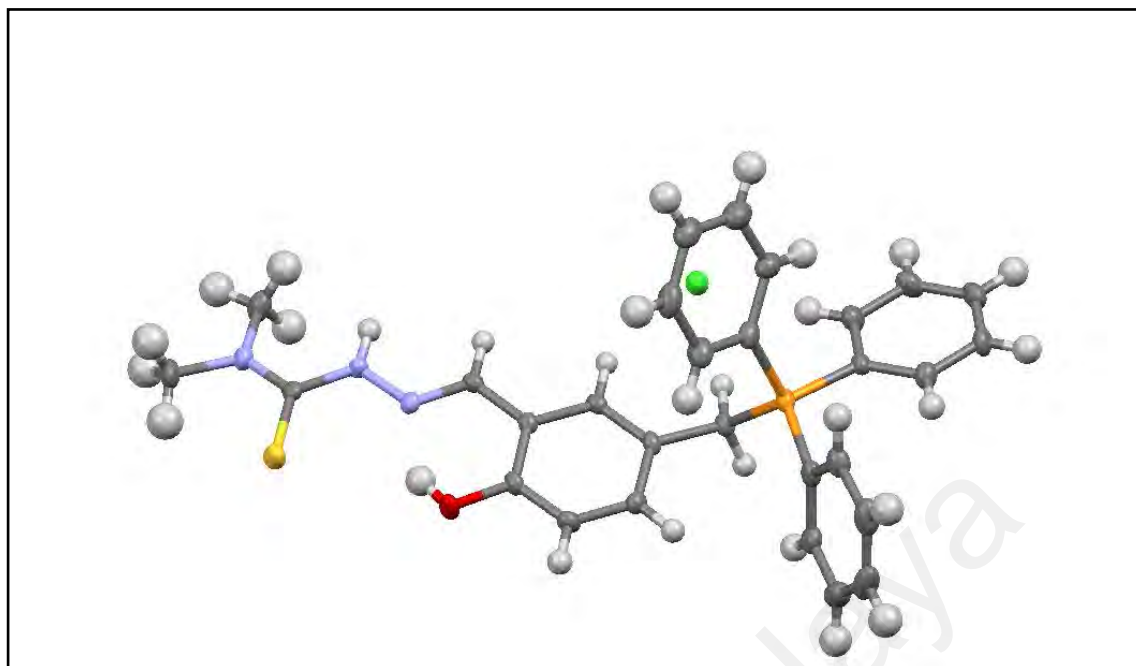


Figure 4.6: ORTEP diagram of C₂₉H₂₉N₃OPS.Cl [DM(tsc)T]. Thermal ellipsoids are shown at 50 % probability.

4.5 Growth inhibitory effect of thiosemicarbazone compounds on human cancer cells as determined by MTT assay

In present study, growth inhibitory effect of the compounds were performed against six human cell lines, namely PC-3 (prostate adenocarcinoma), A549 (non-small cell lung cancer), MCF7 (breast carcinoma), MDA-MB-231 (breast adenocarcinoma), HCT 116 (colorectal carcinoma) and RWPE-1 (prostate normal). Prostate cancer is the second-most frequent diagnosed malignancy globally (R. Siegel et al., 2013). The hormone independent PC-3 cell line which is the more aggressive forms of prostatic adenocarcinoma was tested in present study as their growth are not affected by the absence of androgen (Jayakumar et al., 2014; Tai et al., 2011)

As shown in Table 4.7, out of eight tested compounds, four compounds namely **T**, **(tsc)T**, **E(tsc)T** and **M(tsc)T** showed poor inhibitory effect (IC₅₀ values > 30 μM) against PC-3, MCF7 and A549 cells. These four compounds that showed poor

inhibitory effects were not further tested against MDA-MB-231 and HCT 116 cells. The thiosemicarbazone with ethylphenyl moiety **EP(tsc)T** displayed most potent activity against PC-3 and HCT 116 cells with IC_{50} values of 1.07 ± 0.38 and 0.90 ± 0.10 μM respectively, surpassing that of the positive control cis-platin (IC_{50} value of 5.47 ± 0.06 and 4.8 ± 0.35 μM , respectively). The results in Table 4.7 showed that **EP(tsc)T** exerted least damage to RWPE-1 cells (IC_{50} value of 6.60 ± 0.10 μM ; selectivity index of 6.2 and 7.3 against PC-3 and HCT 116 cells, respectively). It is highly desirable to have a compound that actively kills cancer cells but exerted least damage to the normal cells (Mahavorasirikul et al., 2010). This result suggests thiosemicarbazone with ethylphenyl substituent at N4 atom exerted the highest cytotoxic properties. The value is closely followed by three other N4 substituents, namely **P(tsc)T**, **FP(tsc)T** and **DM(tsc)T** with IC_{50} values of 3.73 ± 0.42 , 2.47 ± 0.12 and 2.64 ± 0.33 μM against PC-3 cells, respectively. Whilst, the same N4 substituents **P(tsc)T**, **FP(tsc)T** and **DM(tsc)T** showed inhibitory properties towards HCT 116 cells with IC_{50} values of 3.00 ± 0.40 , 6.73 ± 0.12 and 3.33 ± 0.70 μM , respectively.

In this study, the results showed that phenyl compound further enhances the cytotoxic properties of the compound. Phenyl group was proven to have cytotoxic activity towards other cancer cell line such as MRC5 fibroblasts and A375 melanoma cells in previous studies (Veselinović et al., 2015). Similarly in another structure and activity study, it showed that presence of phenyl group at N(4) position of 2-hydroxy-5-methoxyacetophenone thiosemicarbazone enhances its antiproliferative activity (Akgemci et al., 2015).

Dimethyl substituent on the other hand was shown to exert *in vitro* cytotoxic properties against human lung cancer cells (DMS-53) and act as an effective inhibitor of tumour growth for DMS-53 tumour xenografts in mice (Yu et al., 2012). In this study,

dimethyl is the only non-phenyl N(4) substituent that exerts good antiproliferative activity. As illustrated in Table 4.7, apart from showing growth inhibition towards PC-3 and HCT 116; **DM(tsc)T** also showed inhibition towards MCF7 and A549 cell lines with IC_{50} values of 19.73 ± 1.50 and 10.80 ± 1.71 μ M, respectively. There is very limited research reporting on enhanced cytotoxicity properties with dimethyl substituent; therefore these encouraging results will give insight to further studies on mechanism action of this new compound.

Fluorouracil unique structure is known to interfere with DNA and RNA replication in cells, and concurrently stops cancer cell growth (An et al., 2007; Arias, 2008; Çetin & Denizli, 2015; Kovács et al., 2015; Mojardín et al., 2013; Silverstein et al., 2011). Fluorouracil is still a widely used antineoplastic agent which plays a major role in treatment of various cancer types such as colorectal, breast, stomach, head and neck cancer (Koyuncu Zeybek et al., 2015). Similarly in this study, **FP(tsc)T** showed good inhibitory towards PC-3, MCF7, MDA-MB-231 and HCT 116 cells.

As **P(tsc)T**, **FP(tsc)T**, **EP(tsc)T** and **DM(tsc)T** exhibited significant inhibitory effect on PC-3 cells with least damage to RWPE-1 cells, thus these four compounds were selected for further investigation on their modes of cell death in PC-3 cells.

Table 4.7: Growth inhibitory effect (IC₅₀ μM) of thiosemicarbazone compounds on human cell lines

Compounds	IC ₅₀ ^A μM (SI) ^D					
	PC-3	MCF7	A549	MDA-MB-231	HCT 116	RWPE-1 ^C
T	> 30	>30	>30	NT ^E	NT	9.70 ± 0.84
(tsc)T	> 30	>30	>30	NT	NT	>30
P(tsc)T	3.73 ± 0.42	5.63 ± 0.93	6.94 ± 0.98	28.47 ± 0.81	3.00 ± 0.40 (1.2)	3.57 ± 0.25
FP(tsc)T	2.47 ± 0.12 (2.0)	10.40 ± 1.06	>30	27.20 ± 0.20	6.73 ± 0.12	4.83 ± 0.06
E(tsc)T	>30	>30	>30	NT	NT	17.11 ± 3.32
EP(tsc)T	1.07 ± 0.38 (6.2)	9.13 ± 0.64	7.53 ± 1.21	6.07 ± 0.92 (1.1)	0.90 ± 0.10 (7.3)	6.60 ± 0.10
M(tsc)T	>30	>30	>30	NT	NT	25.09 ± 2.39
DM(tsc)T	2.64 ± 0.33 (1.5)	19.73 ± 1.50	10.80 ± 1.71	>30	3.33 ± 0.70 (1.2)	3.99 ± 0.15
Cis-platin^B	5.47 ± 0.06 (2.2)	5.10 ± 0.10 (2.4)	4.2 ± 0.79 (2.9)	3.47 ± 0.23 (3.5)	4.80 ± 0.35 (2.5)	12.04 ± 1.63

^AData are presented as mean ± SD from of three independent experiments triplicate for each; ^B Positive control; ^C Non-cancerous cell line;

^DSI= Selectivity Index (normal cells/cancer cells); ^ENT= not tested

4.6 Modes of cell death of selected thiosemicarbazone compounds

In continuation of growth inhibition studies, modes of cell death against PC-3 cells were further investigated. The number of PC-3 cells used was set at 300,000 cells/culture dish in contrast to 3000 cells/well used for MTT assay. In this study, higher number of cells was used in accordance to the protocol set by the product manufacturer and to fulfill the minimum cell number requirements. In all flow cytometric assays, a minimum number of 10,000 events were collected from each individual sample. Therefore, compounds concentrations ranging from 10-100 μM were used instead of IC_{50} concentration as the number of cells has been amplified significantly in contrast to MTT assay. In addition, the study on mode of cell death, the treatment duration of 24, 48 and 72 hours were used instead of just 72 hours as reported in MTT assay. Similar experimental condition has been reported in literatures by Hasinoff *et al.* (2015) to compensate for greater amplification of cells.

In order to distinguish the mode of cell death, morphological changes on the PC-3 cells were assessed using phase-contrast inverted microscope. In this study, the morphological changes in PC-3 cells were pictured at lower magnification of 50x to present a complete picture of the treated cells. Some of the common apoptotic characteristics such as rounding, shrinkage, membrane blebbing, anoikis and loss of cell to cell contacts were monitored between different treatment concentration and durations (Bottone *et al.*, 2013).

AO/EB fluorescent staining was used to identify apoptosis associated changes of cell membranes by visualizing under a fluorescent microscope. Concentrations ranging from 50-100 μM were used for this assay. Compound with 10 μM concentration was omitted as it did not show any significant changes comparing to negative control. Application of this method would help to distinguish cells undergoing different types of cell death. AO is a vital dye, which penetrates an intact cell membrane and emits green

fluorescence if it intercalates into DNA; while EB will only intercalate DNA of the cells that have lost their membrane integrity and emits red fluorescence (Ribble et al., 2005; Zhou et al., 2012). Therefore, this assay is able to distinguish between normal, apoptotic and necrotic cells. AO/EB staining is used to study cell shrinkage, membrane blebbing, membrane bound apoptotic bodies, condensed chromatin and nuclear fragmentation of apoptotic cells. In this study, high magnification of 400x was used to give close up picture of the cells.

In present study, FITC Annexin V is used to quantitatively determine the percentage of cells within a population that are undergoing apoptosis. Compound concentrations ranging from 10-50 μM were used for this assay. 100 μM compound concentration was not tested as 50 μM concentration is sufficient to show significant increase in cells undergoing apoptosis. Annexin V is a calcium-dependent phospholipid binding protein that has a very high affinity for phosphatidylserine and is useful in identifying early apoptotic cells. One of the early characteristic of apoptosis is phosphatidylserine externalization prior to the loss of membrane integrity; hence, Annexin V is a good probe indicating early stage of apoptosis (Ashokkumar et al., 2014; Lee et al., 2014; Rogalska et al., 2013). Propidium iodide (PI) on the other hand is a standard viability probe that is widely used to distinguish viable and non-viable cells. Viable cells with intact membranes will exclude PI whereas the cell with damaged membrane will be stained with PI indicating late apoptosis and/or necrosis. The cells are considered viable when they are both Annexin V negative and PI negative (lower left quadrant), early apoptosis when the cells are Annexin V positive and PI negative (lower right quadrant), where else late apoptosis occurs when the cells are Annexin V positive and PI positive (upper right quadrant) and lastly debris/necrosis occur when the cells are annexin V negative and PI positive (upper left quadrant). This method involves dissolving the cell membrane lipids with non-ionic detergent and eliminating the cell

cytoskeleton. It also dissolves the nuclear protein with trypsin and digests the cellular RNA with an enzyme and finally stabilizes the nuclear chromatin with spermine. In this method, PI is stoichiometrically bound to the clean, isolated nuclei which will be able to electronically discriminate doublets when run on a flow cytometer.

Cell cycle is a set of tightly regulated events that is responsible for the formation of two daughter cells from one cell. Compound concentrations ranging from 10-50 μM were used for this assay. 100 μM concentration was not tested as 10, 30 and 50 μM compound concentrations is sufficient to establish that the cell cycle was arrested at G0/G1 phase. Cell proliferation is dependent on the progression of the cell cycle, which consist of G1 (growth phase 1), S (DNA synthesis phase), G2 (growth phase 2) and M (mitosis phase). The transition from one phase to the next phase is critical as it is tightly controlled by checkpoints. At the G1 checkpoint, a cell ensures that the cell internal and external condition is ready for DNA synthesis. In case a cell does not get to go ahead at the G1 checkpoint; it may enter a resting state called G0 phase. G2 cell cycle checkpoint ensures the DNA condition of cell is fit to enter M phase and lastly M phase ensures that the cell is ready for complete cell division. Cancer cells often deregulate the normal cell cycle checkpoints; thus, cell cycle arrest represents a good opportunity for therapeutic intervention in treating proliferative disease like cancer (Senese et al., 2014). In this assay, PI fluorescence was used as it is proportional to the amount of chromosomal DNA and it allows us to identify different stages in the cell cycle distribution (Ziegler & Groscurth, 2004).

Flow cytometry has emerged as the most popular method for analyzing mitochondrial membrane potential ($\Delta\Psi_m$) in cells which is a hallmark of apoptosis. It is an important parameter of mitochondrial function and has been used as an indicator of cell's health. Compound concentrations ranging from 10-50 μM were used for this assay. 100 μM concentration was not tested as 10, 30 and 50 μM compound

concentrations were sufficient to show the cells are losing its mitochondrial membrane potential. The 5',6,6'-tetrachloro-1,1',3,3'-tetraethylbenzimidazolylcarbocyanine-iodide (JC-1), a cationic fluorescent dye used in this assay, exhibits potential-dependent accumulation in mitochondria, indicated by a fluorescence emission shift from green (~525 nm) to red (~590nm). In healthy cells with high $\Delta\Psi_m$, JC-1 forms complexes known as J-aggregates with intense red fluorescence. On the other hand, in apoptotic or unhealthy cells with low $\Delta\Psi_m$, JC-1 remains in the monomeric form exhibiting green fluorescence. The ratio of red to green fluorescence determines the polarization of the mitochondrial membrane (Perelman et al., 2012).

4.6.1 Modes of cell death with P(tsc)T

Previous studies on structure activity relationship of various 4-phenylhydroxycoumarins against human MRC5 fibroblasts and A375 melanoma cells have shown that phenyl group can be considered as good molecular templates for potential cytotoxic agents (Veselinović et al., 2015). Research carried out by Alam *et al.* (2011) suggested that, an optimum electron density, a substituent bulkiness or a proton donating ability in the C-5 phenyl ring may be closely related for maximum cytotoxic activity against human cancer cell lines such as lung cancer (A549), ovarian cancer (SK-OV-3), skin cancer (SK-MEL-2) and colon cancer (HCT15). In addition, there are studies reported that phenyl groups at N(4) of the thiosemicarbazone moiety are essential contributor to antimalarial activity (Klayman et al., 1979). Soares *et al.* (2012) reported the N(4)-Phenyl-substituted 2-acetylpyridine thiosemicarbazone was highly cytotoxic against human breast cancer (MCF7) and glioma (T98G and U87) cells.

4.6.1.1 Morphological assessment of apoptotic cells by phase-contrast inverted microscope for **P(tsc)T**

Figure 4.7 showed that there were distinctive morphological changes in PC-3 cells after treatment with **P(tsc)T** at concentrations of 10, 30, 50 and 100 μM . The untreated cells (Neg) maintained their original morphology and adhered to the bottom of the culture dish surface. Whilst, treated cells showed common apoptotic characteristics such as rounding, shrinkage, membrane blebbing and loss of cell to cell contacts as reported in the literatures (Bortner & Cidlowski, 2002; Ziegler & Groscurth, 2004). Appearance of apoptotic bodies (floating cells) was more prominent with increased concentration of **P(tsc)T**. This is a process of programmed cell death known as anoikis whereby the cells that detached from the extracellular matrix dies (Liotta & Kohn, 2004).

As exhibited in Figure 4.7, treatment with 10 μM of **P(tsc)T** resulted in reduction of PC-3 cells compared to the untreated cells. The changes observed are rounding and loss of contact with the neighboring cells. With treatment of 50 μM of **P(tsc)T**, the cells loss their original morphology with concomitant reduction in the total cell numbers. Figure 4.7 presented that with 100 μM treatment of **P(tsc)T**, for 72 hours treatment duration, PC-3 cells showed significant reduction in the cell number compared to untreated cells and the presence of apoptotic bodies were more prominent at this concentration. Treatment duration of 24 and 48 hours illustrates that the reduction of cell numbers were only prominent for treatment at the concentration of 50 μM and above which displayed about 50 % reduction in cell number. Meanwhile, for treatment duration of 72 hours, a drastic drop of more than 50 % was observed for treatment concentration of 10 μM .

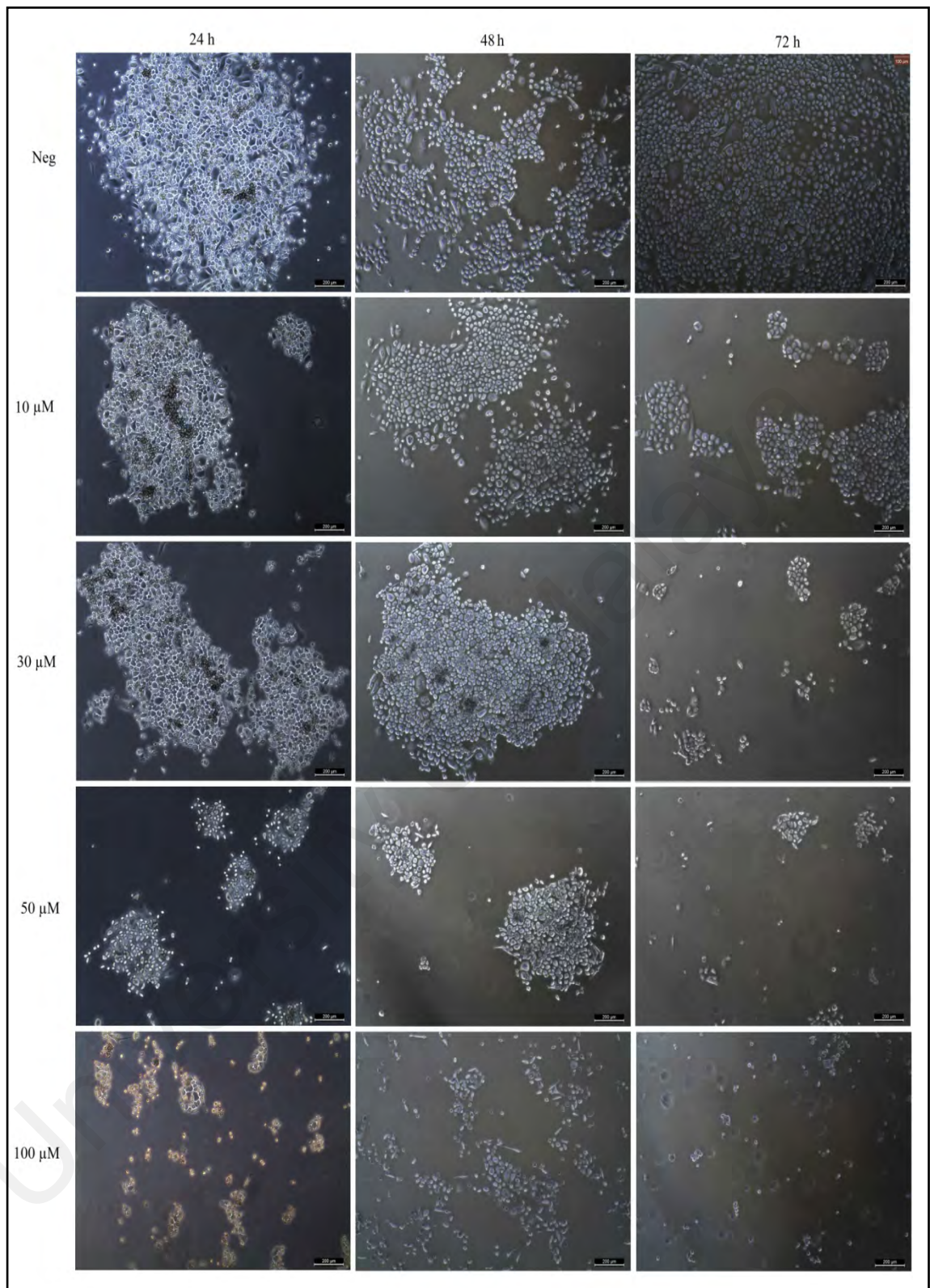


Figure 4.7: Morphological observation of PC-3 cells treated with [P(tsc)T] at concentrations of 10, 30, 50 and 100 μM under phase-contrast inverted microscope (magnification 50x) for 24, 48 and 72 hours. Figure shown were obtained from at least three independent experiments with similar parameters. Neg (untreated cells).

4.6.1.2 Morphological observation of apoptosis cells by fluorescent microscope for **P(tsc)T**

AO/EB fluorescent staining is used to identify apoptosis associated changes of cell membranes by visualizing under a fluorescent microscope. This assay helps to distinguish between normal, apoptotic and necrotic cells.

The result obtained from AO/EB double staining against **P(tsc)T** treated cells is pictured in Figure 4.8. In this study, a magnification of 400x was used to give a clearer picture of the treated cells. The untreated cells (Neg) emit green fluorescent uniformly for 24, 48 and 72 hours, which indicates healthy living cells without any penetration of EB dye. PC-3 cells treated with **P(tsc)T** for 24 hours did not exhibit any chromatin condensation morphology, only a slight membrane blebbing was observed at treatment concentration of 30 μ M. Meanwhile, treatment with the same concentration for 48 and 72 hours duration showed presence of fragmented DNA and condensed chromatin which indicated early apoptosis. Treatment duration of 72 hours for 30 μ M in particular, showed penetration of EB, whereby the nucleus was stained reddish orange, indicating late apoptosis. Treatment at 50 μ M of **P(tsc)T** showed similar apoptotic morphology such as membrane blebbing, chromatin condensation and DNA fragmentation for all three duration as shown in Figure 4.8.

Figure 4.8 showed that treatment with 100 μ M of **P(tsc)T** for 24 hours displayed characteristics of early apoptosis such as membrane blebbing and chromatin condensation. Meanwhile, at the same concentration and duration, some of the cells were stained bright orange which indicated late apoptosis due to EB penetration. Treatment with 100 μ M for 48 and 72 hours showed most of the cells were stained bright orange to red as an indication for late apoptosis and necrosis. Apart from that, most of the cells underwent chromatin condensation and size shrinkage as presented in Figure 4.8. The results were more prominent for 72 hours treatment duration whereby

some of the cells have burst and release its content which is a characteristic of necrosis.

The results showed that **P(tsc)T** exhibited cytotoxic properties in a time- and concentration-dependent manner.

University of Malaya

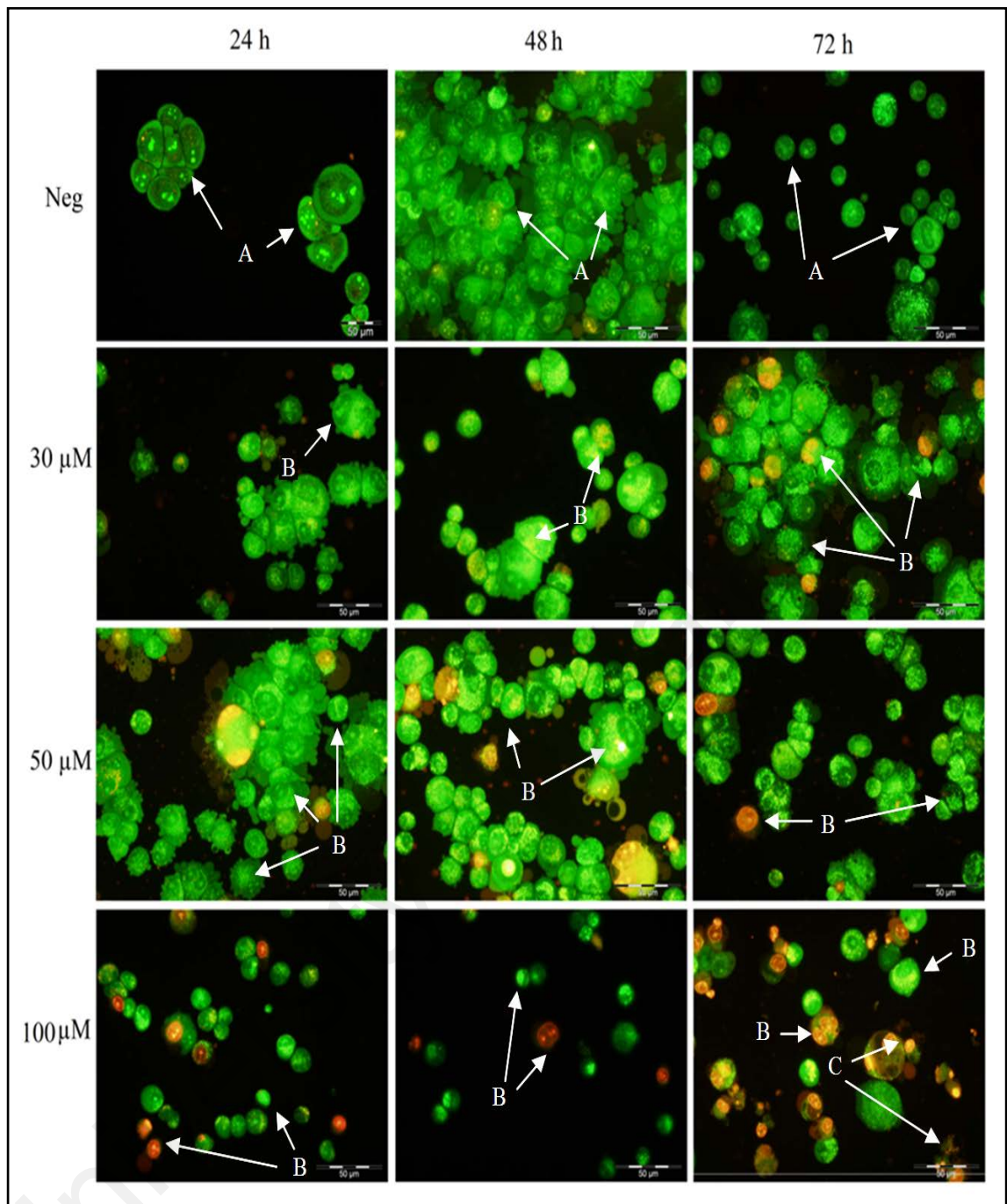


Figure 4.8: Cell death morphological changes in PC-3 cells treated with [P(tsc)T] for 24, 48 and 72 hours detected by AO/EB double staining. The cell morphology was visualized under inverted fluorescent microscope (magnification 400x). Control cells showing normal epithelial morphology followed by cells treated with [P(tsc)T] compound (30, 50 and 100 μM). Arrows indicate (A) live cells, (B) apoptotic cells and (C) necrotic cells. Figure shown represents outcome from at least three experiments with similar parameters. Neg (untreated cells).

4.6.1.3 Annexin V-FITC/PI double staining analysis using flow cytometry for **P(tsc)T**

In present experiment, FITC Annexin V is used to quantitatively determine the percentage of cells within a population that are undergoing apoptosis. Figure 4.9 illustrates flow cytometric results for PC-3 cells treated with **P(tsc)T** at concentrations of 10, 30 and 50 μM for 24, 48 and 72 hours. All the untreated cells (Neg) showed more than 90 % of viable cells when treated for 24, 48 and 72 hours. The percentage of viable cells did not change much in all treatment concentrations (10, 30, and 50 μM) at 24 hours. Even with treatment of 50 μM , the percentage of viable cells was 83.2 % and percentage of apoptotic cells was 16.1 %. The results illustrate that treatment duration of 24 hours is not sufficient to induce cell death when treated with **P(tsc)T**.

Referring to Figure 4.9, at the concentration of 10 μM **P(tsc)T**, there were approximately 10 % drop in the cell viability for 48 hours and a significant drop of approximately 36 % for 72 hours treatment duration. For treatment duration of 48 hours, when the cells were treated with 30 μM **P(tsc)T**, there were approximately 20 % drop in the cell viability and a drastic drop of approximately 40 % when treated with 50 μM **P(tsc)T**. The percentage of viable cells in Q3 quadrant remains approximately the same (30 - 40 %) throughout all concentrations for treatment duration of 72 hours. The percentage of apoptotic cells, for 72 hours treatment duration were approximately 55 % and 5 % of the cells were debris and/or necrosis. The result showed that for treatment duration of 48 hours a minimum of 50 μM **P(tsc)T** is required for 40 % cell apoptosis event to occur. Meanwhile for treatment duration of 72 hours, **P(tsc)T** did not show much increment in apoptotic level when the PC-3 cell were treated with concentration above 10 μM .

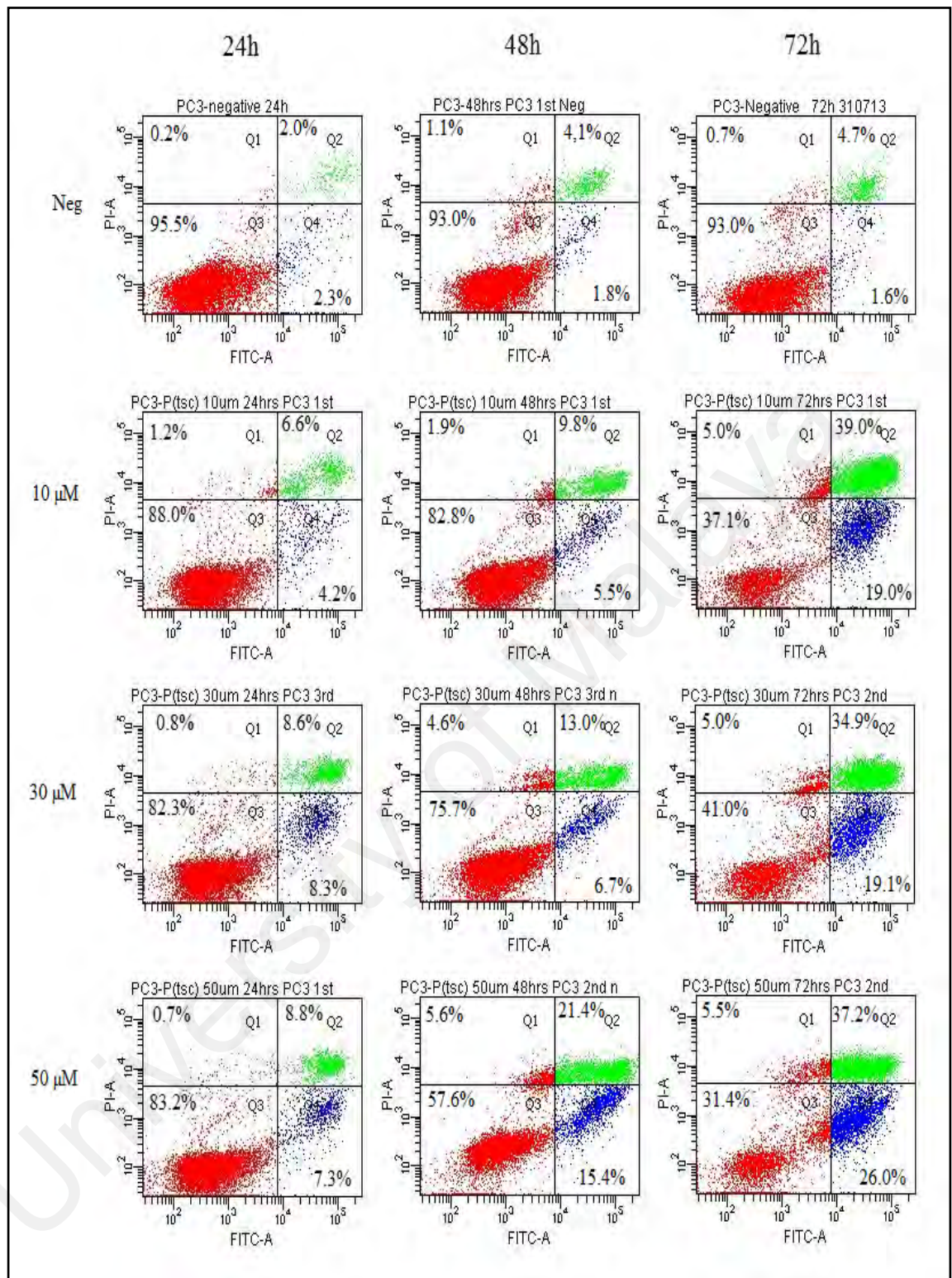


Figure 4.9: Annexin V/PI double staining analysis on PC-3 cells treated with [P(tsc)T] at concentrations of 10, 30 and 50 μM for 24, 48 and 72 hours. Results were analyzed by flow cytometry. At least 10,000 cells were counted in each sample. Neg (untreated cells).

4.6.1.4 Cell cycle analysis using flow cytometry for **P(tsc)T**

This method involves dissolving the cell membrane lipids with non-ionic detergent and eliminating the cell cytoskeleton. It also dissolves the nuclear protein with trypsin and digests the cellular RNA with an enzyme and finally stabilizes the nuclear chromatin with spermine. In this method, PI is stoichiometrically bound to the clean, isolated nuclei which will be able to electronically discriminate doublets when run on a flow cytometer.

Figure 4.10 presents PC-3 cells which was treated with **P(tsc)T** for 24, 48 and 72 hours in order to determine the distribution of cells in different phases of the cell cycle. There is a mild cell cycle arrest observed at S phase for 24 hours treatment. Meanwhile, for 48 and 72 hours treatment, the cell cycle results showed more prominent cell cycle arrest at G₀/G₁ phase. Similarly, some of the established cancer chemopreventive compounds such as resveratrol (trans-3,4',5,-trihydroxystilbene), a phytoalexin found in grapes, nuts, fruits and red wine also elicited inhibition at the G₀/G₁ phase (Ahmad et al., 2001).

Ahmad *et al.* (2001) reported that cyclins and cyclin dependent kinases (cdks) are often associated by forming complexes, which are inhibited by a class of protein known as ckis (INK4 family and CIP/KIP family). This series of event generally halt the progression of cell cycle from G₁ to S phase and thus causing G₁ phase cell cycle arrest. This cell cycle arrest is an irreversible event that will ultimately lead to apoptotic cell death. Metabolic depletion and DNA damage are some of the general reasons that prevents progression from G₁ to S phase (Linke et al., 1996). The results in this study showed prominent cell cycle arrest at G₀/G₁ phase, therefore indicating that **P(tsc)T** most likely inhibits CDK complexes, thus causing apoptosis.

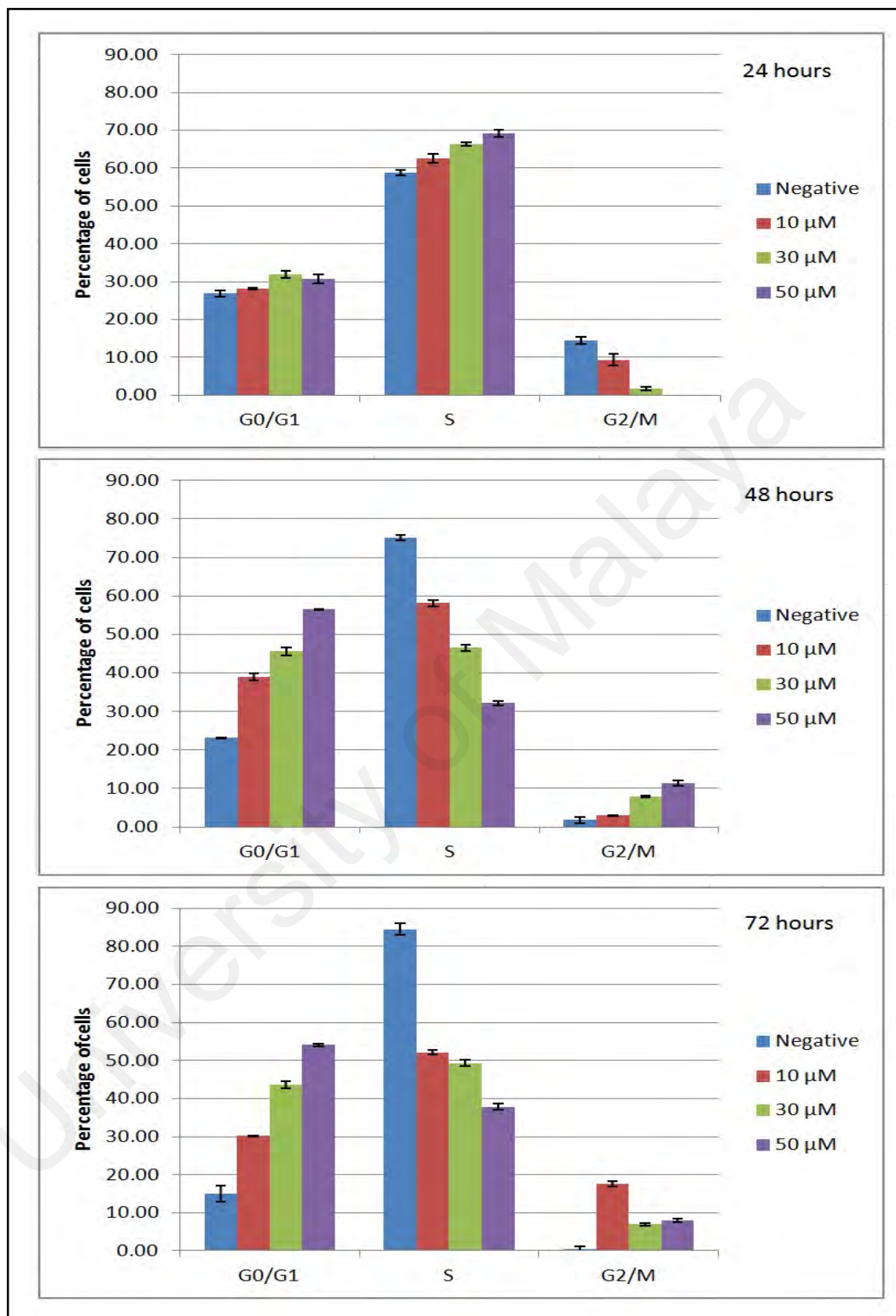


Figure 4.10: Cell cycle arrest analysis on PC-3 cells treated with [P(tsc)T] at concentrations of 10, 30 and 50 μM for 24, 48 and 72 hours. Results were analyzed by flow cytometry. At least 30,000 cells were counted in each sample. Negative (untreated cells).

4.6.1.5 JC-1 Mitochondrial transmembrane potential ($\Delta\Psi_m$) analysis for P(tsc)T

Flow cytometry has emerged as an important parameter to measure mitochondrial membrane potential. The 5',6,6'-tetrachloro-1,1',3,3'-tetraethylbenzimidazolylcarbocyanine-iodide (JC-1), a cationic fluorescent dye used in this assay, exhibits potential-dependent accumulation in mitochondria, indicated by a fluorescence emission shift from green to red.

As illustrated in Figure 4.11, 87.7 % of the cell population showed healthy mitochondria and merely 11.6 % population showed unhealthy mitochondria/apoptosis for 24 hours duration in untreated cells (Negative). Cells treated with P(tsc)T showed a concentration-dependent trend, whereby the cells start to lose its $\Delta\Psi_m$ with increasing concentration of the compound. The depolarized cells increased in an upward trend with increasing concentration of P(tsc)T with 24.2 , 28.7 and 68.5 % for 10, 30 and 50 μM , respectively. The result indicates that the cell death method that is applied by P(Tsc)T might be through the mitochondria mediated intrinsic pathway and with treatment concentration of 50 μM significant effect is observed.

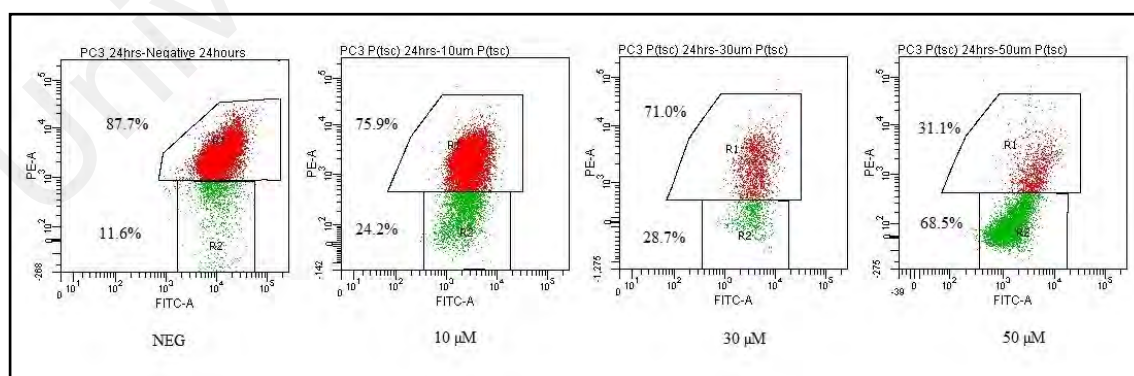


Figure 4.11: Mitochondrial membrane potential analysis against PC-3 cells treated with [P(tsc)T] at concentration of 10, 30 and 50 μM for 24 hours. Results were analyzed by flow cytometry. At least 50,000 cells were counted in each sample. Neg (untreated cells).

4.6.2 Modes of cell death with FP(tsc)T

The role of fluorine atom in enhancing the cytotoxicity of a compound has been exemplified by the advent of fluorouracil (5-FU), an analog of uracil with a fluorine atom at C-5 position in the place of hydrogen. Its unique structure is known to interfere with DNA and RNA replication in cells, and concurrently stops cancer cell growth (An et al., 2007; Arias, 2008; Çetin & Denizli, 2015; Kovács et al., 2015; Mojardín et al., 2013; Silverstein et al., 2011). 5-FU is a widely used antineoplastic agent which played a major role in treatment of various cancer types such as colorectal, breast, stomach, head and neck cancer (Koyuncu Zeybek et al., 2015). The growth inhibitory result in this study (Table 4.7) and vast literature reports suggest that **FP(tsc)T** would be a great candidate to further investigate the modes applied to induce programmed cell death in tumor cells.

4.6.2.1 Morphological assessment of apoptotic cells by phase-contrast inverted microscope for FP(tsc)T

As show in Figure 4.12, there were distinctive morphological changes in PC-3 cells after treatment with **FP(tsc)T** at concentrations of 10, 30, 50 and 100 μM . The untreated cells (Neg) maintained their original morphology and adhered to the bottom of the culture dish surface. Whilst, treated cells showed some common apoptotic characteristics such as rounding, shrinkage, membrane blebbing and loss of cell to cell contacts as reported in the literatures (Bortner & Cidlowski, 2002; Ziegler & Groscurth, 2004).

Treatment with 10 μM of **FP(tsc)T** resulted in slight reduction of PC-3 cells compared to control at treatment duration of 24 and 48 hours. For treatment duration of 24 and 48 hours, reduction of cell number was only prominent for treatment

concentration of 50 μM and above which displayed about 50 % reduction in cell numbers. Meanwhile, at treatment duration of 72 hours, a drastic drop of more than 50 % was observed at the lowest treatment duration of 10 μM . The changes observed are rounding and the loss of contact with the neighboring cells. With treatment of 50 μM of **FP(tsc)T**, the cells lose their original morphology with concomitant reductions in the total cell numbers. In addition, presence of apoptotic bodies was observed at 50 μM treatment concentration. As displayed in Figure 4.12, treatment with 100 μM of **FP(tsc)T** showed significant reduction in the cell numbers compared to untreated cells. Furthermore, the shrinkage of cells and presence of apoptotic bodies were more prominent with 100 μM treatment.

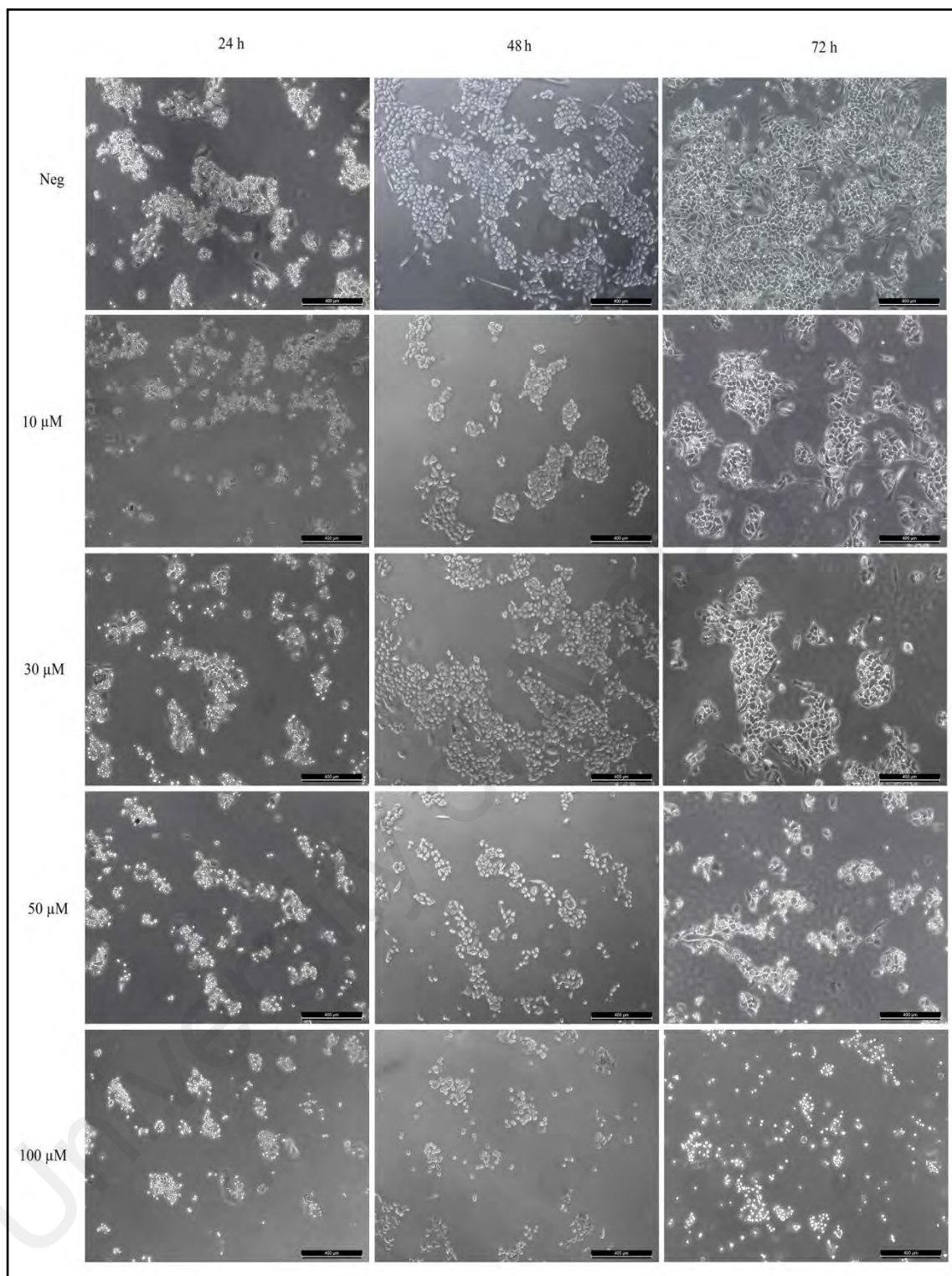


Figure 4.12: Morphological observation of PC-3 cells treated with [FP(tsc)T] at concentrations of 10, 30, 50 and 100 μM under phase-contrast inverted microscope (magnification 50x) for 24, 48 and 72 hours. Figure shown were obtained from at least three independent experiments with similar parameters. Neg (untreated cells).

4.6.2.2 Morphological observation of apoptosis cells by fluorescent microscope for **FP(tsc)T**

The morphological changes of PC-3 cells treated with [**FP(tsc)T**] detected by AO/EB double staining are illustrated in Figure 4.13. The untreated cells (Neg) were stained green uniformly for 24, 48 and 72 hours, which indicate healthy living cells without penetration of EB dye. After 24 hours treatment, the cells did not exhibit any apoptotic morphology with treatment concentration of 30 μ M. Meanwhile, for 48 hours duration, 30 μ M **FP(tsc)T** treatment displayed membrane blebbing characteristics. Figure 4.13 showed that after 72 hours of treatment for same concentration, characteristics of early apoptotic such as membrane blebbing were observed and some of the cells were stained bright orange as indication of late apoptosis. Similar apoptotic characteristics were observed in treatment concentrations of 30 and 50 μ M **FP(tsc)T**.

As illustrated in Figure 4.13, some of the cells were stained bright orange to red as an indication of late apoptosis and necrosis after treatment of 100 μ M **FP(tsc)T** for 24, 48 and 72 hours. Apart from that, most of the cells underwent chromatin condensation and size shrinkage. The results were more prominent for 72 hours treatment duration. Lastly, the results indicated that **FP(tsc)T** exhibited cytotoxic properties in a time and concentration-dependent manner.

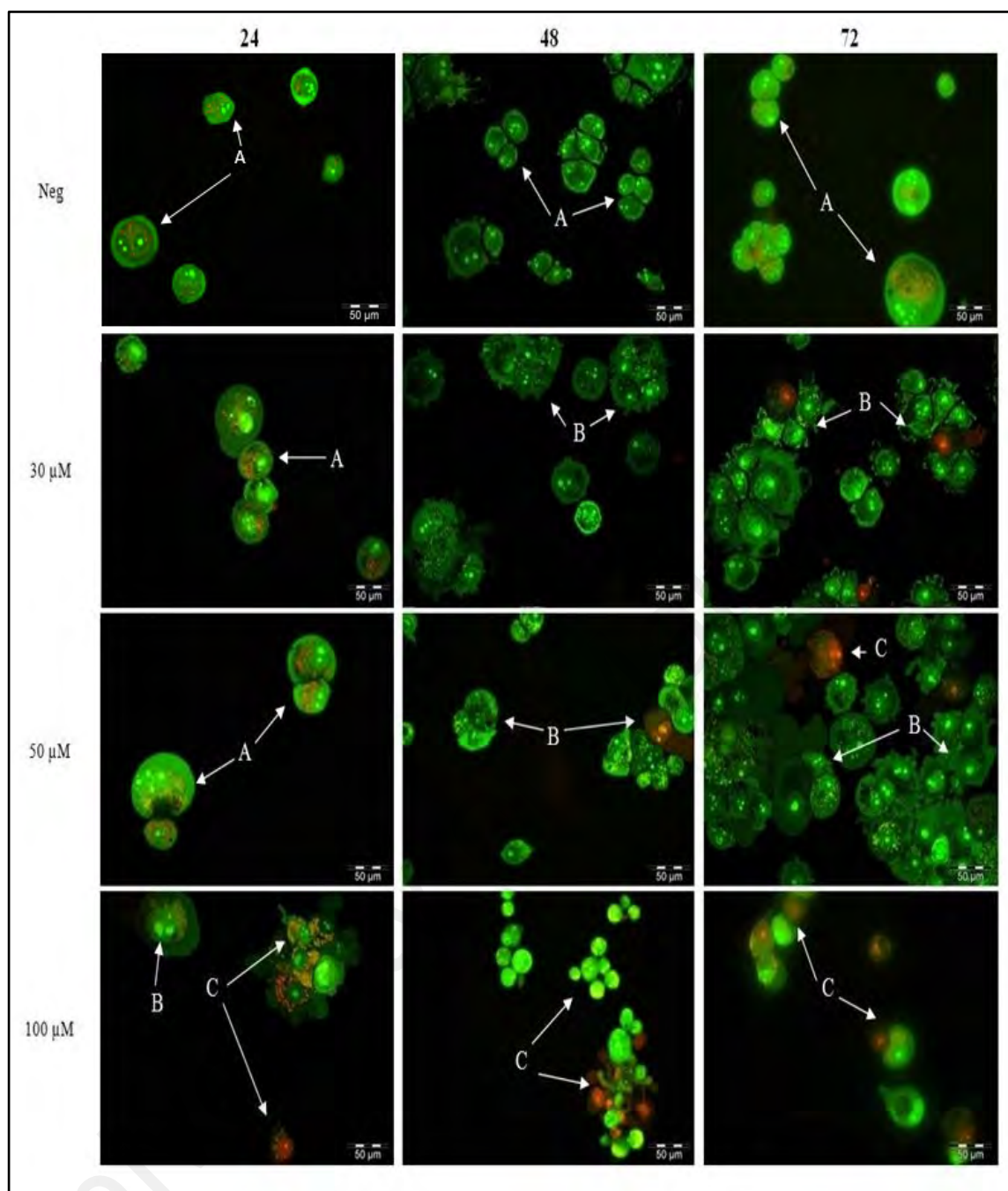


Figure 4.13: Cell death morphological changes in PC-3 cells treated with [FP(tsc)T] for 24, 48 and 72 hours detected by AO/EB double staining. The cell morphology was visualized under inverted fluorescent microscope (magnification 400x). Control cells showing normal epithelial morphology followed by cells treated with [FP(tsc)T] compound (30, 50 and 100 μM). Arrows indicate (A) live cells, (B) apoptotic cells and (C) necrotic cells. Figure shown represents outcome from at least three experiments with similar parameters. Neg (untreated cells).

4.6.2.3 Annexin V-FITC/PI double staining analysis using flow cytometry for **FP(tsc)T**

As illustrated in Figure 4.14, untreated cells (Neg) showed 93 % and above of viable cells. After treatment duration of 24 hours, most of the cells were in lower left quadrant (Q3; AV⁻/PI⁻) which is an indication of viable cells, with percentage of cell viability above 90 % in all tested concentrations (30, 50 and 100 μ M). At 24 hours, there is no significant cytotoxic effect shown. When PC-3 cells were treated with 30 μ M **FP(tsc)T**, there was a minimal drop of approximately 3 % in cell viability for 48 and 72 hours. For treatment duration of 48 hours, cells undergoing early and late apoptosis were only prominent at treatment concentration of 100 μ M which showed about 20 % increase compared to control.

After 72 hours of 50 μ M **FP(tsc)T** treatment, there was an approximately 10 % drop in cell viability. A significant drop of 30 % viable cells was observed after treatment of 100 μ M at same duration, meanwhile cells undergoing early/late apoptosis were about 30 % as well. Taken together, the results clearly indicated that **FP(tsc)T** can only induce significant apoptosis in PC-3 cell with treatment duration of 72 hours and with minimal concentration of 100 μ M.

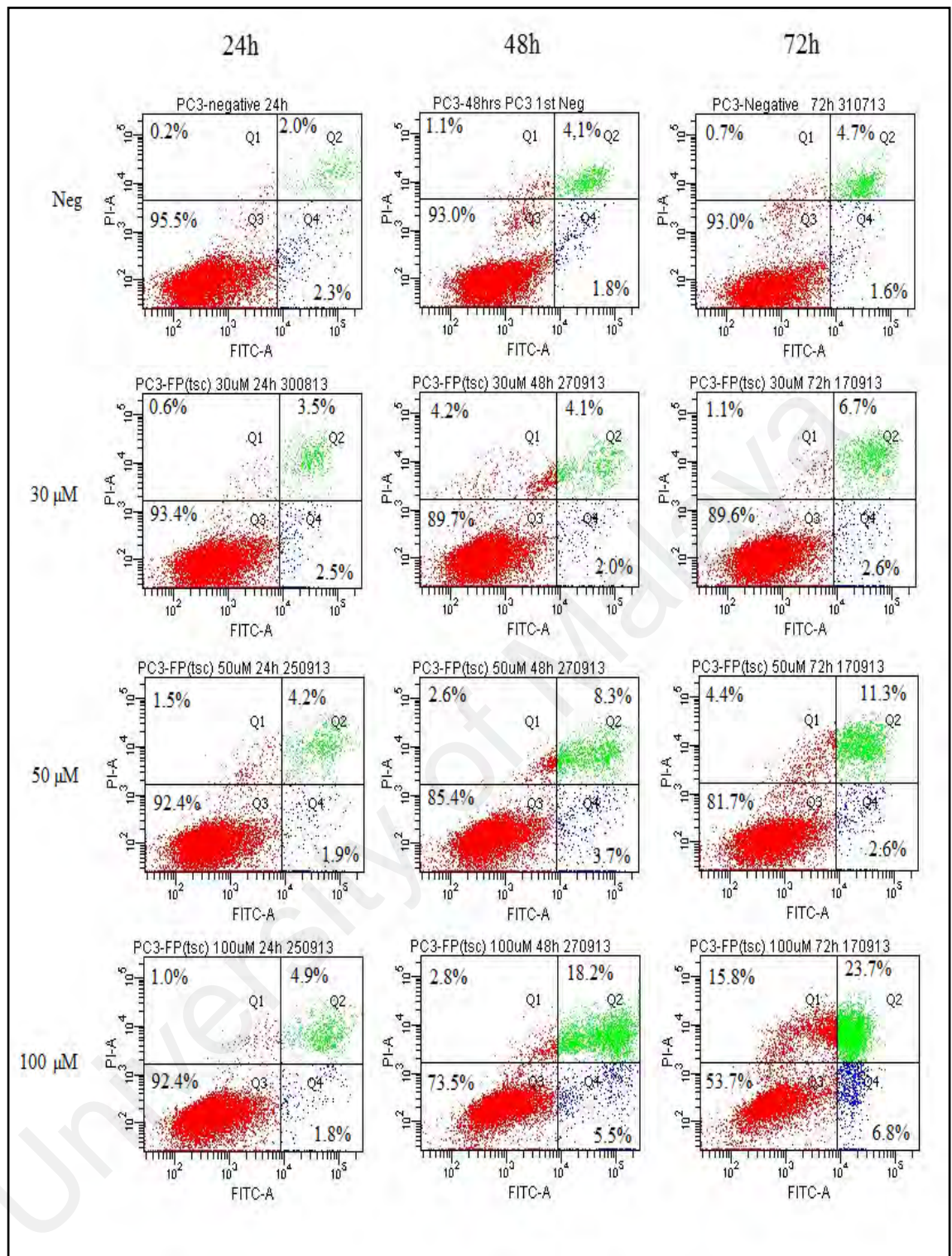


Figure 4.14: Annexin V/PI double staining on PC-3 cells treated with [FP(tsc)T] at concentrations of 30, 50 and 100 μM for 24, 48 and 72 hours. Results were analyzed by flow cytometry. At least 10,000 cells were counted in each sample. Neg (untreated cells).

4.6.2.4 Cell cycle analysis using flow cytometry for FP(tsc)T

Cell cycle analysis was studied in present study to comprehend the influence of **FP(tsc)T** on cell cycle distribution. The PC-3 cells were treated with **FP(tsc)T** for 24, 48 and 72 hours in order to determine the distribution of cells in different phases of the cell cycle. As illustrated in Figure 4.15, the cell cycle was arrested at G0/G1 phase for treatment duration of 24, 48 and 72 hours. Treatment duration of 48 and 72 hours showed that there was reduction in S phase compared with the negative control. As shown in previous reports, some established gold and platinum drugs also showed inhibition at the same phase (Lauková et al., 2015; X. Li et al., 2015; Zhang et al., 2015). The cells arrest at the G0/G1 phase could be due to DNA damage and/or hindrance in the cell growth (Fofaria et al., 2014; Huang et al., 2013). The cell cycle arrest at different phases implies different mechanisms involved in the arrest. Therefore, one of the factor for cell cycle arrest by **FP(tsc)T** could be due to the presence of damaged DNA which hinders cell cycle progression.

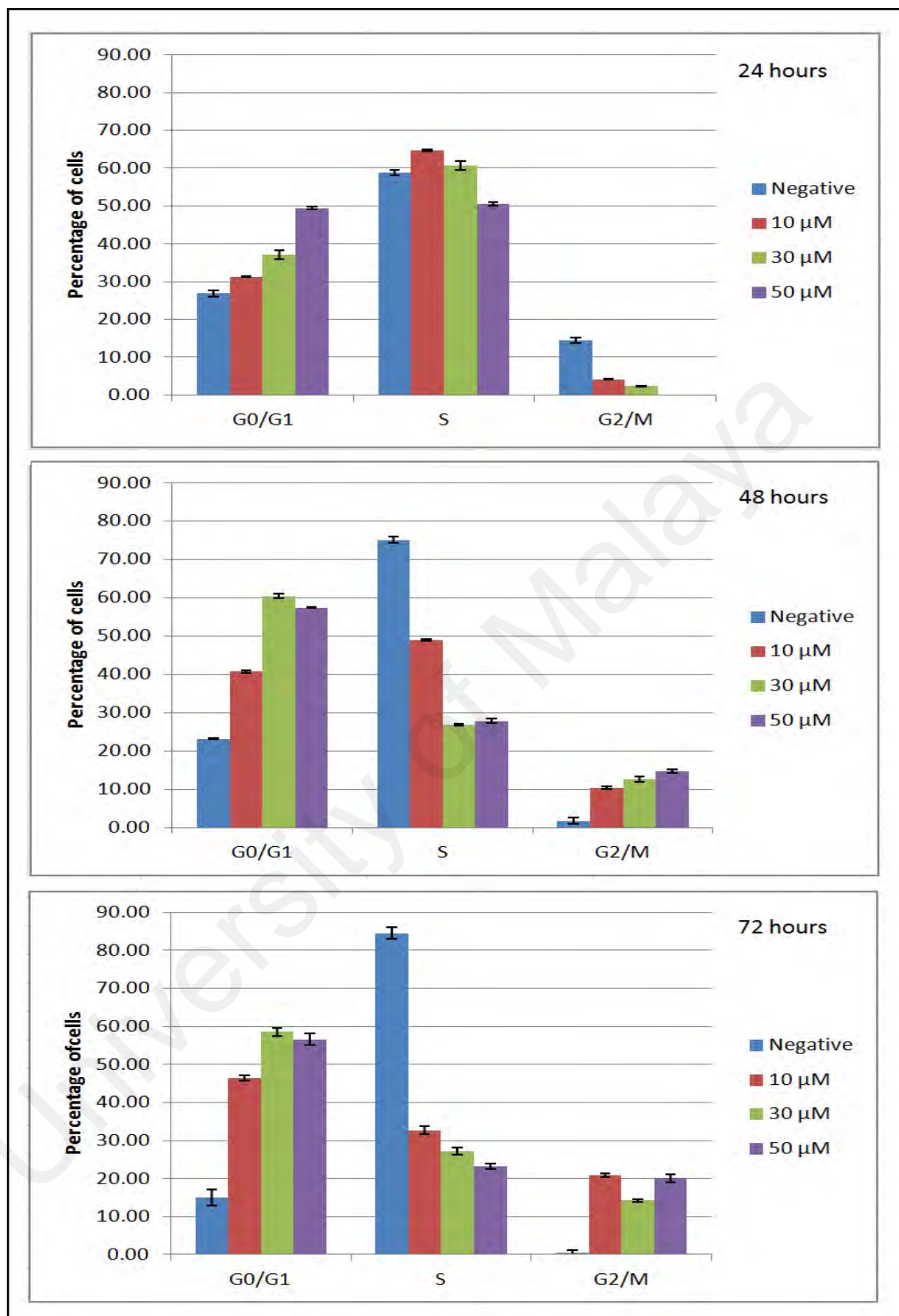


Figure 4.15: Cell cycle analysis against PC-3 cells treated with [FP(tsc)T] at concentrations of 10, 30 and 50 μM for 24, 48 and 72 hours. Results were analyzed by flow cytometry. At least 30,000 cells were counted in each sample. Negative (untreated cells).

4.6.2.5 JC-1 Mitochondrial transmembrane potential ($\Delta\Psi_m$) analysis for FP(tsc)T

Mitochondria-mediated (intrinsic pathway) apoptosis which could be triggered by various apoptotic stimuli is generally known as the functional route for anticancer drugs (Christensen et al., 2013). Generally depolarized mitochondria emits green fluorescence from monomers present in the cytoplasm, whilst polarized mitochondria generally emits red fluorescence from J-aggregates of the dye (Reardon et al., 2014). Figure 4.16 illustrated that 89.9 % of population in untreated cells (Negative) showed healthy mitochondria and merely 9.5 % population showed apoptosis after 24 hours of treatment. When treated with increasing concentrations of FP(tsc)T, the cells start to lose their mitochondrial membrane potential ($\Delta\Psi_m$). As indicated in Figure 4.16, the amount of healthy cells dropped in a concentration-dependent manner. Meanwhile, depolarized cells increased in orderly manner from 11.7 % at 10 μ M, 25.3 % at 30 μ M to 37.2 % at 50 μ M. With the above results taken together, it implies that the cell apoptosis induced by FP(tsc)T might be due to, but not limited to mitochondria mediated pathway.

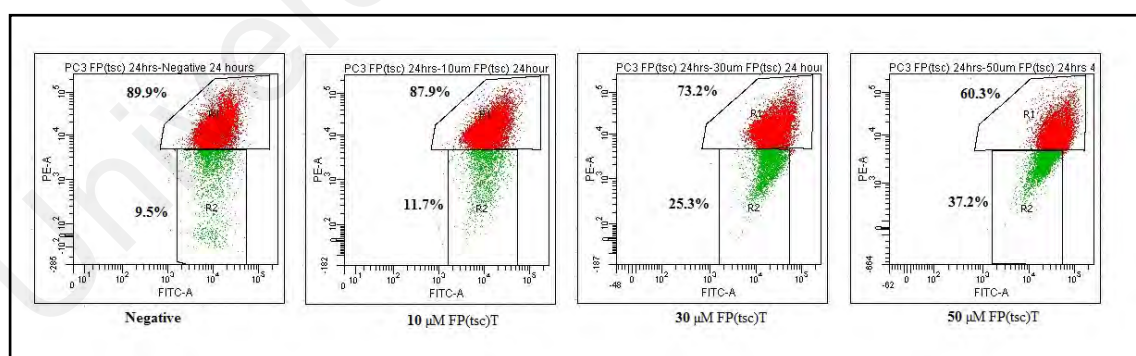


Figure 4.16: Mitochondrial membrane potential analysis against PC-3 cells treated with [FP(tsc)T] at concentrations of 10, 30 and 50 μ M for 24 hours. Results were analyzed by flow cytometry. At least 50,000 cells were counted in each sample. Figure shown represents outcome from at least three experiments with similar parameters. Negative (untreated cells).

4.6.3 Modes of cell death with EP(tsc)T

Literature on ethylphenyl substituent at the N(4) atom of the thiosemicarbazone, particularly in the context of their medicinal uses is sparse, with references being limited to its chemical and physical properties. **EP(tsc)T** displayed the most potent inhibitory effect in this study (Table 4.7), however, research papers are very limited for this compound. Thus, pursuing in detail for this particular compound would give a good insight in drug discovery and development.

4.6.3.1 Morphological assessment of apoptotic cells by phase-contrast inverted microscope for EP(tsc)T

Figure 4.17 illustrates the distinctive morphological changes in PC-3 cells treated with **EP(tsc)T** at concentrations of 10, 30, 50 and 100 μM . The untreated cells (Neg) maintained their original morphology and adhered to the bottom of culture dish. As reported in literatures on apoptosis morphology, cells treated with **EP(tsc)T** showed some common apoptotic characteristics such as rounding, shrinkage, membrane blebbing and loss of cell to cell contacts (Bottone et al., 2013).

Treatment with 10 μM of **EP(tsc)T** resulted in slight reduction of PC-3 cells compared to control at all treatment durations. As illustrated in Figure 4.17, at 24 hours treatment duration, with concentration up to 50 μM , **EP(tsc)T** did not induce much changes to the morphology of PC-3 cells. Whilst, PC-3 cells treated with 50 μM **EP(tsc)T** and above for 48 and 72 hours elicited amplification in appearance of apoptotic bodies (floating cells in culture media) and decrease in cell numbers compared to control. This process is known as anoikis where the cells loose contact with the matrix die (Liotta & Kohn, 2004). On the other hand, treatment with 100 μM of **EP(tsc)T** at all durations showed significant shrinkage of cells and appearance of apoptotic bodies were more prominent with 100 μM treatment.

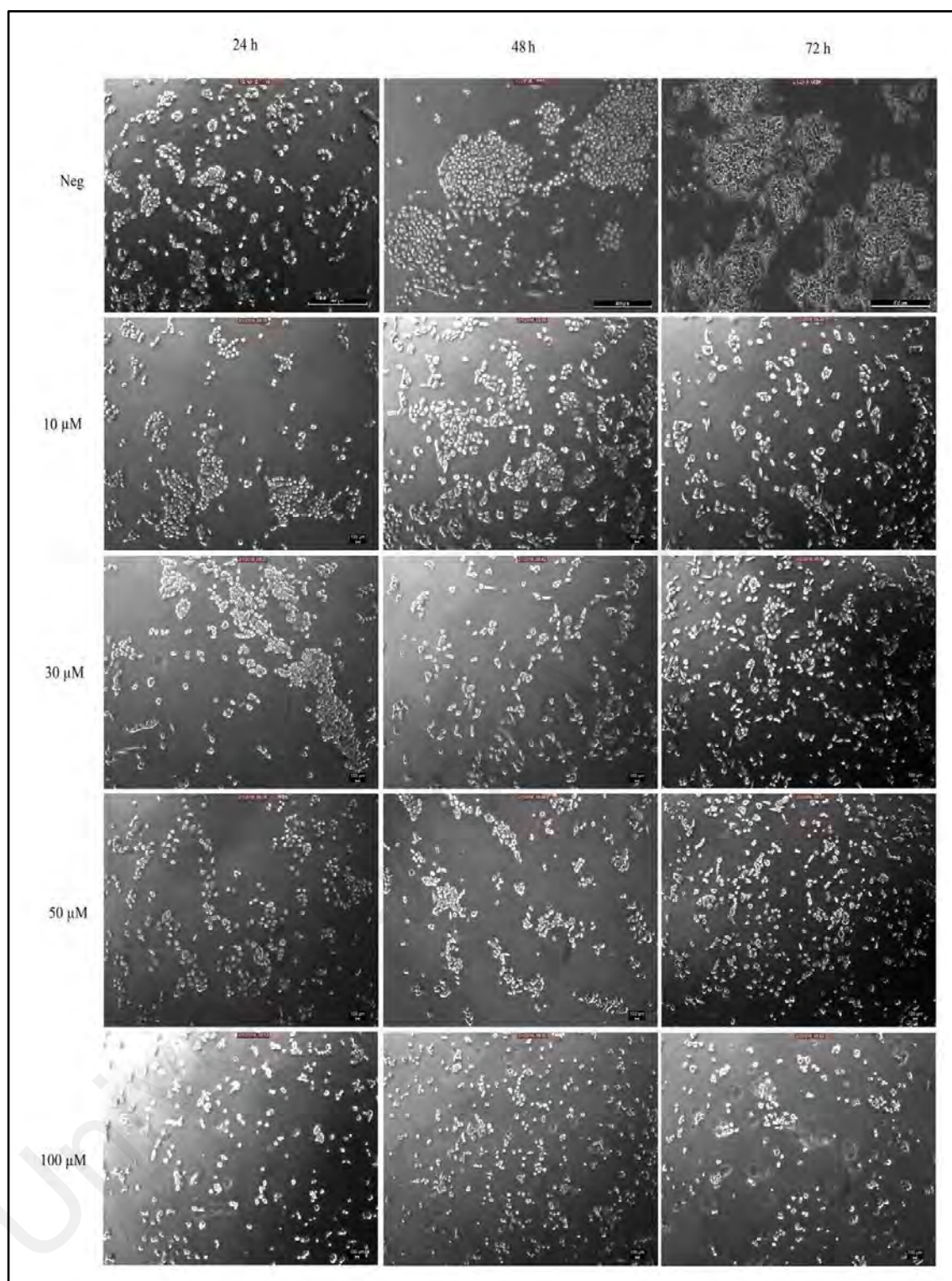


Figure 4.17: Morphological observation of PC-3 cells treated with [EP(tsc)T] at concentrations of 10, 30, 50 and 100 μM under phase-contrast inverted microscope (magnification 50x) for 24, 48 and 72 hours. Figure shown were obtained from at least three independent experiments with similar parameters. Neg (untreated cells).

4.6.3.2 Morphological assessment of cells stained with AO/EB double staining using fluorescent microscope for EP(tsc)T

Some of the common morphological features of apoptosis such as chromatin condensation, nuclear fragmentation, alteration in the size and shape of cells as revealed by fluorescent microscope of EP(tsc)T treated cells were pictured in Figure 4.18. The untreated cells emit green fluorescent uniformly for 24, 48 and 72 hours, which indicates healthy living cells without any penetration of EB dye.

PC-3 cells treated with 30 μ M EP(tsc)T for 24 hours exhibited chromatin condensation and DNA fragmentation morphology. Meanwhile, same concentration of treatment at 48 hours duration showed intercalation of DNA with EB whereby some of the cells were stained reddish orange indicating late apoptosis. Treatment duration of 72 hours at 30 μ M in particular showed more prominent penetration of EB whereby the entire cell nucleus was stained reddish orange. A similar condition was observed for treatment at 50 μ M EP(tsc)T throughout all duration as shown in Figure 4.18. Characteristics of late apoptotic was observed when the cells were treated with 100 μ M of EP(tsc)T for 24 hours whereby some of the cells were stained bright orange as indication of late apoptosis due to EB penetration. Most of the cells were stained bright orange as an indication of late apoptosis and necrosis after treatment with 100 μ M for 48 and 72 hours. Apart from that, presence of apoptotic bodies and size shrinkage were more prominent as presented in Figure 4.18. For the same treatment duration and concentration, some of the cells have ruptured membrane and released their content which is characteristic of necrosis. The results signifies that EP(tsc)T exhibited strong cytotoxic properties even with merely 30 μ M treatment concentration.

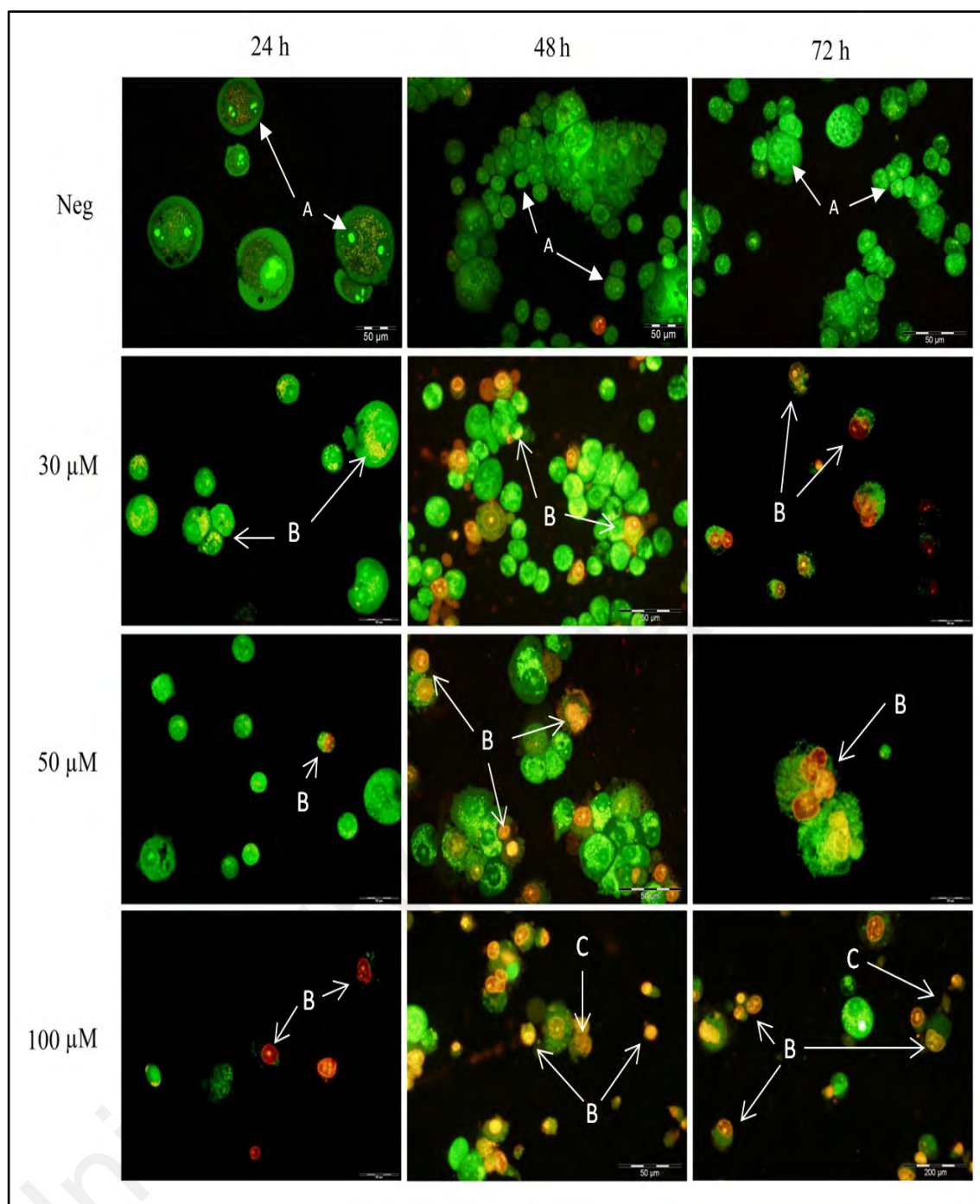


Figure 4.18: Cell death morphological changes in PC-3 cells treated with [EP(tsc)T] for 24, 48 and 72 hours detected by AO/EB double staining. The cell morphology was visualized under inverted fluorescent microscope (magnification 400x). Control cells showing normal epithelial morphology followed by cells treated with [EP(tsc)T] compound (30, 50 and 100 μM). Arrows indicate (A) live cells, (B) apoptotic cells and (C) necrotic cells. Figure shown represents outcome from at least three experiments with similar parameters. Neg (untreated cells).

4.6.3.3 Annexin V-FITC/PI double staining analysis using flow cytometry for **EP(tsc)T**

As shown in Figure 4.19, all untreated cells (Neg) showed percentage of viable cells of above 90 %. Surprisingly, **EP(tsc)T** did not show any apoptotic effect in PC-3 cells after treatment duration of 24 hours. At 24 hours, most of the cells were in lower left quadrant (Q3; AV⁻/PI⁻) with percentage of cell viability above 90 % at all concentrations (30, 50 and 100 μ M) tested. At 48 hours, PC-3 cells which underwent early and late apoptosis were only prominent with treatment concentration of 50 μ M. Significant drop of approximately 40 % of viable cells was observed meanwhile cells undergoing early/late apoptosis were about 40 % as well for the same treatment duration and concentration.

At 72 hours treatment duration, there is an approximately 10 % drop in cell viability for treatment of 10 μ M **EP(tsc)T**, followed by 30 % drop in cell viability for 30 μ M. Significant drop of approximately 70 % viable cells in comparison to untreated cells was observed with treatment of 50 μ M for the same duration, meanwhile cells undergoing early/late apoptosis were about 65 %. Taken together, the results clearly indicated that **EP(tsc)T** can induce significant apoptosis in PC-3 cells with treatment duration of 72 hours and minimal concentration of 30 μ M **EP(tsc)T**.

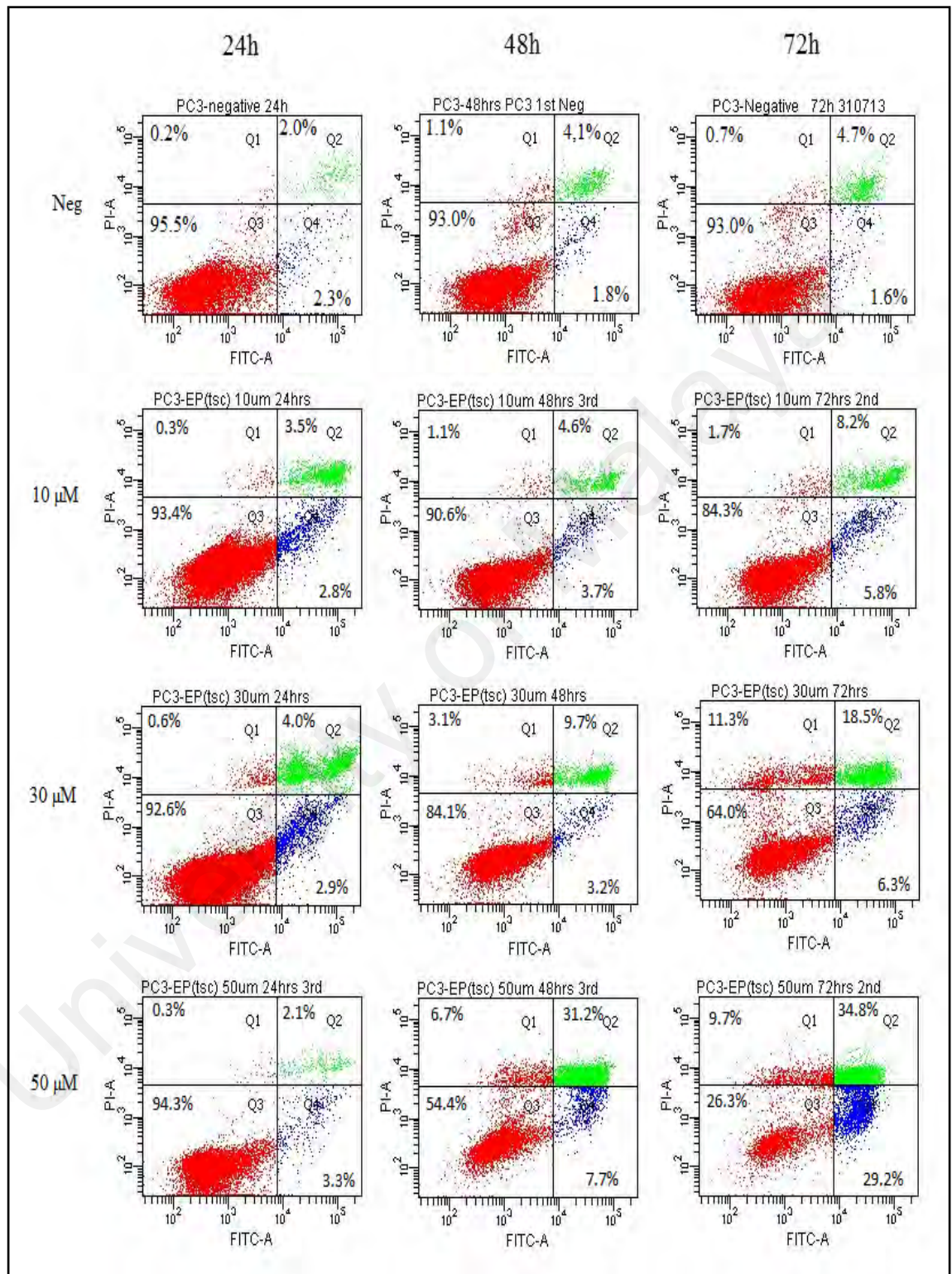


Figure 4.19: Annexin V/PI double staining analysis on PC-3 cell lines treated with [EP(tsc)T] at concentrations of 10, 30 and 50 μ M for 24, 48 and 72 hours. Results were analyzed by flow cytometry. At least 10,000 cells were counted in each sample. Neg (untreated cells).

4.6.3.4 Cell cycle analysis using flow cytometry for EP(tsc)T

As illustrated in Figure 4.20, the cell cycle results showed gradual cell cycle arrest at the G0/G1 phase for all the three durations tested. The results were more prominent with longer treatment duration. Cell cycle progression can be arrested under conditions that are not suitable for DNA replication, including nutrient depletion, DNA damage and growth factor withdrawal (Jones et al., 2005). Similarly, established antitumor compound metformin induces G0/G1 phase arrest as well. Cyclin and Cyclin dependent kinases complexes are essential for driving the cells across the checkpoints in cell cycle, thus compounds that could activate its suppressor such as p53 and protein known as ckis (INK4 family and CIP/KIP family) would prevent inappropriate activity in the cell (Cai et al., 2015). Cell cycle regulatory functions in cancer cells are usually impaired; hence arresting cell cycle progression might be an effective strategy in preventing proliferation of cancer cells.

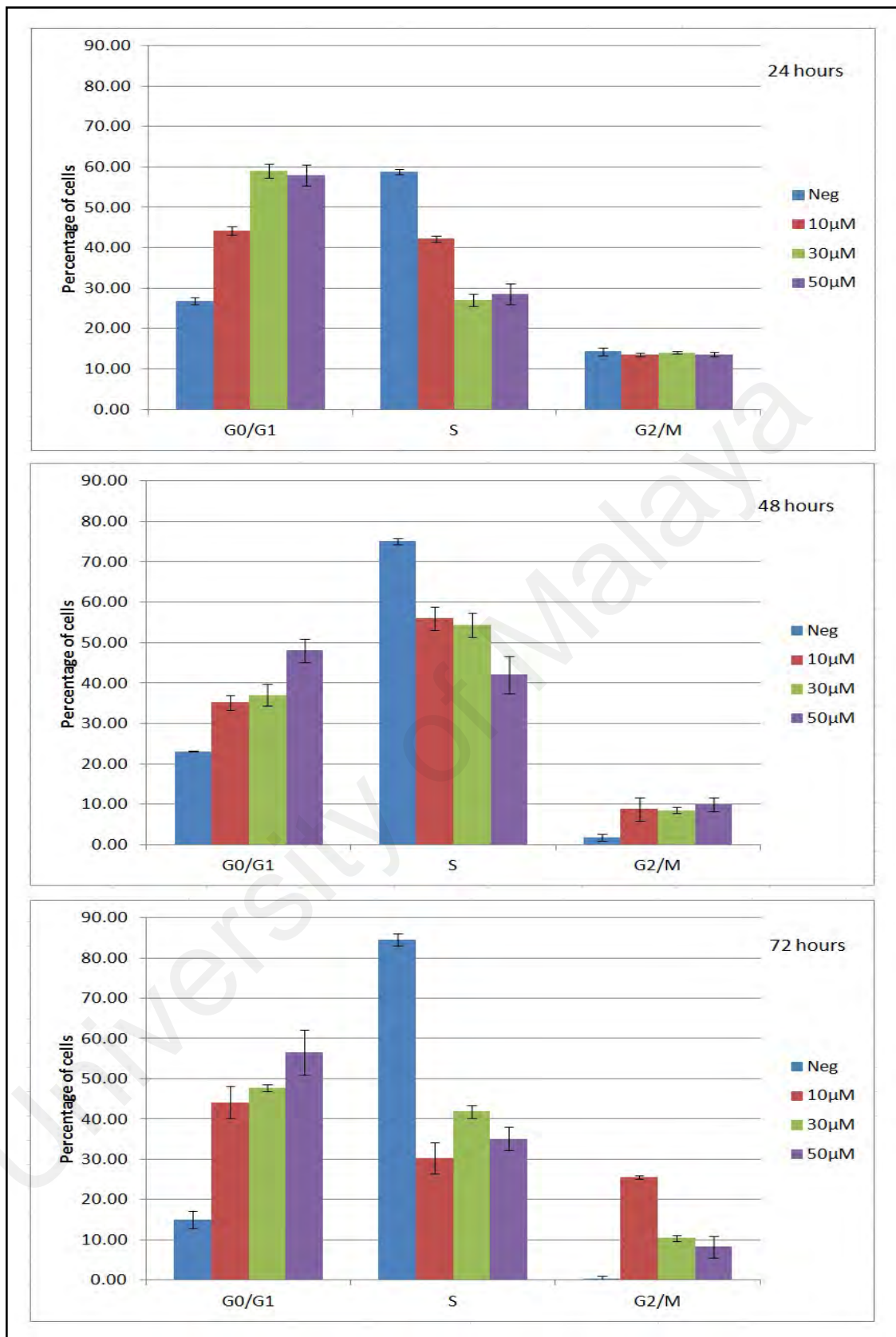


Figure 4.20: Cell cycle arrest analysis by flow cytometry in PC-3 cells treated with [EP(tsc)T] at concentration of 10, 30 and 50 μM for 24, 48 and 72 hours. Results were analyzed by flow cytometry. At least 30,000 cells were counted in each sample. Results are the mean ± SD from three independent experiments. Neg (untreated cells).

4.6.3.5 JC-1 Mitochondrial transmembrane potential ($\Delta\Psi_m$) analysis for EP(tsc)T

As pictured in Figure 4.21, 87.7 % of the population in untreated cells (NEG) emits red fluorescent indicating healthy mitochondria; while only 11.6 % cells were unhealthy. When the cells were treated with increasing concentrations of EP(tsc)T, the cells lost their mitochondrial membrane potential ($\Delta\Psi_m$). The amount of polarized cells showed a drastic drop of healthy cells from 73.1, 52.4 to 40.3 % at increasing concentrations from 10, 30 to 50 μM , respectively. Meanwhile, depolarized cells increased in orderly manner from 11.7 % at 10 μM , 25.3 % at 30 μM and 37.2 % at 50 μM . The result assures that the cell death pathway applied by EP(tsc)T could be through the mitochondrial mediated intrinsic pathway.

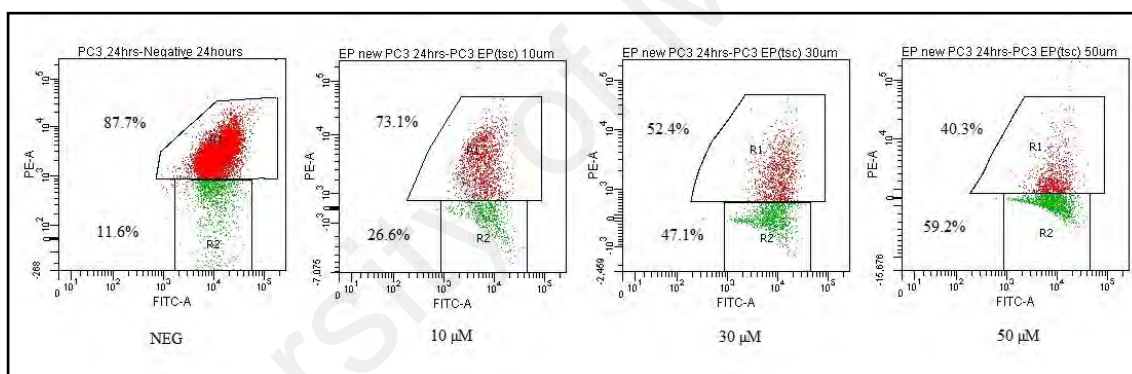


Figure 4.21: Mitochondrial membrane potential analysis against PC-3 cells treated with [EP(tsc)T] at concentrations of 10, 30 and 50 μM for 24 hours. Results were analyzed by flow cytometry. At least 50,000 cells were counted in each sample. Figure shown represents outcome from at least three experiments with similar parameters. Neg (untreated cells).

4.6.4 Modes of cell death analysis with DM(tsc)T

Schiff bases from the thiosemicarbazones family having a substituent at the N4 atom, are known to show enhanced cytotoxic properties (Pervez et al., 2011). Structure activity relationships of the ligands showed that dimethylation of the terminal NH₂ group enhance the cytotoxic properties by 300 – 700-folds (Kowol et al., 2009). Thiosemicarbazone ligand, di-2-pyridylketone 4,4-dimethyl-3-thiosemicarbazone (Dp44mT) and its analog were shown to have potent *in vitro* and *in vivo* antitumor activity (Anand et al., 2015) and possess marked antimetastatic properties. This drug accumulates within lysosomes where it could form a redox-active metal complex that mediates lysosomal membrane permeabilization and consequently inducing apoptosis (Jansson et al., 2015). In addition, the ligand is also known to inhibit the rate limiting step of DNA synthesis which is catalyzed by ribonucleotide reductase causing inhibition of cell proliferation. Previous reports showed that this ligand could up-regulate N-myc downstream regulated gene 1 which results in metastasis suppression (Kovacevic et al., 2016; Merlot et al., 2015). Yuan *et al.*, (2004) reported that Dp44mT is a great cytotoxic agent with activity comparable with antitumor agent doxorubicin. This ligand significantly reduces the tumor weight by 47 % for *in vivo* studies using mice (J. Yuan et al., 2004). Furthermore, Lukmantara *et al.*, (2014) reported that complexation of the chelator ligand with Fe results in 2 to 20 fold decrease in antiproliferative activity compared to the free ligand. This could be attributed to their inability to chelate intracellular Fe that is required for DNA synthesis. With all the burgeoning reports on the effectiveness of dimethyl substituted ligand, this ligand will definitely be worth to further access on its potential mode of cell death.

4.6.4.1 Morphological assessment of apoptotic cells by phase-contrast inverted microscope for **DM(tsc)T**

PC-3 cells treated with **DM(tsc)T** were examined for morphology changes and photographs were taken. The result shown in Figure 4.22 exhibited that there were distinctive morphological changes in PC-3 cells after treatment with **DM(tsc)T**. The control cells (Neg) maintained their original morphology (judging by ATCC image), cell numbers and adhered to the bottom of the culture dish surface. **DM(tsc)T** treated cells showed apoptotic characteristics such as rounding, shrinkage, membrane blebbing and loss of cell to cell contacts as reported in the literature. Higher treatment concentration of 50 μM and above elicited amplification in appearance of apoptotic bodies (floating cells in culture media) and decrease in cell numbers compared to control. According to Liotta and Kohn (2004), this is a process called anoikis where the cells that lose contact with the matrix die.

As shown in Figure 4.22, treatment with 10 μM **DM(tsc)T** resulted in significant reduction of about 50 % of cell number compared to control. The changes observed are rounding and loss of contact with neighboring cells. With treatment of 50 μM **DM(tsc)T**, the cells lose their original morphology with concomitant reductions in the total cell numbers. Treatment with 100 μM **DM(tsc)T** caused losing of cell to cell contact and common characteristics of apoptosis such as shrinkage and rounding were observed. Presence of apoptotic bodies were observed with treatment duration of 50 μM and above.

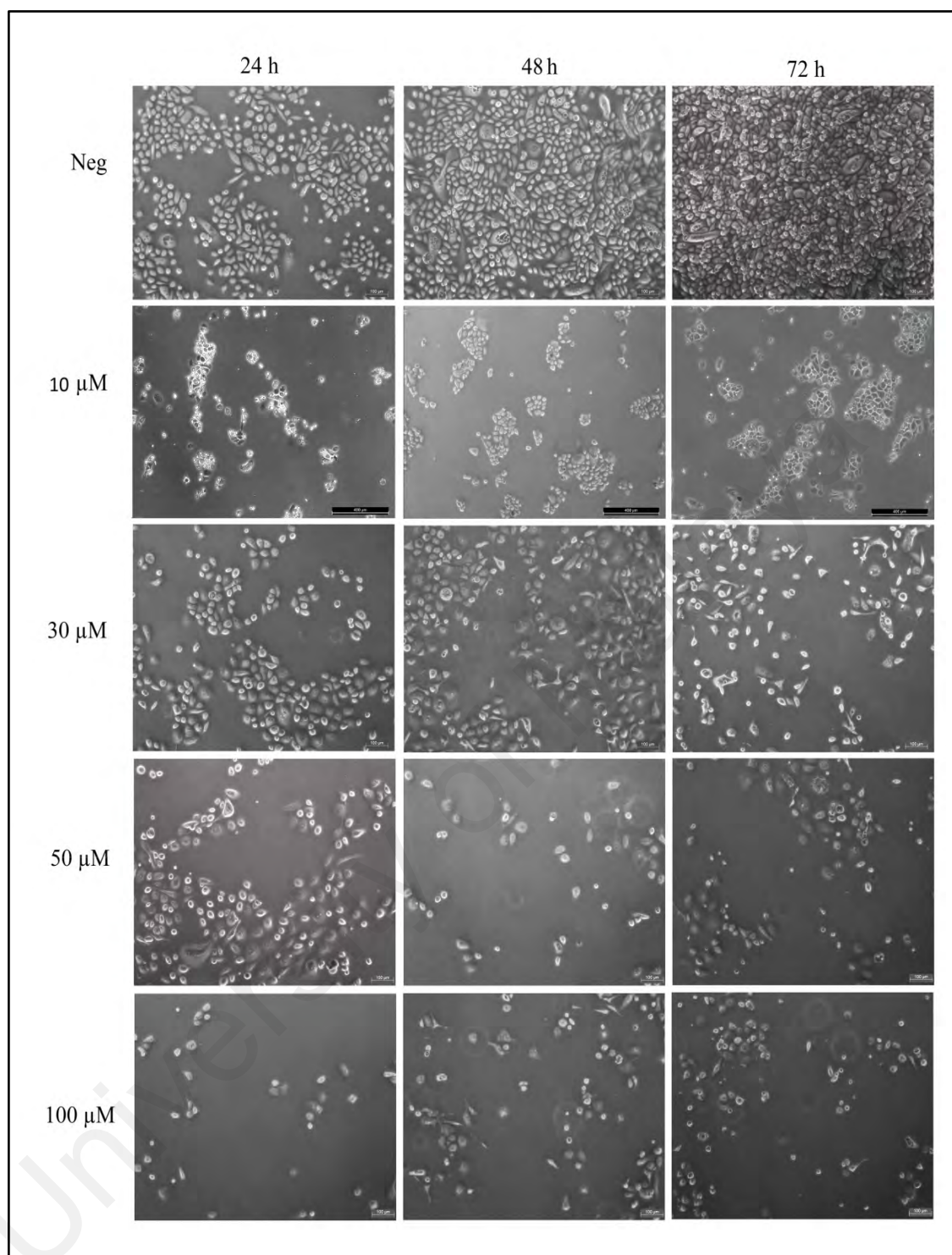


Figure 4.22: Morphological observation of PC-3 cells treated with [DM(tsc)T] at concentrations of 30, 50 and 100 μM under phase-contrast inverted microscope (magnification 50 x) for 24, 48 and 72 hours. Figure shown represents results obtained from at least three independent experiments with similar parameters. Neg (untreated cells).

4.6.4.2 Morphological assessment of cells stained with AO/EB staining using fluorescent microscope for DM(tsc)T

In cell death induction, cell death by apoptosis is preferred over necrosis; as apoptosis is a step wise well organized cell death that seldom results in inflammation, while necrotic cell death is caused by external injury and almost always results in inflammation (Amaravadi & Thompson, 2007; Okada et al., 2004). AO/EB staining is used to study cell shrinkage, membrane blebbing, membrane bound apoptotic bodies, condensed chromatin and nuclear fragmentation of apoptotic cells.

As illustrated in Figure 4.23, the cells treated with **DM(tsc)T** for 24, 48 and 72 hours showed morphological changes compared to untreated cells (Neg). The untreated cells appeared to be intact and rounded in shape with their normal morphology. They were stained green uniformly for 24, 48 and 72 hours, which is an indication of healthy living cells without any penetration of EB dye. Late apoptosis/ necrosis cells were stained bright orange to red due to EB dye penetration. **DM(tsc)T** exhibited cytotoxic properties in a time- and concentration-dependent manner.

Cells treated with 30 μM **DM(tsc)T** for 24 and 48 hours showed chromatin condensation whereby the nucleus clumped together and aggregated at a corner of the cells; meanwhile, treatment for 72 hours showed chromatin condensation and loss of membrane integrity. Membrane blebbing was observed in 50 μM treatment with **DM(tsc)T** after 24 hours. Figure 4.23 showed treatment with 50 μM **DM(tsc)T** for 48 and 72 hours causes some PC-3 cells to undergo late apoptosis. With treatment of 100 μM **DM(tsc)T** at all three durations, most of the cells were stained bright orange to red, which are characteristics of late apoptosis and/or necrosis. These results were more prominent in the cells treated with duration of 48 and 72 hours.

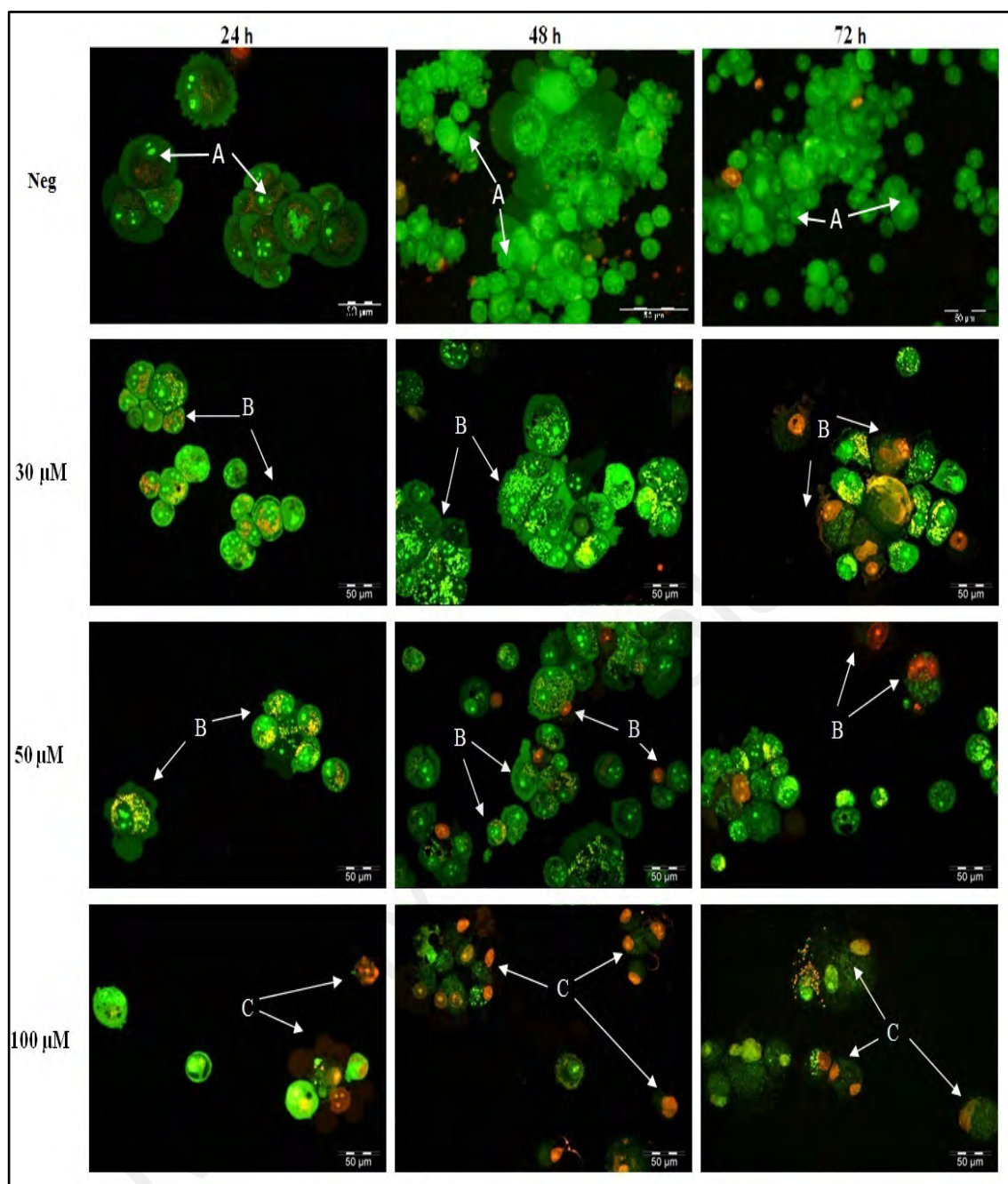


Figure 4.23: Cell death morphological changes in PC-3 cells treated with [DM(tsc)T] for 24, 48 and 72 hours detected by AO/EB double staining. The cell morphology was visualized under inverted fluorescent microscope (magnification 400x). Control cells showing normal epithelial morphology followed by cells treated with [DM(tsc)T] compound (30, 50 and 100 μM). Arrows indicate (A) live cells, (B) apoptotic cells and (C) necrotic cells. Figure shown represents outcome from at least three experiments with similar parameters. Neg (untreated cells).

4.6.4.3 Annexin V-FITC/PI double staining study using flow cytometry for **DM(tsc)T**

Figure 4.24 illustrates flow cytometric results for PC-3 cells treated with **DM(tsc)T** at various concentrations and duration. The results showed that **DM(tsc)T** exhibited cytotoxic properties in concentration- and time-dependent manner. All the untreated cells (Neg) showed percentages of viable cells of more than 90 % for 24, 48 and 72 hours. Referring to Figure 4.24, at the concentration of 30 μM **DM(tsc)T**, most of the cells were in the lower left quadrant (Q3; AV⁻/PI⁻) which is an indication of viable cells with the percentage of cells that were alive 92.9 , 83.1 and 85.2 % for 24, 48 and 72 hours, respectively. The result showed that when the cells were treated with 30 μM **DM(tsc)T**, there were approximately 10 % drop in the cell viability for 48 and 72 hours. As illustrated in Figure 4.24, the percentage of viable cells in the Q3 quadrant were reduced to 87.4 , 84.0 and 74.4 % for 24, 48 and 72 hours respectively, upon treatment with 50 μM **DM(tsc)T**.

At the concentration of 100 μM **DM(tsc)T** for all the durations, it can be observed that most of the spots in the Q3 quadrant have moved to the right quadrant; (Q2; AV⁺/PI⁻) and (Q4; AV⁺/PI⁺) that show cells undergoing late apoptosis and early apoptosis respectively. The result in Figure 4.24 shows that the diminution of cell viability was observed with prolonged treatment duration. For treatment duration of 24 hours, a minimum concentration of 100 μM is required to show significant drop in percentage of viable cells as shown in Figure 4.24. Treatment at 30 and 50 μM for 48 hours did not show much change in early and late apoptotic cells. Treatment with 100 μM of **DM(tsc)T** showed approximately 30 % reduction in cell viability compared to the untreated cells for both 24 and 48 hours, meanwhile approximately 50 % decrease in cell viability were observed for 72 hours. Taken together the results clearly indicated that **DM(tsc)T** has great potential in inducing apoptosis in PC-3 cell.

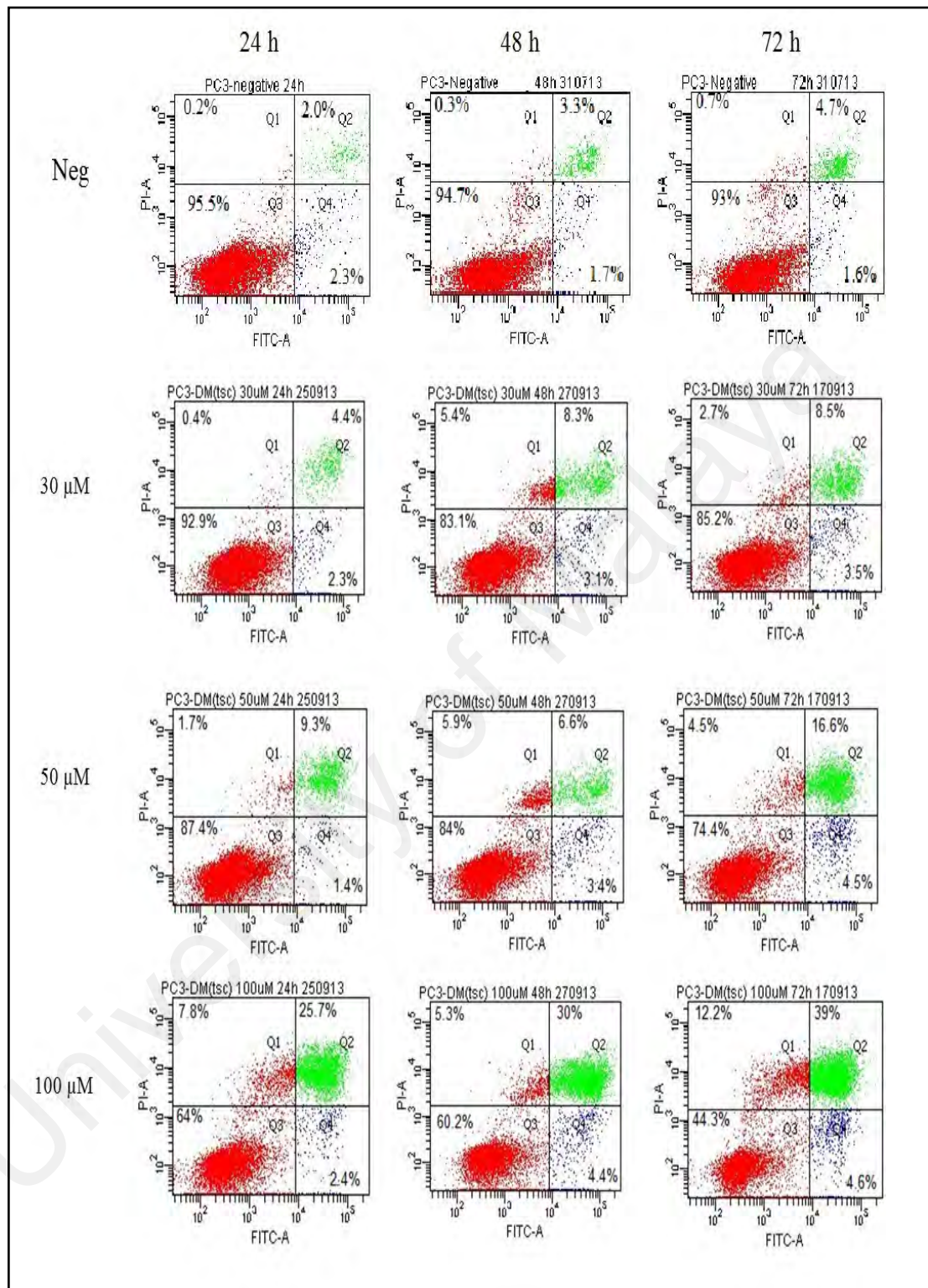


Figure 4.24: Annexin V/PI assay against PC-3 cell lines treated with [DM(tsc)T] at concentrations of 30, 50 and 100 μM for 24, 48 and 72 hours. Results were analyzed by flow cytometry. At least 10,000 cells were counted in each sample. Neg (untreated cells).

4.6.4.4 Cell cycle analysis using flow cytometry for DM(tsc)T

Flow cytometric analysis was carried out to analyze the influence of **DM(tsc)T** on cell cycle distribution. Cell cycle analyses were performed after treatment duration of 24, 48 and 72 hours. In this assay, PI fluorescence was used as it is proportional to the amount of chromosomal DNA and it allows us to identify different stages in the cell cycle distribution (Ziegler & Groscurth, 2004).

As illustrated in Figure 4.25, there is no prominent cell cycle arrest observed for 24 hours treatment. Meanwhile, for 48 and 72 hours treatment, the cell cycle results showed gradual cell cycle arrest at the G0/G1 phase. Similarly, some of the established compounds derived from platinum and gold also elicited inhibition at the G0/G1 phase as well (Choudhury et al., 2013; Huang et al., 2013; Tu et al., 2009). The general reasons/possibilities for the cells arrest at G0/G1 are DNA damage and insufficient materials for cell growth (Fofaria et al., 2014). The difference in type of phase arrest implies a different mechanistic pathway involved (Ng et al., 2014).

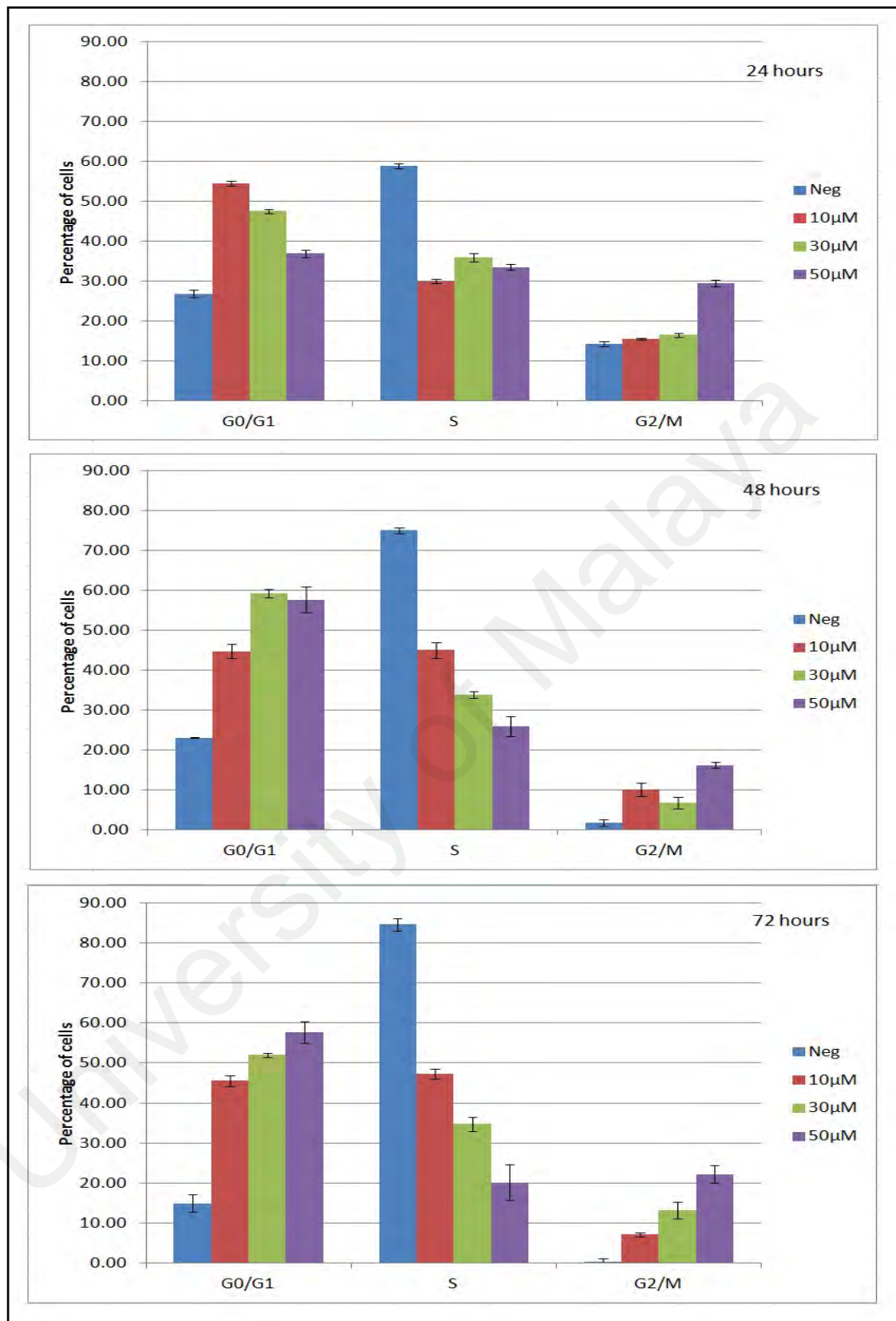


Figure 4.25: Cell cycle analysis by flow cytometry in PC-3 cells treated with [DM(tsc)T] at concentrations of 10, 30 and 50 μM for 24, 48 and 72 hours. Results were analyzed by flow cytometry. At least 30,000 cells were counted in each sample. Results are the mean ± SD from three independent experiments. Neg (untreated cells).

4.6.4.5 JC-1 Mitochondrial transmembrane potential ($\Delta\Psi_m$) assay for DM(tsc)T

Apoptosis could occur by many pathways, however mitochondria-mediated (intrinsic pathway) apoptosis is generally known as the functional pathway for anticancer drugs (Christensen et al., 2013). Mitochondria play important roles in apoptosis through the release of proapoptotic factors such as cytochrome c and other apoptosis-inducing factors. As shown in figure 4.26, 85.7 % of the population in untreated cells emits red fluorescent indicating healthy mitochondria. Gradual mitochondrial membrane potential loss was observed when the cells treated with increasing concentration of **DM(tsc)T**. Figure 4.26 showed that polarized cells drop in a concentration-dependent manner with 83.4, 77.7 and 69.9 % for 10, 30 and 50 μM , respectively. The result implies that the apoptosis by **DM(tsc)T** could be due to mitochondria mediated pathway, although this may not be the only conclusive pathway.

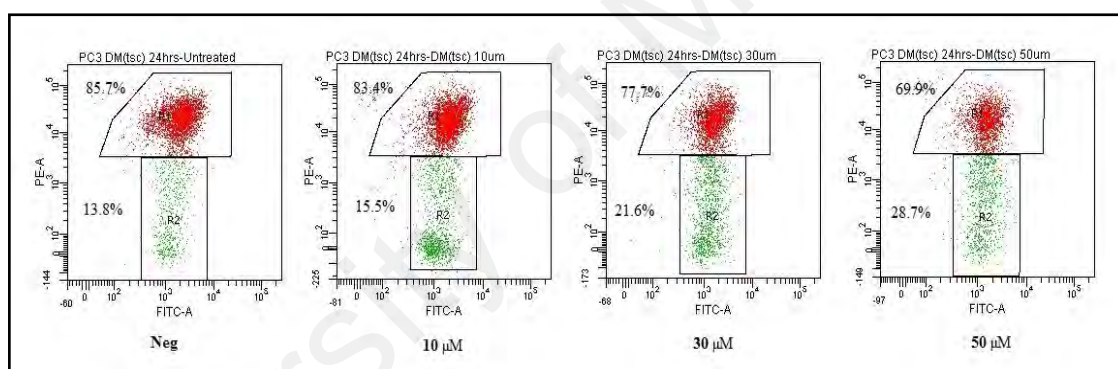


Figure 4.26: Mitochondrial membrane potential analysis against PC-3 cells treated with [DM(tsc)T] at concentrations of 10, 30 and 50 μM for 24 hours. Results were analyzed by flow cytometry. At least 30,000 cells were counted in each sample. Figure shown represents outcome from at least three experiments with similar parameters. Neg (untreated cells).

4.7 General discussion

The thiosemicarbazone with ethylphenyl moiety displayed most potent activity against PC-3 and HCT 116 cells. At the same time, **EP(tsc)T** exerted least damage to RWPE-1 cells with IC_{50} value of $6.60 \pm 0.10 \mu\text{M}$; giving selectivity index of 6.2 and 7.3 against PC-3 and HCT 116, respectively. Mahavorasirikul *et al.* (2010) reported that selectivity index of greater than three is considered as highly selective. Growth inhibitory results illustrates that **P(tsc)T**, **FP(tsc)T**, **EP(tsc)T** and **DM(tsc)T** exhibited significant inhibitory effect on PC-3 cells with least damage to RWPE-1 cells. Based on MTT results and burgeoning literature reports, the modes of cell death against PC-3 cells for the thiosemicarbazone with selected N(4) substituent were further accessed.

PC-3 cells treated with selected compounds showed distinctive morphological changes in comparison with untreated cells, which maintained their original morphology and adhered to the bottom of culture dish surface. In this study, lower magnification of 50x was used to present a complete picture of the treated cells. The selected compounds exhibited cytotoxic properties in a time- and concentration-dependent manner. For 24 hours treatment duration, the compounds did not induce much change to the morphology of PC-3 cells for treatment concentration up to $30 \mu\text{M}$. The results clearly indicated that the compound can induce significant cell death with prominent appearance of apoptosis bodies in PC-3 cells, with treatment duration of 72 hours and minimal concentration of $50 \mu\text{M}$.

The AO/EB fluorescent staining has been used to visualize apoptosis associated changes on cell morphology and distinguish cells undergoing different types of cell death. The results showed that a minimal concentration of $30 \mu\text{M}$ and treatment duration of 24 hours is sufficient to induce early apoptotic characteristics such as membrane blebbing and chromatin condensation. Treatment with $100 \mu\text{M}$ for 48 and 72 hours showed most of the cells were stained bright orange to red as an indication for

late apoptosis and necrosis. Apart from that, most of the cells underwent chromatin condensation and size shrinkage. The results were more prominent for 72 hours treatment duration whereby some of the cells membranes have ruptured and releases its content which is a characteristic of necrosis. This assay establishes that necrosis cell death only occur with minimal treatment of 100 μ M of the selected compounds.

Staining cells simultaneously with Annexin V-FITC/PI dye allows the differentiation of healthy cells, early apoptosis, late apoptosis and debris/necrosis. All the untreated cells showed percentage of viable cells of above 90 %. For treatment duration of 24 hours, most of the cells showed percentage of cell viability above 80 % for concentration up to 50 μ M. Annexin V-FITC/PI assay showed that there are only minimal changes in number of healthy and apoptotic cells for 24 hours treatment duration. **P(tsc)T** exhibited the most potent cytotoxic property with significant drop of approximately 50 % cell viability for 72 hours treatment duration with merely 10 μ M of the compound. **EP(tsc)T** also exhibited potent cytotoxic property with significant drop of approximately 70 % viable cells in comparison to the untreated cells, with treatment of 50 μ M for the same duration.

Cell cycle regulatory functions in cancer cells are usually impaired; hence arresting cell cycle progression might be an effective strategy in preventing proliferation of cancer cells. In this study, the cell cycle results clearly indicate that all the selected compounds were able to arrest the cell cycle at the G0/G1. The results were more prominent with 72 hours treatment duration. Metabolic depletion and DNA damage are some of the general reason that prevents progression from G1 to S phase. Cyclins and cyclin dependent kinases (cdks) are often associated with progression of cell cycle from G1 to S phase. The results in this study showed prominent cell cycle arrest at G0/G1 phase, therefore indicates that the compounds might have indirectly suppress CDK complexes, thus causing apoptosis.

Mitochondrial membrane potential $\Delta\psi_m$, is a valuable indicator which can be used to measure the mitochondrial health. Mitochondria are known to play important roles in the apoptotic mechanism via several pathways which include disrupting electron transport chain and energy metabolism, releasing or activating proteins that mediate apoptosis and altering cellular redox potential (D'Souza et al., 2011). All the selected compounds showed a drastic drop in the membrane potential with increasing concentration of the compounds. The result implies that the apoptosis by the compounds could be due to mitochondria mediated pathway, although this may not be the only conclusive pathway. Currently it is widely accepted that mitochondria play a key role in the regulation of apoptosis. Depletion of mitochondrial membrane potential releases pro-apoptotic proteins such as cytochrome C, that normally present in the intermembrane space of these organelles. These led to the cleavage of caspases and activation of downstream cell death mechanisms (Esmaeili et al., 2016).

CHAPTER 5

CONCLUSIONS AND RECOMMENDATIONS

Thiosemicarbazone has been the subject of great interest of many researchers for its wide spectrum of pharmaceutical properties. Keeping in mind a mitochondria-targeting treatment strategy could be a promising avenue for cancer therapy, therefore in this study lipophilic triphenylphosphonium moiety have been successfully conjugated to thiosemicarbazone. Since Schiff bases from thiosemicarbazone family with N(4) substituent have been reported to boost cytotoxic properties, compounds that could penetrate mitochondrial membrane and accumulate inside mitochondrial matrix have been developed in present study. There is strong evidence to support the rationale for the development of anticancer compound based on mitochondrial targeting.

Seven triphenylphosphonium containing thiosemicarbazone derivatives [**(tsc)T**, **P(tsc)T**, **FP(tsc)T**, **E(tsc)T**, **EP(tsc)T**, **M(tsc)T** and **DM(tsc)T**] and (3-formyl-4-hydroxyphenyl)methyltriphenylphosphonium (**T**) itself as the starting material were successfully prepared in this research. The thiosemicarbazones were prepared by condensation reaction of (**T**) with thiosemicarbazide and its N-(4)-substituted derivatives. The compounds were characterized by CHN, IR, ¹H NMR, ¹³C NMR and HRMS which were in conformity with the structure of targeted compounds. The results from elemental analysis are in good agreement with the proposed structures and thus strongly affirm that the proposed compounds have been formed. The structure of **(tsc)T**, **P(tsc)T**, **E(tsc)T**, **FP(tsc)T** and **DM(tsc)T** have been solved by single crystal X-ray crystallography and the analysis reveals that all compounds crystallized in the monoclinic system except for **P(tsc)T** in the triclinic form.

The structure activity relationship showed that thiosemicarbazone N(4) atom substituted with phenyl compound enhances the cytotoxicity properties of the compound. These compounds showed that an optimum electron density, a substituent bulkiness or a proton donating ability in the C-5 phenyl ring may be closely related for maximum cytotoxic activity against human cancer cell lines. Ethyl and fluorine attached to the phenyl ring further enhance the growth inhibitory effect of the compound. The findings from the current research will definitely provide an insight in drug discovery and development.

Among all the human cell lines tested, the compounds exhibit most potent cytotoxic properties towards PC-3 cell line. Biological studies reveals that, the ethylphenyl moiety at the N(4) atom of thiosemicarbazone exerts the strongest cytotoxic activity among all the compounds tested. This finding clearly showed that presence of bulky group at N(4) positions of the thiosemicarbazone moiety; somehow, enhances the cytotoxic effect of the compounds as claimed in literatures.

With all the results taken together, these selected compounds would serve as a lead scaffold for rational anticancer agent development. For future studies incorporation of metal complexes into this ligand might enhance the cytotoxicity and selectivity of the compounds. Consequently, *in vivo* research will definitely give a better overall effect of an experiment as *in vivo* studies will provide information for various pharmacokinetic/pharmacodynamics of a drug such as absorption, distribution, metabolism, elimination and toxicity. For targeted therapies, measuring the tissue concentration and whether the compound has successfully modulated the target would provide a major insight in this research.

REFERENCES

- Abu-Gosh, S. E., Kolvazon, N., Tirosh, B., Ringel, I., & Yavin, E. (2009). Multiple Triphenylphosphonium Cations Shuttle a Hydrophilic Peptide into Mitochondria. *Molecular Pharmaceutics*, 6(4), 1138-1144.
- Adams, M., Li, Y., Khot, H., De Kock, C., Smith, P. J., Land, K. (2013). The synthesis and antiparasitic activity of aryl- and ferrocenyl-derived thiosemicarbazone ruthenium(ii)-arene complexes. *Dalton Transactions*, 42(13), 4677-4685.
- Ahmad, N., Adhami, V. M., Afaq, F., Feyes, D. K., & Mukhtar, H. (2001). Resveratrol causes WAF-1/p21-mediated G(1)-phase arrest of cell cycle and induction of apoptosis in human epidermoid carcinoma A431 cells. *Clinical Cancer Research*, 7(5), 1466-1473.
- Akbar Ali, M., & Livingstone, S. E. (1974). Metal complexes of sulphur-nitrogen chelating agents. *Coordination chemistry reviews*, 13(2-3), 101-132.
- Akgemci, E. G., Saf, A. O., Tasdemir, H. U., Türkan, E., Bingol, H., Turan, S. O. (2015). Spectrophotometric, voltammetric and cytotoxicity studies of 2-hydroxy-5-methoxyacetophenone thiosemicarbazone and its N(4)-substituted derivatives: A combined experimental-computational study. *Spectrochimica Acta Part A: Molecular and Biomolecular Spectroscopy*, 136, Part B(0), 719-725.
- Aljahdali, M., & El-Sherif, A. A. (2013). Synthesis, characterization, molecular modeling and biological activity of mixed ligand complexes of Cu(II), Ni(II) and Co(II) based on 1,10-phenanthroline and novel thiosemicarbazone. *Inorganica Chimica Acta*, 407(0), 58-68.
- Allen, R. T., Hunter, W. J., 3rd, & Agrawal, D. K. (1997). Morphological and biochemical characterization and analysis of apoptosis. *Journal of Pharmacological and Toxicological Methods*, 37(4), 215-228.
- Alomar, K., Landreau, A., Allain, M., Bouet, G., & Larcher, G. (2013). Synthesis, structure and antifungal activity of thiophene-2,3-dicarboxaldehyde bis(thiosemicarbazone) and nickel(II), copper(II) and cadmium(II) complexes: Unsymmetrical coordination mode of nickel complex. *Journal of Inorganic Biochemistry*, 126(0), 76-83.
- Amaravadi, R. K., & Thompson, C. B. (2007). The roles of therapy-induced autophagy and necrosis in cancer treatment. *Clinical Cancer Research*, 13(24), 7271-7279.
- An, Q., Robins, P., Lindahl, T., & Barnes, D. E. (2007). 5-Fluorouracil Incorporated into DNA Is Excised by the Smug1 DNA Glycosylase to Reduce Drug Cytotoxicity. *Cancer Research*, 67(3), 940-945.
- Anand, S. A. A., Loganathan, C., Thomas, N. S., Saravanan, K., Alphonsa, A. T., & Kabilan, S. (2015). Synthesis, structure prediction, pharmacokinetic properties, molecular docking and antitumor activities of some novel thiazinone derivatives. *New Journal of Chemistry*, 39(9), 7120-7129.

- Anbazhagan, R., & Sankaran, K. R. (2015). Design, synthesis, computational calculation and biological evaluation of some novel 2-thiazolyl hydrazones. *Spectrochimica Acta Part A: Molecular and Biomolecular Spectroscopy*, 135(0), 984-993.
- Anitha, P., Chitrapriya, N., Jang, Y. J., & Viswanathamurthi, P. (2013). Synthesis, characterization, DNA interaction, antioxidant and anticancer activity of new ruthenium(II) complexes of thiosemicarbazone/semicarbazone bearing 9,10-phenanthrenequinone. *Journal of Photochemistry and Photobiology B: Biology*, 129(0), 17-26.
- Arias, J. (2008). Novel Strategies to Improve the Anticancer Action of 5-Fluorouracil by Using Drug Delivery Systems. *Molecules*, 13(10), 2340-2369.
- Ashokkumar, T., Prabhu, D., Geetha, R., Govindaraju, K., Manikandan, R., Arulvasu, C. (2014). Apoptosis in liver cancer (HepG2) cells induced by functionalized gold nanoparticles. *Colloids and Surfaces B: Biointerfaces*, 123(0), 549-556.
- Bauer, D. J., & Apostolov, K. (1966). Adenovirus Multiplication: Inhibition by Methisazone. *Science*, 154(3750), 796-797.
- Beckford, F. A., Thessing, J., Shaloski Jr, M., Mbarushimana, P. C., Brock, A., Didion, J. (2011). Synthesis and characterization of mixed-ligand diimine-piperonal thiosemicarbazone complexes of ruthenium(II): Biophysical investigations and biological evaluation as anticancer and antibacterial agents. *Journal of Molecular Structure*, 992(1-3), 39-47.
- Bello, D., Webber, M. M., Kleinman, H. K., Wartinger, D. D., & Rhim, J. S. (1997). Androgen responsive adult human prostatic epithelial cell lines immortalized by human papillomavirus 18. *Carcinogenesis*, 18(6), 1215-1223.
- Bortner, C. D., & Cidlowski, J. A. (2002). Apoptotic volume decrease and the incredible shrinking cell. *Cell Death & Differentiation*, 9(12), 1307-1310.
- Bottone, M., Santin, G., Aredia, F., Bernocchi, G., Pellicciari, C., & Scovassi, A. (2013). Morphological Features of Organelles during Apoptosis: An Overview. *Cells*, 2(2), 294.
- Cai, X., Hu, X., Tan, X., Cheng, W., Wang, Q., Chen, X. (2015). Metformin Induced AMPK Activation, G0/G1 Phase Cell Cycle Arrest and the Inhibition of Growth of Esophageal Squamous Cell Carcinomas In Vitro and In Vivo. *PLoS ONE*, 10(7), e0133349.
- Castro, E. F., Campos, R. H., & Cavallaro, L. V. (2014). Stability of the Resistance to the Thiosemicarbazone Derived from 5,6-Dimethoxy-1-Indanone, a Non-Nucleoside Polymerase Inhibitor of Bovine Viral Diarrhea Virus. *PLoS ONE*, 9(6), e100528.
- Çetin, K., & Denizli, A. (2015). 5-Fluorouracil delivery from metal-ion mediated molecularly imprinted cryogel discs. *Colloids and Surfaces B: Biointerfaces*, 126, 401-406.

- Chavez, K. J., Garimella, S. V., & Lipkowitz, S. (2010). Triple Negative Breast Cancer Cell Lines: One Tool in the Search for Better Treatment of Triple Negative Breast Cancer. *Breast disease*, 32(1-2), 35-48.
- Chew, S. T., Lo, K. M., Lee, S. K., Heng, M. P., Teoh, W. Y., Sim, K. S. (2014). Copper complexes with phosphonium containing hydrazone ligand: Topoisomerase inhibition and cytotoxicity study. *European Journal of Medicinal Chemistry*, 76(0), 397-407.
- Choudhury, D., Xavier, P. L., Chaudhari, K., John, R., Dasgupta, A. K., Pradeep, T. (2013). Unprecedented inhibition of tubulin polymerization directed by gold nanoparticles inducing cell cycle arrest and apoptosis. *Nanoscale*, 5(10), 4476-4489.
- Christensen, M. E., Jansen, E. S., Sanchez, W., & Waterhouse, N. J. (2013). Flow cytometry based assays for the measurement of apoptosis-associated mitochondrial membrane depolarisation and cytochrome c release. *Methods*, 61(2), 138-145.
- D'Souza, G. G. M., Wagle, M. A., Saxena, V., & Shah, A. (2011). Approaches for targeting mitochondria in cancer therapy. *Biochimica et Biophysica Acta (BBA) - Bioenergetics*, 1807(6), 689-696.
- DeNardo, D. G., Andreu, P., & Coussens, L. M. (2010). Interactions between lymphocytes and myeloid cells regulate pro- versus anti-tumor immunity. *Cancer Metastasis Reviews*, 29(2), 309-316.
- Dowling, R. J. O., Niraula, S., Stambolic, V., & Goodwin, P. J. (2012). Metformin in cancer: translational challenges. *Journal of Molecular Endocrinology*, 48(3), R31-R43.
- Ebrahimi, H. P., Hadi, J. S., Alsalim, T. A., Ghali, T. S., & Bolandnazar, Z. (2015). A novel series of thiosemicarbazone drugs: From synthesis to structure. *Spectrochimica Acta Part A: Molecular and Biomolecular Spectroscopy*, 137(0), 1067-1077.
- Eissa, H. (2013). Synthesis, Characterization and Antibacterial Activity of Macrocyclic Schiff Bases Based on 1, 3-Docarbonyl Phenyl Dihydrazide, 1, 4-Docarbonyl Phenyl Dihydrazide. *Organic Chemistry: Current Research*, 2(3), 1000122.
- El-Sonbati, A. Z., El-Bindary, A. A., & Rashed, I. G. A. (2002). Polymer complexes XXXVII novel models and structural of symmetrical poly-Schiff base on heterobinuclear complexes of dioxouranium(VI). *Spectrochimica Acta Part A: Molecular and Biomolecular Spectroscopy*, 58(7), 1411-1424.
- Elledge, S. J. (1996). Cell Cycle Checkpoints: Preventing an Identity Crisis. *Science*, 274(5293), 1664-1672.
- Elmore, S. (2007). Apoptosis: A Review of Programmed Cell Death. *Toxicologic pathology*, 35(4), 495-516.

- Esmaili, M. A., Abagheri-Mahabadi, N., Hashempour, H., Farhadpour, M., Gruber, C. W., & Ghassempour, A. (2016). Viola plant cyclotide vigno 5 induces mitochondria-mediated apoptosis via cytochrome C release and caspases activation in cervical cancer cells. *Fitoterapia*, *109*, 162-168.
- Feldman, B. J., & Feldman, D. (2001). The development of androgen-independent prostate cancer. *Nature Reviews Cancer*, *1*(1), 34-45.
- Ferguson, D. L. (1964). Some observations on the role of methisazone ('Marboran') in the prophylaxis of smallpox in a rural area. *South African medical journal*, *38*, 868-869.
- Finch, Liu, M.-C., Grill, S. P., Rose, W. C., Loomis, R., Vasquez, K. M. (2000). Triapine (3-aminopyridine-2-carboxaldehyde- thiosemicarbazone): A potent inhibitor of ribonucleotide reductase activity with broad spectrum antitumor activity. *Biochemical Pharmacology*, *59*(8), 983-991.
- Finch, Liu, M. C., Cory, A. H., Cory, J. G., & Sartorelli, A. C. (1999). Triapine (3-aminopyridine-2-carboxaldehyde thiosemicarbazone; 3-AP): an inhibitor of ribonucleotide reductase with antineoplastic activity. *Advances in Enzyme Regulation*, *39*, 3-12.
- Finichiu, P., James, A., Larsen, L., Smith, R. J., & Murphy, M. (2013). Mitochondrial accumulation of a lipophilic cation conjugated to an ionisable group depends on membrane potential, pH gradient and pK a: implications for the design of mitochondrial probes and therapies. *Journal of Bioenergetics and Biomembranes*, *45*(1-2), 165-173.
- Fofaria, N. M., Kim, S.-H., & Srivastava, S. K. (2014). Piperine Causes G1 Phase Cell Cycle Arrest and Apoptosis in Melanoma Cells through Checkpoint Kinase-1 Activation. *PLoS ONE*, *9*(5), e94298.
- Foster, K. A., Oster, C. G., Mayer, M. M., Avery, M. L., & Audus, K. L. (1998). Characterization of the A549 cell line as a type II pulmonary epithelial cell model for drug metabolism. *Experimental Cell Research*, *243*(2), 359-366.
- Fulda, S., Galluzzi, L., & Kroemer, G. (2010). Targeting mitochondria for cancer therapy. *Nature Reviews Drug Discovery*, *9*(6), 447-464.
- Funk, J. O. (2001). *Cell Cycle Checkpoint Genes and Cancer eLS*: John Wiley & Sons, Ltd.
- Galanello, R. (2007). Deferiprone in the treatment of transfusion-dependent thalassemia: a review and perspective. *Therapeutics and Clinical Risk Management*, *3*(5), 795-805.
- Galluzzi, L., Aaronson, S. A., Abrams, J., Alnemri, E. S., Andrews, D. W., Baehrecke, E. H. (2009). Guidelines for the use and interpretation of assays for monitoring cell death in higher eukaryotes. *Cell Death & Differentiation*, *16*(8), 1093-1107.
- Gil-Araujo, B., Toledo Lobo, M.-V., Gutiérrez-Salmerón, M., Gutiérrez-Pitalúa, J., Roperio, S., Angulo, J. C. (2013). Dual specificity phosphatase 1 expression

inversely correlates with NF- κ B activity and expression in prostate cancer and promotes apoptosis through a p38 MAPK dependent mechanism. *Molecular Oncology*(0).

Green, D. R., & Reed, J. C. (1998). Mitochondria and apoptosis. *Science*, 281(5381), 1309-1312.

Grönberg, H. (2003). Prostate cancer epidemiology. *The Lancet*, 361(9360), 859-864.

Gurumoorthy, P., Mahendiran, D., Prabhu, D., Arulvasu, C., & Rahiman, A. K. (2015). Mixed-ligand copper(II) phenolate complexes: Synthesis, spectral characterization, phosphate-hydrolysis, antioxidant, DNA interaction and cytotoxic studies. *Journal of Molecular Structure*, 1080(0), 88-98.

Han, J., Zhong, C.-Q., & Zhang, D.-W. (2011). Programmed necrosis: backup to and competitor with apoptosis in the immune system. *Nature Immunology*, 12(12), 1143-1149.

Hanahan, D., & Folkman, J. (1996). Patterns and emerging mechanisms of the angiogenic switch during tumorigenesis. *Cell*, 86(3), 353-364.

Hanahan, D., & Weinberg, R. A. (2000). The Hallmarks of Cancer. *Cell*, 100(1), 57-70.

Hanahan, D., & Weinberg, Robert A. (2011). Hallmarks of Cancer: The Next Generation. *Cell*, 144(5), 646-674.

Harris, C. C. (1996). p53 tumor suppressor gene: from the basic research laboratory to the clinic--an abridged historical perspective. *Carcinogenesis*, 17(6), 1187-1198.

Hayflick, L. (1997). Mortality and immortality at the cellular level. A review. *Biochemistry (Mosc)*, 62(11), 1180-1190.

Hengartner, M. O. (2000). The biochemistry of apoptosis. *Nature*, 407(6805), 770-776.

Huang, Chen, Z.-F., Liu, Y.-C., Li, Z.-Q., Wei, J.-H., Wang, M. (2013). Platinum(II) complexes with mono-aminophosphonate ester targeting group that induce apoptosis through G1 cell-cycle arrest: Synthesis, crystal structure and antitumour activity. *European Journal of Medicinal Chemistry*, 63(0), 76-84.

Huang, C., Gou, S., Zhu, H., & Huang, W. (2007). Cleavage of C-S Bonds with the Formation of a Tetranuclear Cu(I) Cluster. *Inorganic Chemistry*, 46(14), 5537-5543.

Hussein, M. A., Iqbal, M. A., Umar, M. I., Haque, R. A., & Guan, T. S. (2015). Synthesis, structural elucidation and cytotoxicity of new thiosemicarbazone derivatives. *Arabian Journal of Chemistry*.

Jagadeesh, M., Lavanya, M., Kalangi, S. K., Sarala, Y., Ramachandraiah, C., & Varada Reddy, A. (2015). Spectroscopic characterization, antioxidant and antitumour studies of novel bromo substituted thiosemicarbazone and its copper(II), nickel(II) and palladium(II) complexes. *Spectrochimica Acta Part A: Molecular and Biomolecular Spectroscopy*, 135(0), 180-184.

- Jansson, P. J., Yamagishi, T., Arvind, A., Seebacher, N., Gutierrez, E., Stacy, A. (2015). Di-2-pyridylketone 4,4-dimethyl-3-thiosemicarbazone (Dp44mT) overcomes multidrug resistance by a novel mechanism involving the hijacking of lysosomal P-Glycoprotein (Pgp). *Journal of Biological Chemistry*, 290(15), 9588-9603.
- Jaroszyńska-Weinberger, B. (1970). Treatment with methisazone of complications following smallpox vaccination. *Archives of Disease in Childhood*, 45(242), 573-580.
- Jayakumar, S., Kunwar, A., Sandur, S. K., Pandey, B. N., & Chaubey, R. C. (2014). Differential response of DU145 and PC3 prostate cancer cells to ionizing radiation: Role of reactive oxygen species, GSH and Nrf2 in radiosensitivity. *Biochimica et Biophysica Acta*, 1840(1), 485-494.
- Jones, R. G., Plas, D. R., Kubek, S., Buzzai, M., Mu, J., Xu, Y. (2005). AMP-activated protein kinase induces a p53-dependent metabolic checkpoint. *Molecular Cell*, 18(3), 283-293.
- Joseph, M., Kuriakose, M., Kurup, M. R. P., Suresh, E., Kishore, A., & Bhat, S. G. (2006). Structural, antimicrobial and spectral studies of copper(II) complexes of 2-benzoylpyridine N(4)-phenyl thiosemicarbazone. *Polyhedron*, 25(1), 61-70.
- Kaini, R. R., & Hu, C.-A. A. (2012). Synergistic killing effect of chloroquine and androgen deprivation in LNCaP cells. *Biochemical and Biophysical Research Communications*, 425(2), 150-156.
- Kalaivani, P., Saranya, S., Poornima, P., Prabhakaran, R., Dallemer, F., Vijaya Padma, V. (2014). Biological evaluation of new nickel(II) metallates: Synthesis, DNA/protein binding and mitochondrial mediated apoptosis in human lung cancer cells (A549) via ROS hypergeneration and depletion of cellular antioxidant pool. *European Journal of Medicinal Chemistry*, 82(0), 584-599.
- Karp, J. E., Giles, F. J., Gojo, I., Morris, L., Greer, J., Johnson, B. (2008). A Phase I study of the novel ribonucleotide reductase inhibitor 3-aminopyridine-2-carboxaldehyde thiosemicarbazone (3-AP, Triapine®) in combination with the nucleoside analog fludarabine for patients with refractory acute leukemias and aggressive myeloproliferative disorders. *Leukemia Research*, 32(1), 71-77.
- Kelso, G. F., Porteous, C. M., Coulter, C. V., Hughes, G., Porteous, W. K., Ledgerwood, E. C. (2001). Selective Targeting of a Redox-active Ubiquinone to Mitochondria within Cells: ANTIOXIDANT AND ANTIAPOPTOTIC PROPERTIES. *Journal of Biological Chemistry*, 276(7), 4588-4596.
- Khamis, E., Ameer, M. A., AlAndis, N. M., & Al-Senani, G. (2000). Effect of Thiosemicarbazones on Corrosion of Steel in Phosphoric Acid Produced by Wet Process. *Corrosion*, 56(2), 127-138.
- Kiriy, N., Bocharova, V., Kiriy, A., Stamm, M., Krebs, F. C., & Adler, H.-J. (2004). Designing Thiophene-Based Azomethine Oligomers with Tailored Properties: Self-assembly and Charge Carrier Mobility. *Chemistry of Materials*, 16(23), 4765-4771.

- Klayman, D. L., Bartosevich, J. F., Griffin, T. S., Mason, C. J., & Scovill, J. P. (1979). 2-Acetylpyridine thiosemicarbazones. 1. A new class of potential antimalarial agents. *Journal of Medicinal Chemistry*, 22(7), 855-862.
- Knox, J. J., Hotte, S. J., Kollmannsberger, C., Winqvist, E., Fisher, B., & Eisenhauer, E. A. (2007). Phase II study of Triapine® in patients with metastatic renal cell carcinoma: a trial of the National Cancer Institute of Canada Clinical Trials Group (NCIC IND.161). *Investigational New Drugs*, 25(5), 471-477.
- Kovacevic, Z., Menezes, S. V., Sahni, S., Kalinowski, D. S., Bae, D.-H., Lane, D. J. R. (2016). The Metastasis Suppressor, N-MYC Downstream-regulated Gene-1 (NDRG1), Down-regulates the ErbB Family of Receptors to Inhibit Downstream Oncogenic Signaling Pathways. *Journal of Biological Chemistry*, 291(3), 1029-1052.
- Kovács, R., Csenki, Z., Bakos, K., Urbányi, B., Horváth, Á., Garaj-Vrhovac, V. (2015). Assessment of toxicity and genotoxicity of low doses of 5-fluorouracil in zebrafish (*Danio rerio*) two-generation study. *Water Research*, 77, 201-212.
- Kowol, C. R., Trondl, R., Heffeter, P., Arion, V. B., Jakupec, M. A., Roller, A. (2009). Impact of Metal Coordination on Cytotoxicity of 3-Aminopyridine-2-carboxaldehyde Thiosemicarbazone (Triapine) and Novel Insights into Terminal Dimethylation. *Journal of Medicinal Chemistry*, 52(16), 5032-5043.
- Koyuncu Zeybek, D., Demir, B., Zeybek, B., & Pekyardımcı, Ş. (2015). A sensitive electrochemical DNA biosensor for antineoplastic drug 5-fluorouracil based on glassy carbon electrode modified with poly(bromocresol purple). *Talanta*, 144, 793-800.
- Kroemer, G., Galluzzi, L., Vandenabeele, P., Abrams, J., Alnemri, E. S., Baehrecke, E. H. (2009). Classification of cell death: recommendations of the Nomenclature Committee on Cell Death 2009. *Cell Death and Differentiation*, 16(1), 3-11.
- Kung, G., Konstantinidis, K., & Kitsis, R. N. (2011). Programmed Necrosis, Not Apoptosis, in the Heart. *Circulation Research*, 108(8), 1017-1036.
- Lauková, J., Kozubík, A., Hofmanová, J., Nekvindová, J., Sova, P., Moyer, M. P. (2015). Loss of PTEN facilitates rosiglitazone-mediated enhancement of platinum(IV) complex LA-12-induced apoptosis in colon cancer cells. *PLoS ONE*, 10(10).
- Lee, C.-C., Hsieh, H. J., Hsieh, C.-H., & Hwang, D.-F. (2014). Spine venom of crown-of-thorns starfish (*Acanthaster planci*) induces antiproliferation and apoptosis of human melanoma cells (A375.S2). *Toxicon*, 91(0), 126-134.
- Levenson, A. S., & Jordan, V. C. (1997). MCF-7: the first hormone-responsive breast cancer cell line. *Cancer Research*, 57(15), 3071-3078.
- Li, M., Ganea, G. M., Lu, C., De Rooy, S. L., El-Zahab, B., Fernand, V. E. (2012). Lipophilic phosphonium-lanthanide compounds with magnetic, luminescent, and tumor targeting properties. *Journal of Inorganic Biochemistry*, 107(1), 40-46.

- Li, X., Tian, J., Bo, Q., Li, K., Wang, H., Liu, T. (2015). Targeting DNA-PKcs increased anticancer drug sensitivity by suppressing DNA damage repair in osteosarcoma cell line MG63. *Tumor Biology*, 36(12), 9365-9372.
- Linke, S. P., Clarkin, K. C., Di Leonardo, A., Tsou, A., & Wahl, G. M. (1996). A reversible, p53-dependent G0/G1 cell cycle arrest induced by ribonucleotide depletion in the absence of detectable DNA damage. *Genes & Development*, 10(8), 934-947.
- Liotta, L. A., & Kohn, E. (2004). Anoikis: Cancer and the homeless cell. *Nature*, 430(7003), 973-974.
- Liu, M. C., Lin, T. C., & Sartorelli, A. C. (1992). Synthesis and antitumor activity of amino derivatives of pyridine-2-carboxaldehyde thiosemicarbazone. *Journal of Medicinal Chemistry*, 35(20), 3672-3677.
- Lobana, T. S., & Castineiras, A. (2002). Metal-heterocyclic thione interactions. 13. Pyridine-2-thione derivatives of copper(I): Crystal structure of dinuclear [bromo(pyridine-2-thione)(tri-p-tolylphosphine)copper(I)]₂ complex. *Polyhedron*, 21(16), 1603-1611.
- Luengo-Fernandez, R., Leal, J., Gray, A., & Sullivan, R. (2013). Economic burden of cancer across the European Union: a population-based cost analysis. *The Lancet Oncology*, 14(12), 1165-1174.
- Lukmantara, A. Y., Kalinowski, D. S., Kumar, N., & Richardson, D. R. (2013). Synthesis and biological evaluation of substituted 2-benzoylpyridine thiosemicarbazones: Novel structure-activity relationships underpinning their anti-proliferative and chelation efficacy. *Bioorganic & Medicinal Chemistry Letters*, 23(4), 967-974.
- Mahavorasirikul, W., Viyanant, V., Chaijaroenkul, W., Itharat, A., & Na-Bangchang, K. (2010). Cytotoxic activity of Thai medicinal plants against human cholangiocarcinoma, laryngeal and hepatocarcinoma cells in vitro. *BMC Complementary and Alternative Medicine*, 10(1), 1-8.
- Matesanz, A. I., Tapia, S., & Souza, P. (2016). First 3,5-diacetyl-1,2,4-triazol derived mono(thiosemicarbazone) and its palladium and platinum complexes: Synthesis, structure and biological properties. *Inorganica Chimica Acta*, 445, 62-69.
- McIlwain, D. R., Berger, T., & Mak, T. W. (2013). Caspase Functions in Cell Death and Disease. *Cold Spring Harbor Perspectives in Biology*, 5(4).
- Meier, P., Finch, A., & Evan, G. (2000). Apoptosis in development. *Nature*, 407(6805), 796-801.
- Merlot, A. M., Sahni, S., Lane, D. J. R., Fordham, A. M., Pantarat, N., Hibbs, D. E. (2015). Potentiating the cellular targeting and anti-tumor activity of Dp44mT via binding to human serum albumin: Two saturable mechanisms of Dp44mT uptake by cells. *Oncotarget*, 6(12), 10374-10398.

- Millard, M., Pathania, D., Shabaik, Y., Taheri, L., Deng, J., & Neamati, N. (2010). Preclinical Evaluation of Novel Triphenylphosphonium Salts with Broad-Spectrum Activity. *PLoS ONE*, 5(10), e13131.
- Mitchell, T., Rotaru, D., Saba, H., Smith, R. A. J., Murphy, M. P., & MacMillan-Crow, L. A. (2011). The Mitochondria-Targeted Antioxidant Mitoquinone Protects against Cold Storage Injury of Renal Tubular Cells and Rat Kidneys. *Journal of Pharmacology and Experimental Therapeutics*, 336(3), 682-692.
- Modica-Napolitano, J. S., & Singh, K. (2002). Mitochondria as targets for detection and treatment of cancer. *Expert Reviews in Molecular Medicine*, 4(09), 1-19.
- Modica-Napolitano, J. S., & Weissig, V. (2015). Treatment Strategies that Enhance the Efficacy and Selectivity of Mitochondria-Targeted Anticancer Agents. *International Journal of Molecular Sciences*, 16(8), 17394-17421.
- Mojardín, L., Botet, J., Quintales, L., Moreno, S., & Salas, M. (2013). New Insights into the RNA-Based Mechanism of Action of the Anticancer Drug 5'-Fluorouracil in Eukaryotic Cells. *PLoS ONE*, 8(11), e78172.
- Mosmann, T. (1983). Rapid colorimetric assay for cellular growth and survival: application to proliferation and cytotoxicity assays. *Journal of Immunological Methods*, 65(1-2), 55-63.
- Mrkvičková, Z., Kovaříková, P., Klimeš, J., Kalinowski, D., & Richardson, D. R. (2007). Development and validation of HPLC-DAD methods for the analysis of two novel iron chelators with potent anti-cancer activity. *Journal of Pharmaceutical and Biomedical Analysis*, 43(4), 1343-1351.
- Murphy, M. P., & Smith, R. A. J. (2007) Targeting antioxidants to mitochondria by conjugation to lipophilic cations. *Vol. 47. Annual Review of Pharmacology and Toxicology* (pp. 629-656).
- Murren, J., Modiano, M., Clairmont, C., Lambert, P., Savaraj, N., Doyle, T. (2003). Phase I and Pharmacokinetic Study of Triapine, a Potent Ribonucleotide Reductase Inhibitor, Administered Daily for Five Days in Patients with Advanced Solid Tumors. *Clinical Cancer Research*, 9(11), 4092-4100.
- Negrini, S., Gorgoulis, V. G., & Halazonetis, T. D. (2010). Genomic instability--an evolving hallmark of cancer. *Nature Reviews Molecular Cell Biology*, 11(3), 220-228.
- Ng, C. H., Kong, S. M., Tiong, Y. L., Maah, M. J., Sukram, N., Ahmad, M. (2014). Selective anticancer copper(ii)-mixed ligand complexes: targeting of ROS and proteasomes. *Metallomics*, 6(4), 892-906.
- Oeckinghaus, A., Hayden, M. S., & Ghosh, S. (2011). Crosstalk in NF- κ B signaling pathways. *Nature Immunology*, 12(8), 695-708.
- Okada, M., Adachi, S., Imai, T., Watanabe, K., Toyokuni, S. Y., Ueno, M. (2004). A novel mechanism for imatinib mesylate-induced cell death of BCR-ABL-

positive human leukemic cells: caspase-independent, necrosis-like programmed cell death mediated by serine protease activity. *Blood*, 103(6), 2299-2307.

- Ono, A., Miyauchi, S., Demura, M., Asakura, T., & Kamo, N. (1994). Activation Energy for Permeation of Phosphonium Cations through Phospholipid Bilayer Membrane. *Biochemistry*, 33(14), 4312-4318.
- Ouyang, L., Shi, Z., Zhao, S., Wang, F. T., Zhou, T. T., Liu, B. (2012). Programmed cell death pathways in cancer: a review of apoptosis, autophagy and programmed necrosis. *Cell Proliferation*, 45(6), 487-498.
- Pape, V. F. S., Tóth, S., Füredi, A., Szebényi, K., Lovrics, A., Szabó, P. (2016). Design, synthesis and biological evaluation of thiosemicarbazones, hydrazinobenzothiazoles and arylhydrazones as anticancer agents with a potential to overcome multidrug resistance. *European Journal of Medicinal Chemistry*.
- Perelman, A., Wachtel, C., Cohen, M., Haupt, S., Shapiro, H., & Tzur, A. (2012). JC-1: alternative excitation wavelengths facilitate mitochondrial membrane potential cytometry. *Cell Death & Disease*, 3, e430.
- Pervez, H., Saira, N., Iqbal, M. S., Yaqub, M., & Khan, K. M. (2011). Synthesis and Toxicity Evaluation of Some N4-Aryl Substituted 5-Trifluoromethoxyisatin-3-thiosemicarbazones. *Molecules*, 16(8), 6408-6421.
- Prabhakaran, R., Krishnan, V., Pasumpon, K., Sukanya, D., Wendel, E., Jayabalakrishnan, C. (2006). Preparation, spectral characterization, electrochemistry, EXAFS, antibacterial and catalytic activity of new ruthenium (III) complexes containing ONS donor ligands with triphenylphosphine/arsine. *Applied Organometallic Chemistry*, 20(3), 203-213.
- Proskuryakov, S. Y. a., Konoplyannikov, A. G., & Gabai, V. L. (2003). Necrosis: a specific form of programmed cell death? *Experimental Cell Research*, 283(1), 1-16.
- Rahmani-Nezhad, S., Safavi, M., Pordeli, M., Ardestani, S. K., Khosravani, L., Pourshojaei, Y. (2014). Synthesis, in vitro cytotoxicity and apoptosis inducing study of 2-aryl-3-nitro-2H-chromene derivatives as potent anti-breast cancer agents. *European Journal of Medicinal Chemistry*, 86(0), 562-569.
- Rajput, A., Dominguez San Martin, I., Rose, R., Beko, A., LeVe, C., Sharratt, E. (2008). Characterization of HCT116 Human Colon Cancer Cells in an Orthotopic Model. *Journal of Surgical Research*, 147(2), 276-281.
- Reardon, A. J. F., Elliott, J. A. W., & McGann, L. E. (2014). Fluorescence as an alternative to light-scatter gating strategies to identify frozen-thawed cells with flow cytometry. *Cryobiology*, 69(1), 91-99.
- Reddy, A., Malek, S. N., Ibrahim, H., & Sim, K. (2013). Cytotoxic effect of *Alpinia scabra* (Blume) Naves extracts on human breast and ovarian cancer cells. *BMC Complementary and Alternative Medicine*, 13(1), 314.

- Ribble, D., Goldstein, N. B., Norris, D. A., & Shellman, Y. G. (2005). A simple technique for quantifying apoptosis in 96-well plates. *BMC Biotechnology*, 5, 12-12.
- Rogalska, A., Marczak, A., Gajek, A., Szwed, M., Śliwińska, A., Drzewoski, J. (2013). Induction of apoptosis in human ovarian cancer cells by new anticancer compounds, epothilone A and B. *Toxicology in Vitro*, 27(1), 239-249.
- Ross, M. F., Kelso, G. F., Blaikie, F. H., James, A. M., Cocheme, H. M., Filipovska, A. (2005). Lipophilic triphenylphosphonium cations as tools in mitochondrial bioenergetics and free radical biology. *Biochemistry (Mosc)*, 70(2), 222-230.
- Ryrie, G. (1950). Thiosemicarbazone in the treatment of leprosy. *The Lancet*, 256(6625), 286-287.
- Schiff, H. (1864). Mittheilungen aus dem Universitätslaboratorium in Pisa: Eine neue Reihe organischer Basen. *Justus Liebigs Annalen der Chemie*, 131(1), 118-119.
- Scholar, E. (2007). Alkylating Agents A2 - Enna, S.J. In D. B. Bylund (Ed.), *xPharm: The Comprehensive Pharmacology Reference* (pp. 1-4). New York: Elsevier.
- Senese, S., Lo, Y. C., Huang, D., Zangle, T. A., Gholkar, A. A., Robert, L. (2014). Chemical dissection of the cell cycle: probes for cell biology and anti-cancer drug development. *Cell Death Dis*, 5, e1462.
- Serda, M., Kalinowski, D. S., Mrozek-Wilczkiewicz, A., Musiol, R., Szurko, A., Ratuszna, A. (2012). Synthesis and characterization of quinoline-based thiosemicarbazones and correlation of cellular iron-binding efficacy to anti-tumor efficacy. *Bioorganic & Medicinal Chemistry Letters*, 22(17), 5527-5531.
- Shane, S. J., Riley, C., Laurie, J. H., & Boutilier, M. (1951). Thiosemicarbazones in Tuberculosis. *Canadian Medical Association Journal*, 64(4), 289-293.
- Shao, J., Zhou, B., Di Bilio, A. J., Zhu, L., Wang, T., Qi, C. (2006). A Ferrous-triapipe complex mediates formation of reactive oxygen species that inactivate human ribonucleotide reductase. *Molecular Cancer Therapeutics*, 5(3), 586-592.
- Sheridan, C., & Martin, S. J. (2010). Mitochondrial fission/fusion dynamics and apoptosis. *Mitochondrion*, 10(6), 640-648.
- Sherr, C. J. (1996). Cancer cell cycles. *Science*, 274(5293), 1672-1674.
- Shields, J. D., Kourtis, I. C., Tomei, A. A., Roberts, J. M., & Swartz, M. A. (2010). Induction of Lymphoidlike Stroma and Immune Escape by Tumors That Express the Chemokine CCL21. *Science*, 328(5979), 749-752.
- Siegel, R., Naishadham, D., & Jemal, A. (2013). Cancer statistics, 2013. *CA Cancer Journal for Clinicians*, 63(1), 11-30.
- Siegel, R. L., Miller, K. D., & Jemal, A. (2016). Cancer statistics, 2016. *CA: A Cancer Journal for Clinicians*, 66(1), 7-30.

- Silverstein, R. A., González de Valdivia, E., & Visa, N. (2011). The Incorporation of 5-Fluorouracil into RNA Affects the Ribonucleolytic Activity of the Exosome Subunit Rrp6. *Molecular Cancer Research*, 9(3), 332-340.
- Soares, M. A., Lessa, J. A., Mendes, I. C., Da Silva, J. G., dos Santos, R. G., Salum, L. B. (2012). N4-Phenyl-substituted 2-acetylpyridine thiosemicarbazones: Cytotoxicity against human tumor cells, structure–activity relationship studies and investigation on the mechanism of action. *Bioorganic & Medicinal Chemistry*, 20(11), 3396-3409.
- Sobel, R. E., & Sadar, M. D. (2005). Cell lines used in prostate cancer research: A compendium of old and new lines - Part 1. *J. Urol*, 173(2), 342-359.
- Soengas, M. S., & Lowe, S. W. (2003). Apoptosis and melanoma chemoresistance. *Oncogene*, 22(20), 3138-3151.
- Spano, D., Heck, C., De Antonellis, P., Christofori, G., & Zollo, M. (2012). Molecular networks that regulate cancer metastasis. *Seminars in Cancer Biology*, 22(3), 234-249.
- Sporn, M. B. (1996). The war on cancer. *Lancet*, 347(9012), 1377-1381.
- Stringer, T., Therrien, B., Hendricks, D. T., Guzgay, H., & Smith, G. S. (2011). Mono- and dinuclear (η^6 -arene) ruthenium(II) benzaldehyde thiosemicarbazone complexes: Synthesis, characterization and cytotoxicity. *Inorganic Chemistry Communications*, 14(6), 956-960.
- Suzuki, Y., Sakai, D., Nomura, T., Hirata, Y., & Aihara, K. (2014). A new protocol for intermittent androgen suppression therapy of prostate cancer with unstable saddle-point dynamics. *Journal of Theoretical Biology*, 350, 1-16.
- Tadros, A. B., & El-Batouti, M. (2004). Spectral study and antifouling assessment of some thiosemicarbazone derivatives. *Anti-Corrosion Methods and Materials*, 51(6), 406-413.
- Tai, S., Sun, Y., Squires, J. M., Zhang, H., Oh, W. K., Liang, C. Z. (2011). PC3 is a cell line characteristic of prostatic small cell carcinoma. *Prostate*, 71(15), 1668-1679.
- Tan, K. W., Seng, H. L., Lim, F. S., Cheah, S.-C., Ng, C. H., Koo, K. S. (2012). Towards a selective cytotoxic agent for prostate cancer: Interaction of zinc complexes of polyhydroxybenzaldehyde thiosemicarbazones with topoisomerase I. *Polyhedron*, 38(1), 275-284.
- Taplin, M. E., Bubley, G. J., Shuster, T. D., Frantz, M. E., Spooner, A. E., Ogata, G. K. (1995). Mutation of the androgen-receptor gene in metastatic androgen-independent prostate cancer. *New England Journal of Medicine*, 332(21), 1393-1398.
- Taylor, R. C., Cullen, S. P., & Martin, S. J. (2008). Apoptosis: Controlled demolition at the cellular level. *Nature Reviews Molecular Cell Biology*, 9(3), 231-241.

- Trondl, R., Flocke, L. S., Kowol, C. R., Heffeter, P., Jungwirth, U., Mair, G. E. (2014). Triapine and a More Potent Dimethyl Derivative Induce Endoplasmic Reticulum Stress in Cancer Cells. *Molecular Pharmacology*, 85(3), 451-459.
- Tu, S., Wai-Yin Sun, R., Lin, M. C. M., Tao Cui, J., Zou, B., Gu, Q. (2009). Gold (III) porphyrin complexes induce apoptosis and cell cycle arrest and inhibit tumor growth in colon cancer. *Cancer*, 115(19), 4459-4469.
- Turner, W., Bauer, D. J., & Nimmo-Smith, R. H. (1962). Eczema Vaccinatum Treated with N-Methylisatin β -Thiosemicarbazone. *British Medical Journal*, 1(5288), 1317-1319.
- Velders, A. H., Van Der Geest, B., Kooijman, H., Spek, A. L., Haasnoot, J. G., & Reedijk, J. (2001). Ruthenium(III) coordination to the exocyclic nitrogen of 9-methyladenine and stabilisation of the rare imine tautomer by intramolecular hydrogen bonding. *European Journal of Inorganic Chemistry*(2), 369-372.
- Veselinović, J. B., Kocić, G. M., Pavic, A., Nikodinovic-Runic, J., Senerovic, L., Nikolić, G. M. (2015). Selected 4-phenyl hydroxycoumarins: In vitro cytotoxicity, teratogenic effect on zebrafish (*Danio rerio*) embryos and molecular docking study. *Chemico-Biological Interactions*, 231, 10-17.
- Vyas, S., Zaganjor, E., & Haigis, Marcia C. (2016). Mitochondria and Cancer. *Cell*, 166(3), 555-566.
- Wadler, S., Makower, D., Clairmont, C., Lambert, P., Fehn, K., & Sznol, M. (2004). Phase I and Pharmacokinetic Study of the Ribonucleotide Reductase Inhibitor, 3-Aminopyridine-2-Carboxaldehyde Thiosemicarbazone, Administered by 96-Hour Intravenous Continuous Infusion. *Journal of Clinical Oncology*, 22(9), 1553-1563.
- Warburg, O., Wind, F., & Negelein, E. (1927). The metabolism of tumors in the body. *The Journal of General Physiology*, 8(6), 519-530.
- Waugh, D. J. J., & Wilson, C. (2008). The Interleukin-8 Pathway in Cancer. *Clinical Cancer Research*, 14(21), 6735-6741.
- Wiles, D. M., Gingras, B. A., & Suprunchuk, T. (1967). The C=S stretching vibration in the infrared spectra of some thiosemicarbazones. *Canadian Journal of Chemistry*, 45(5), 469-473.
- Wu, W., & Zhao, S. (2013). Metabolic changes in cancer: beyond the Warburg effect. *Acta Biochimica et Biophysica Sinica*, 45(1), 18-26.
- Xie, W., Xie, S., Zhou, Y., Tang, X., Liu, J., Yang, W. (2014). Design and synthesis of novel 5,6-disubstituted pyridine-2,3-dione-3-thiosemicarbazone derivatives as potential anticancer agents. *European Journal of Medicinal Chemistry*, 81(0), 22-27.
- Xu, R., Zhang, Y., Ye, X., Xue, S., Shi, J., Pan, J. (2013). Inhibition effects and induction of apoptosis of flavonoids on the prostate cancer cell line PC-3 in vitro. *Food Chemistry*, 138(1), 48-53.

- Yildirim, H., Guler, E., Yavuz, M., Ozturk, N., Kose Yaman, P., Subasi, E. (2014). Ruthenium (II) complexes of thiosemicarbazone: Synthesis, biosensor applications and evaluation as antimicrobial agents. *Materials Science and Engineering: C*, 44(0), 1-8.
- Yu, Y., Rahmanto, Y. S., & Richardson, D. R. (2012). Bp44mT: An orally active iron chelator of the thiosemicarbazone class with potent anti-tumour efficacy. *British Journal of Pharmacology*, 165(1), 148-166.
- Yuan, H., Cho, H., Chen, H. H., Panagia, M., Sosnovik, D. E., & Josephson, L. (2013). Fluorescent and radiolabeled triphenylphosphonium probes for imaging mitochondria. *Chemical Communications*, 49(88), 10361-10363.
- Yuan, J., Lovejoy, D. B., & Richardson, D. R. (2004). Novel di-2-pyridyl-derived iron chelators with marked and selective antitumor activity: in vitro and in vivo assessment. *Blood*, 104(5), 1450-1458.
- Zhang, Q., Ma, Y., Yang, S., Xu, B., & Fei, X. (2015). Small-sized gold nanoparticles inhibit the proliferation and invasion of SW579 cells. *Molecular Medicine Reports*, 12(6), 8313-8319.
- Zhou, C., Qian, L., Ma, H., Yu, X., Zhang, Y., Qu, W. (2012). Enhancement of amygdalin activated with β -d-glucosidase on HepG2 cells proliferation and apoptosis. *Carbohydrate Polymers*, 90(1), 516-523.
- Ziegler, U., & Groscurth, P. (2004). Morphological features of cell death. *News in Physiological Sciences*, 19, 124-128.

LIST OF PUBLICATIONS

1. Saravana Kumar Sinniah, Kong Wai Tan, Seik Weng Ng and Kae Shin Sim (2017). Thiosemicarbazone derivative induces in vitro apoptosis in metastatic PC-3 cells via activation of mitochondrial pathway. *Anti-Cancer Agents in Medicinal Chemistry*. **(Accepted)**
2. Saravana Kumar Sinniah, Kong Wai Tan, Kae Shin Sim, Seik Weng Ng and Edward R. T. Tiekink (2012). [3-((E)-2-[(4-Fluorophenyl)carbamothioyl]hydrazinylidene)methyl)-4-hydroxy-benzyl]methyl-triphenyl-phosphonium chloride. *Acta Crystallographica Section E Structure Report Online*. 67:03330-3331.
3. Shin Thung Chew, Kong Mun Lo, Saravana Kumar Sinniah, Kae Shin Sim and Kong Wai Tan (2014). Synthesis, characterization and biological evaluation of cationic hydrazone copper complexes with diverse diimine co-ligands. *RSC Advances*. 4,61232.
4. Mok Piew Heng, Saravana Kumar Sinniah, Wuen Yew Teoh, Kae Shin Sim, Seik Weng Ng, Yoke kqueen Cheah and Kong Wai Tan (2015). Synthesis of a DNA-targeting nickel (II) complex with testosterone thiosemicarbazone which exhibits selective cytotoxicity towards human prostate cancer cells (LNCAP). *Spectrochimica Acta Part A Molecular and Biomolecular Spectroscopy*. 150(1):360-372.

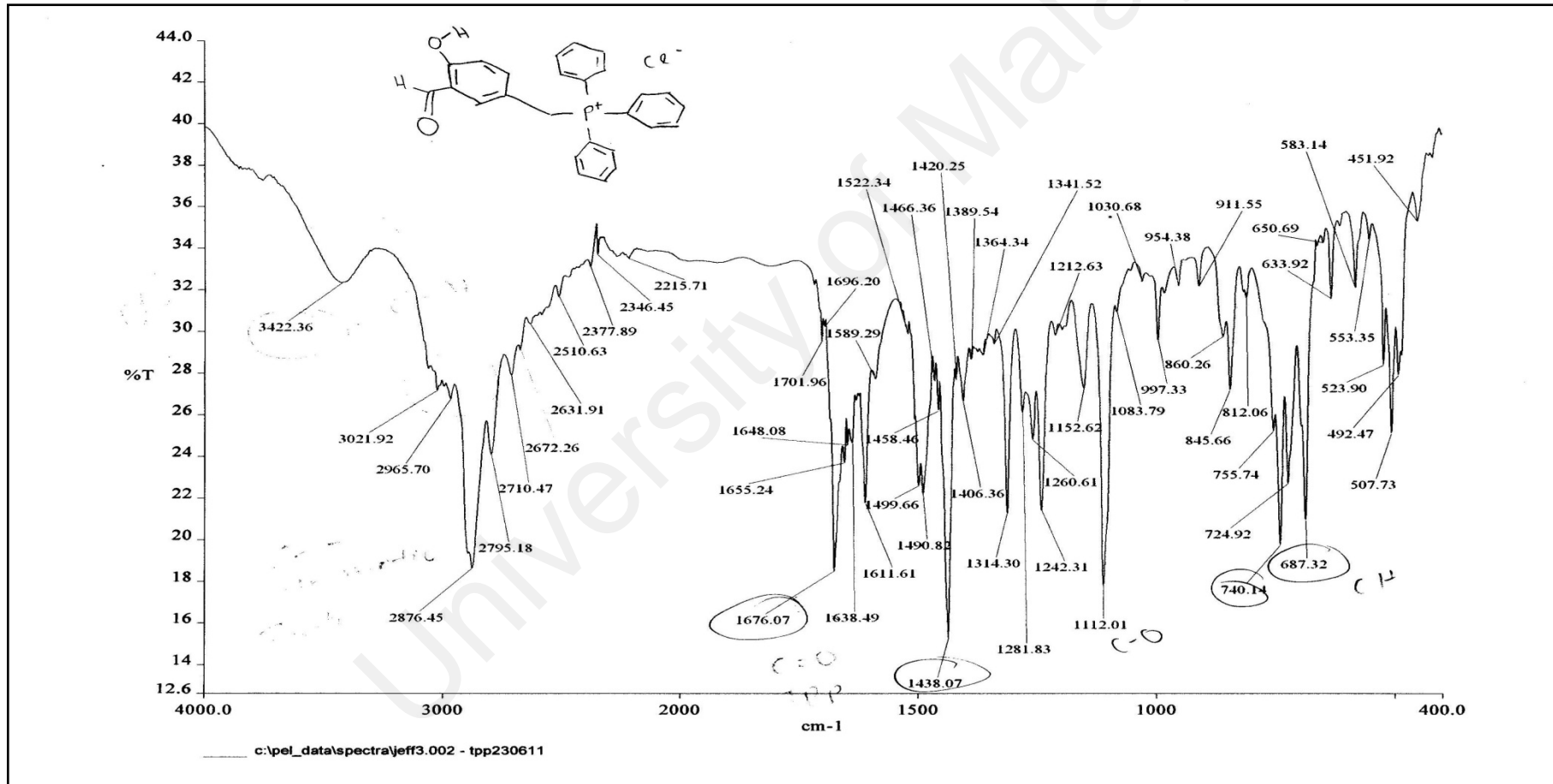
PAPERS PRESENTED IN CONFERENCE

1. Cytotoxic activities of synthetic compounds derived from cationic thiosemicarbazones. Presented at 17th Biological Sciences Graduate Congress (Thailand, Chulalongkorn University) (December 2012).
2. Cytotoxic activities, apoptotic induction and mitochondrial studies of cationic Schiff bases from the thiosemicarbazone family. Presented at Malaysian Toray Science Foundation Grant Research Symposium (Malaysia, University of Malaya) (November 2015)

APPENDICES

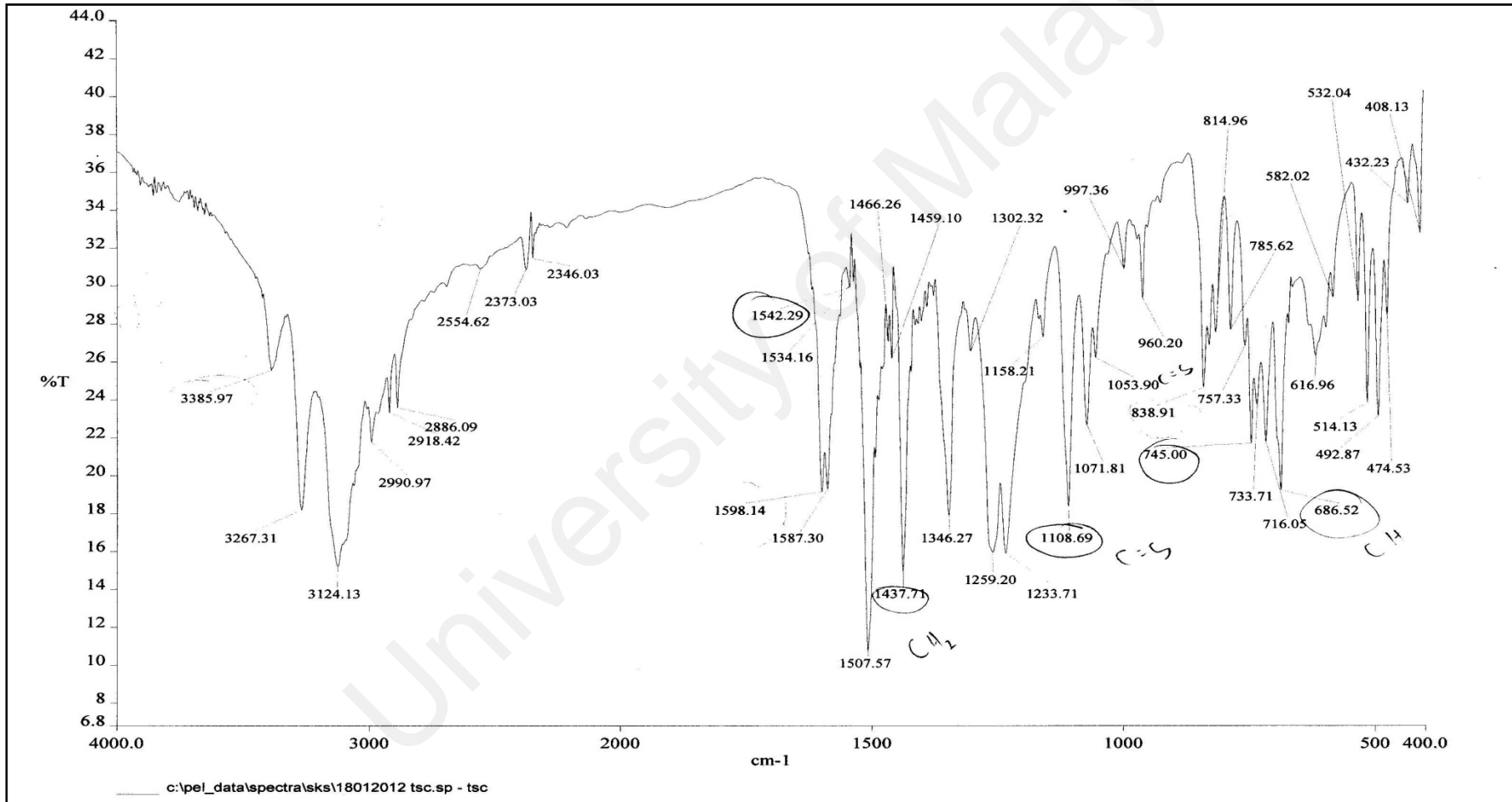
Appendix 1

IR spectrum of T



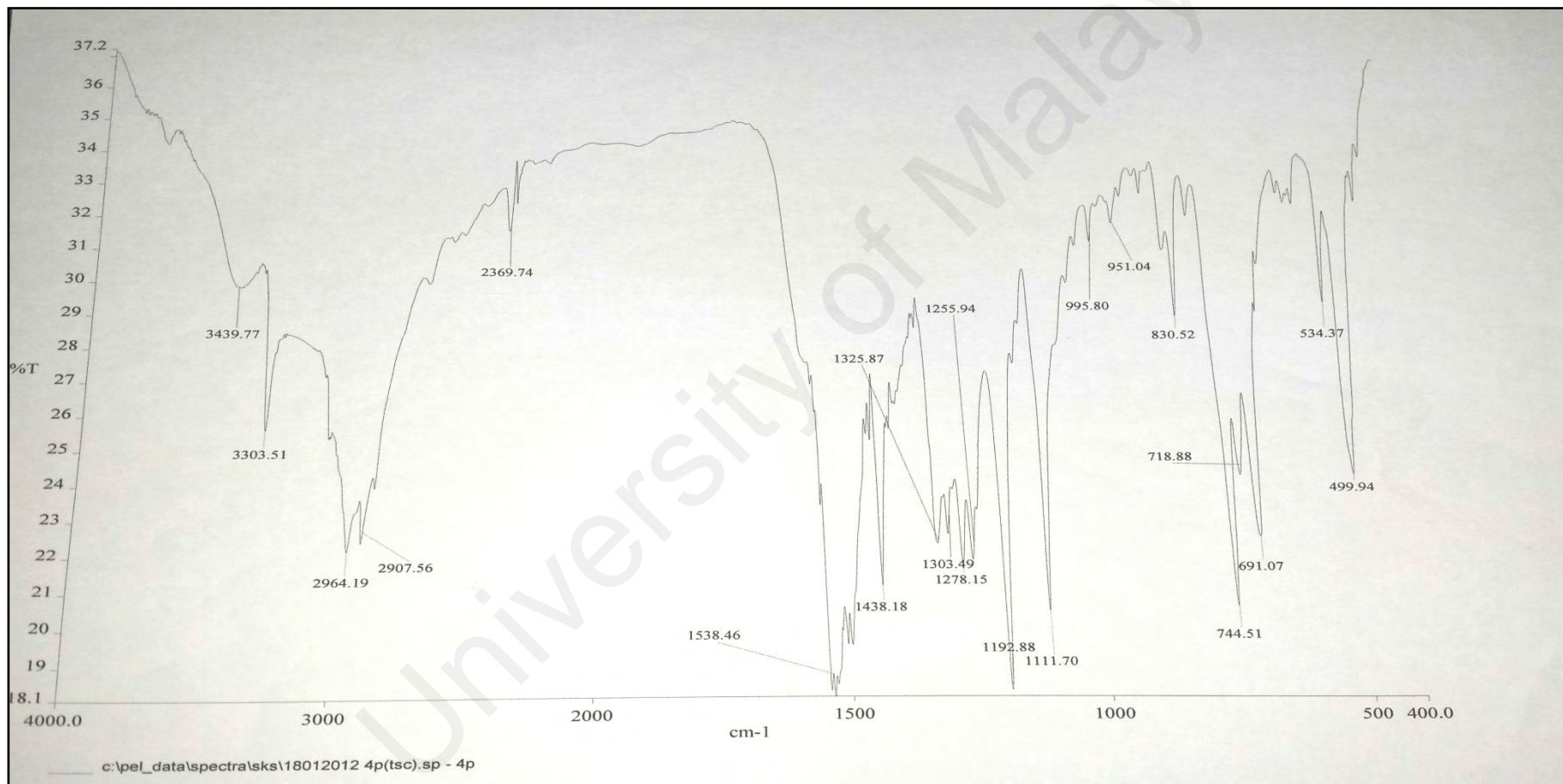
Appendix 2

IR spectrum of T(tsc)T



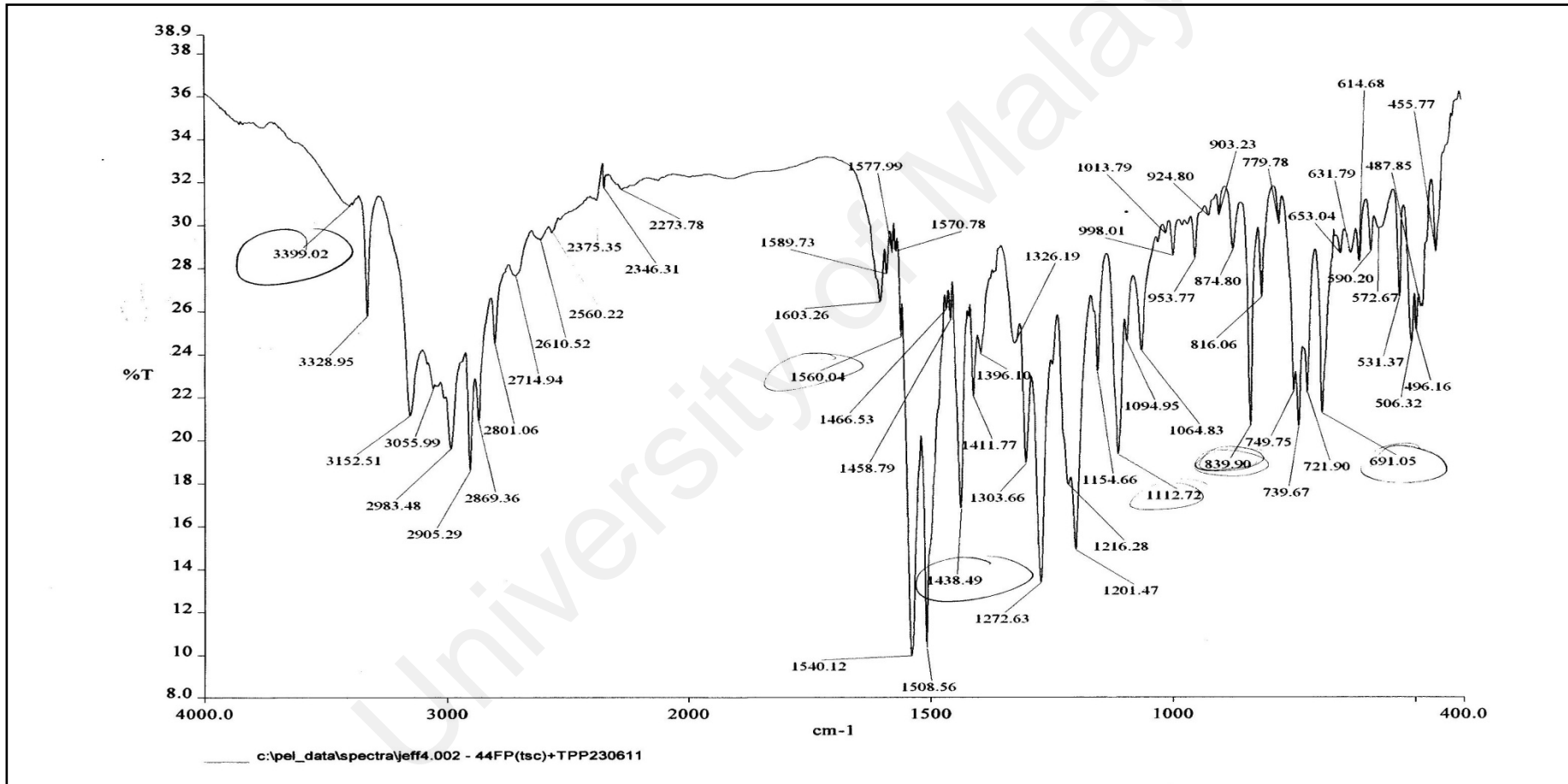
Appendix 3

IR spectrum of P(tsc)T



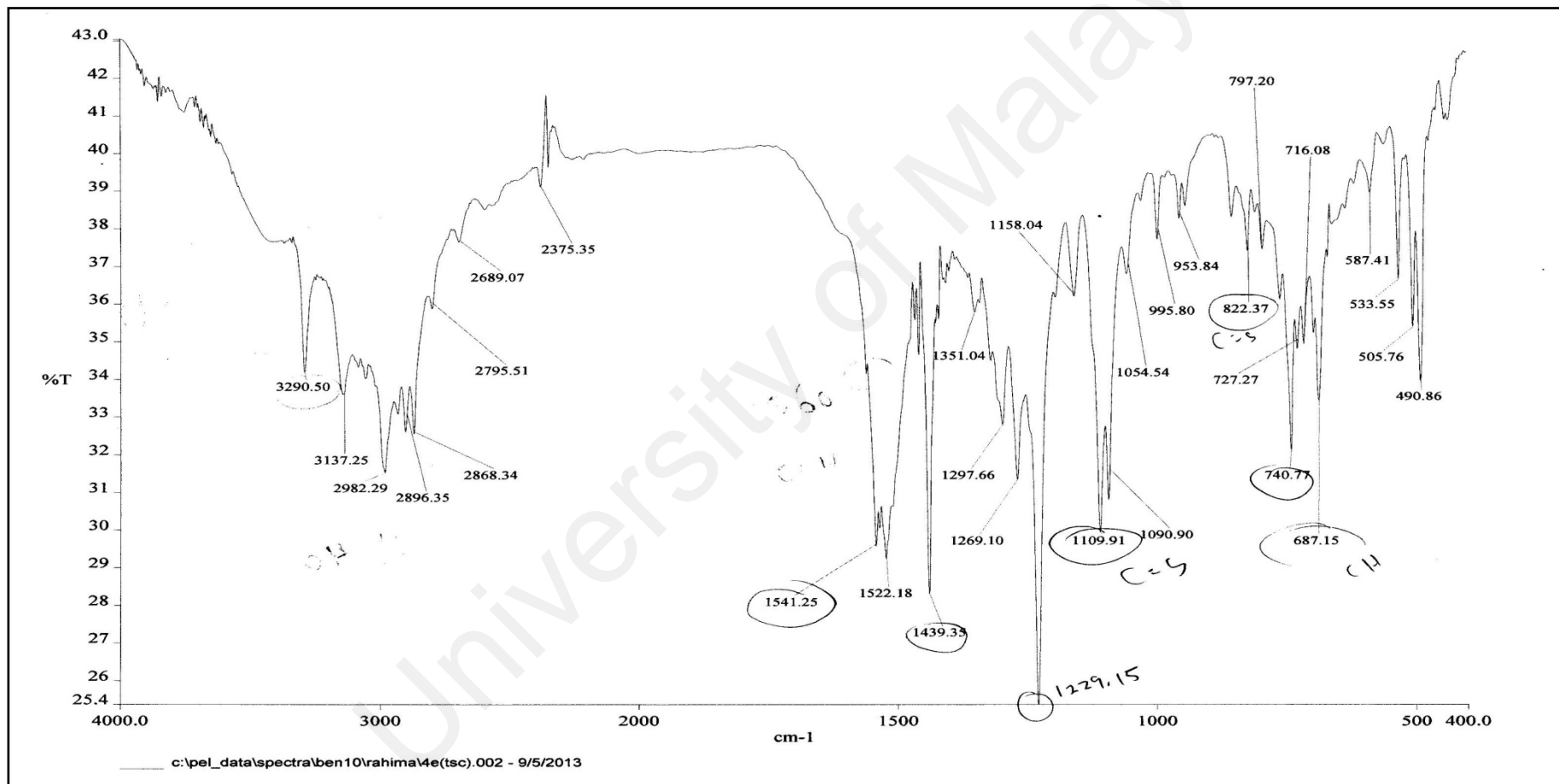
Appendix 4

IR spectrum of FP(tsc)T



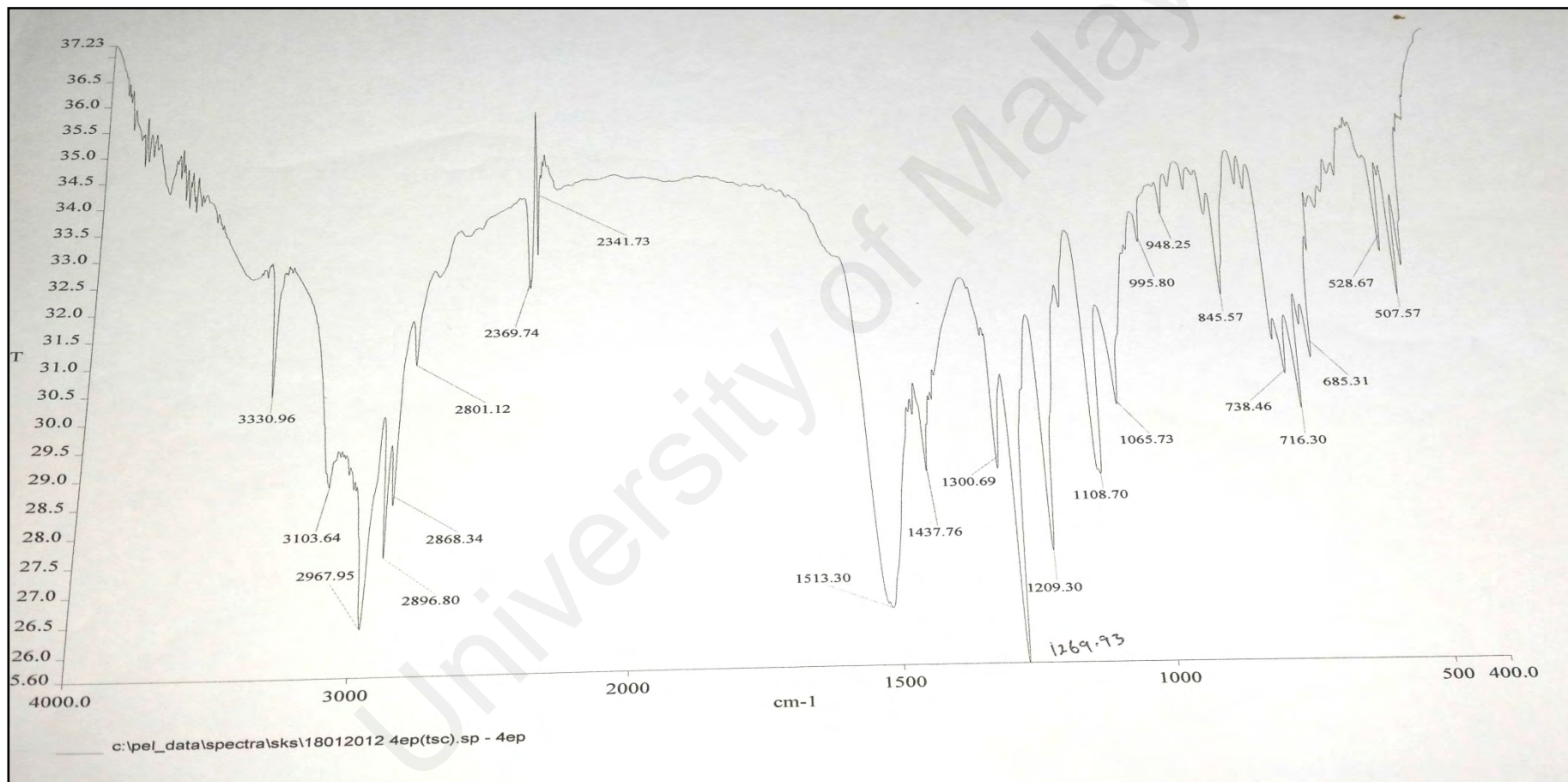
Appendix 5

IR spectrum of E(tsc)T



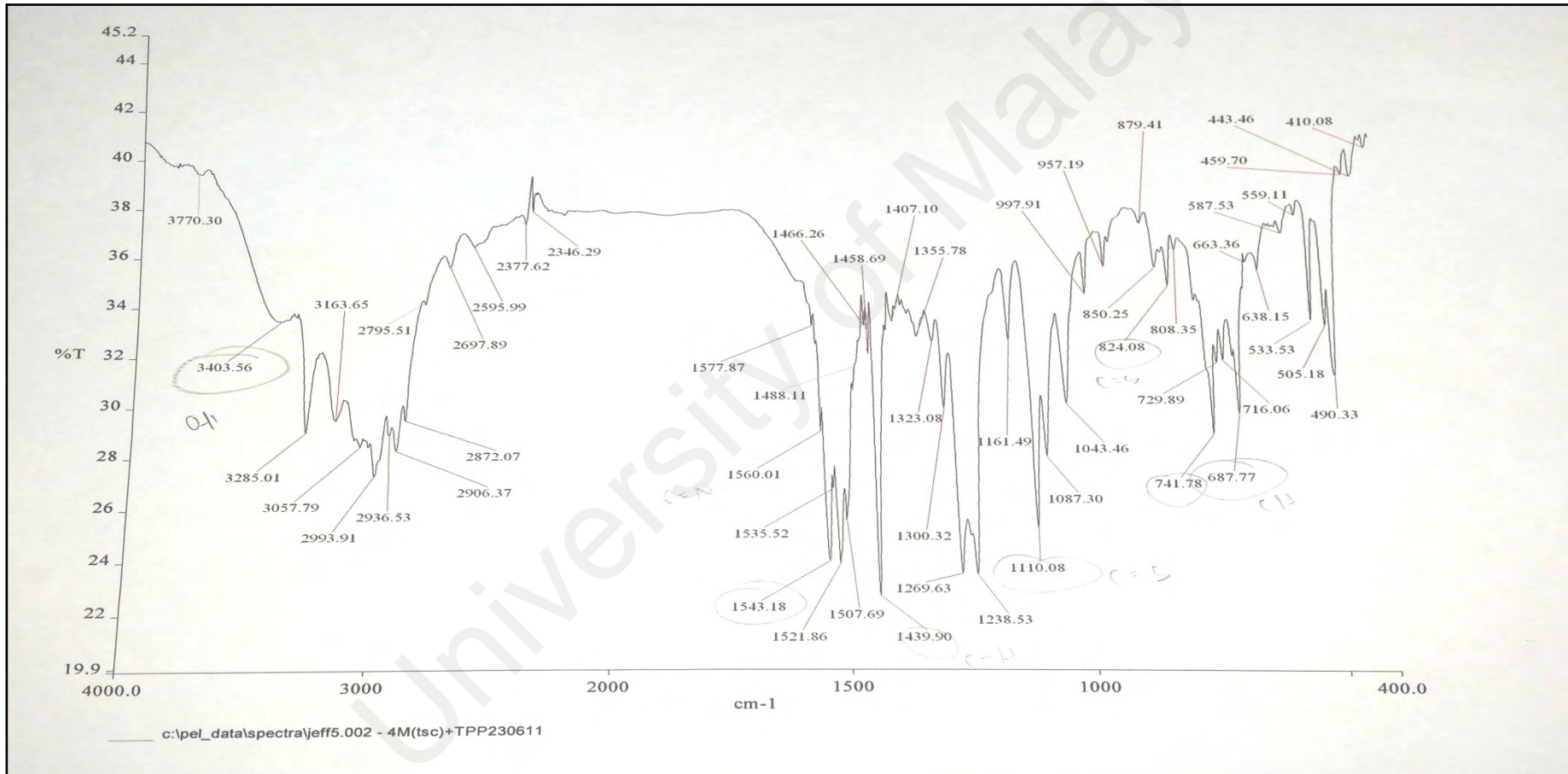
Appendix 6

IR spectrum of EP(tsc)T



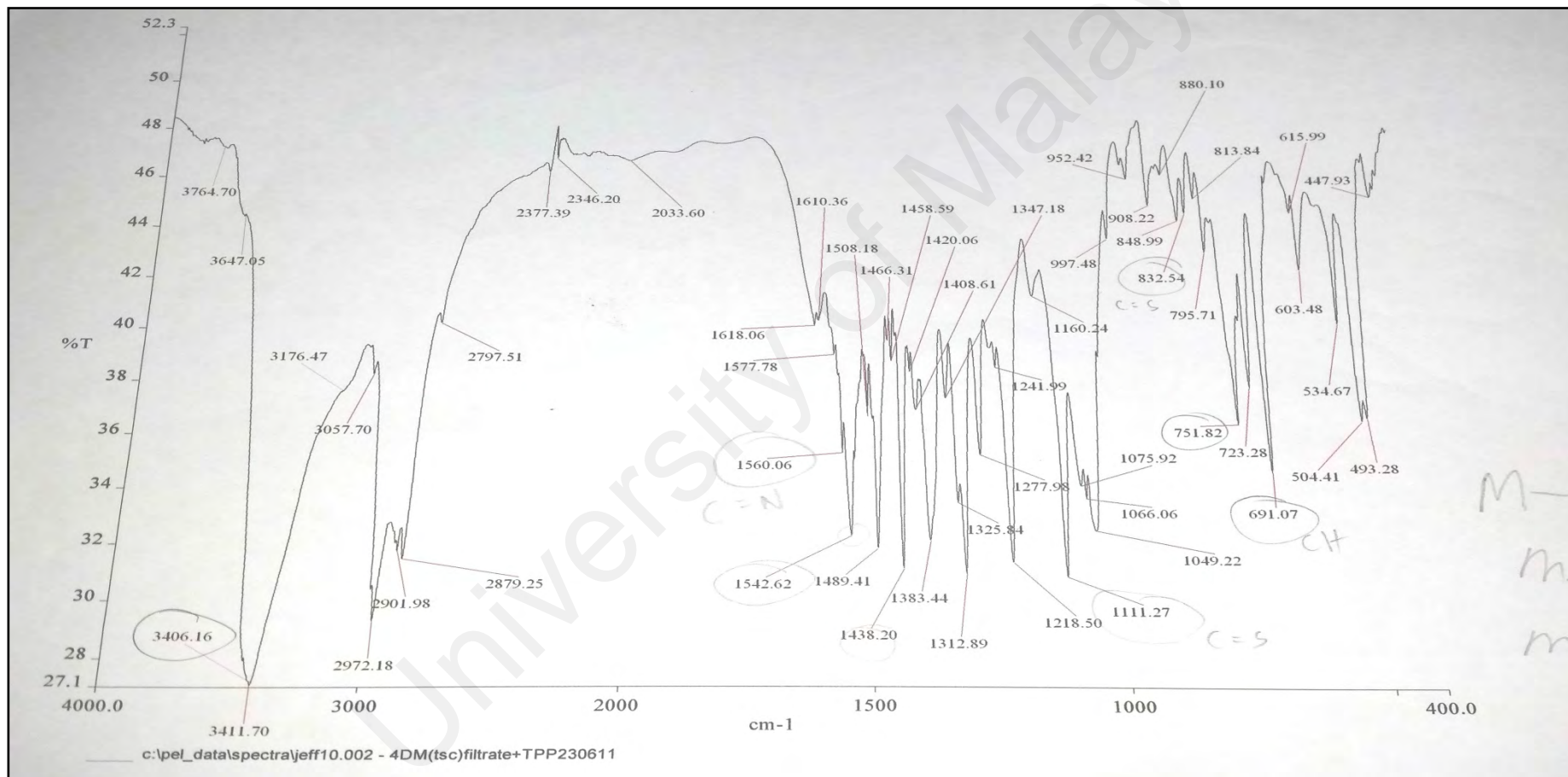
Appendix 7

IR spectrum of **M(tsc)T**



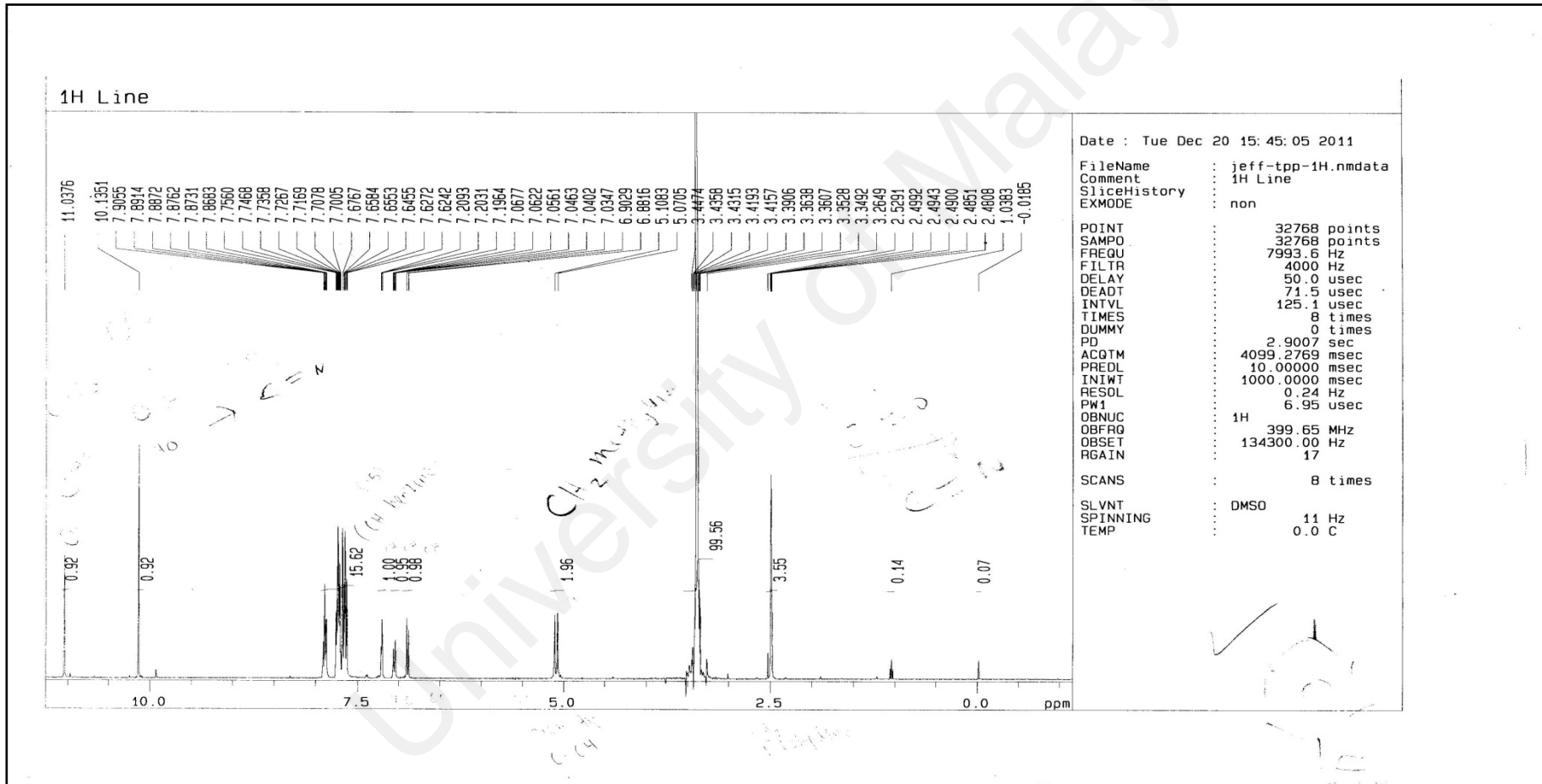
Appendix 8

IR spectrum of DM(tsc)T



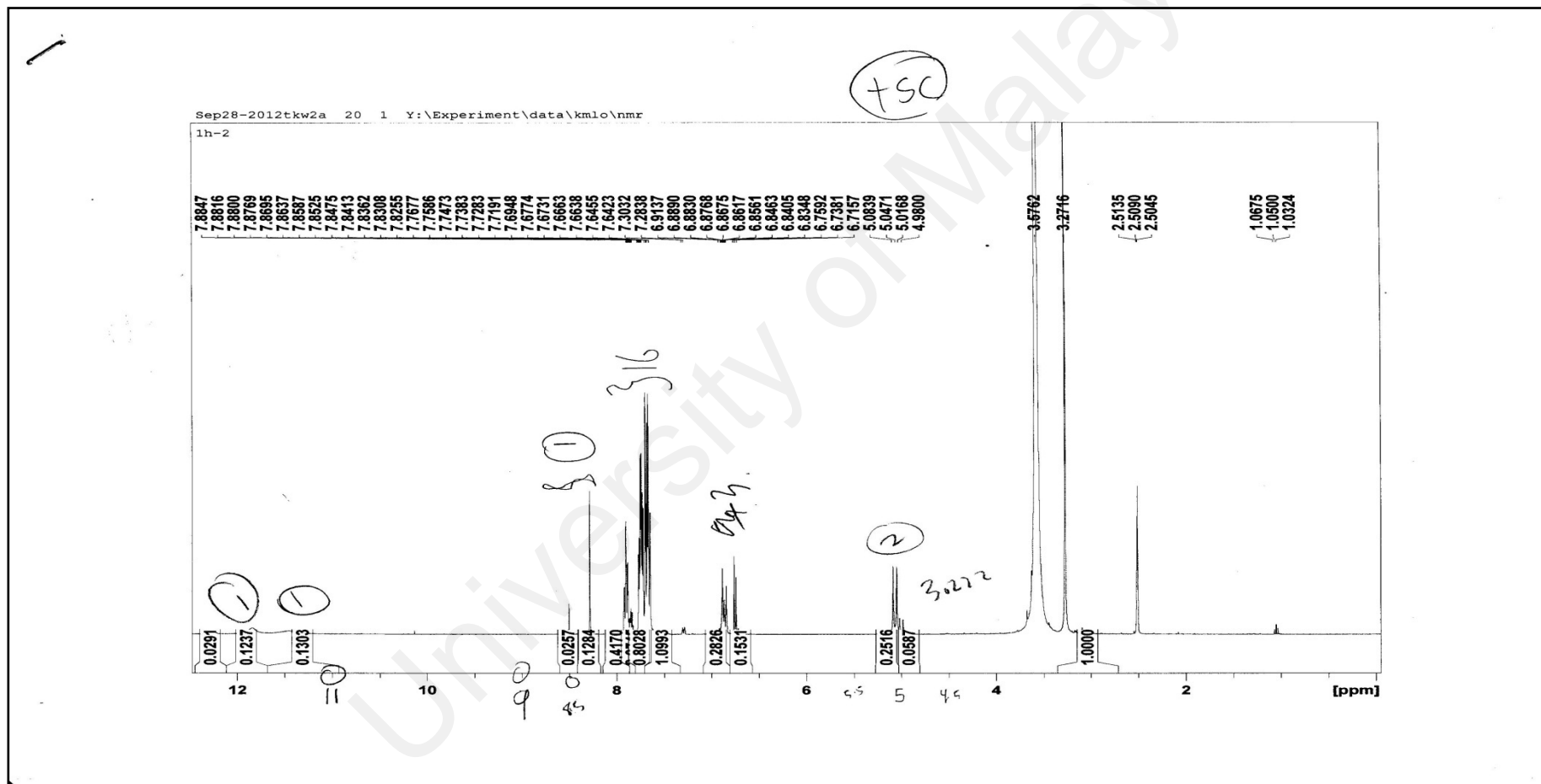
Appendix 9

¹H NMR of T



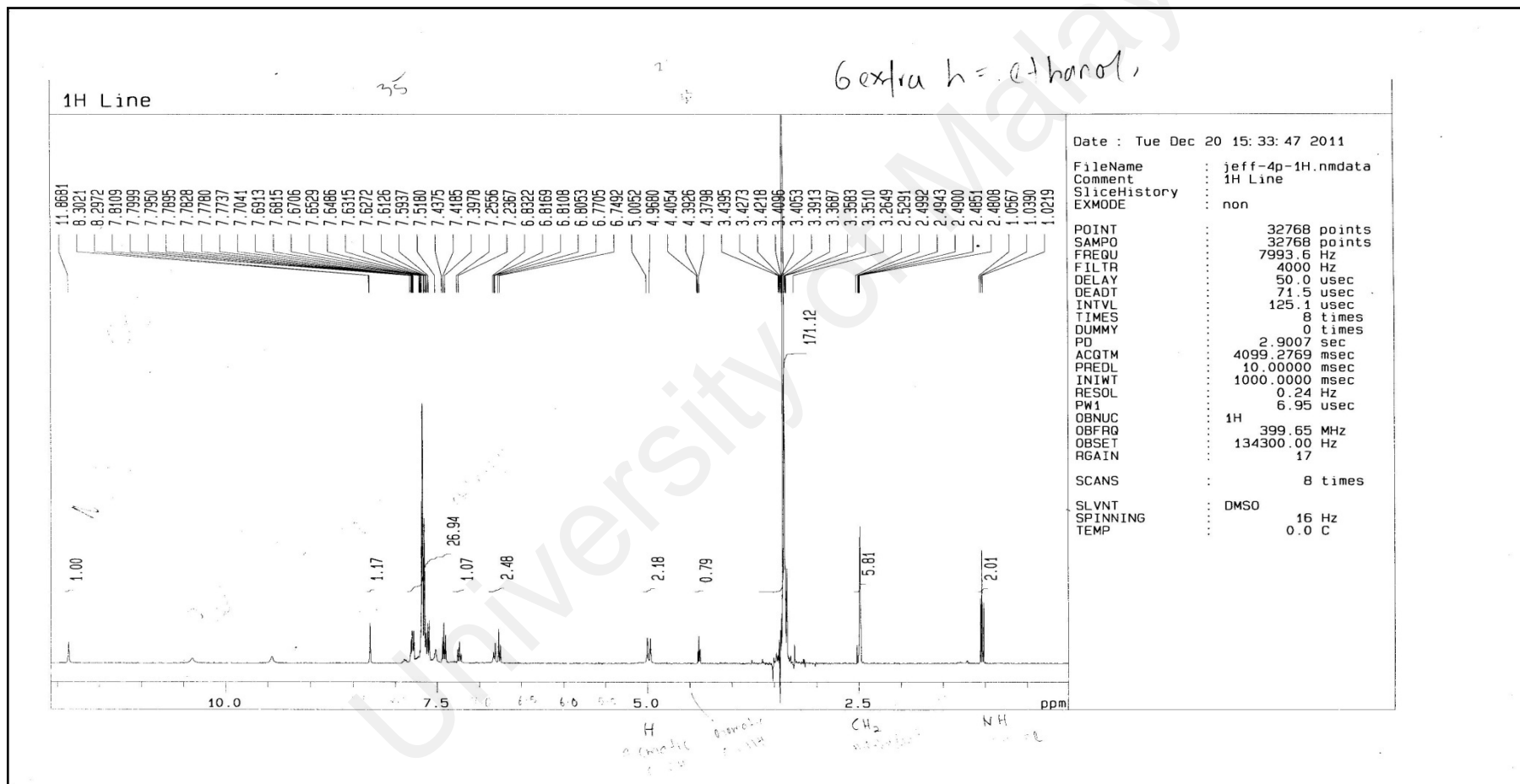
Appendix 10

¹H NMR of T(tsc)T



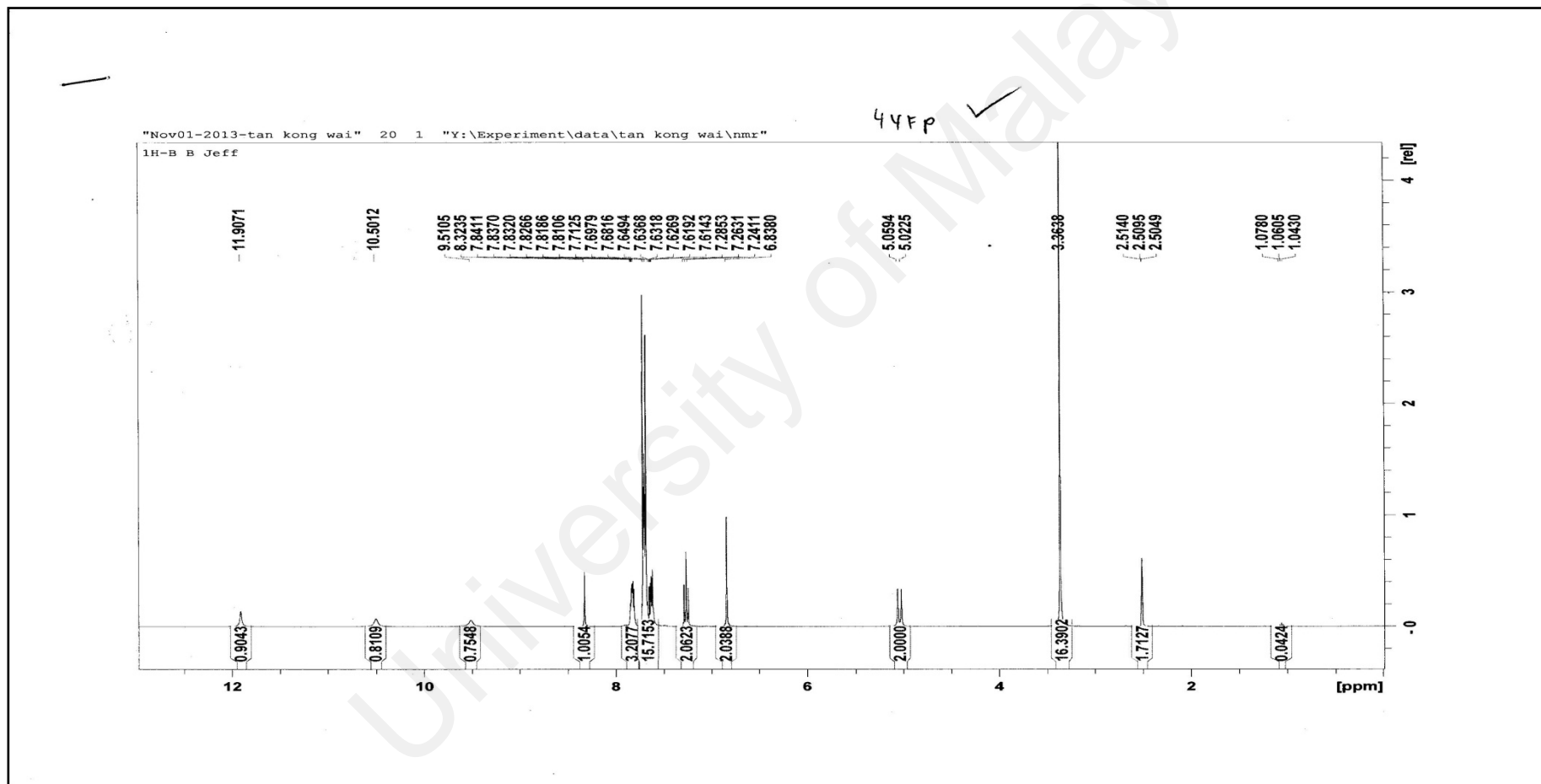
Appendix 11

¹H NMR of P(tsc)T



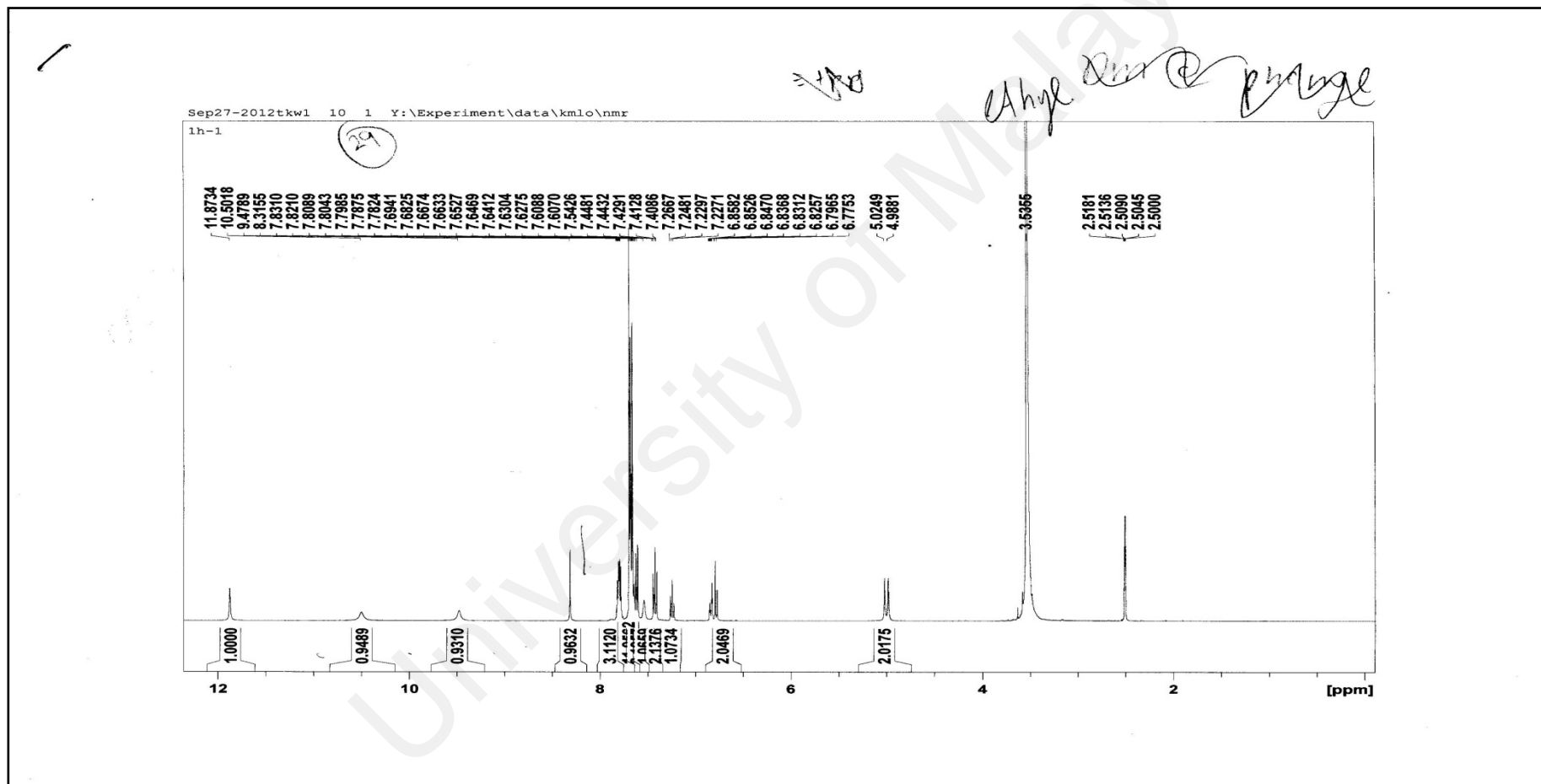
Appendix 12

¹H NMR of FP(tsc)T



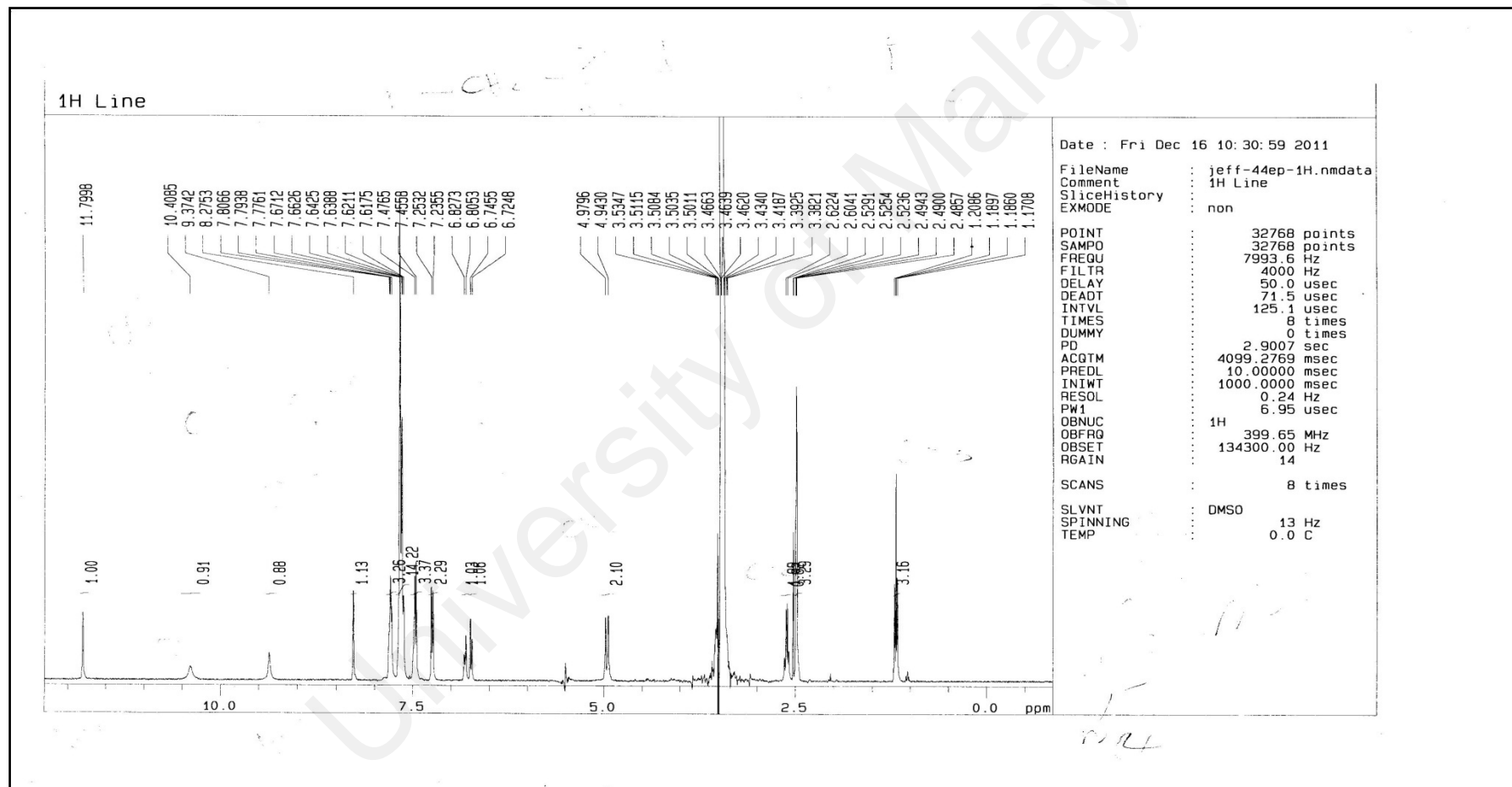
Appendix 13

¹H NMR of E(tsc)T



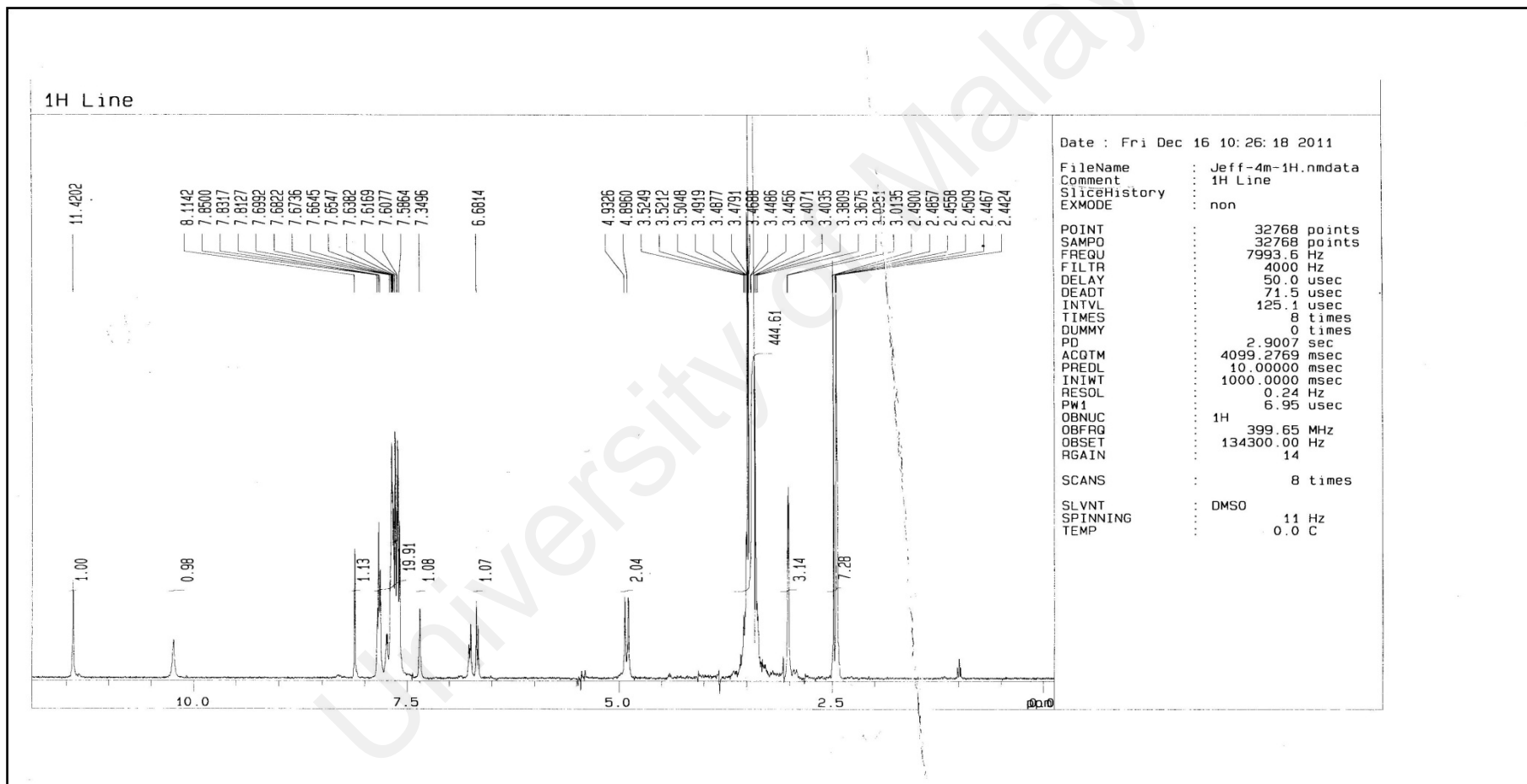
Appendix 14

¹H NMR of EP(tsc)T



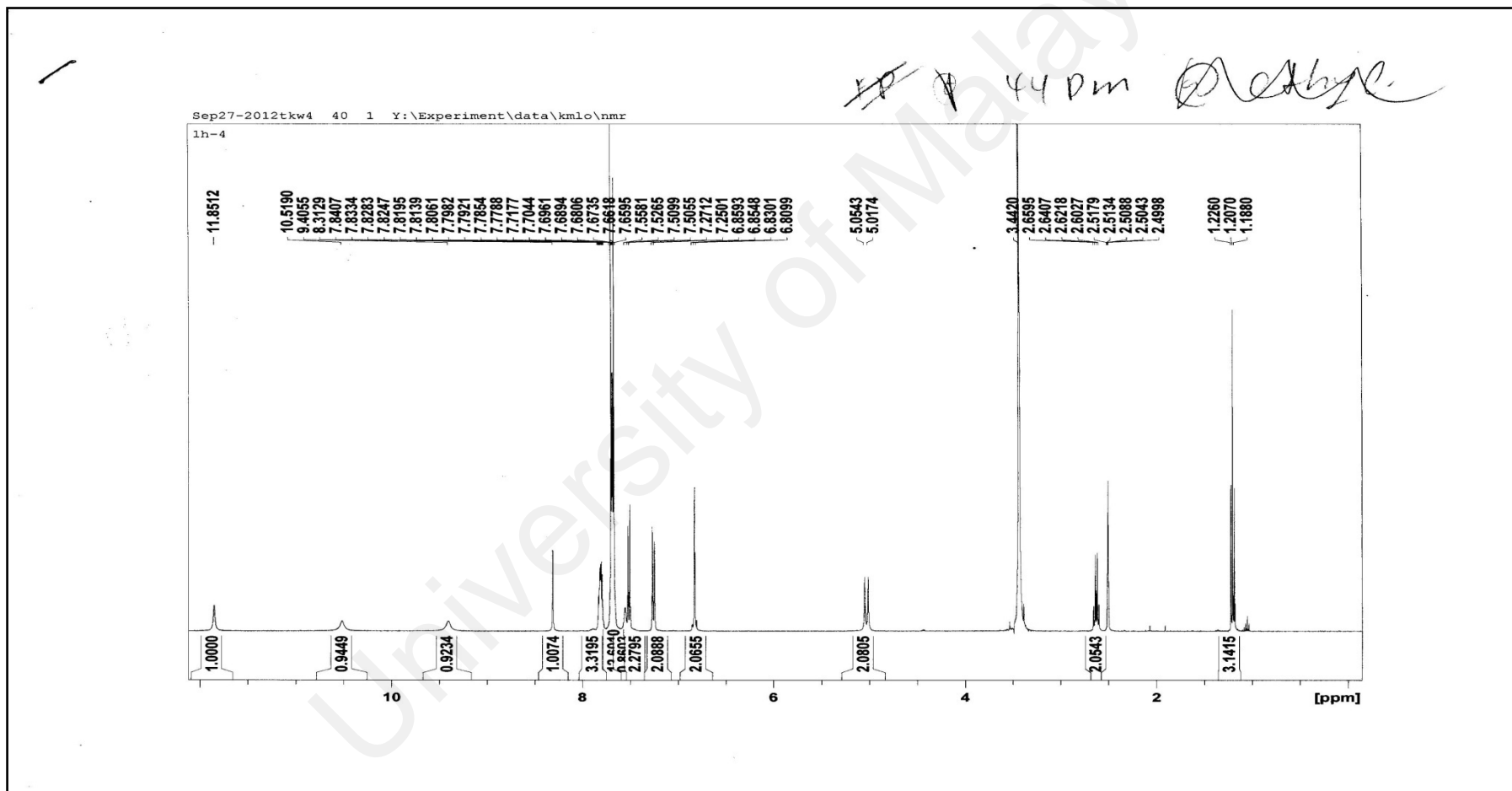
Appendix 15

¹H NMR of M(tsc)T



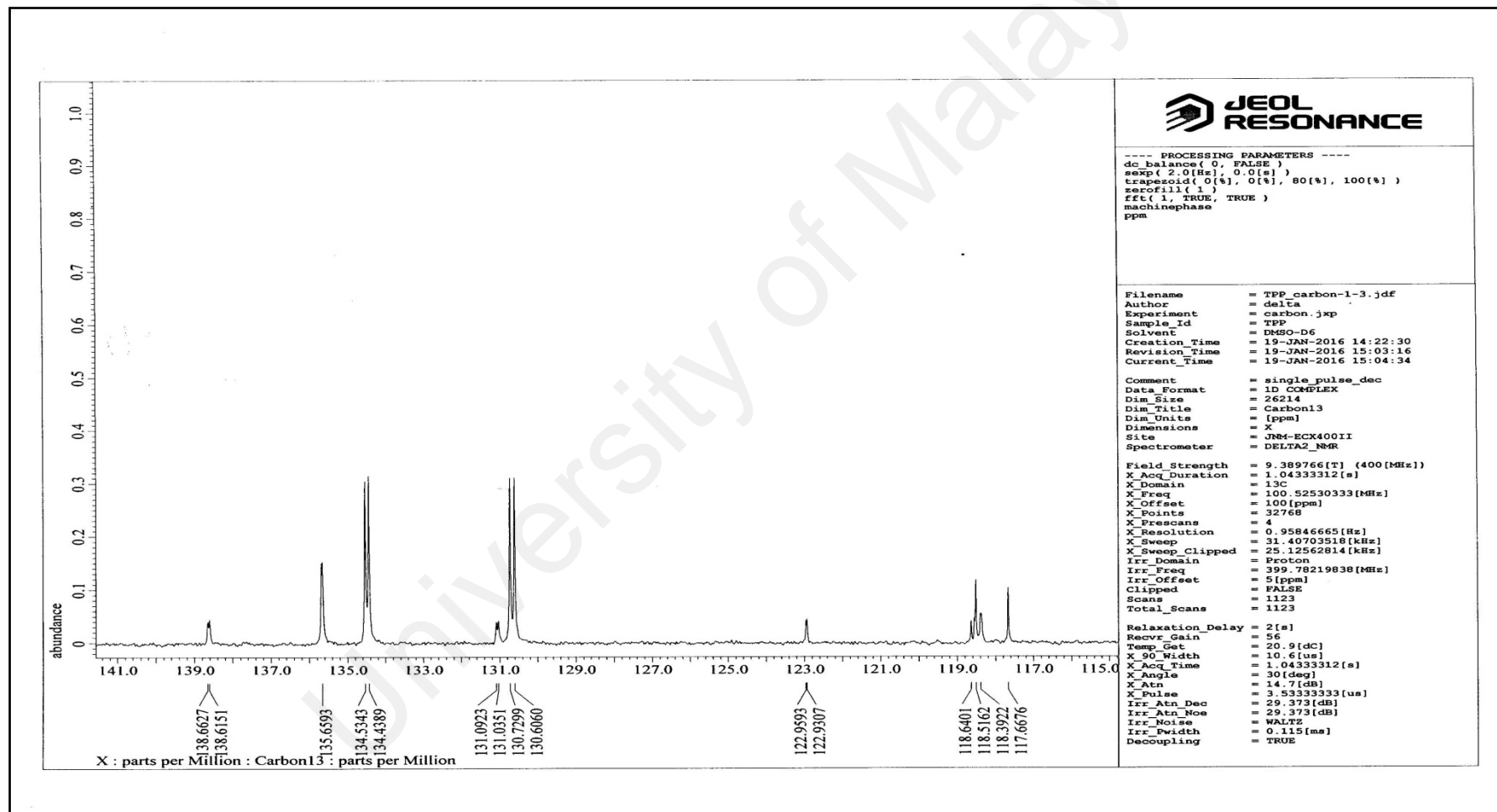
Appendix 16

¹H NMR of DM(tsc)



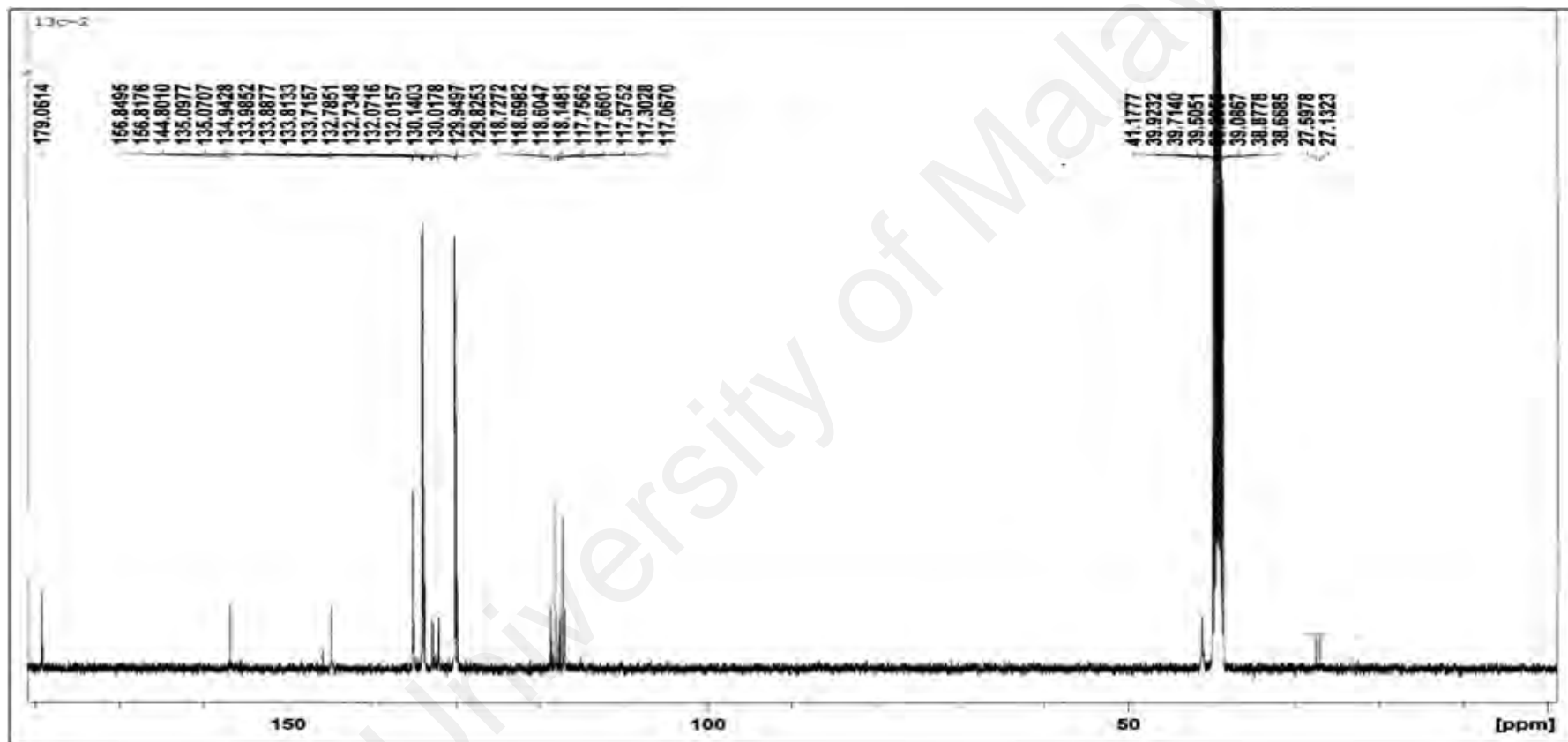
Appendix 17

¹³C NMR of T



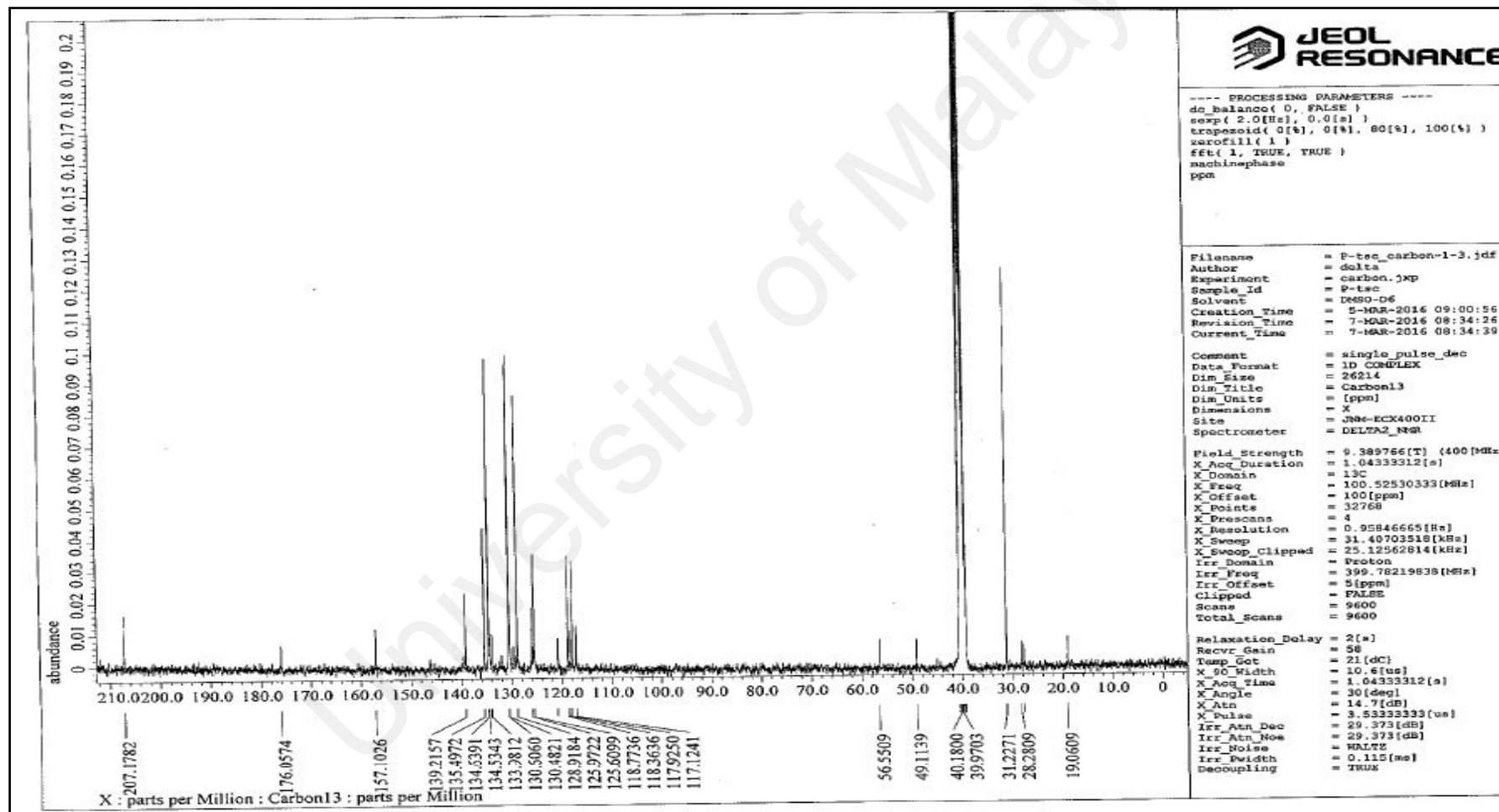
Appendix 18

^{13}C NMR of (tsc)T



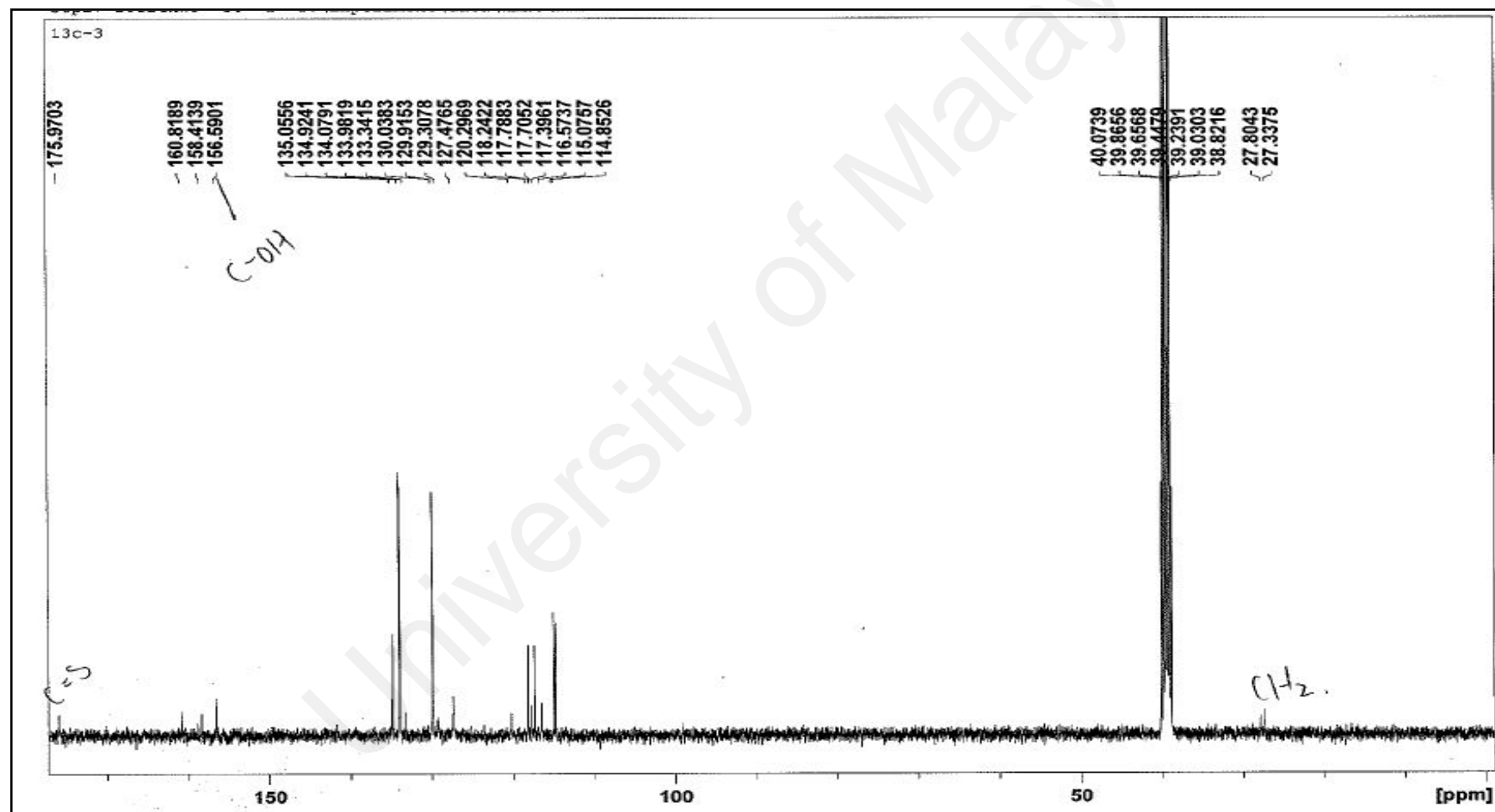
Appendix 19

¹³C NMR of P(tsc)T



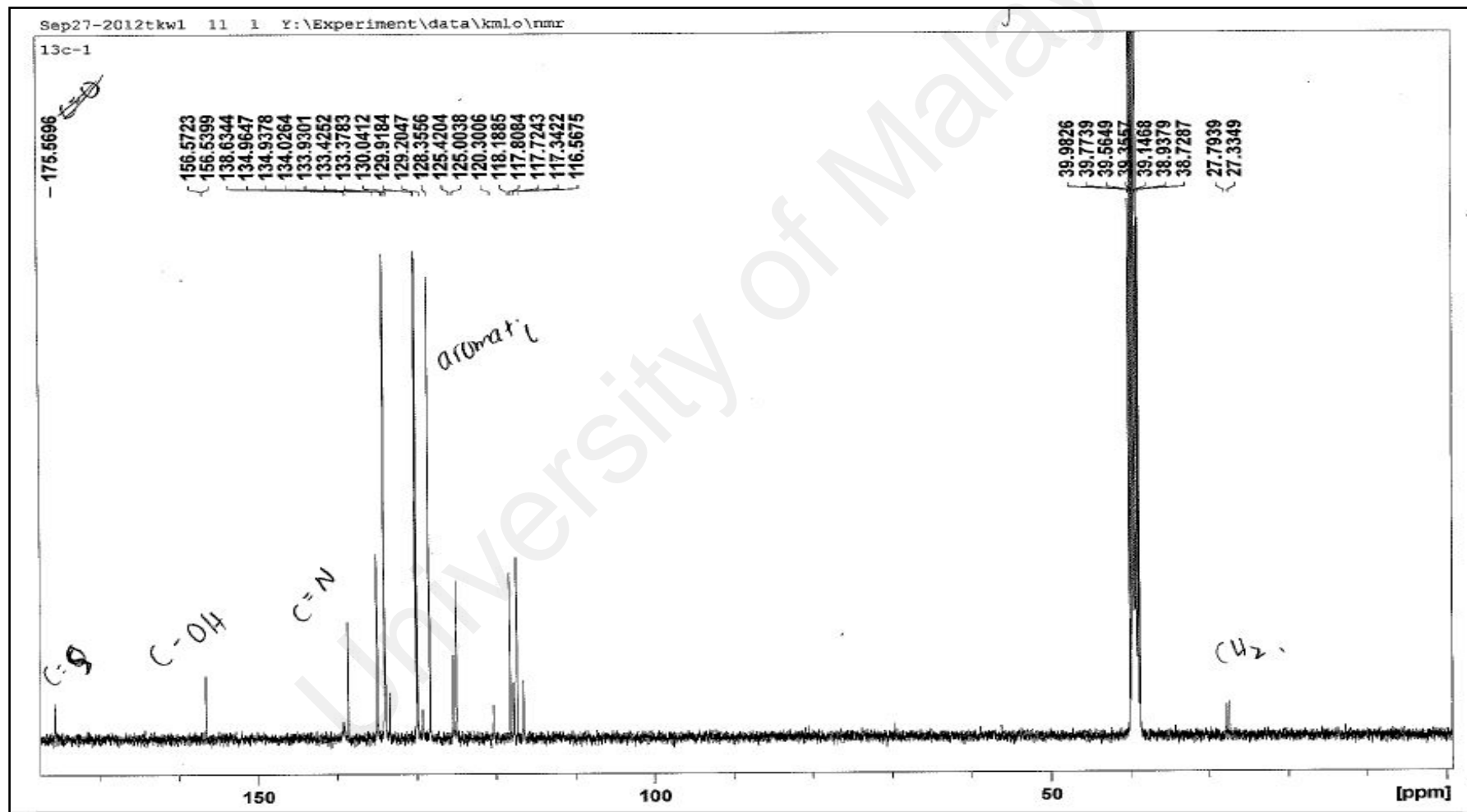
Appendix 20

^{13}C NMR of FP(tsc)T



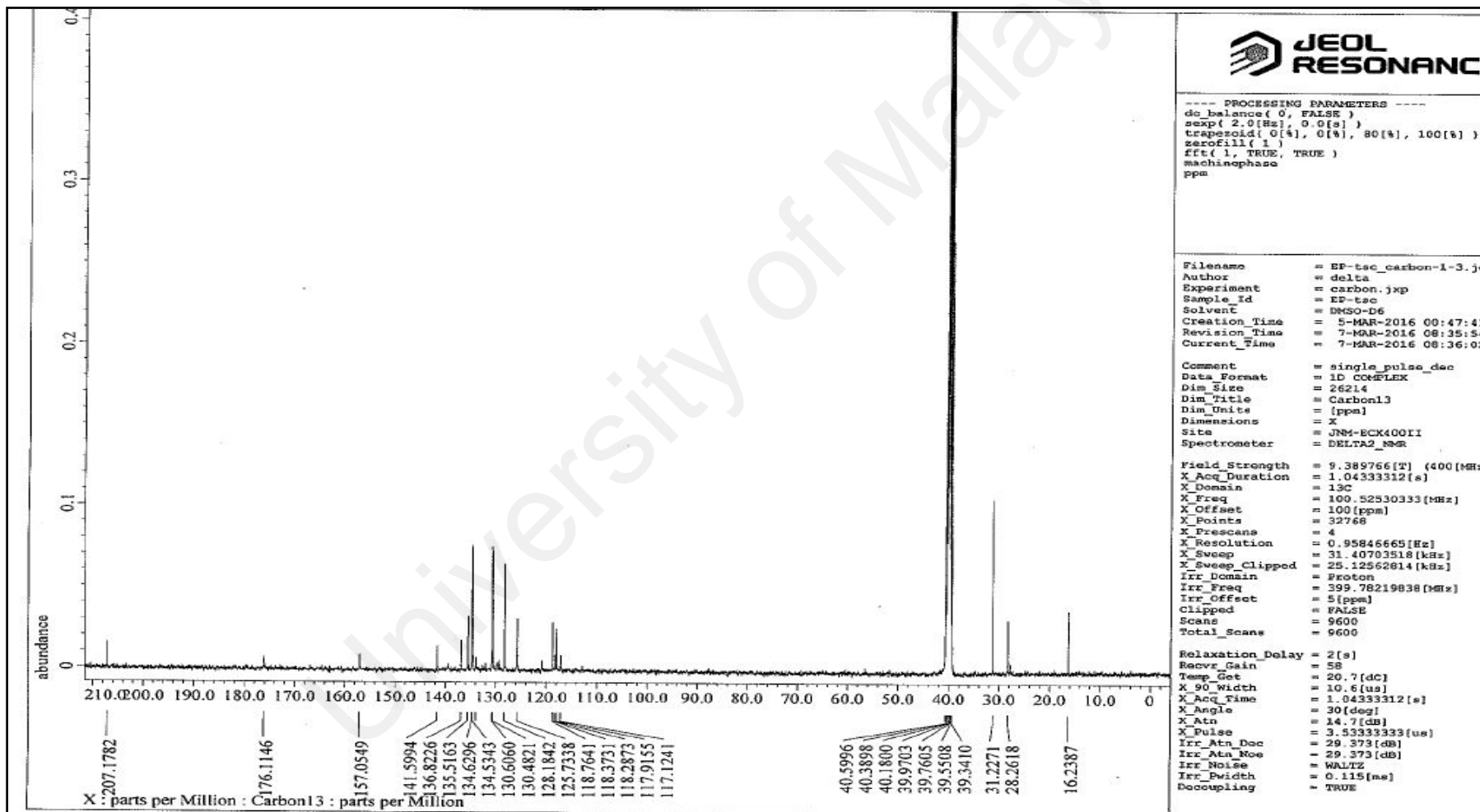
Appendix 21

^{13}C NMR of **E(tsc)T**



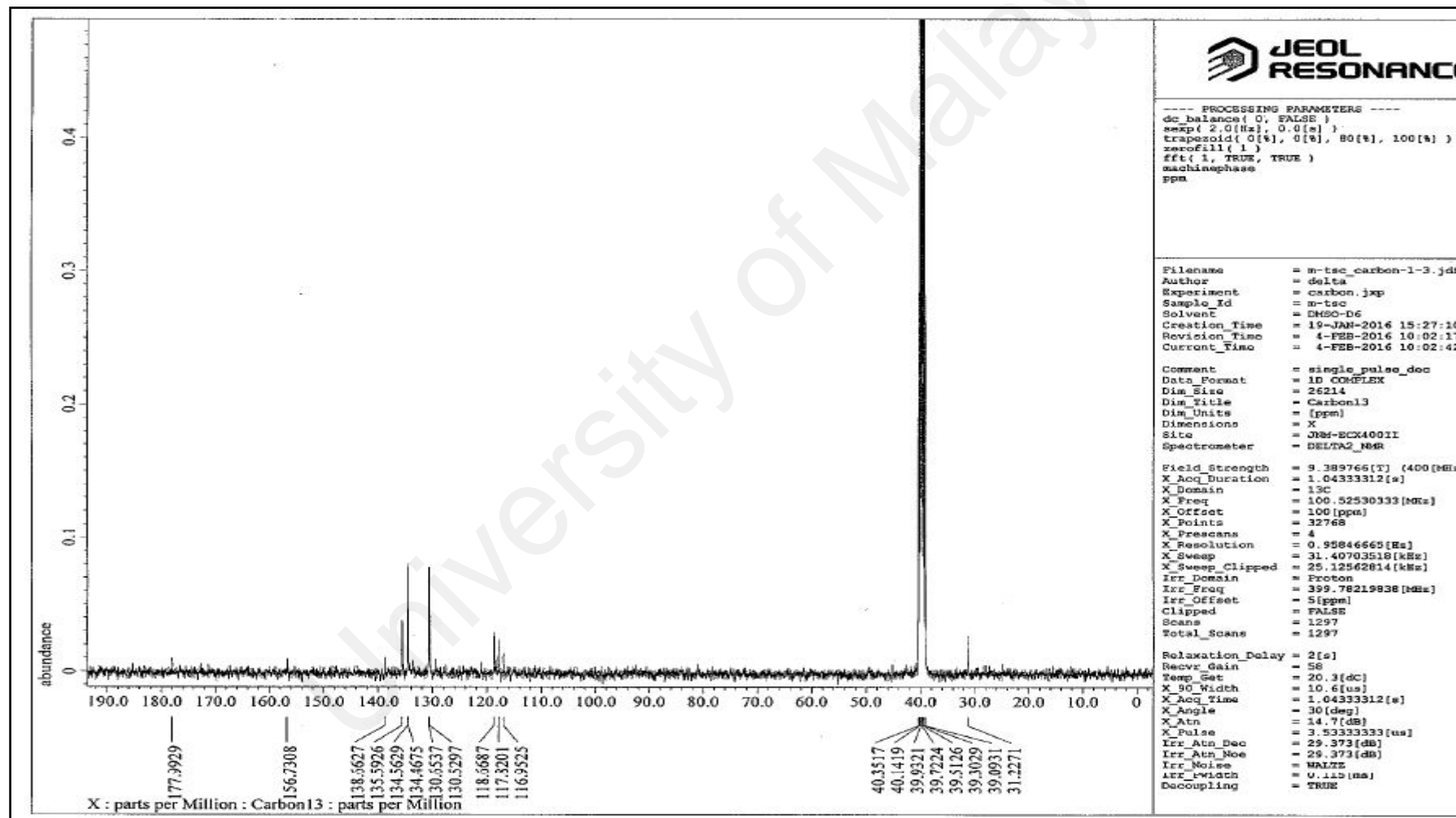
Appendix 22

¹³C NMR of EP(tsc)T



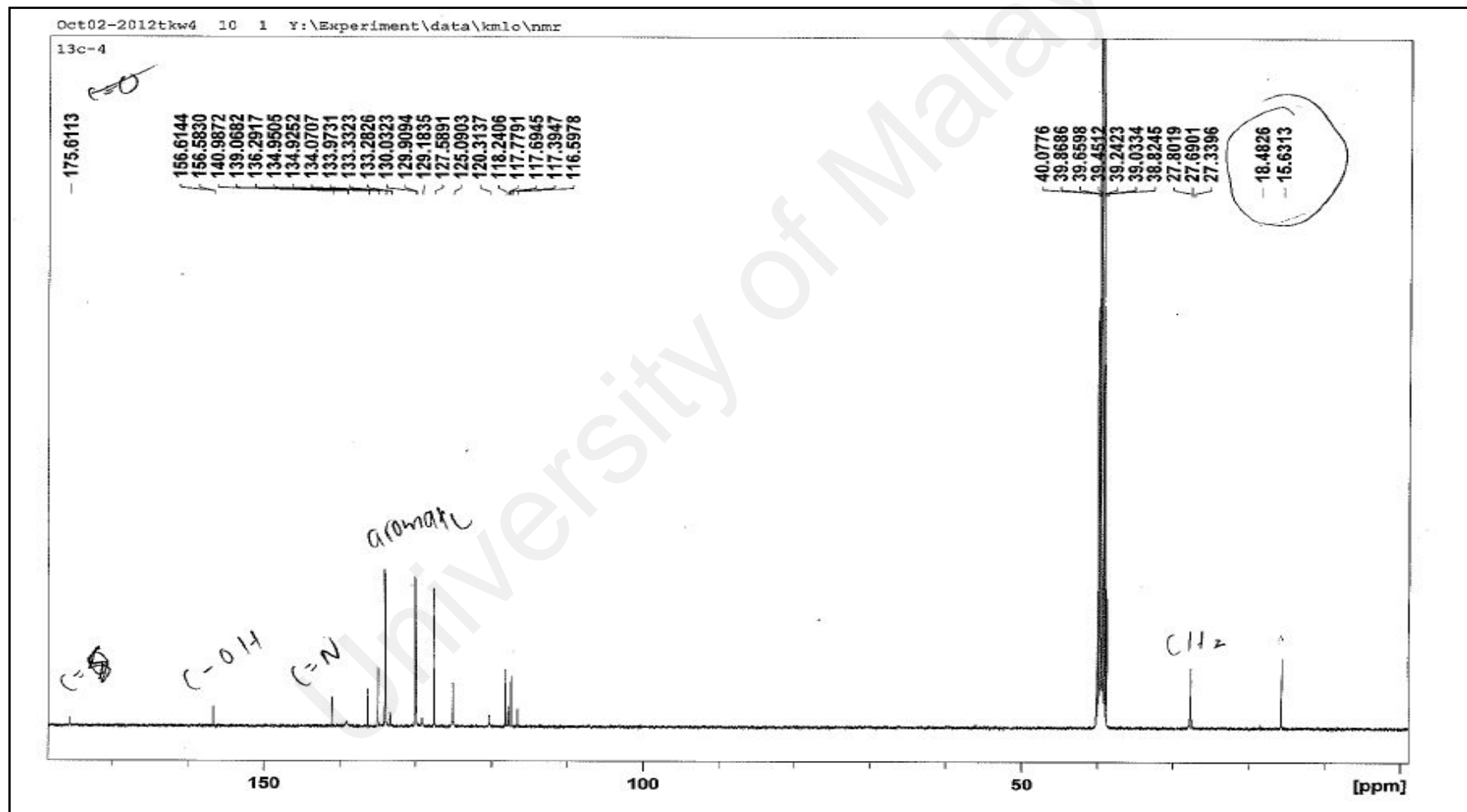
Appendix 23

¹³C NMR of M(tsc)T



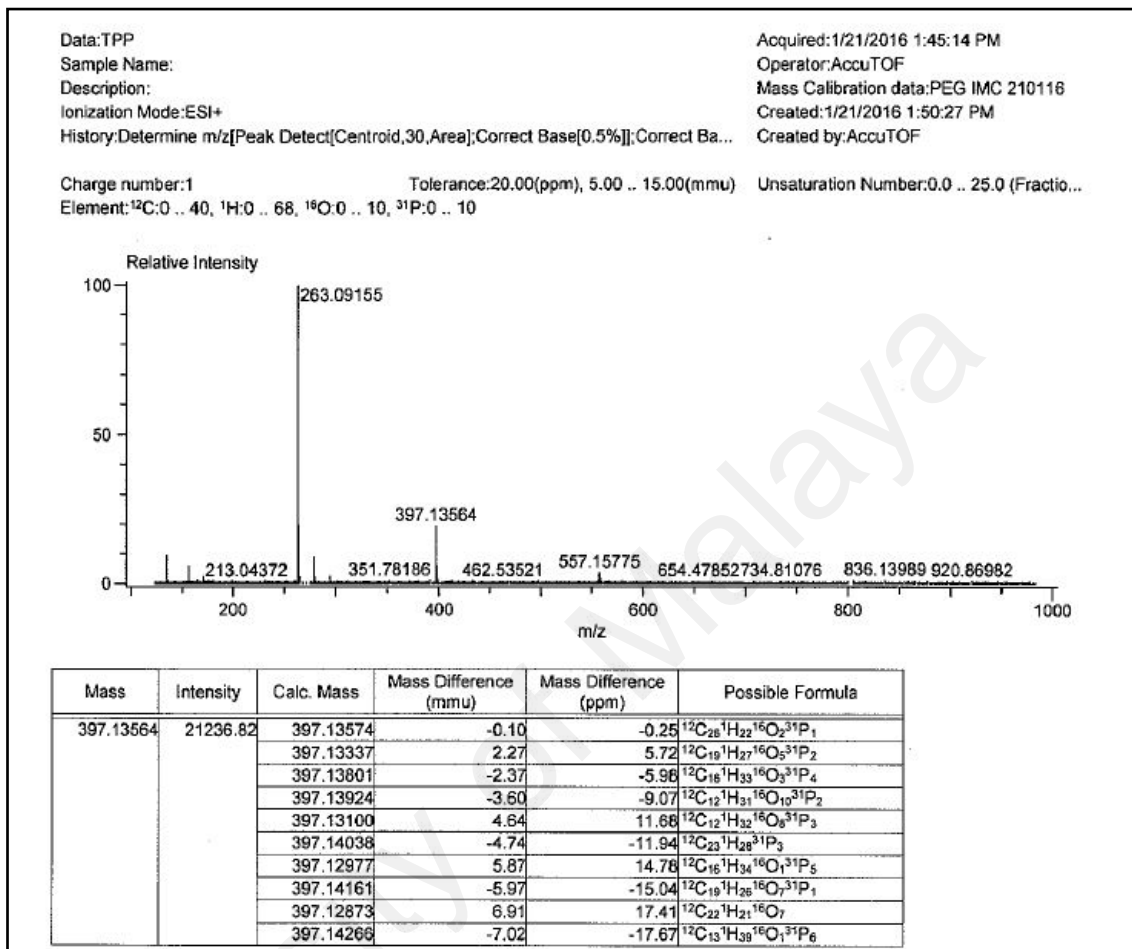
Appendix 24

^{13}C NMR of DM(tsc)T



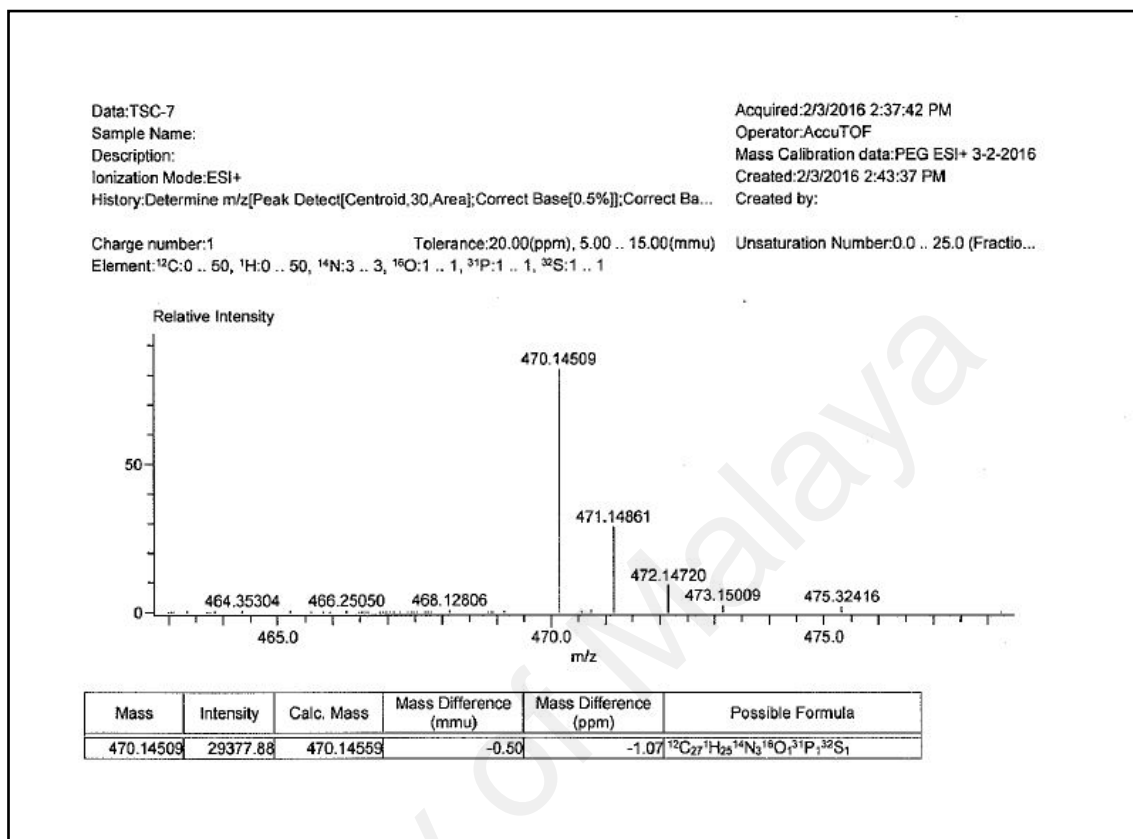
Appendix 25

HRMS of T



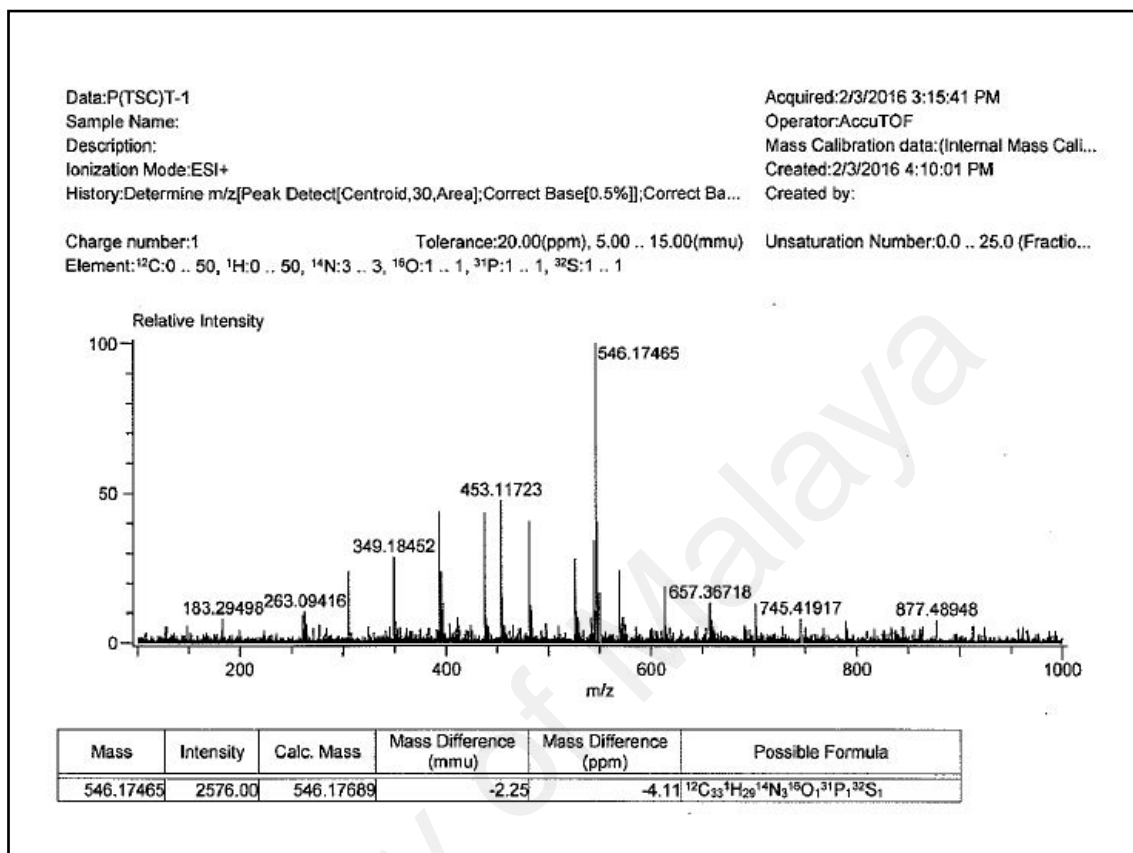
Appendix 26

HRMS of (tsc)T



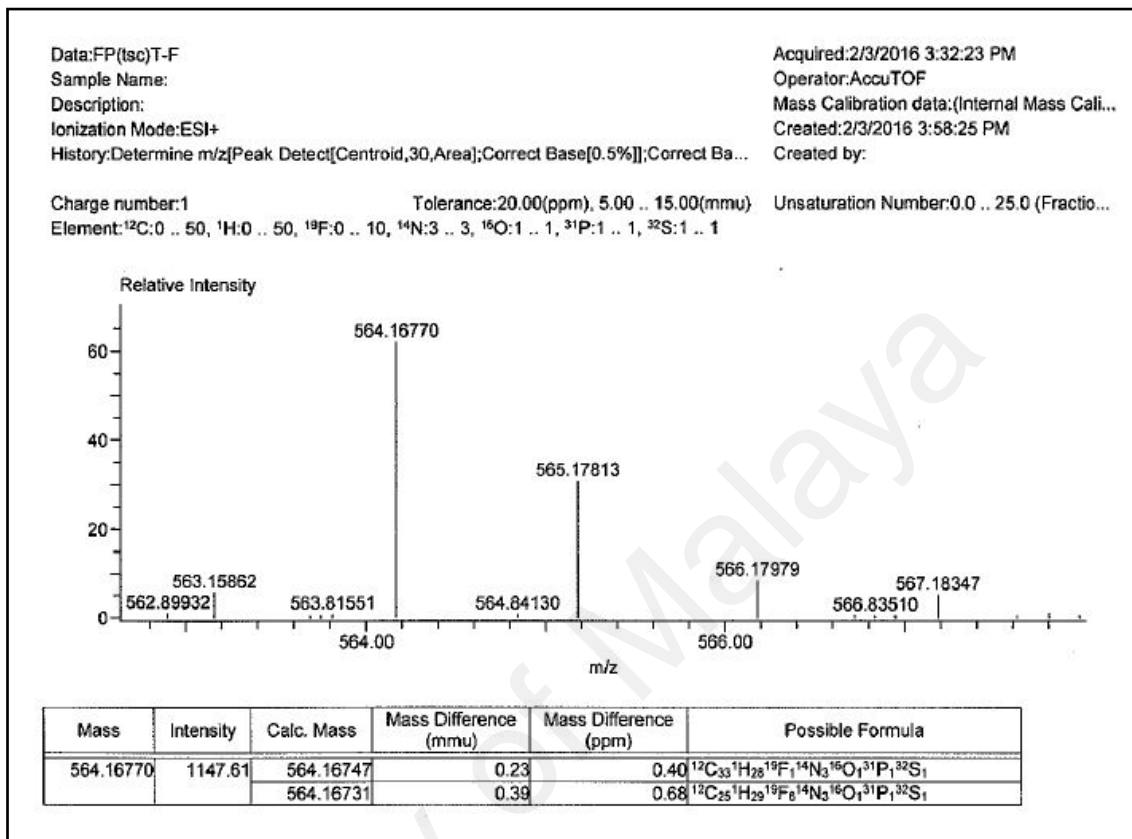
Appendix 27

HRMS of **P(tsc)T**



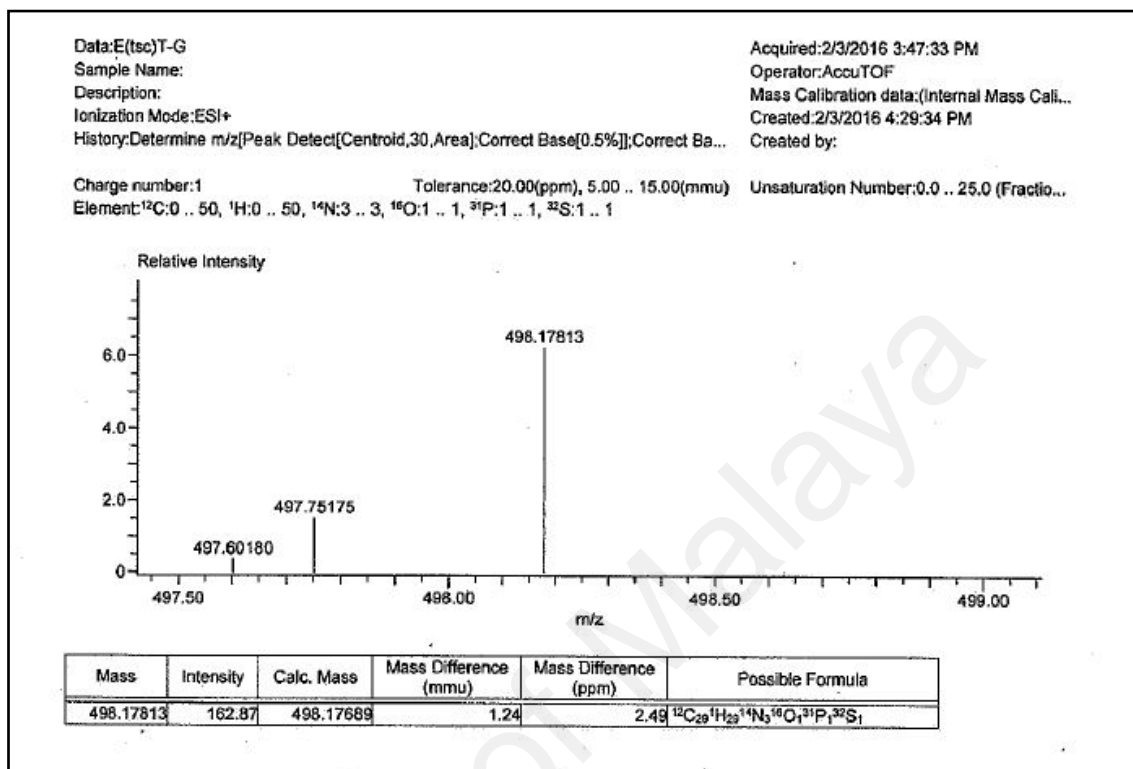
Appendix 28

HRMS of FP(tsc)T



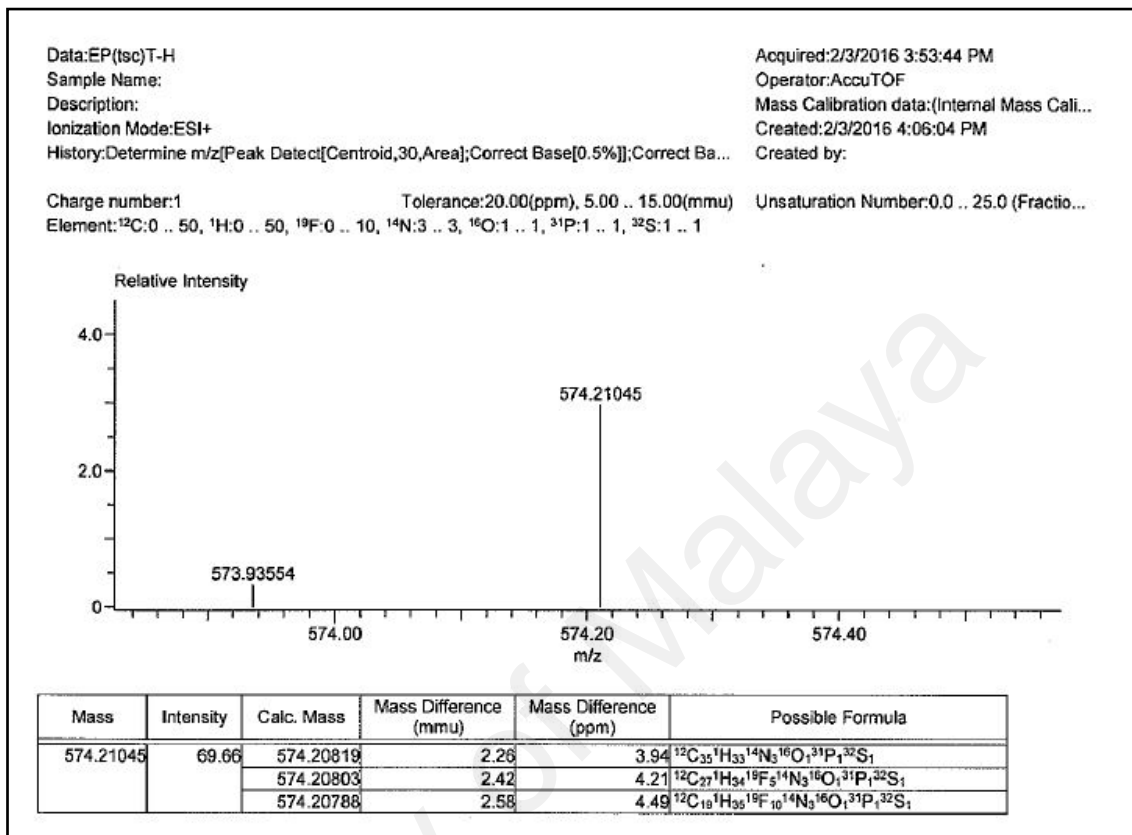
Appendix 29

HRMS of E(tsc)T



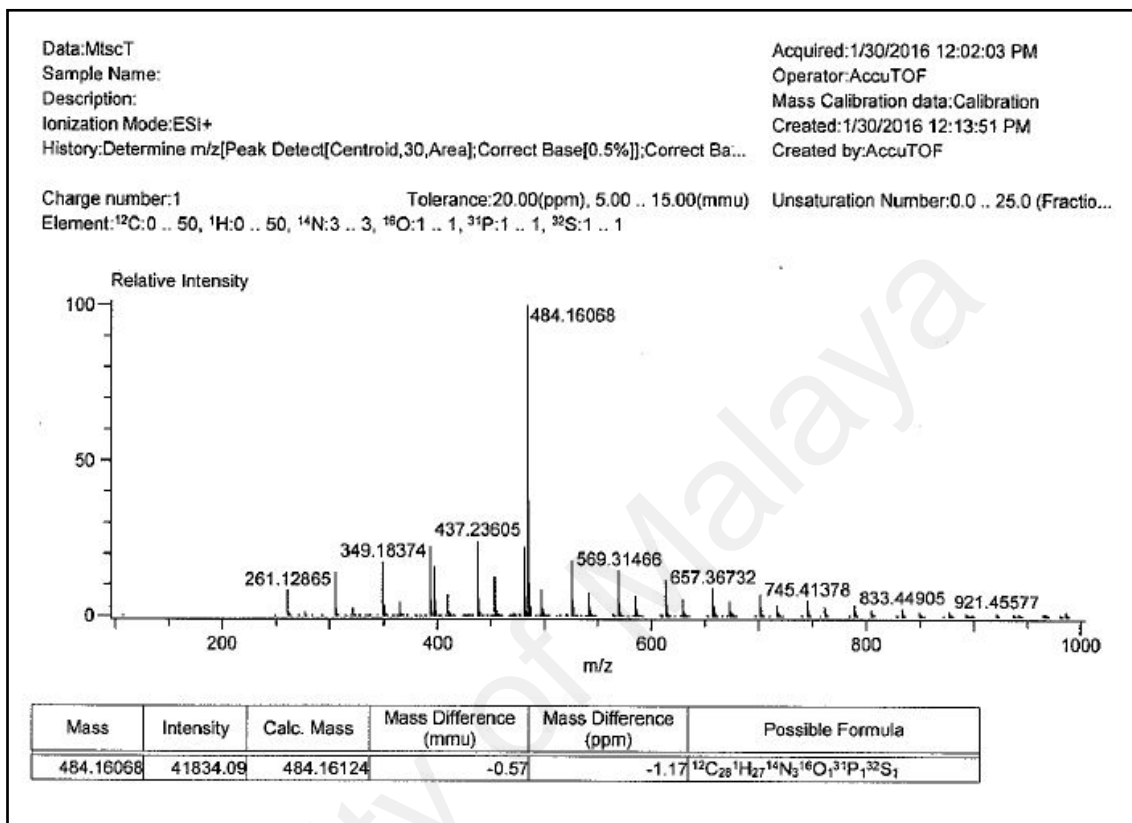
Appendix 30

HRMS of EP(tsc)T



Appendix 31

HRMS of M(tsc)T



Appendix 32

HRMS of DM(tsc)T

